

# Monitoring the Structural Integrity of Packaging Materials Subjected to Sustained Random Loads

By:

Matthew James Lamb B.Eng. (Hons)

School of Engineering and Science, Faculty of Health, Engineering and Science, Victoria  
University

Submitted in fulfilment of the requirements for the degree of Doctor of Philosophy

January 2011

Supervised By:

Associate Professor Vincent Rouillard

Associate Professor Michael Sek

## ABSTRACT

During the distribution phase, packaged consignments are exposed to a variety of environmental hazards, such as vibrations, which, if excessively severe, may cause damage to or even destroy the product. The ability of packaging systems to withstand these dynamic loads is an important factor, since their function is not only to protect the product but also to ensure that damage to the package itself is not evidently apparent as this is likely to affect consumer confidence. Such concerns often result in the use of excessive packaging material and this is no longer acceptable. Therefore, engineered protective packaging systems need to be optimised. Such optimisation requires a suitable technique for continuously monitoring the structural integrity of the systems during laboratory based vibration testing.

Damage within a system can be identified and evaluated using changes in its measured modal parameters, namely natural frequency and damping ratio. Most widely accepted modal parameter identification techniques use the system's frequency response function (FRF), obtained using the Fourier transform, in order to extract modal parameters. However, these techniques cannot be directly applied to time varying systems. In order to circumvent the time invariant requirement, the short-time Fourier transform (STFT) was introduced. However, this technique also has significant limitations with respect to obtaining accurate modal parameter estimates using limited temporal data. Techniques which may reduce the impact of these limitations, such as zero-padding and data overlapping, do exist, however, their effectiveness in modal parameter extraction applications has not been thoroughly evaluated.

An alternative to using frequency domain data to extract modal parameters is to evaluate data in the temporal domain. Many time domain modal parameter extraction techniques make use of the system's free-response impulse response function. These techniques also cannot be directly used to continuously monitor the structural integrity of packaging elements subjected to random loads. For these methods to be applicable to continuous structural integrity assessment, a technique for converting nonstationary forced excitation response data into a series of constant parameter free-response impulse response functions is required. This transformation can be achieved using a digital finite-impulse-response (FIR) filter in conjunction with an algorithm, such as the least-mean-squares (LMS) technique, which is capable of adjusting the filter's tap coefficients in order to minimise the difference between

the measured and estimated response. There is currently no literature on such a continuous structural integrity assessment technique; however, the required tools do exist.

The research presented in this thesis discusses the development of two continuous structural integrity assessment techniques, one which uses an STFT based approach and another which uses an adaptive digital FIR filter. The influence of various analysis parameters used when implementing the STFT, including those of spectral enhancement techniques such as spectral averaging, data overlapping and zero-padding, was also evaluated and discussed.

Both integrity assessment techniques were developed using the results from numerous numerical simulations of single degree-of-freedom (SDoF) systems. This approach was used to avoid the uncontrollable aspects of physical experiments as well as to enable a statistical analysis of the results, which would not otherwise be possible. The results from the numerically simulated experiments were used to develop methods for selecting optimum analysis parameters for both techniques.

The comparative performance of the two techniques was evaluated using a large number of numerical systems, subjected to various stiffness parameter changes (damage scenarios). The sensitivity of the techniques to noise and damping was also evaluated.

Results from the numerically simulated experiments suggest that the adaptive FIR technique is more sensitive to both structural damping and extraneous noise than the STFT based technique. However, for parameters extracted with fine temporal resolution the adaptive FIR technique convincingly outperforms the Fourier based approach, provided that the structural damping is less than approximately 32%. Damping ratios of as much as 16% do not have a significant adverse effect on the results obtained using the adaptive FIR technique, particularly when the level of extraneous noise is low.

The results obtained from the numerical evaluation were compared to those obtained from selected controlled experiments with simulated damage (controlled forced changes in the system's natural frequency). The materials used for the controlled experiments include steel, aluminium, acrylic and carbon fibre.

In the main, the controlled physical experiments confirmed the numerically simulated results. One noticeable difference is a slight increase in the uncertainty of the frequency estimates (for both techniques) despite a relatively low noise to signal ratio (when compared to the numerically simulated experiments containing extraneous noise). This can be attributed to

nonlinearities in the physical arrangements as well as the contamination of the first resonant frequency by higher order modes.

Finally, the ability of integrity assessment techniques to monitor the progression of damage in real packaging elements, such as biodegradable air-cushions and corrugated paperboard containers, was established.

The analysis of random excitation and response data obtained from laboratory tests performed on the packaging elements showed that both techniques are capable of monitoring changes in the structural integrity of complex SDoF systems. However, in general, the adaptive FIR technique was found to be more sensitive in detecting small changes in system characteristics, even when the estimates are obtained with relatively coarse temporal resolution.

Overall, the results presented in this study indicate that the adaptive FIR can be a practical and effective tool for establishing the ability of materials and structures to withstand sustained random loads, provided that the system's damping ratio is limited to approximately 16%.

## STUDENT DECLARATION

“I, Matthew Lamb, declare that the PhD thesis entitled Monitoring the structural integrity of packaging materials subjected to sustained random loads is no more than 100,000 words in length including quotes and exclusive of tables, figures, appendices, bibliography, references and footnotes. This thesis contains no material that has been submitted previously, in whole or part, for the award of any other academic degree or diploma. Except where otherwise indicated, this thesis is my own work”.

Signature:



Date: 28/04/2011

## **ACKNOWLEDGEMENTS**

The author wishes to express his sincere thanks and appreciation to Associate Professor Vincent Rouillard for his encouragement and guidance during the course of the research culminating in this thesis. Thanks are also due to Associate Professor Michael Sek for his conceptual thinking in the initial stages of the research.

The author would also like to thank the technical staff from the School of Engineering and Science. Particular thanks are due to Mr Laszlo Kovacs, for developing the stepper motor controller with limited input from the author.

Finally, the author would like to thank his parents (particularly his father, Walter Lamb) for their unconditional support.

## LIST OF PUBLICATIONS

Rouillard, V, Lamb, M & Sek, M 2007, 'Determining fatigue progression in corrugated paperboard containers subjected to dynamic compression', *Proceedings of the 5th Australasian congress on applied mechanics, ACAM 2007*, vol. 1, Engineers Australia, Brisbane, pp. 331-336

Lamb, M & Rouillard, V 2009, 'Limitations of Fourier-Based spectral analysis for monitoring structural integrity', *Annual conference & exposition on experimental and applied mechanics*, Society of Experimental Mechanics, Albuquerque

Lamb, M, Sek, M & Rouillard, V 2009, 'Adaptive impulse response for determining damage during fatigue testing', *Annual conference & exposition on experimental and applied mechanics*, Society of Experimental Mechanics, Albuquerque

Lamb, M & Rouillard, V 2009, 'Some issues when using Fourier analysis for the extraction of modal parameters', *Journal of physics: Conference series*. vol. 181, no. 1, Institute of Physics

Lamb, M, Rouillard, V & Ainalis, D 2010, 'A practical study of Fourier analysis for monitoring fatigue progression in elements subjected to random loads', *Proceedings of the 6th Australasian congress on applied mechanics*, Engineers Australia, Perth

Lamb, M, Rouillard, V & Ainalis, D 2010, 'A multi-resolution time domain technique for monitoring fatigue progression in elements subjected to random loads', *Proceedings of the 6th Australasian congress on applied mechanics*, Engineers Australia, Perth

Lamb, M, Rouillard, V & Ainalis, D 2010, 'An adaptive impulse response technique for evaluating the performance of structural elements', *Proceedings of the 21st Australasian conference on the mechanics of structures and materials: Incorporating sustainable practice in mechanics of structures and materials*, CRC press, Melbourne, pp. 769-774

Lamb, M, Rouillard, V & Ainalis, D 2010, 'A practical approach to Fourier analysis for monitoring structural integrity', *Proceedings of the 21st Australasian conference on the mechanics of structures and materials: Incorporating sustainable practice in mechanics of structures and materials*, CRC press, Melbourne, pp.763-768

Lamb, M & Rouillard, V 2010, 'Assessing the influence of Fourier analysis parameters on short-time modal parameter extraction', *Journal of the American Society of Mechanical Engineers*, under review

Lamb, M & Rouillard, V 2010, 'An adaptive, multi-resolution, modal parameter extraction technique', *Journal of mechanical systems and signal processing*, under review

Lamb, M & Rouillard, V 2010, 'Monitoring the evolution of damage in packaging systems under sustained random loads', *Journal of packaging technology and science*, in press

# CONTENTS

ABSTRACT .....	ii
STUDENT DECLARATION.....	v
ACKNOWLEDGEMENTS .....	vi
LIST OF PUBLICATIONS .....	vii
LIST OF FIGURES .....	xii
GLOSSARY OF SYMBOLS .....	xx
Chapter 1 INTRODUCTION.....	1-1
1.1 . PACKAGING AND THE ENVIRONMENT .....	1-1
1.2 . EVALUATION OF PACKAGING PERFORMANCE .....	1-4
1.3 . SCOPE OF RESEARCH.....	1-7
REFERENCES.....	1-8
Chapter 2 PRELIMINARY LITERATURE REVIEW .....	2-1
2.1 . THE FOURIER TRANSFORM.....	2-1
2.1.1 . Fourier Analysis for Continuous Integrity Assessment .....	2-2
2.2 . THE HILBERT-HUANG TRANSFORM.....	2-3
2.1.2 . The Hilbert-Huang Transform for Continuous Integrity Assessment .....	2-4
2.3 . THE WAVELET TRANSFORM.....	2-5
2.1.3 . The Wavelet Transform for Continuous Integrity Assessment.....	2-5
2.4 . COMBINED AND COMPARATIVE STUDIES .....	2-6
2.5 . ADAPTIVE TECHNIQUES.....	2-8
2.1.4 . Adaptive Techniques for Continuous Integrity Assessment .....	2-8
2.6 . LITERATURE REVIEW SUMMARY .....	2-11
REFERENCES .....	2-12
Chapter 3 HYPOTHESIS .....	3-1

Chapter 4 METHODOLOGY .....	4-1
4.1 . PERFORMANCE EVALUATION OF ANALYSIS TECHNIQUES .....	4-1
4.2 . NUMERICAL MODEL .....	4-3
4.3 . PHYSICAL EXPERIMENTS.....	4-5
REFERENCES.....	4-6
 Chapter 5 FOURIER ANALYSIS.....	 5-1
5.1 . BACKGROUND .....	5-1
5.2 . MODAL PARAMETER ESTIMATION .....	5-8
5.2.1 . Modal Parameter Estimation From Nonstationary Signals .....	5-12
5.2.2 . Fourier Analysis Enhancement Techniques .....	5-14
5.3 . INFLUENCE OF SPECTRAL (STFT) ANALYSIS PARAMETERS AND ENHANCEMENT TECHNIQUES.....	5-19
5.3.1 . Influence of Spectral Averaging and Sub-record Length .....	5-20
5.3.2 . Influence of Zero-Padding on Modal Parameter Estimation .....	5-22
5.3.3 . Influence of Overlapped Averages on Modal Parameter Estimation .....	5-29
5.4 . CONCLUSIONS.....	5-34
REFERENCES .....	5-35
 Chapter 6 ADAPTIVE CONDITION ASSESSMENT .....	 6-1
6.1 . MODAL PARAMETER EXTRACTION: FREE-RESPONSE .....	6-1
6.1.1 . Logarithmic Decrement Technique .....	6-4
6.1.2 . Hilbert Envelope Technique.....	6-5
6.2 . NONSTATIONARY FORCED EXCITATION/RESPONSE .....	6-7
6.2.1 . Impulse Response Functions and Finite-Impulse-Response Filters.....	6-7
6.2.2 . Least-Mean-Square Adaptive Filters .....	6-9
6.2.3 . SUMMARY OF LEAKY, NLMS ADAPTATION FOR MODAL PARAMETER ESTIMATION.....	6-16
6.2.4 . EXPERIMENTAL EVALUATION OF ADAPTIVE FINITE-IMPULSE- RESPONSE PARAMETERS .....	6-20
6.3 . CONCLUSIONS.....	6-46
REFERENCES .....	6-47

Chapter 7 NUMERICAL COMPARATIVE STUDY .....	7-1
7.1 . SELECTION OF ANALYSIS PARAMETERS .....	7-1
7.1.1 . Fourier Based Technique .....	7-2
7.1.2 . Overview of Fourier Based Technique .....	7-7
7.1.3 . Adaptive Finite Impulse Response Technique .....	7-11
7.1.4 . Overview of Adaptive Finite-Impulse-Response Techniques .....	7-14
7.2 . COMPARATIVE INFLUENCE OF NOISE .....	7-20
7.3 . COMPARATIVE INFLUENCE OF DAMPING.....	7-21
7.4 . STEP CHANGES IN NATURAL FREQUENCY .....	7-24
7.5 . PROGRESSIVE DAMAGE .....	7-33
7.6 . SELECTING A TECHNIQUE BASED ON TEMPORAL RESOLUTION .....	7-40
 Chapter 8 PHYSICAL EXPERIMENTS.....	 8-1
8.1 . CONTROLLABLE EXPERIMENTS.....	8-1
8.1.1 Experimental Setup for Controlled Experiments.....	8-1
8.1.2 . Calibration of Natural Frequency .....	8-3
8.1.3 . Preliminary Experiments.....	8-4
8.1.3.1 . <i>Fourier based technique</i> .....	8-5
8.1.3.2 . <i>Adaptive finite-impulse-response technique</i> .....	8-8
8.1.4 . Stepped Damage Scenarios.....	8-12
8.1.4.1 . <i>Steel cantilever results</i> .....	8-12
8.1.4.2 . <i>Aluminium cantilever results</i> .....	8-15
8.1.4.3 . <i>Acrylic cantilever results</i> .....	8-18
8.1.4.4 . <i>Carbon fibre cantilever results</i> .....	8-21
8.1.5 . Discussion of Controlled Experiment Results.....	8-24
8.2 . ASSESSMENT OF REAL PACKAGING ELEMENTS .....	8-25
8.3 . CONCLUSION .....	8-34
REFERENCES .....	8-35
 Chapter 9 CONCLUSION .....	 9-1
9.1. SUMMARY OF GENERAL TECHNICAL CONTRIBUTIONS.....	9-4
9.2. FUTURE WORK.....	9-5

# LIST OF FIGURES

## Chapter 1: INTRODUCTION

*Figure 1-1: Illustration of packaging optimisation* ..... 1-6

## Chapter 4: METHODOLOGY

*Figure 4-1 (a) Packaging testing arrangement (b) Equivalent SDoF model*. .... 4-3

*Figure 4-2: SDoF free-body force diagram*..... 4-3

*Figure 4-3: Schematic of Simulink model for simulation of foundation displacement*..... 4-4

## Chapter 5: FOURIER ANALYSIS

*Figure 5-1: Random signal (top left) followed by its harmonic components*. .... 5-5

*Figure 5-2: Time-Frequency-Amplitude representation of the harmonics of a random signal*..... 5-5

*Figure 5-3: (a) Magnitude spectrum, (b) Phase spectrum, for the time signal shown in Figure 5-1* ..... 5-6

*Figure 5-4: Common windowing functions*. .... 5-15

*Figure 5-5: Reduced leakage by the application of windowing functions*..... 5-16

*Figure 5-6: Schematic of spectral analysis identifying overlap*. .... 5-17

*Figure 5-7: Spectral estimate overlap*. .... 5-17

*Figure 5-8: Zero-padding*. .... 5-18

*Figure 5-9: Experiment 1 - Spectral resolution and uncertainty*. .... 5-21

*Figure 5-10: Experiment 2 - Results of increased zero-padding*..... 5-24

*Figure 5-11: Experiment 2 – Results of increased zero-padding (10% noise)*..... 5-24

*Figure 5-12: FRF estimates and zero-padding: Left – No zero-padding*, ..... 5-25

*Figure 5-13: Spectral resolution and uncertainty with zero-padding*. .... 5-26

*Figure 5-14: Experiment 3 - Results from improved temporal resolution using zero-padding* ..... 5-28

*Figure 5-15: Experiment 3 – Results of improved temporal resolution using zero-padding from signals (10% noise)*. .... 5-28

<i>Figure 5-16: Experiment 4 - Effect of overlapped averages.</i> .....	5-30
<i>Figure 5-17: Experiment 4 - Estimated natural frequency variance versus increased spectral overlapping (where <math>x</math> is the number of overlapped averages).</i> .....	5-32
<i>Figure 5-18: Enhancement of FRF estimates using overlapped averaging.</i> .....	5-33
<i>Figure 5-19: Influence of overlapped averaging on the natural frequency estimate variance with zero-applied (<math>T_{sr} \times 16</math>).</i> .....	5-34

## Chapter 6: TIME DOMAIN PARAMETER EXTRACTION

<i>Figure 6-1: Comparison of overdamped, critical and underdamped response (Reproduced from: Rao 2005, p.145)</i> .....	6-2
<i>Figure 6-2: Free vibration free-body diagram.</i> .....	6-2
<i>Figure 6-3: Free vibration response of a viscously underdamped SDoF system (Reproduced from: Rao 2005, p. 143)</i> .....	6-4
<i>Figure 6-4: FIR filter schematic.</i> .....	6-8
<i>Figure 6-5: Adaptive FIR filter schematic.</i> .....	6-9
<i>Figure 6-6: Total misadjustment and the optimum step-size (Reproduced from: Haykin 1986, p. 254)</i> .....	6-13
<i>Figure 6-7: NLMS adaptive modal parameter estimation algorithm.</i> .....	6-16
<i>Figure 6-8: Technique one, mean of the derivative of the <math>n^{\text{th}}</math> instantaneous phase vector.</i> 6-17	
<i>Figure 6-9: Technique two, polynomial fit of the <math>n^{\text{th}}</math> instantaneous phase vector.</i> .....	6-17
<i>Figure 6-10: Phase curve- fit with contaminated data.</i> .....	6-19
<i>Figure 6-11: Sinusoidal curve- fit with contaminated data.</i> .....	6-19
<i>Figure 6-12: Effect of normalised step-size on nonstationary parameter extraction.</i> .....	6-21
<i>Figure 6-13: Zoomed section from Figure 6 12 showing steady-state error.</i> .....	6-21
<i>Figure 6-14: Effect of normalised step-size on RMS filter error.</i> .....	6-22
<i>Figure 6-15: Zoomed section of Figure 6-14 showing convergence and steady-state error</i> .....	6-23
<i>Figure 6-16: Experiment 5 - Effect of normalised step-size on overall RMS filter error, linear decay.</i> .....	6-24
<i>Figure 6-17: Experiment 5 - Effect of normalised step-size on overall RMS filter error, linear decay (10% noise)</i> .....	6-24

<i>Figure 6-18: Experiment 6 parameter summary</i> .....	6-25
<i>Figure 6-19: Experiment 6 - Effect of normalised step-size on final RMS filter error, sudden damage</i> .....	6-26
<i>Figure 6-20: Experiment 6 - Effect of normalised step-size on final RMS filter error, sudden damage (10% noise)</i> .....	6-26
<i>Figure 6-21: Experiment 6 - Effect of normalised step-size and leakage on final RMS filter error, 25% sudden damage</i> .....	6-27
<i>Figure 6-22: Experiment 6 - Effect of normalised step-size and leakage on final RMS filter error, 25% sudden damage (10% noise)</i> .....	6-28
<i>Figure 6-23: Reduction in the required calculations for determining the optimum normalised step-size by implementing the sequential dichotomy technique</i> .....	6-29
<i>Figure 6-24: Introduction of a fixed optimised normalised step-size</i> .....	6-30
<i>Figure 6-25: Compromise between convergence and steady-state error when using a fixed optimised normalised step-size</i> .....	6-31
<i>Figure 6-26: Introduction of a fixed optimised normalised step-size (10% noise)</i> .....	6-32
<i>Figure 6-27: Compromise between convergence and steady-state error when using a fixed optimised normalised step-size (10% noise)</i> .....	6-33
<i>Figure 6-28: Introduction of a variable optimised normalised step-size</i> .....	6-33
<i>Figure 6-29: Reduced compromise between convergence and steady-state error when using a variable optimised normalised step-size</i> .....	6-34
<i>Figure 6-30: Reduced compromise between convergence and steady-state error when using a variable optimised normalised step-size (10% noise)</i> .....	6-34
<i>Figure 6-31: Example damage pattern</i> .....	6-35
<i>Figure 6-32: Filter error corresponding to the damage pattern in Figure 6-31</i> .....	6-36
<i>Figure 6-33: Variable normalised step-size corresponding to the damage pattern in Figure 6-31</i> .....	6-36
<i>Figure 6-34: Reduction of filter error by improving the initial filter tap coefficients</i> .....	6-39
<i>Figure 6-35: Convergence of the initial filter tap coefficients through iteration</i> .....	6-39
<i>Figure 6-36: Experiment 7 - Portion of the system's impulse response function described by the given number of filter tap coefficients</i> .....	6-40
<i>Figure 6-37: Experiment 7 - Portion of the system's impulse response function used for parameter extraction</i> .....	6-41

<i>Figure 6-38: Experiment 7 - Converged damped natural frequencies (natural duration approximately 300-350 coefficients).....</i>	<i>6-42</i>
<i>Figure 6-39: Experiment 7 - RMS Filter error signal. ....</i>	<i>6-43</i>
<i>Figure 6-40: Experiment 7 - RMS Filter error signal (10% noise).....</i>	<i>6-43</i>
<i>Figure 6-41: Experiment 8 - Influence of sampling frequency on results extracted from a system with 20Hz natural frequency and 11% damping (inset clean results for 500Hz-4000Hz sampling frequencies).....</i>	<i>6-45</i>
<i>Figure 6-42: Experiment 8 - Influence of sampling frequency on results extracted from a system with 40Hz natural frequency and 11% damping (inset clean results for 500Hz-4000Hz sampling frequencies).....</i>	<i>6-45</i>
<i>Figure 6-43: Experiment 8 - Influence of sampling frequency on results extracted from a system with 80Hz natural frequency and 11% damping (inset clean results for 500Hz-4000Hz sampling frequencies).....</i>	<i>6-46</i>

## Chapter 7: NUMERICAL COMPARATIVE STUDY

<i>Figure 7-1: Importance of sub-record length versus spectral averaging.....</i>	<i>7-2</i>
<i>Figure 7-2: Effect of overlapped averages (x) on estimated natural frequency variance... </i>	<i>7-3</i>
<i>Figure 7-3: Dependence of optimum averaging amount on sampling frequency and temporal resolution (sampling frequency: 2048Hz, temporal resolution: 5 seconds) .....</i>	<i>7-4</i>
<i>Figure 7-4: Dependence of optimum averaging amount on sampling frequency and temporal resolution (sampling frequency: 1000Hz, temporal resolution: 1 second).....</i>	<i>7-5</i>
<i>Figure 7-5: Improvements though zero-padding.....</i>	<i>7-6</i>
<i>Figure 7-6: Schematic representation of algorithm for Fourier based integrity assessment technique. ....</i>	<i>7-7</i>
<i>Figure 7-7: Evolution of a system's FRF .....</i>	<i>7-8</i>
<i>Figure 7-8: FRF spectrogram .....</i>	<i>7-9</i>
<i>Figure 7-9: Parameter extraction from final (295<sup>th</sup> second) FRF estimate.....</i>	<i>7-10</i>
<i>Figure 7-10: Damped natural frequency as a function of time. ....</i>	<i>7-10</i>
<i>Figure 7-11: Demonstration of filter tap coefficient vector length and impulse response natural duration.....</i>	<i>7-11</i>
<i>Figure 7-12: Influence of filter tap coefficient vector length on damped natural frequency estimates (inset clean results for 400-1600 filter tap coefficients). ....</i>	<i>7-12</i>

<i>Figure 7-13: Typical example of stages in the initial filter tap reiteration procedure.....</i>	<i>7-13</i>
<i>Figure 7-14: Schematic representation of algorithm for adaptive FIR integrity assessment technique. ....</i>	<i>7-14</i>
<i>Figure 7-15: Evolution of a system's FIR function. ....</i>	<i>7-15</i>
<i>Figure 7-16: Parameter extraction from final (300<sup>th</sup> second) instantaneous FIR function .....</i>	<i>7-16</i>
<i>Figure 7-17: Un-wrapped instantaneous phase vector for the final (300<sup>th</sup> second) FIR function. ....</i>	<i>7-17</i>
<i>Figure 7-18: Evolution of the system's normalised FIR function.....</i>	<i>7-18</i>
<i>Figure 7-19: Normalised FIR function spectrogram.....</i>	<i>7-18</i>
<i>Figure 7-20: Sinusoidal curve- fit of the final (300<sup>th</sup> second) normalised instantaneous impulse response function.....</i>	<i>7-19</i>
<i>Figure 7-21: Damped natural frequency as a function of time. ....</i>	<i>7-20</i>
<i>Figure 7-22: Comparison of the influence of noise on the adaptive FIR and Fourier based techniques. ....</i>	<i>7-21</i>
<i>Figure 7-23: Comparison of the influence of increased damping on the adaptive FIR and Fourier based techniques (0% noise). ....</i>	<i>7-22</i>
<i>Figure 7-24: Comparison of the influence of increased damping on the adaptive FIR and Fourier based techniques (8% noise). ....</i>	<i>7-23</i>
<i>Figure 7-25: Typical filter tap coefficient vector (impulse response function) for various damping ratios. ....</i>	<i>7-23</i>
<i>Figure 7-26: Step change results for a damping ratio of 1% (0% noise).....</i>	<i>7-25</i>
<i>Figure 7-27: Figure 7-26 rescaled to better reveal the response of the adaptive FIR technique (0% noise).....</i>	<i>7-25</i>
<i>Figure 7-28: Step change results for a damping ratio of 1% (8% noise).....</i>	<i>7-26</i>
<i>Figure 7-29: Figure 7-28 rescaled to better reveal the response of the adaptive FIR technique (8% noise).....</i>	<i>7-26</i>
<i>Figure 7-30: Step change results for a damping ratio of 8% (0% noise).....</i>	<i>7-27</i>
<i>Figure 7-31: Figure 7-30 rescaled to better reveal the response of the adaptive FIR technique (0% noise).....</i>	<i>7-27</i>
<i>Figure 7-32: Step change results for a damping ratio of 8% (8% noise).....</i>	<i>7-28</i>

<i>Figure 7-33: Figure 7-32 rescaled to better reveal the response of the adaptive FIR technique (8% noise).....</i>	<i>7-28</i>
<i>Figure 7-34: Step change results for a damping ratio of 16% (0% noise).....</i>	<i>7-29</i>
<i>Figure 7-35: Figure 7-34 rescaled to better reveal the response of the adaptive FIR technique (0% noise).....</i>	<i>7-29</i>
<i>Figure 7-36: Step change results for a damping ratio of 16% (8% noise).....</i>	<i>7-30</i>
<i>Figure 7-37: Step change results for a damping ratio of 1%, Fourier technique with 10 second temporal resolution (0% noise) .....</i>	<i>7-31</i>
<i>Figure 7-38: Improved results from the adaptive FIR technique using a moving average filter.....</i>	<i>7-32</i>
<i>Figure 7-39: Progressive damage, increasing rate of change, 1% damping (0% noise) ...</i>	<i>7-34</i>
<i>Figure 7-40: Progressive damage, increasing rate of change, 1% damping (8% noise) ...</i>	<i>7-34</i>
<i>Figure 7-41: Progressive damage, increasing rate of change, 8% damping (0% noise) ...</i>	<i>7-35</i>
<i>Figure 7-42: Progressive damage, increasing rate of change, 8% damping (8% noise) ...</i>	<i>7-35</i>
<i>Figure 7-43: Progressive damage, increasing rate of change, 16% damping (0% noise). ...</i>	<i>7-36</i>
<i>Figure 7-44: Progressive damage, increasing rate of change, 16% damping (8% noise). ...</i>	<i>7-36</i>
<i>Figure 7-45: Progressive damage, decreasing, rate of change, 1% damping (0% noise)..</i>	<i>7-37</i>
<i>Figure 7-46: Progressive damage, decreasing rate of change, 1% damping (8% noise)...</i>	<i>7-38</i>
<i>Figure 7-47: Progressive damage, decreasing rate of change, 8% damping (0% noise)...</i>	<i>7-38</i>
<i>Figure 7-48: Progressive damage, decreasing rate of change, 8% damping (8% noise)...</i>	<i>7-39</i>
<i>Figure 7-49: Progressive damage, decreasing rate of change, 16% damping (0% noise)</i>	
<i>.....</i>	<i>7-39</i>
<i>Figure 7-50: Progressive damage, decreasing, rate of change, 16% damping (8% noise).....</i>	<i>7-40</i>
<i>Figure 7-51: Total error versus temporal resolution (4% noise).....</i>	<i>7-41</i>
<i>Figure 7-52: Results obtained using a temporal resolution of 3 seconds for a system with 16% damping and signals containing 4% extraneous noise.....</i>	<i>7-42</i>

## Chapter 8: PHYSICAL EXPERIMENTS

<i>Figure 8-1: Variable length cantilever rig.</i>	8-2
<i>Figure 8-2: Schematic of experimental arrangement - controllable experiments.</i>	8-3
<i>Figure 8-3: Bode plot of physical steel cantilever arrangement.</i>	8-4
<i>Figure 8-4: Influence of zero-padding, sub-record length and spectral averaging.</i>	8-6
<i>Figure 8-5: Influence of overlapped spectral averages.</i>	8-7
<i>Figure 8-6: Compromise between temporal and spectral uncertainty.</i>	8-7
<i>Figure 8-7: Influence of normalised step-size on natural frequency estimates.</i>	8-9
<i>Figure 8-8: Optimisation of fixed normalised step-size.</i>	8-10
<i>Figure 8-9: Filter error signals for a fixed optimised step-size and a fixed step-size of 0.1.</i>	8-10
<i>Figure 8-10: Improvement from error magnitude optimised normalised step-size.</i>	8-11
<i>Figure 8-11: Values of step-size selected by error magnitude optimisation.</i>	8-11
<i>Figure 8-12: Step change results for a physical steel cantilever.</i>	8-13
<i>Figure 8-13: Error signal for the fixed step-size the results presented in Figure 8-12.</i>	8-14
<i>Figure 8-14: Comparison of the adaptive FIR and Fourier based results, steel cantilever.</i>	8-14
<i>Figure 8-15: Bode plot of physical aluminium cantilever arrangement.</i>	8-16
<i>Figure 8-16: Step change results for a physical aluminium cantilever.</i>	8-16
<i>Figure 8-17: Error signal for the fixed step-size the results presented in Figure 8-16.</i>	8-17
<i>Figure 8-18: Comparison of the adaptive FIR and Fourier based results, aluminium cantilever.</i>	8-17
<i>Figure 8-19: Bode plot of physical acrylic cantilever arrangement.</i>	8-19
<i>Figure 8-20: Step change results for a physical acrylic cantilever.</i>	8-19
<i>Figure 8-21: Error signal for the fixed step-size results presented in Figure 8-20.</i>	8-20
<i>Figure 8-22: Comparison of the adaptive FIR and Fourier based results, acrylic cantilever.</i>	8-20

<i>Figure 8-23: Bode plot of physical carbon fibre cantilever arrangement.....</i>	<i>8-22</i>
<i>Figure 8-24: Step change results for a physical carbon fibre cantilever. ....</i>	<i>8-22</i>
<i>Figure 8-25: Error signal for the fixed step-size results presented in Figure 8-24. ....</i>	<i>8-23</i>
<i>Figure 8-26: Comparison of the adaptive FIR and Fourier based results, carbon fibre cantilever.....</i>	<i>8-23</i>
<i>Figure 8-27: Opus biodegradable air cushion typical compression curves – full compression. ....</i>	<i>8-26</i>
<i>Figure 8-28: Corrugated paperboard container compression curves – full compression..</i>	<i>8-26</i>
<i>Figure 8-29: Opus biodegradable air cushion pre-compression characteristics. ....</i>	<i>8-27</i>
<i>Figure 8-30: Bio-degradable air-cushion experimental arrangement.....</i>	<i>8-28</i>
<i>Figure 8-31: Structural integrity assessment results – Opus biodegradable air cushion..</i>	<i>8-29</i>
<i>Figure 8-32: Structural integrity assessment results – zoomed section of Figure 8-31.....</i>	<i>8-29</i>
<i>Figure 8-33: Evolution of the air cushion system’s FRF with the induction of damage (line colours correspond with those given in Figure 8-29). ....</i>	<i>8-30</i>
<i>Figure 8-34: Evolution of the paperboard container system’s FRF during random fatigue testing.....</i>	<i>8-31</i>
<i>Figure 8-35: Corrugated paperboard experimental arrangement.....</i>	<i>8-31</i>
<i>Figure 8-36: Visual wavelength photograph (top row) and thermal (bottom row) image sequence of sample during random fatigue testing (arbitrary temperature scale). ....</i>	<i>8-32</i>
<i>Figure 8-36 Continued: Naked eye (top row) and thermal (bottom row) image sequence of sample during random fatigue testing (arbitrary temperature scale). ....</i>	<i>8-33</i>
<i>Figure 8-37: Paperboard container sample at 7th minute – Left: Naked eye (top row) Right: Thermal image (arbitrary temperature scale). ....</i>	<i>8-33</i>
<i>Figure 8-38: Structural integrity assessment results – paperboard container.....</i>	<i>8-34</i>

## GLOSSARY OF SYMBOLS

$a$	Constant
$A$	Constant
$b$	Constant
$B$	Constant
$c$	Damping coefficient or constant
$c_r$	Correlation coefficient
$C$	Unknown constant
$e$	Base of natural logarithms or filter error
$f$	Frequency
$f_n$	Natural frequency
$\overline{f_n}$	Mean Natural frequency
$f_s$	Sampling frequency
$h$	Filter tap coefficient
$\mathbf{h}$	Filter tap coefficient vector
$\hat{\mathbf{h}}$	Least-mean-squares estimate of $\mathbf{h}$
$h(\tau)$	Impulse response function
$H(f)$	Frequency response function
$H_1$	Definition of frequency response function
$H_2$	Definition of frequency response function
$i$	Integer
$j$	$\sqrt{-1}$
$J$	Mean squared error
$k$	Stiffness or integer
$m$	Mass or number of cycles averaged
$M$	Total number of filter coefficients
$n$	Integer
$n_d$	Number of distinct averages
$N$	Total number of points
$\mathbf{p}$	Cross-correlation vector
$\hat{\mathbf{p}}$	Least-mean-squares estimate of $\mathbf{p}$
$q$	Integer
$r$	Overlap percentage
$\mathbf{R}$	Correlation matrix
$\hat{\mathbf{R}}$	Least-mean-squares estimate of $\mathbf{R}$
$s$	Exponential coefficient or root of an equation
$t$	Time
$T$	Total record duration
$T_{IR}$	Impulse response function natural duration
$T_p$	Period

$T_r$	Temporal resolution
$T_{sr}$	Sub-record length
$w$	Windowing function (Time history tapering)
$x$	Variable, often excitation
$\mathbf{x}$	Adaptive filter input vector
$\bar{x}$	Mean of $x$
$\tilde{x}$	Hilbert transform of $x$
$X$	Fourier transform or amplitude $x$
$y$	Variable, often response
$\hat{y}$	Least-mean-squares estimate of $y$
$Y$	Fourier transform of $y$
$\alpha$	Constant, Tukey window weighting
$\delta$	Logarithmic decrement
$\Delta f$	Spectral resolution
$\Delta t$	Increment in time
$\varepsilon_r$	Spectral uncertainty/error
$\zeta$	Damping ratio
$\lambda$	Eigenvalue of correlation matrix
$\mu$	Step-size
$\mu_N$	Normalised step-size
$\sigma$	Standard deviation
$\sigma_{avg.}^2$	Average spectral variance
$\sigma_{meas.}^2$	Individual spectral variance of measurements
$\phi$	Phase
$\omega_d$	Damped natural frequency
$\omega_{int}$	Intermittency frequency
$\omega_n$	Natural frequency
$\omega_0$	Instantaneous natural frequency
$\mathcal{F}$	Fourier transform
$\mathcal{H}$	Hilbert transform
$\mathcal{X}_n$	Space spanned by $\mathbf{x}$
$\nabla$	Gradient vector

# Chapter 1 INTRODUCTION

Protective packaging has a significant influence on modern society, particularly at an environmental and economical level. This chapter discusses the increasing impact of packaging on the environment, social and governmental pressures on the packaging industry, current packaging performance evaluation procedures and the importance of improving such procedures.

## 1.1. PACKAGING AND THE ENVIRONMENT

Distribution services are the basis on which national economies are built. They remain as one of the key components of modern industry as a whole. During the three decades leading to 2004, distribution services in Europe grew by an average of 12 percent each year (European Commission: White Paper 2004). This increase in distribution services not only brings evident benefits, but also inflicts burdens on society and the environment. In order to ensure sustainability, a modern economy must strive to limit its volume of transport. Limiting this volume will enable the financial, social and ecological burdens of distribution to be kept within acceptable bounds. To ensure that these bounds are maintained, improvements must be made in all areas of the distribution industry, including protective packaging waste.

Packaging, in some form, has been in existence for centuries, with growth in its usage being particularly rapid in the second half of the twentieth century (PCA 2005). Packaging is an essential part of most people's lives and is fundamental to the way commerce is organised. It has been estimated that the annual expenditure on packaging materials and machinery worldwide is in excess of \$AUD330 billion (PCA 2005). In Australia the value of packaging is estimated to be between \$AUS10-10.5 billion and approximately 30,000 people are directly employed in its production (PCA 2005). Even though packaging is often overlooked or disregarded by critics focusing only on environmental issues, without it materials handling would be inefficient and modern consumer marketing would be extremely difficult. By the time of its disposal protective packaging has provided a means of clean and safe delivery, increased handling ease and warehousing.

One of the most difficult issues that confronts packaging engineers and designers is that of optimisation; in other words, how much protective packaging is sufficient to reasonably expect its effectiveness for a particular distribution environment?

Insufficient or ineffective packaging is easily identified as it is manifested through the occurrence of damage to the consignment during transport and handling. Over-packaging, however, is more difficult to establish. Over-packaging can be defined as the excess of protective material with respect to the expected risks of damage. In general, much of the material that makes up packaging consists of protective cushioning which is included to guard products against mechanical damage. The hidden cost associated with over-packaging, in the European Union (E.U) alone, was valued at an estimated €130 billion per year in 1991 (Oestergaard, 1991). These hidden costs include those associated with disposal, increased traffic, pollution, and accelerated road deterioration as a result of over-packaging. Clearly, a reduction in over-packaging would lead to significant economical, environmental and social savings.

In the packaging industry there are ever increasing environmental concerns, particularly in relation to excessive waste. As a result of packaging's generally short functional life span, compared with the product it protects, packaging is often considered wasteful or excessive. Its durability and visibility in domestic waste, tends to strengthen the perception that there is just too much packaging. Its function is taken for granted and its contribution to our modern way of life is not appreciated or well understood. Consumers are now becoming increasingly concerned about the environmental credentials of packaging, which in turn forces action from the government and the packaging industry. Today, all sectors involved with packaging are contributing to programs which reduce the adverse environmental effects of packaging. Some retail chains and governments have banned environmentally unacceptable packaging such as those made from expanded polystyrene (EPS). Furthermore, governments around the world are beginning to place mandates on packaging recycling rates (PCA 2005).

To tackle the problem of excessive packaging waste, the directive 94/62/EC of the European Parliament on Packaging and Packaging Waste was introduced in December 1994. Directive 94/62/EC and its later equivalent, 2005/20/EC, say in part that, packaging must now be manufactured so that *“its volume and weight is limited to the minimum adequate amount to maintain the necessary level of safety, hygiene and acceptance of the packed product for the consumer.”*

In the past, much of the drive for packaging companies to engineer protective packaging has been based on immediate economic benefits during production since the final disposal responsibility was passed on to the consumer. However, within Europe, particularly Germany, the disposal responsibility has been legislated back to the manufacturer in order to motivate companies to reduce packaging waste (Eichstadt *et al.* 1999).

The European directives stem directly from the pressures of waste disposal. Australia, as a large, sparsely populated continent, is not yet under such immediate visible pressures. However, a growing awareness of the Australian population's impact, particularly its waste products on the environment, has initiated responsible packaging practices.

In 1999 the Australian National Packaging Covenant (NPC), a voluntary, co-regulatory agreement between the government and the packaging industry, was introduced to provide packaging companies with practical guidelines to evaluate the impact of new and existing packaging. Under the updated 2005 NPC, it was proposed to increase the recycling rate of packaging waste from 48% in 2003 to 65% by 2010 (NPCC 2007). The current (2009) overall recycling rate is approximately 57% (NPCC 2010).

One method which may be used to increase the recycling rate is to utilise "green" packaging materials, such as paperboard which has a target recycling rate of approximately 70-80% (NPCC 2010).

Overall, it is evident that the costs associated with excess packaging are substantial and are of particular concern to modern society. Therefore, there is a strong case for continued research aimed at developing better techniques to optimise the design of protective packaging systems, which will in turn reduce the level of over-packaging. In order to achieve a beneficial level of packaging optimisation, a thorough understanding of the continuous progression of damage, as a result of environmental distribution loads, within the packages is required. This understanding is of particular importance when comparing the relative performance of materials (for example the performance of "green" materials compared with that of those which are environmentally unacceptable), performing accelerated tests (where the nature in which a system decays needs to be establish over a very short time interval) and when performing nonstationary (fluctuating root-mean square excitation) or shock on random tests (where the influence of the excitation on the condition of the system needs to be monitored at precise intervals).

## **1.2. EVALUATION OF PACKAGING PERFORMANCE**

During the distribution phase, shipments are often exposed to a variety of environmental hazards which, if excessively severe, may cause damage to or even destroy products. Among those hazards, mechanical shocks are potentially the most damaging and being so are commonly used as the main parameter for designing protective packaging systems. Vibrations, however, also play a significant role. Road distribution vibrations are primarily caused by the interaction between wheeled vehicles and uneven pavement surfaces. As a result of the randomness of pavement irregularities distribution vibrations are also random in nature. These random vibrations, though not as severe in magnitude as shocks, are generally sustained and their cumulative effect can result in the damage of packaging and/or its contained product.

Most mechanical systems exhibit resonances when subjected to vibration inputs which often create considerable response amplitudes. It has been demonstrated that, at resonance, paperboard boxes and cushioning packs can exhibit vibration transmissibilities in excess of 6 and 10, respectively (Godshall 1971; Zell 1969). Premature collapse of paperboard boxes due to excessive vibrations has also been observed (Gordon 1980).

Stresses below the strength limit of materials such as hard plastics and glass have negligible effect on their ability to withstand further stress. However, the ability of ductile materials, which are often used for packaging, to withstand stresses is gradually lost with the repetitive application of stress, even at relatively low amplitudes (Kipp 2000). These occurrences highlight the importance of understanding the effect of distribution vibrations on packages and packaged goods.

Various laboratory validation methods have been designed to emulate the random vibrations that occur naturally during transport. The most widely used methods to evaluate the performance of packaging elements during distribution are given under the American Society of Testing and Materials (ASTM) standard ASTM-D 4169. Under ASTM-D 4169 the following testing procedure is used to evaluate the performance of packaging elements (ASTM 2009, pp. 1-14):

- **Define shipping unit in terms of size, weight and form of construction**
- **Establish assurance level:** This should be one of three predetermined levels based on product value, anticipated damage and the tolerated level of damage.
- **Determine acceptance criteria:** In general cases the criteria used are 1) no damage to the product 2) package remains intact and 3) both condition 1) and 2). These criteria are to be evaluated following the test based on the structural integrity, functionality of the enclosed item and the evaluation of shock magnitude during testing. The evaluation of structural integrity is based solely on visual inspection and may be judged using a simple pass-fail or through quantitative scoring analysis (ASTM 2009, p.4).
- **Select a distribution cycle:** This is based on climate, handling conditions, transportation procedures and storage.
- **Write a test plan:** The test plan is to follow a predetermined sequence outlined in Table 1 of the ASTM-D 4169 standard (ASTM 2009, pp. 4-5). This may include (ASTM 2009, pp. 1-14):
  - Climate conditioning (subject to ASTM-D 4332)
  - Impact and tip/tip-over testing to simulate handling conditions
  - Vibration simulation (subject to ASTM-D 4728 or ASTM-D 999) to simulate transportation
  - Variable static (subject to ASTM-D 642) to simulate warehouse/transportation stacking
- **Perform test and report results**

An alternative to the ASTM testing procedure is given under the International Safe Transit Association (ISTA) standards 3A – 4AB (ISTA 2008). Each of these standards follows a similar testing procedure to that given by the ASTM with the cycle consisting of climate conditioning, impact/tip testing, vibration simulation and static loading. The acceptance criteria given by the ISTA is also similar to that given by the ASTM in that it is evaluated using visual inspection at the completion of each test.

Overall, it is apparent that the current methods for comparing the performance of protective packaging elements are limited to static, impact and vibration tests whereby visual inspection, at the completion of testing, alone is used to evaluate damage. This provides a very limited means for optimisation, which requires the condition of the packaging to be continually monitored and quantified during distribution testing.

For all protective packaging designs there must exist an environmental and economic optimum, as in *Figure 1-1*. Research towards the development of tools that enable the progression of damage (as a result of laboratory simulated environmental loads) to be monitored will allow for the comparative performance of packaging materials and configurations to be accurately established. This in turn will aid packaging engineers in finding the optimum design.

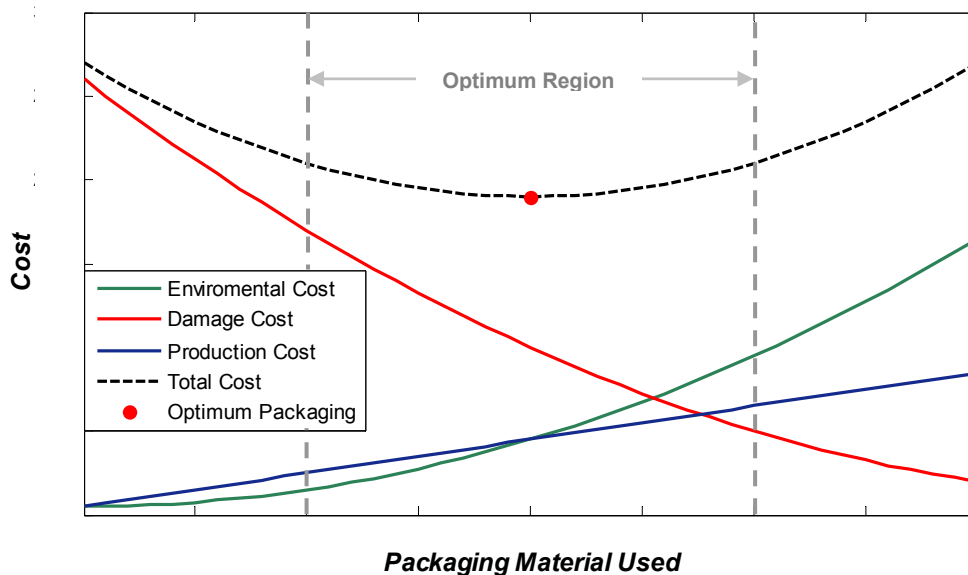


*Figure 1-1: Illustration of packaging optimisation*

### **1.3. SCOPE OF RESEARCH**

The purpose of this study is to develop a fundamental approach of rapidly detecting small changes in the natural frequency of systems subjected to sustained random loads during laboratory tests. Such a technique will provide a means for establishing the fatigue characteristics of materials and structures, thereby aiding the development of optimised protective packaging elements. It is acknowledged that the relationship between modal parameter variations and actual damage in complex materials and systems may not be completely clear, as it may well be influenced by the type and location of damage. However, the research presented in this thesis is the first stage of a broader research effort and the discussions will be limited single degree-of-freedom (SDoF) vibratory systems. This does not represent a significant limitation to the research, as it is common practice to perform laboratory tests on packaging elements using an SDoF configuration (refer to section 4.2 of this thesis).

Chapter 2 provides a brief review of various signal processing techniques which can be used to monitor the condition of structures.

The hypothesis of the research is presented in Chapter 3.

Chapter 4 provides information on the methodology to be applied.

Reviews of the techniques under analysis, as well as, preliminary results (obtained using a numerical evaluation) which aid the implementation of the techniques, are provided in Chapters 5 and 6.

A comparative evaluation of the techniques, using numerically simulated data, is given in Chapter 7.

The results obtained from physical experiments are given in Chapter 8.

Chapter 9 concludes the thesis by providing a summary of the results.

## REFERENCES

American Society of Testing and Materials (ASTM) 2009, 'Standard practice for performance testing of shipping containers and systems: D4169-08', *ASTM Standards on disk: Standards worldwide*, vol. 15.10, ASTM, West Conshohocken

Eichstadt, T, Carius, A & Andreas Kraemer, R 1999, 'Producer responsibility within policy networks: the case of German packaging policy', *Journal of environmental policy & planning*, vol. 1, no. 2, Routledge, pp. 133 - 153

European Commission 2004, 'European transport policy', *White paper 2004*

Godshall, W 1971, *Frequency response, damping and transmissibility characteristics of top loaded corrugated cases*, USDA Fed. Res. Paper FPL 160

Gordon, G 1980, 'Developing better vibration tests for packages', *Journal of the Society of Environmental Engineers*, December 1980

International Safe Transit Association (ISTA) 2008, 'Testing procedures', viewed 23 June 2010, < <http://www.ista.org/pages/procedures/ista-procedures.php>>

Kipp, W 2000, 'Developments in testing products for distribution', *International journal of packaging technology and science*, vol. 13, pp. 89-98

National Packaging Covenant Council (NPCC) 2007, *The National Packaging Covenant: 2005-2006 annual report*, Parsons Brinkerhoff, Brisbane

National Packaging Covenant Council (NPCC) 2010, *The National Packaging Covenant: 2005-2006 annual report*, Parsons Brinkerhoff, Brisbane

Oestergaard, S 1991, 'Packaging goals in transport quality', *Proceedings of the 7th IAPRI world conference on packaging*, Utrecht

Packaging Council of Australia (PCA) 2005, *Australian packaging issues and trends*, viewed 7 July 2008, < <http://www.pca.org.au/uploads/00499.pdf>>

Zell, G 1969, 'Vibration testing of resilient packaging cushioning material', Report PA-T-3610, Piccatinny Arsenal, Dover

## Chapter 2 PRELIMINARY LITERATURE REVIEW

The previous chapter discussed the limitations of current procedures for evaluating the performance of protective packaging systems subjected to random loads, particularly with respect to their inability to accurately quantify the level of damage within the system. As discussed, the optimisation of protective packaging requires a quantitative measure of the level of damage within the system as a function of time. The most common approach to evaluating damage within a single degree-of-freedom (SDoF) system is to measure changes in its modal parameters, mainly its natural frequency. Comprehensive reviews of the state-of-the-art in the field have been presented by Norwood (1990) and Doebling *et al.* (1996). Most of the published damage detection techniques only identify relative changes in system properties without addressing the progression of damage. The purpose of this study is to develop a fundamental approach of rapidly detecting small changes in the natural frequency of systems subjected to random loads. Various nonstationary signal processing methods can be applied for continuous structural integrity assessment. However, despite various claims of effectiveness and accuracy, most have significant limitations. A review of the most commonly applied techniques is given in sections (2.1-2.5).

### 2.1. THE FOURIER TRANSFORM

The Fourier transform is a technique for converting periodic data from the time domain to the frequency domain by separating a number of sinusoids (Donnelly 2006).

One limitation of the Fourier transform is that it requires the data under analysis to be stationary (Huang *et al.* 1998; Newland 1993, p. 295). In order to circumvent this stationary requirement, the short-time Fourier transform (STFT) was developed by Gabor (1946). The STFT works by computing the Fourier transform of data in shorter sub-records (Bendat & Piersol 2000, p. 504). Results from the STFT are generally displayed using a three-dimension spectrogram, which contains both temporal and spectral information (Bendat & Piersol 2000, p. 505). A significant limitation of the STFT is that a compromise needs to be made between the spectral and temporal resolutions (Newland 1993 p. 218; Bendat & Piersol 2000, p. 505). This limitation conforms to Heisenberg's uncertainty principle, as applied to signal analysis, which states the product of the temporal and spectral resolutions is always at least a minimum constant (Burke-Hubbard 1998, pp. 203-208).

### **2.1.1. Fourier Analysis for Continuous Integrity Assessment**

A study of the effect of earthquake excitation on civil structures was undertaken by Udawadia & Trifunac (1974). The study was based on the use of the STFT (referred to as moving window Fourier analysis by Udawadia & Trifunac) to monitor variations in the natural frequency of the structures during excitation. The study showed that as a result of earthquakes the stiffness of civil structures can reduce by 70%. Udawadia & Trifunac were also able to suggest that shifts in structural characteristics during excitation are significantly larger than those found through post-earthquake analysis and that they are strongly time dependent.

Trifunac *et al.* (2001) studied the variations in the natural frequency of civil structures subjected to earthquake excitation. Analysis of the structures was achieved using two methods 1) the STFT and 2) by measuring the time between zero-crossings in band-pass filtered response data. The results obtained by this analysis were used to demonstrate a reduction in natural frequency as a function of time, during excitation, and an apparent “self-healing” (increase of instantaneous natural frequency towards its original state) after the excitation ceased. The authors attributed this variation to loosening of foundation soil during excitation.

A technique for detecting faults in brushless direct current motors (BLDC) subjected to varying levels of nonstationarity was developed by Rajagopalan *et al.* (2005). The technique determines the existence of “instantaneous” fault frequencies using the local maxima in a filtered spectrogram obtained using STFT. Filtering of the spectrogram is carried out to remove the fundamental frequency amplitudes and any frequency amplitudes above the second harmonic. This approach is used in an attempt to improve the sensitivity of the method and is based on the fact that the fundamental frequency amplitudes are much higher than the fault frequency amplitudes. After obtaining the filtered spectrum the root-mean-squared (RMS) of its local maxima are used to create a fault matrix, which is in turn used to indicate a developing rotor fault. The results obtained by the application of the technique suggest that it can identify the presence of both fault types.

Garcia-Romeu-Martinez *et al.* (2007) implemented a modal parameter extraction technique which used a least-means-squares fit of the magnitude of the system’s FRF in the region of resonance, in an attempt to monitor damage in paperboard containers. The authors subjected a sample container to various preloads to induce damage. Subsequent to each pre-load, the

FRF of the sample was obtained with the container sample subjected to random base excitation with a dead load applied. The dynamic stiffness and damping ratio, for each pre-compression level, was then computed using the least squares algorithm. The dynamic stiffness for each pre-compression level was compared with the static stiffness obtained from the tangent of the force-deflection curve. A strong correlation between the changes in static and dynamic stiffness of the system was found. After establishing this correlation Garcia-Romeu-Martinez *et al.* (2007), and later Rouillard *et al.* (2007), performed a series of experiments designed to evaluate the effectiveness of the modal parameter extraction method, in combination with a modified STFT, for monitoring the level of cumulative damage in corrugated containers continuously subjected to random dynamic compressive loads. The method was found to be sensitive to changes in the structural integrity of the paperboard containers. However, the technique lacks temporal resolution as a result of spectral averaging, which was deemed necessary to keep the statistical uncertainty in the frequency domain results small (Rouillard *et al.* 2007). This highlights the main shortcoming of the modified STFT technique, which is poor temporal resolution.

## **2.2. THE HILBERT-HUANG TRANSFORM**

The Hilbert-Huang transform (HHT), originally developed by Huang *et al.* 1998 (with modifications by Huang 2005 and Wu & Huang 2008), was developed as a nonstationary analysis technique which produces fine resolution in both the temporal and spectral domains. The HHT is performed in two stages: 1) empirical mode decomposition (EMD) and 2) extraction of temporal and spectral information. During stage 1, EMD, a series of siftings are performed to find the individual oscillation modes imbedded in the data; these oscillation modes are referred to as intrinsic mode functions (IMF). In the second stage of HHT the instantaneous frequencies and instantaneous amplitudes of each IMF are computed using the Hilbert Transform. The information calculated by the application of the Hilbert transform is generally displayed using the Hilbert spectrum, which contains the absolute values of instantaneous amplitude, at each frequency, as a function of time. An alternative to the Hilbert spectrum is the marginal spectrum. The marginal spectrum offers a measure of the total amplitude contribution from each frequency in a probabilistic sense (Huang *et al.* 1998, p.929).

### 2.1.2. The Hilbert-Huang Transform for Continuous Integrity Assessment

The HHT was used by Ratneshwar *et al.* (2004) to monitor damage within a finite element model of an aluminium plate. Damage within the plate was simulated by reducing the stiffness of 2 out of 144 elements within the FEM by 50%. The evaluation of damage was achieved by applying sine sweep excitation and tracking changes in the model's natural frequency using the Hilbert and marginal spectra. The results obtained using these spectra were compared to those obtained using the traditional spectrogram, obtained using STFT, and the Fourier spectrum, respectively. Both methods (the HHT and the Fourier transform) suggested similar changes in natural frequency. However, the authors suggest that the HHT better describes the variations in vibration magnitude, particularly when comparing the marginal and Fourier spectra.

Yang *et al.* 2004 suggested that the temporal location and extent of damage within a structure can be determined using the HHT by making use of a parameter referred to as the intermittency frequency  $\omega_{\text{int}}$  (Huang *et al.* 1998). In this study damage was applied to a numerical model of a four story building subjected to random base excitation. The HHT, along with  $\omega_{\text{int}}$  and the Fourier transform, was used to identify the damage time instant (instant when damage occurs). After determining the damage time instant the signal was broken into two components (before damage and after damage) and the HHT was used to determine the instantaneous damped natural frequencies. The instantaneous damped natural frequencies were then averaged to give the damped natural frequencies before and after damage. The random decrement technique (Ibrahim 1977) was also applied to the two signal components to extract the system's damping ratio and undamped natural frequency. The results obtained were sufficiently accurate, however, the averaging and random decrement techniques applied do not allow for estimates to be obtained with fine temporal resolution. This creates practical limitations when using the technique for continuous condition assessment.

In 2005 Oliver & Kosmatka presented a preliminary study on defining a damage index using the HHT. The paper was mostly devoted to identifying single changes in system properties rather than continuous assessment. However, a section dedicated to the use of the HHT for the continuous monitoring of an eight degree-of-freedom (DoF) system with nonstationary stiffness characteristics was included. Based on the results obtained, the authors suggested

that the HHT is insufficiently sensitive and that the results obtained by its application are highly subjective.

## **2.3. THE WAVELET TRANSFORM**

The wavelet transform is a nonstationary signal analysis technique which is most commonly applied to image processing (Huang *et al.* 1998, p.908). However, the wavelet transform has also been used for the development of time-frequency distribution estimates. The wavelet transform works by breaking the original time signal into a number of levels, with each level consisting of a different number, scaling and spacing of an analysis wavelet (basis function used to describe the signal, equivalent to a sinusoid when using Fourier analysis). The position and distribution of the wavelets along the horizontal axis is set by the structure of the wavelet transform, meaning only the vertical size of each wavelet can be altered (Newland 1993, pp. 299-300). The level of detail produced by the wavelet transform is limited only by the analysis wavelet and the duration of the time signal, with longer signals resulting in more wavelet levels and hence finer detail. While the wavelet transform is still limited by Heisenberg's uncertainty principle, it provides potential benefits over the Fourier transform by automatically scaling components with respect to time and frequency (Burke-Hubbard 1998, p. 53).

### **2.1.3. The Wavelet Transform for Continuous Integrity Assessment**

Ghanem & Romeo 2000 developed a procedure for the identification of time-varying linear discrete models from noise contaminated data. The technique is based on representing the governing differential equations of motion, which describe the motion of single and two DoF mathematical excitation response systems, with respect to a wavelet base. The authors use a Galerkin approach (Glowinski *et al.* 1990), with a wavelet base, to discretise the differential equations. Subsets of the discretised equations, along with a least squares algorithm, are used to continuously extract the modal parameters (damping ratio and stiffness) of progressively damaged systems. The authors apply the technique to a numerical model with three theoretical, time dependent, modal parameter variation types; 1) quadratic 2) sinusoidal and 3) sudden step. The authors demonstrate that the technique can accurately describe the model when the level of extraneous noise is low and that the trend of the variations is followed for noise levels of up to 10%. However, it is also shown that the damping ratio estimates, for noise contaminated signals, can have errors as large as 30% of the RMS value. As well as the

large errors shown for the damping ratios, the technique is also limited to applications where an accurate dynamic model of the structure is known.

A study on detecting damage time instants within a single DoF system, using the level 1 results produced by the wavelet transform, was presented by Hou *et al.* (2000). The technique was tested using a numerical model consisting of a damper and three breakable springs which were designed to fail as a result of either excessive loading or fatigue. The authors demonstrated that the technique was capable of detecting the time instant of large levels of damage, with a spike appearing in the level 1 results when a spring failed. However, the method appears to be insufficiently sensitive, particularly with the presence of extraneous noise.

Alonso *et al.* 2004 continued the work of Hou *et al.* 2000 using orthogonal wavelet decomposition (OWD). In this study the authors focused on the effect of excitation frequency on the accuracy of damage detection. The authors demonstrate the presence of corrupt results as a consequence of pseudo-aliasing effects even when the sampling frequency is as much as ten times the maximum frequency within the signal. The authors attribute this pseudo-aliasing effect to inherent down-sampling and up-sampling processes of OWD and suggest that the sampling rate be increased in order to push the effect of aliasing into higher levels of the decomposition.

## **2.4. COMBINED AND COMPARATIVE STUDIES**

Shinde *et al.* (2004) proposed a method based on wavelet packet sifting and the Hilbert transform to extract the instantaneous frequencies of a time varying system, named wavelet packet sifting (WPS). The method uses wavelet decomposition, to break the signal into multiple levels with a zero mean, to which the Hilbert transform is applied to extract the instantaneous frequencies. Since the number of decomposition levels can be quite large sifting is limited to the significant components. An attempt to validate the technique was made by comparing the results obtained from the WPS results to those estimated using the HHT. Two numerical experiments were carried out using a three DoF spring mass system. During these experiments the stiffness of the second DoF was reduced by 10% and the time for the damage was varied from sudden (damaged over 0.05 seconds) to progressive (linearly increasing damage over 30 seconds). The physical experiments carried out consisted of a two story wooden frame subjected to damage through vibration excitation. The results from the numerical experiments were similar to those obtained using the HHT and were able to

identify the damage time instant and magnitude of the damage. However, the authors did not explore the sensitivity of the method with respect to extraneous noise or consistency of results.

Hou *et al.* (2006) used the WPS technique introduced by Shinde & Hou (2004) along with a confidence index, to verify the validity of results, to monitor the changes in mode shapes of a three DoF numerical model, subjected to random base excitation, as a result of damage. Two damage instances were studied, sudden and progressive. In each case damage was modelled by reducing the stiffness of the first DoF. The results obtained were able to identify the damage time instants for large amounts of damage. However, the results were only sensitive for the first vibration mode, even with a stiffness reduction of 20% and zero instrumentation noise. The authors also performed a sensitivity analysis on the technique with regards to the level of instrumentation noise and the level of damage. However, the results were limited and their interpretation subjective.

Hartin (2001) compares the use of both Fourier and wavelet analysis to extract the instantaneous frequencies and mode shapes of a linear and bilinear ten DoF numerical model. In this study Hartin proposes the use of a wavelet based FRF, which for the linear model is shown to be equivalent to the Fourier based FRF. Hartin does not apply the technique to a damage detection situation; however, the suggestion that the wavelet based FRF is equivalent to the Fourier based FRF may allow for the use of conventional Fourier based modal parameter extraction techniques while including the potential nonstationary analysis improvements offered by the wavelet transform.

Kim & Melham (2003) compared the use of the Fourier and wavelet transforms for monitoring the progression of damage within a simply supported prismatic concrete beam. Damage was induced to the beam to develop a crack after which sinusoidal fatigue loading was applied. The change in natural frequency of the beam was evaluated using the Fourier and wavelet transforms. The natural frequency estimates obtained using both techniques were similar; however, the authors suggested that the wavelet transform was more appropriate for identifying damage time instants.

Hera *et al.* (2004) presented a comparative study of the wavelet, WPS and HHT signal processing techniques in application to continuous structural integrity assessment. During the study the damage evolution within a numerical three DoF system, for two different damage cases (sudden and gradual degradation), was monitored. Sudden damage was modelled by

reducing the stiffness of the first DoF by 40% at an arbitrary point in time. Gradual degradation was modelled by reducing the stiffness of the first DoF linearly, as a function of time, up to 40% cumulative damage. The authors concluded that each method is effective in accurately extracting the variations in modal parameters. However, it was suggested that the wavelet transform method results in poor time localisation of damage. The authors performed preliminary experiments focused on the effect of noise contaminated data and suggested that the wavelet transform method was the least sensitive to noise and that band-pass filtering is required during the EMD process if HHT is to be applied.

## **2.5. ADAPTIVE TECHNIQUES**

The limitations of common modal parameter extraction techniques, particularly those which rely on the use of the Fourier transform, have motivated research into adaptive techniques which can provide accurate estimates of structural integrity with fine temporal resolution. A particular interest in adaptive techniques which make use of digital filters is evident in recent literature.

A brief review of recent work using adaptive techniques to monitor the integrity of various systems is given in the following sections.

### **2.1.4. Adaptive Techniques for Continuous Integrity Assessment**

Cooper & Worden (2000) developed a recursive parameter extraction technique which directly extracts physical properties, such as mass and stiffness, rather than relying on modal parameters. The recursive least-squares (RLS), double least-squares (DLS) and instrumental variables (IV) techniques, with constant forgetting factors, were compared. Similar results were obtained using each algorithm; however, those obtained using the IV technique had a higher variance.

In order to avoid the trade-off between rate of response to change and sensitivity to extraneous noise, which is associated with a constant forgetting factor, an algorithm which allows for a variable forgetting factor was introduced. The technique was capable of selecting appropriate forgetting factors and the changes in system properties extracted, from both physical and numerical experiments, matched those described by Cooper & Worden (2000). It is difficult to assess the actual sensitivity of the technique (significant variability is evident); however, it appears to provide reasonable estimates over a wide range of situations.

An adaptive structural identification algorithm which uses the RLS Kalman filter technique, along with a variable forgetting factor, was developed by Lin & Betti (2004). Lin & Betti (2004) used the technique to analyse several polynomial type nonlinear numerical models including the Bouc-Wen hysteretic model. In order to test the technique's ability to monitor progressive damage, a simulated reduction in damping was included in each of the models analysed. The technique was shown to provide significant improvements over the traditional Kalman algorithm, which uses a constant forgetting factor, and for cases with no extraneous noise it appeared to track the variations described by the authors (the authors did not plot the actual decay against the extracted results). However, for cases including extraneous noise the technique suffered significant errors. These errors were attributed to the integration of extraneous noise when calculating the required velocity and displacement vectors from the measured (simulated) acceleration signals.

A technique which uses RLS filtering to monitor variations in the stiffness matrix of a multiple DoF numerical model was developed by Chase (*et al.* 2005a). The technique was used to analyse two multistorey frame structures, one four DoF and the other twelve DoF, subjected to various damage patterns. The results produced indicated that the technique has the ability to extract the correct stiffness trends, in terms of detecting damage time instants and the order of stiffness reduction. The technique also has the potential for implementation in real time as a result of its fast convergence rate. However, the authors did not analyse the technique in terms of sensitivity to stiffness variations (the stiffness changes monitored were large). As well as the lack of sensitivity analysis, the technique requires measurements of acceleration, velocity and displacement vectors, which significantly limits its practical applicability (generally, only acceleration is recorded).

Chase (*et al.* 2005b) developed an adaptive least-mean-squares (LMS) filtering technique, very similar to the RLS technique of Chase (*et al.* 2005a), which identifies changes in a simple baseline model. The authors applied the technique to a physical rocking structure to track its changes in stiffness as a result of damage induced by earthquake excitation. Since the experiments undertaken to validate the technique were physical, and were thereby unable to be repeated, the sensitivity of the method was not thoroughly evaluated. One notable advantage of the technique over the RLS technique of Chase (*et al.* 2005a), is that it does not require the measurement of velocity and displacement. The velocity and displacement vectors are determined by integrating the acceleration records. The vectors are also corrected by removing the offset and drift resulting from the integration of extraneous noise. It is expected

that this approach could be successfully applied to the techniques described by Chase (*et al.* 2005a) and Lin & Betti (2004).

An adaptive structural parameter tracking technique based on the extended Kalman filter approach (Hoshiya & Saito 1984) and constrained optimisation procedures was proposed by Yang (*et al.* 2006). Yang (*et al.* 2006) demonstrated the applicability of the proposed technique to continuous structural integrity assessment by using it to analyse a series of numerical linear and nonlinear structures with abrupt changes in structural parameters (mainly stiffness). The stiffness trends extracted using the technique were shown to closely match the actual damage patterns for up to 5% extraneous noise. However, the stiffness reductions were large (~20%) and the true sensitivity of the technique was not analysed.

An attempt to develop a robust structural health monitoring technique, aimed specifically at structures containing nonlinearities, was made by Ghanem & Ferro (2006). The technique uses the ensemble Kalman filter (Evensen 1994) to track variations in the unknown parameters of a nonparametric, nonlinear, model as a result of damage. The technique was applied to a damped (5%) numerical model of a four DoF multistorey structure with a degrading hysteretic element. Excitation was achieved using both sinusoidal and random excitation (recorded from an earthquake) and the simulated damage event was modelled as an instantaneous change. The technique was able to detect the damage time instant, and subjectively, the space location of damage. The technique was also shown to be superior to the extended Kalman filter technique in terms of robustness. However, the level of damage analysed was very large and not quantified, thereby not allowing the true sensitivity of the technique to be revealed. As well as the lack of sensitivity analysis, the technique requires measurements of acceleration, velocity and displacement. This limitation may be overcome by implementing the integration technique described by Chase (*et al.* 2005a).

Various other adaptive approaches have been modified to suit continuous condition assessment. These approaches include the adaptive least squares estimation, sequential nonlinear least squares, and quadratic sum-squares error techniques. Huang (*et al.* 2008) provides a review of each of these techniques, including appropriate references, and compares their performance as continuous structural integrity assessment tools. Huang (*et al.* 2008) found the sequential nonlinear least squares and the quadratic sum-squares error techniques to be the most suitable for online structural integrity assessment, in terms of accuracy, convergence and efficiency. The authors also suggest that common adaptive least

squares estimation techniques are significantly limited, in a practical sense, since they require displacement, velocity and acceleration measurements.

An extensive discussion on various adaptive techniques is also given by Yang (*et al.* 2006).

The aforementioned adaptive techniques have not made use of traditional modal parameter extraction procedures. However, the tools required to develop an adaptive technique, which uses modal properties to determine variations in structural integrity, do exist. Such a technique would use an adaptive finite-impulse-response (FIR) filter to continually extract the instantaneous (for each new sample point) impulse response function of the system. The use of impulse response functions for modal parameter extraction is well established (Rao 2005, pp. 139-149; Jackson 1991, pp. 243-246). This type of approach has received very limited attention in the literature. However, Ploj Virtic *et al.* (2006) used an adaptive FIR filter, which used a least squares algorithm for adaptation, in conjunction with the Fourier transform to establish the remaining service life of a numerically modelled gear. The technique developed by Ploj Virtic *et al.* (2006) relied on a *priori* knowledge of the response of an undamaged gear and a gear with a crack of critical length. Although the work by Ploj Virtic *et al.* did not directly extract modal properties from the impulse response functions obtained using the adaptive filter, and is significantly limited, it does suggest that least squares adaptive FIR filters may be suitable for continuous structural integrity assessment.

## **2.6. LITERATURE REVIEW SUMMARY**

Estimating the condition of structures using modal parameters is well established. Initial findings suggest that the most widely accepted approach to extracting modal parameters from structures is to apply techniques which use the Fourier transform. However, continuous integrity assessment techniques which rely on the Fourier transform are significantly limited, as a result of the compromise required between the temporal and spectral resolutions. The potential for wavelet transform based techniques is also limited as it also conforms to Heisenberg's uncertainty principle. Literature has suggested that a HHT based approach may be better suited; however, the sensitivity of the technique is questionable.

Adaptive digital filters provide an alternative to monitoring systems in the frequency domain and have been shown to be capable of providing reasonable estimates of damage with fine temporal resolution.

In most cases adaptive filter based techniques do not directly extract modal parameters from the system under analysis. However, tools which can be used to extract modal parameters using digital filtering techniques do exist.

## REFERENCES

Alonso, R, Noori, M, Saadat, S, Masuda, A & Hou, Z 2004, 'Effects of excitation frequency on detection accuracy of orthogonal wavelet decomposition for structural health monitoring', *Earthquake engineering and engineering vibration*, vol. 3, n 1, Institute of Engineering Mechanics, pp. 101-106

Bendat, J & Priesol, A 2000, *Random data: Analysis and measurement procedures*, 3<sup>rd</sup> Edition, John Wiley & Sons, New York

Burke-Hubbard, B 1998, *The world according to wavelets*, A. K. Peters, Natick

Chase, G, Begoc, V & Barroso, L 2005a, 'Efficient structural health monitoring for a bench mark structure using adaptive RLS filters', *Computers and structures*, vol. 83, no. 8-9, Elsevier, pp. 639-647

Chase, G, Spieth, H, Blome, F & Mander, J 2005b, 'LMS-based structural health monitoring of a non-linear structure', *Earthquake engineering and structural dynamics*, vol. 34, no. 8, John Wiley and Sons, pp. 909-930

Cooley, J. W. & J. W. Tukey 1965, 'An algorithm for the machine computation of the complex Fourier series', *Mathematics of Computation*, vol. 19, pp. 297-301.

Cooper, J & Warden, K 2000, 'On-line physical parameter estimation with adaptive forgetting factors', *Mechanical systems and signal processing*, vol. 14, no. 5, Academic Press, London

Doebbling, S, Farrar, C, Prime, M, & Shevitz, D 1996, *Damage identification and health monitoring of structural mechanical systems from changes in their vibration characteristics: A literature review*, Los Alamos National Laboratory, Los Alamos

Donnelly, D 2006, 'The fast Fourier and Hilbert-Huang transforms: A comparison', *Proceedings of the IMACS multiconference on computational engineering in systems applications*, Beijing, pp. 84-88

Evensen, G 1994, 'Sequential data assimilation with nonlinear quasi- geostrophic model using Monte Carlo methods to forecast error statistics', *Journal of geophysical research*, vol. 99, pp. 10143-10162

Gabor, D 1946, 'Theory of communication', *Journal of the Institution of Electrical Engineers 1889-1948*, Part 3, vol. 93, London, pp.429-457

Garcia-Romeu-Martinez, M.A, Rouillard, V, Sek, M & V.A Cloquell-Ballester 2007, 'Monitoring the evolution of fatigue in corrugated paperboard under random loads', *Proceedings of the 5<sup>th</sup> BSSM international conference on advances in experimental mechanics*

Ghanem, R & Romeo, F 2000, 'A wavelet based approach for the identification of linear time-varying dynamic systems', *Journal of sound and vibration*, vol. 234, no. 4, Academic Press, pp. 555-576

Ghanem, R & Ferro, G 2006, 'Health monitoring for strongly non-linear systems using the ensemble Kalman filter', *Structural control and health monitoring*, vol. 13, no. 1, John Wiley and Sons, pp. 245-259

Glowinski, R, Lawton, W, Ravachol, M & Tenenbaum, E 1990, *Computing methods in applied science and engineering*, pp. 5-120

Hartin, J 2001, 'Application of a wavelet based FRF to the analysis of a bilinear structure', *Proceedings of the international modal analysis conference*, vol. 2, Society of experimental mechanics, pp. 1414-1419

Hera, A, Shinde, A & Hou, Z 2004, 'A comparative study of the empirical mode decomposition and wavelet analysis on their application for structural health monitoring', *American Society of Mechanical Engineers, design engineering division (publication) DE*, vol. 117, American Society of Mechanical Engineers, New York, pp. 449-458

Hoshiya, M & Saito, E 1984, 'Structural identification by extended Kalman filter', *Journal of engineering mechanics*, vol. 110, no. 12, pp.1757-1771

- Hou, Z, Noori, M & St. Amand, R 2000, 'Wavelet based approach for structural damage detection', *Journal of engineering mechanics*, vol. 126, no. 7, American Society of Civil Engineers, pp.677-683
- Hou, Z, Hera, A & Shinde, A 2006, 'Wavelet based structural health monitoring of earthquake excited structures', *Computer-aided civil and infrastructure engineering*, vol. 27, Blackwell Publishing, pp. 268-279
- Huang, N, Shen, Z, Long, S, Wu, M, Shih, H, Zheng, Q, Yen, N, Tung, C & Liu, H 1998, 'The empirical mode decomposition and the Hilbert spectrum for non-linear and non-stationary time series analysis', *Proceedings of the Royal Society*, The Royal Society, London, pp. 903-995
- Huang, N 2005, 'Introduction to the Hilbert-Huang transform and its related mathematics problems', *Hilbert-Huang transform and its applications*, World Scientific, Singapore
- Huang, H, Yang, J & Zhou, L 2008, 'Comparison of various structural damage tracking techniques based on experimental data', *Proceedings of SPIE – International society for optical engineering*, vol. 6932, SPIE, pp. 693225-693235
- Ibrahim, R 1977, 'Random decrement technique for modal identification of structures', *Journal of spacecrafts and rockets*, vol. 4, no. 11, pp. 696-700
- Jackson, L 1991, *Signals, systems and transforms*, Addison-Wesley Publishing Company
- Kay, S 1988, 'Spectral estimation', in J Lim & A Oppenheim (eds), *Advanced Topics in Signal Processing*, Prentice Hall, Englewood Cliffs
- Kim, H & Melhem 2003, 'Fourier and wavelet analyses for fatigue assessment of concrete beams', *Experimental mechanics*, vol. 43, no. 2, Society for Experimental Mechanics
- Lin, J-W & Betti, R 2004, 'On-line identification and damage detection in non-linear structural systems using a variable forgetting factor', *Earthquake engineering and structural dynamics*, vol. 33, no. 4, John Wiley and Sons, pp. 419-444
- National Packaging Covenant Council (NPCC) 2007, *The National Packaging Covenant: 2005-2006 Annual*, Parsons Brinkerhoff, Brisbane

Newland 1993, *An introduction to random vibrations, spectral and wavelet analysis*, 3<sup>rd</sup> Edition, Longman Scientific & Technical

Norwood, C 1990, 'The use of vibration techniques in non-destructive testing', *Proceedings of the vibration and noise conference, 1990*, no. 90, The Institute of Engineers Australia, Barton, pp. 270-275

Oliver, J & Kosmatka, J 2005, 'Evaluation of the Hilbert-Huang transform for modal-based structural health monitoring applications', *Proceedings of SPIE – The International Society for Optical Engineering*, vol. 5767, SPIE, pp. 274-285

Ploj Virtic, M, Abersek, B, Cudina, M & Belsak, A 2006, 'Development of mathematical model for detection of cracks in tooth root using an adaptive algorithm', *Key engineering materials*, vols. 324-325, Trans Tech Publications, Stafa-Zuerich, pp. 793-798

Rajagopalan, S, Habbetler, T, Harley, R, Alerr, J & Restrepo, J 2005, 'Diagnosis of rotor faults in brushless DC (BLDC) motors operating under non-stationary conditions using windowed Fourier ridges', *Conference record of the 2005 IEEE industry applications conference*, vol. 1, Institute of Electrical and Electronics Engineers, Hong Kong, pp. 26-33

Rao, S 2005, *Mechanical Vibrations*, SI Edition, Prentice Hall

Ratneshwar, J, Feng, Y & Goodarz, A 2004, 'Energy-frequency-time analysis of structural vibrations using Hilbert-Huang transform', *Collection of technical papers – AIAA/ASME/ACSE/AHS/ASC structures, structural dynamics and materials conference*, vol. 6, American Institute of Aeronautics and Astronautics, Reston, pp. 4897-4096

Rouillard, V, Lamb, M & Sek, M 2007, 'Determining fatigue progression in corrugated paperboard containers subjected to dynamic compression', *Proceedings of the 5<sup>th</sup> Australasian Congress on Applied Mechanics, ACAM 2007*, vol. 1, Engineers Australia, Brisbane, pp. 331-336

Ruzzene, M, Fasana, A, Garibaldi, L & Piombo, B 1997, 'Natural frequencies and damping identification using wavelet transform: Application to real data', *Mechanical systems and signal processing*, vol. 11, no. 2, Academic Press, pp. 207-218

Shinde, A & Hou, Z 2004, 'A wavelet based sifting process and its application for structural health monitoring', *Proceedings of the 2004 American control conference*, vol. 5, Institute of Electrical and Electronics Engineers, pp. 4219-4224

Trifunac, M, Ivanovic, S & Todorovska, M 2001, 'Apparent periods of a building II: Time-frequency analysis', *Journal of structural engineering*, vol. 127, no. 5, American Society of Civil Engineers, pp. 527-537

Udwadia, F & Trifunac, M 1974, 'Time and amplitude dependent response of structures', *Earthquake engineering & structural dynamics*, vol. 2, no. 4

Wu, Z & Huang, N 2008, 'Ensemble empirical mode decomposition: A noise related analysis method', *Advances in adaptive data analysis*

Yang, J, Lei, S, Lin & Huang, N 2004, 'Hilbert-Huang based approach for structural damage detection', *Journal of engineering mechanics*, vol. 130, no. 1, pp. 85-95

Yang, J, Lin, S, Huang, H & Zhou, L 2006, 'An adaptive extended Kalman filter for structural damage identification', *Structural control and health monitoring*, vol. 13, no. 4, John Wiley and Sons, pp. 849-867

## Chapter 3 HYPOTHESIS

Various techniques which have been used in an attempt to monitor the integrity of structural elements have been discussed. It was made clear that the condition of structures can be quantitatively assessed using changes in their modal parameter, most commonly natural frequency, hence stiffness.

This study will test the hypothesis that established constant parameter modal estimation techniques, combined with suitable signal processing, can be used to continually monitor small changes in the structural integrity of protective packaging materials.

Two techniques for monitoring structural integrity will be considered. The first technique will evaluate a modified version of the short-time Fourier transform (STFT) to obtain a series of “instantaneous”, or short-time, frequency response functions (FRF). These FRFs will be used to obtain estimates of natural frequency and equivalent viscous damping of the system.

Methods for estimating FRFs using Fourier analysis are well established. However, without careful consideration and enhancement these techniques require a significant compromise between the accuracy of the estimates and the rate at which they can be obtained. This study will also test the hypothesis that spectral enhancement techniques, such as zero-padding and data overlapping can be used to limit the compromise between the spectral and temporal accuracies when using a Fourier based approach.

The second technique will test the hypothesis that an adaptive digital finite-impulse-response (FIR) filter can be used to continually extract accurate estimates the system’s instantaneous impulse response function, from which estimates of the system’s instantaneous natural frequency can be made.

## Chapter 4 METHODOLOGY

When assessing the performance of structural integrity assessment techniques it is important to ensure that they are operating at their full potential. This requires a comprehensive evaluation of the influence of the analysis parameters used. For this evaluation to provide meaningful results, any experiments undertaken must be carefully designed so as to avoid any uncontrollable external influences.

Once the correct parameters for analysis have been established the performance of the techniques can be compared. This comparison will include a variety of extraneous noise levels, material characteristics and damage scenarios.

Discussions in this chapter will include:

- The experimental design of numerically simulated and physical experiments
- Optimisation in terms of parameter selection
- Sensitivity analysis with respect to extraneous noise and temporal resolution

### 4.1. PERFORMANCE EVALUATION OF ANALYSIS TECHNIQUES

The research to be undertaken deals with stochastic processes. Therefore, the accurate quantification of outcomes requires an exhaustive statistical analysis of the assessment techniques with variations in damage patterns, system properties and level of extraneous noise. A complete statistical analysis will allow for the accuracy, reliability and sensitivity of the structural integrity assessment techniques to be accurately established. Such a statistical analysis requires a significant number of experiments to be undertaken and each of these experiments must be perfectly repeatable.

In some simplistic physical experiments it is possible to study the effectiveness of the structural integrity assessment techniques, in regards to modal parameter tracking, by directly altering physical properties such as mass, stiffness and damping. Physical experiments on real packaging elements, however, are more complex. Generally, variations in the modal parameters of real packaging systems are generated by allowing the system to deteriorate (structurally) under dynamic (random) compressive loads (ASTM 2009; Rouillard *et al.* 2007; Garcia-Romeu-Martinez *et al.* 2007). This type of procedure is not easily controllable

and more often than not is very time consuming, unreliable and requires subjective interpretation.

In many cases, physical systems can be modelled as a series of vibratory mechanical systems consisting of mass, spring and damper elements (Sek 2007). This means that reliable results can be produced by realistically mimicking physical experimental phenomena using numerical simulations, which take into account salient aspects of real processes, including extraneous noise and stochasticity. These numerical simulations enable full control of any variations in the system's modal properties, predominantly mass, stiffness and damping, as well as the presence of otherwise uncontrollable influences such as extraneous noise. The use of numerical simulations is advantageous as they also allow for the statistical analysis of results.

Extraneous noise is always present, at some degree of severity, when capturing experimental data from fatigue tests. Consequently, any analysis tool which monitors shifts in modal characteristics must compensate for its presence. This study will include a statistical analysis which is used to assess the influence of extraneous noise on both of the previously mentioned structural integrity assessment techniques. The experiments used for the statistical analysis will be carried-out using numerical simulations that include controllable levels of extraneous noise. Preliminary experiments, designed to enable the selection of appropriate analysis parameters for the structural integrity assessment techniques, will be performed using data containing 0% and 10% extraneous noise (root-mean-square of the excitation and response signal pair). The upper limit of extraneous noise (10%) was chosen as literature suggests that it is a reasonable estimate of the highest expected level of extraneous noise (Cooper & Warden 2000; Ghanem & Romeo 2000; Lin & Betti 2004; Hera *et al.* 2004). This upper limit will be used to establish the robustness of the parameter extraction techniques.

Every nonstationary structural integrity assessment technique has an inherent uncertainty when detecting a damage instant. This is particularly the case for Fourier transform based integrity assessment procedures which require a compromise between temporal sensitivity and the accuracy of the estimates obtained (spectral resolution is inversely proportional to temporal resolution). This study will include a statistical analysis of the uncertainties associated with detecting a damage instant when using the structural integrity assessment techniques. The results used for the statistical analysis will be obtained using numerically simulated data. The ability to reduce the level of temporal uncertainty when applying the Fourier transform based technique will also be established.

---

## 4.2. NUMERICAL MODEL

Under the testing standards ASTM-D 4169 schedules D and E (ASTM 2009, pp. 7-8) protective packages are subjected to synthesised vibration simulation. During vibration simulation packages are subjected to excitations  $x(t)$  using a vibrating base (shaker) along with appropriate loading  $m$  to simulate stacked transportation conditions, as depicted in *Figure 4-1(a)*. This arrangement is most simply modelled using a single degree-of-freedom (SDoF) system, in a moving base configuration, where the protective packaging element represents a spring and damper, with a stiffness  $k$  and damping coefficient  $c$ , as depicted in *Figure 4-1(b)*.

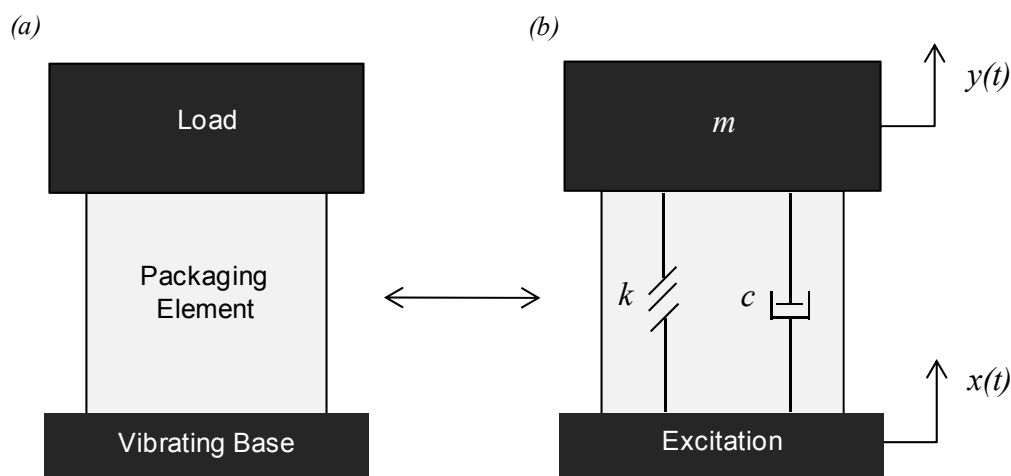


Figure 4-1 (a) Packaging testing arrangement (b) Equivalent SDoF model.

The free-body force diagram of the SDoF model is as follows:

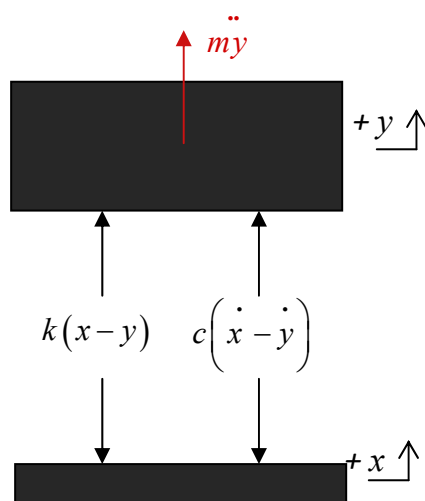


Figure 4-2: SDoF free-body force diagram.

By applying Newton's 2<sup>nd</sup> law of motion we can derive the following differential equation of motion:

$$m \ddot{y} = c(\dot{x} - \dot{y}) + k(x - y) \quad (4-1)$$

With the introduction of time variant parameters the equation of motion becomes:

$$m \ddot{y}(t) + c(t)\{\dot{y}(t) - \dot{x}(t)\} + k(t)\{y(t) - x(t)\} = 0 \quad (4-2)$$

In this study excitation for the described SDoF system will be synthesised using a band-limited spectral function (magnitude) coupled with a uniformly-distributed phase spectrum to form a complex spectrum. The inverse Fourier transform of the complex spectrum will be taken to produce a Gaussian random signal. This process will be undertaken repeatedly to produce a random signal of arbitrary duration and spectral content. The resulting signal will be later uploaded into a simulation tool developed using the Simulink® package in Matlab® which uses the Dormand-Prince method to incrementally solve Equation 4-2. A simplified schematic of the Simulink model is given in *Figure 4-3*.

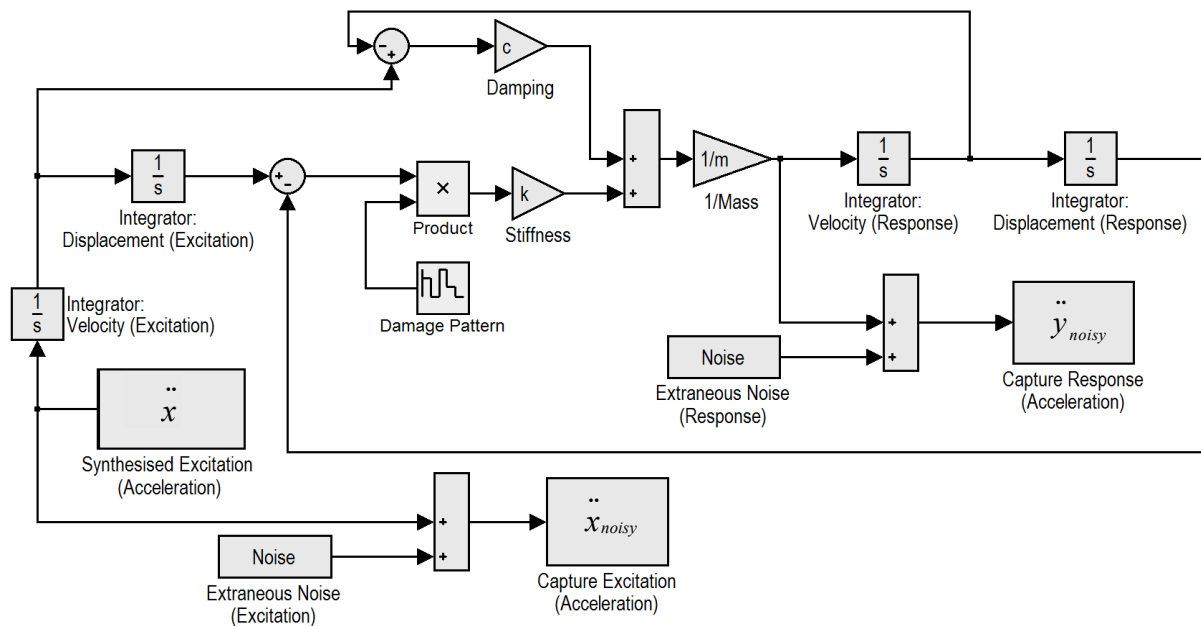


*Figure 4-3: Schematic of Simulink model for simulation of foundation displacement.*

The numerical software tool will be designed such that the mass, stiffness and damping of the SDoF system can be independently set. Extraneous noise will be added to both the excitation and response signals prior to post processing. Variations in the magnitude of extraneous noise, as well as specific modal parameters, will enable a working range for the parameter extraction techniques to be found.

### 4.3. PHYSICAL EXPERIMENTS

Selected physical experiments will be designed to validate the numerically simulated experiments, as well as the ability of the integrity assessment techniques to track changes in real materials. Each physical experiment will be performed using a moving base configuration in order to match the procedures used during packaging evaluation.

It is important to perform some controllable physical experiments which exhibit characteristics which closely reflect those of the numerical systems analysed.

Cooper & Warden (2000) made use of a cantilever beam arrangement in an attempt to validate results obtained from numerically simulated experiments using their recursive, physical parameter extraction technique. This arrangement is well suited since physical parameters, mainly applied load and stiffness, are easily controlled. A further advantage of this arrangement is the ability to adjust how closely the system matches an SDoF. For these reasons, a cantilever arrangement will be used for the preliminary physical experiments in this study (details of the cantilever arrangement are given in Chapter 8: Physical Experiments). During these experiments the cantilevers will be subjected to continuous random excitation and damage will be simulated by varying the length of the cantilever (hence changing its natural frequency).

As previously mentioned, the ability of the integrity assessment technique to track the changes in the modal characteristics of real systems is of the utmost importance. Therefore, experiments will be performed using real packaging elements such as containers and protective cushions. These experiments will be performed in two ways. The first approach will use controlled levels of induced damage (by subjecting packaging elements to various levels of pre-compression) at regular intervals during vibration testing, while the second will allow for the elements to deteriorate naturally under random compressive loads. The packaging elements selected for the physical experiments will exhibit nonlinear stiffness characteristics. This is to help establish the ability of the introduced structural integrity assessment technique to provide estimates of the condition of systems where nonlinear behaviour is present.

## REFERENCES

- American Society of Testing and Materials (ASTM) 2009, 'Standard practice for performance testing of shipping containers and systems: D4169-08', *ASTM Standards on disk: Standards worldwide*, vol. 15.10, ASTM, West Conshohocken
- Cooper, J & Warden, K 2000, 'On-line physical parameter estimation with adaptive forgetting factors', *Mechanical systems and signal processing*, vol. 14, no. 5, Academic Press, London
- Garcia-Romeu-Martinez, M.A, Rouillard, V, Sek, M & Cloquell-Ballester, V.A. 2007, 'Monitoring the evolution of fatigue in corrugated paperboard under random loads', *Proceedings of the 5<sup>th</sup> BSSM international conference on advances in experimental mechanics*
- Ghanem, R & Romeo, F 2000, 'A wavelet based approach for the identification of linear time-varying dynamic systems', *Journal of sound and vibration*, vol. 234, no. 4, Academic Press, pp. 555-576
- Hera, A, Shinde, A & Hou, Z 2004, 'A comparative study of the empirical mode decomposition and wavelet analysis on their application for structural health monitoring', *American Society of Mechanical Engineers, design engineering division (publication) DE*, vol. 117, American Society of Mechanical Engineers, New York, pp. 449-458
- Lin, J-W & Betti, R 2004, 'On-line identification and damage detection in non-linear structural systems using a variable forgetting factor', *Earthquake engineering and structural dynamics*, vol. 33, no. 4, John Wiley and Sons, pp. 419-444
- Newland 1993, *An introduction to random vibrations, spectral and wavelet analysis*, 3<sup>rd</sup> Edition, Longman Scientific & Technical
- Rouillard, V, Lamb, M & Sek, M 2007, 'Determining fatigue progression in corrugated paperboard containers subjected to dynamic compression', *Proceedings of the 5<sup>th</sup> Australasian Congress on Applied Mechanics, ACAM 2007*, vol. 1, Engineers Australia, Brisbane, pp. 331-336
- Sek, M 2007, 'Numerical simulation of impacts involving a collapsible nonlinear multilayer structure', *Proceedings of the world conference of engineering*, London, pp. 1367-1372

## Chapter 5 FOURIER ANALYSIS

Many common structural integrity assessment techniques make use of Fourier analysis for modal parameter extraction, although the intermediate processes for each technique can vary significantly. For continual modal parameter extraction, the Fourier transform requires that a compromise be made between the accuracy of the estimates and how frequently they can be obtained. It is believed that the limitations brought forth by this compromise can be significantly reduced by selecting suitable values for the analysis parameters when implementing the techniques. Further improvements are also expected by making use of various spectral enhancement techniques. This chapter provides a review of Fourier analysis and methods of modal parameter extraction. Also included are detailed discussions on the influence of various analysis parameters and spectral enhancement techniques on short-time modal parameter extraction.

### 5.1. BACKGROUND

The possibility of a string vibrating in several of its harmonics at the same time was proven by Daniel Bernoulli in 1755 (Cannon & Dostrovsky 1981). Bernoulli developed his proof using the principle of the coexistence of small oscillations, which in modern terminology is referred to as the principle of superposition (Rao 2005, p.5). This principle made it possible to express any arbitrary function using an infinite series of sines and cosines. Initially, Bernoulli's work was not accepted by mathematicians D'Alembert and Euler. However, the validity of superposition was proved in 1822 (initially in 1807 and published in 1822) by Joseph Fourier who used the technique to solve the partial differential equation for the propagation of heat in solid bodies (University of St Andrews 1997). Prior to the findings made by Fourier there was no solution to the heat propagation equation for general conditions. However, particular solutions were known if the heat source behaved as a sinusoidal or co-sinusoidal wave. Fourier's work was based on the hypothesis that complicated heat sources could be modelled using the superposition of sinusoidal and co-sinusoidal waves, and that their effect could be modelled as the superposition of the resulting particular solutions. Although initially not well received by mathematicians such as Lagrange and Laplace, Fourier's work was eventually acknowledged and his superposition principle is now known as the Fourier series (University of St Andrews 1997).

Further development of Fourier's work has since provided an alternative to analysing signals in the time domain, namely frequency domain analysis.

Using the modern formality provided by Dirichlet & Riemann the Fourier series of an infinite periodic signal  $x(t)$ , of period  $T_p$  and fundamental frequency  $f_1$ , is represented as follows (Crandall 1958, p.9; Bendat & Piersol 2000, p. 5):

$$x(t) = \frac{a_o}{2} + \sum_{q=1}^{\infty} \left[ a_q \cos(2\pi q f_1 t) + b_q \sin(2\pi q f_1 t) \right], \quad (5-1)$$

where

$$a_q = \frac{2}{T_p} \int_0^{T_p} x(t) \cos(2\pi q f_1 t) \cdot dt \quad q = 0, 1, 2, \dots$$

$$b_q = \frac{2}{T_p} \int_0^{T_p} x(t) \sin(2\pi q f_1 t) \cdot dt \quad q = 1, 2, 3, \dots$$

If the duration of a finite record is equal to its period, and the record consists of  $N$  points, spaced  $\Delta t$  apart, the Fourier series at any time  $t$  over the interval  $(0, T_p)$  can be written as (Bendat & Piersol 2000, p. 402-403):

$$x(t) = A_o + \sum_{q=1}^{N/2} \left[ A_q \cos\left(\frac{2\pi q t}{T_p}\right) \right] + \sum_{q=1}^{(N/2)-1} \left[ B_q \sin\left(\frac{2\pi q t}{T_p}\right) \right] \quad (5-2)$$

Given that,

$$x_n = x(n\Delta t) \quad n = 1, 2, \dots, N$$

Equation 5-2, at points  $n$ , becomes:

$$x_n = A_o + \sum_{q=1}^{N/2} \left[ A_q \cos\left(\frac{2\pi q n}{N}\right) \right] + \sum_{q=1}^{(N/2)-1} \left[ B_q \sin\left(\frac{2\pi q n}{N}\right) \right], \quad (5-3)$$

where

$$A_0 = \frac{1}{N} \sum_{n=1}^N x_n = \bar{x}$$

$$A_q = \frac{2}{N} \sum_{n=1}^N x_n \cos\left(\frac{2\pi qn}{N}\right) \quad q = 1, 2, \dots, \frac{N}{2} - 1$$

$$A_{N/2} = \frac{1}{N} \sum_{n=1}^N x_n \cos(n\pi)$$

$$B_q = \frac{2}{N} \sum_{n=1}^N x_n \sin\left(\frac{2\pi qn}{N}\right) \quad q = 1, 2, \dots, \frac{N}{2} - 1$$

In engineering practice signals, acquired from physical experiments or numerical simulations, are generally discretised by  $N$  points sampled at time intervals of  $\Delta t$  (inverse of the sampling frequency  $f_s$ ) for a duration  $T$ . These signals are always finite and are generally not the same length as the period required by the Fourier series; in fact the signals may not be periodic at all. As a result, it is necessary to devise a method capable of extracting estimates of the frequency content within nondeterministic discrete time signals.

The Fourier transform converts signals from the time domain to the frequency domain by extracting a number of sinusoids and co-sinusoids. The first step towards understanding this extraction is to recognise the signal under analysis as a collection of rotating vectors in the form  $e^{j(2\pi ft + \phi)}$ , where  $f$  and  $\phi$ , respectively, represent the circular frequency and phase of one component of the signal. If such a signal is multiplied by  $e^{-j(2\pi ft)}$  its component corresponding to the frequency  $f$  will become stationary and will integrate to single finite value, whilst vectors at other frequencies will continue to rotate and will integrate to zero. Thus, it can be seen that the Fourier transform of a continuous signal  $x(t)$  is defined as (Crandall 1958, p.13-15; Bendat & Piersol 2000, p. 404):

$$X(f) = \int_{-\infty}^{\infty} x(t)e^{-j(2\pi ft)} \quad (5-4)$$

Equation 5-4 is impractical for signals sampled at discrete times  $n\Delta t$  ( $n=0,1,2..N-1$ ) and of finite duration. For this reason, the following variation known as the discrete Fourier transform is used (Bendat & Piersol 2000, p. 404; Randall 1987, pp. 26-28):

$$X(f_k) = \frac{1}{N} \sum_{n=0}^{N-1} x(n\Delta t) e^{-j\left(\frac{2\pi nk}{N}\right)} \quad k = 0, 1, 2, \dots, N-1 \quad (5-5)$$

With the application of Equation 5-5 the Fourier coefficients of the discrete time signal are spaced at equal intervals of  $\Delta f$ . This spacing is referred to as the spectral (or frequency) resolution and can be determined using the following (Bendat & Piersol 2000, p. 404):

$$\Delta f = \frac{1}{T} = \frac{1}{N\Delta t} = \frac{f_s}{N} \quad (5-6)$$

An algorithm known as the fast Fourier transform (FFT) has been developed to efficiently extract the coefficients of the DFT. The most well known, and most commonly applied, variation of the FFT was developed by Cooley & Tukey (1965). The Cooley-Tukey procedure is a special case of the general FFT algorithm that is applicable to calculations made using binary digital computers. For a detailed discussion of the FFT and the Cooley-Tukey algorithms refer to Cooley & Tukey (1965, pp. 297-301) and Bendat & Piersol (2000, pp.405-412).

By applying the Fourier transform, to extract the harmonics of a signal, it is possible to present the signal in a way that highlights its frequency content rather than its temporal content. If a third axis, which represents frequency, is introduced perpendicular to the time-amplitude plane each harmonic component can be displayed against its corresponding frequency. An example of the harmonic decomposition is given in *Figure 5-1*.

The harmonics shown in *Figure 5-1* can also be represented using a third axis which represents frequency as shown in *Figure 5-2*.

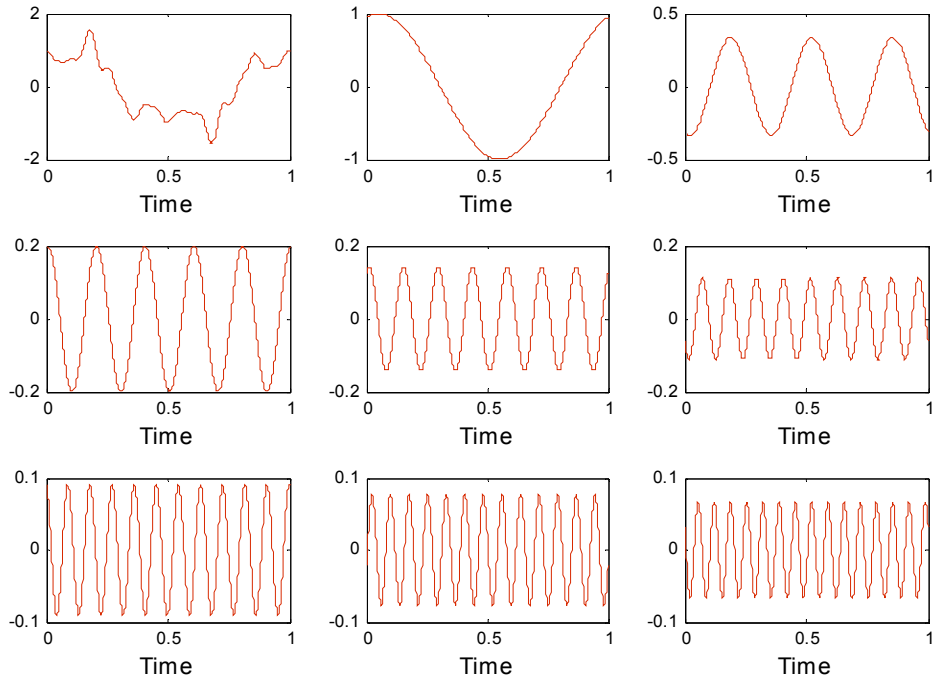


Figure 5-1: Random signal (top left) followed by its harmonic components.

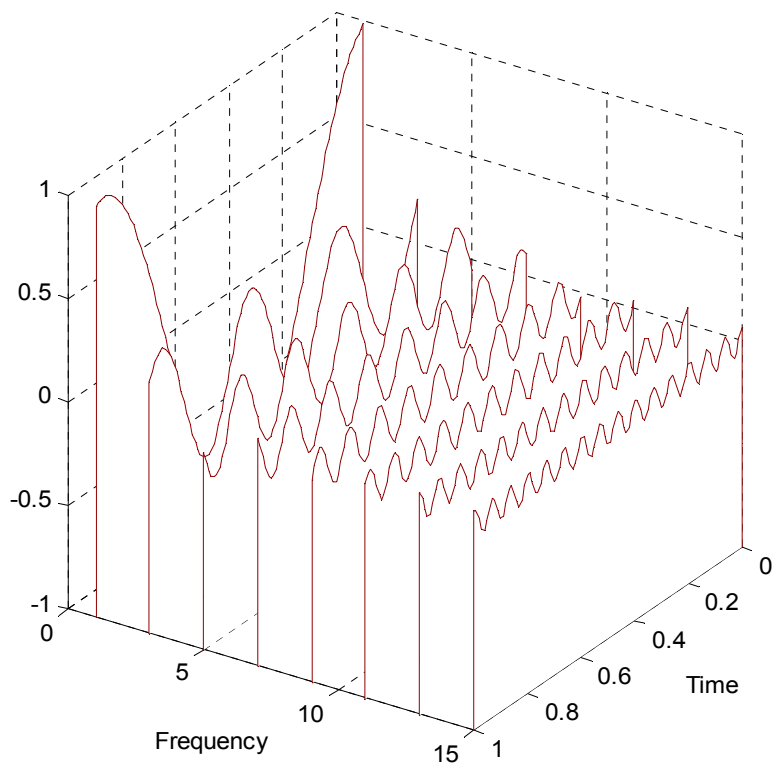
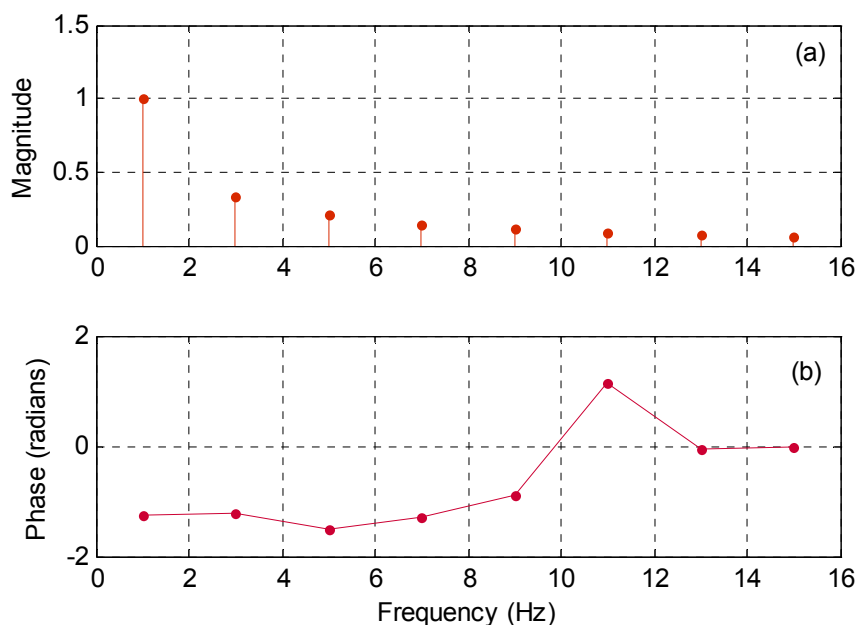


Figure 5-2: Time-Frequency-Amplitude representation of the harmonics of a random signal.

When *Figure 5-2* is rotated so that the time axis is perpendicular to the page the signal is represented in the frequency domain. This procedure provides what is often referred to as a magnitude spectrum. The magnitude spectrum only displays the magnitude of the harmonic components of the signal, as shown in *Figure 5-3* (a). The magnitude spectrum is a useful descriptor of random signals; however, both the magnitude and phase of the harmonic components are required to fully describe the signal. A phase spectrum, as in *Figure 5-3* (b), is obtained by converting the complex signal obtained using the Fourier transform to its polar form and displaying the extracted phase values against their corresponding frequency.



*Figure 5-3: (a) Magnitude spectrum, (b) Phase spectrum, for the time signal shown in Figure 5-1*

Data obtained using the Fourier transform is displayed using various techniques. One of the most common displays used in modal parameter extraction, thereby making it most relevant to continuous structural integrity assessment, is the frequency response function (FRF). FRFs are used to compare the excitation and response of an input-output system in the frequency domain. In general terms, this is achieved by calculating the ratio of the excitation and response frequency spectra (Randall 1987, p. 239). FRFs are described in further detail in section 5.2.

One limitation of the Fourier transform is that it is used to extract sinusoids which persist throughout the entire length of data (Huang *et al.* 1998, p. 907; Newland 1993, p. 295), which in turn requires the data being analysed to be stationary. However, applications such as continuous structural integrity assessment require a technique which can monitor variations

in a system's modal characteristics. These variations make the signals under analysis nonstationary, which in turn makes the Fourier transform unsuitable. The inability of the Fourier transform to track variations with respect to time was overcome by Gabor (1946) who wrote "...our every day experiences – especially our auditory sensations – insist on a description in terms of both time and frequency". Gabor achieved this description using what is known as either the windowed or short-time Fourier transform (STFT). The STFT works by capturing the Fourier transform of data over limited time periods  $T_{sr}$  (where  $sr$  represents sub-record length), during which the data should be piecewise stationary, in successive groups along the length of data. The results from each sub-record are displayed against their corresponding time forming a three-dimensional figure called a spectrogram or waterfall diagram (Bendat & Piersol 2000, p. 505). One limitation of STFT is that a compromise needs to be made between the spectral and temporal resolutions (Newland 1993 p. 218; Bendat & Piersol 2000, p. 505). This limitation is easily identified if one recalls, from Equation 5-6, that:

$$\Delta f = \frac{1}{T} \quad (5-6a)$$

Given that each estimate is obtained using only one sub-record length of data Equation 5-6a becomes:

$$\Delta f = \frac{1}{T_{sr}} \quad (5-7)$$

Also, provided that there is no spectral estimate overlap, the sub-record length effectively becomes the temporal resolution  $T_r$ . This means that the temporal and spectral resolutions become the reciprocal of one another, thereby generating the required compromise:

$$\Delta f \cdot T_r = 1 \quad (5-8)$$

Equation 5-8 conforms to Heisenberg's uncertainty principle, in application to signal analysis, which states that the product of the temporal and spectral resolutions is always at least a minimum constant (Burke-Hubbard 1998, pp. 203-208), with that constant being equal to unity for the STFT.

It must be noted that temporal resolution is independent of the sampling frequency  $f_s$ ; however, according to Shannon's sampling theorem,  $f_s$  must be at least twice the maximum expected analysis frequency to avoid aliasing (Burke-Hubbard 1998, p. 16; Randall 1987, pp. 30-31).

## 5.2. MODAL PARAMETER ESTIMATION

The dynamic characteristics of a time-invariant linear system can be described using an impulse response function  $h(\tau)$ , which is defined as the response of a system at any point in time as a result of a unit impulse applied at a time  $\tau$  earlier. Impulse response functions are useful as system descriptors as they can be used to determine a system's response  $y(t)$ , for any arbitrary excitation  $x(t)$ , using the convolution integral shown in Equation 5-9 (Bendat & Piersol. 2000, p. 29):

$$y(t) = \int_{-\infty}^{\infty} h(\tau)x(t-\tau)d\tau \quad (5-9)$$

Such characterisation can also be achieved in the frequency domain using the system's FRF  $H(f)$ . FRFs are used to represent the ratio of output/response to input/excitation in the frequency domain and are defined as the Fourier transform of the system's impulse response function as shown in Equation 5-10 (Bendat & Piersol 2000, p. 31):

$$H(f) = \int_0^{\infty} h(\tau)e^{-j2\pi f\tau} \quad (5-10)$$

By taking the Fourier transform of both sides of Equation 5-9, it follows that

$$Y(f) = H(f) \cdot X(f) , \quad (5-11)$$

where  $Y(f)$  and  $X(f)$  represent the Fourier transform of the response and excitation, respectively.

From Equation 5-11 the FRF is defined as follows:

$$H(f) = \frac{Y(f)}{X(f)} \quad (5-12)$$

It is often found advantageous to modify Equation 5-12. One modification is to multiply the equation's numerator and denominator by the complex conjugate of  $X(f)$ . In doing so a version of the FRF often referred to as  $H_1$  is obtained (Randall 1987, p.240):

$$H_1(f) = \frac{Y(f)}{X(f)} \cdot \frac{X^*(f)}{X^*(f)} \quad (5-13)$$

Another version of the FRF known as  $H_2$  is obtained by multiplying the numerator and denominator of  $H_1$  by the complex conjugate of  $Y(f)$  (Randall 1987, p.240):

$$H_2(f) = \frac{Y(f) \cdot Y^*(f)}{X(f) \cdot Y^*(f)} \quad (5-14)$$

Randall (1987, pp. 241-250) demonstrates that the  $H_1$  definition can be used to minimise the effect of extraneous noise, and that the  $H_2$  definition is superior in the reduction of frequency domain leakage (to be discussed later in section 5.2.2.1).

The most common application of FRFs is in modal analysis where they are used to extract the global properties of mechanical systems, namely their damping ratios and natural frequencies (the mode shapes a mechanical system are also defined by the residuals of its FRF). This modal parameter extraction requires the application of appropriate curve-fitting techniques in order to extract the required modal properties.

A number of techniques to extract modal parameters from the Fourier transform exist. For single degree-of-freedom (SDoF) systems, Ewins (1995, pp. 178-199) recommends a technique based on the circle fit of the Nyquist plot. Another common technique uses the polynomial fit of the magnitude of the FRF in the region of resonance (Bruel & Kjaer 1987 pp.31-32; Avitabile 2006). Various other frequency domain techniques, such as the Peak Amplitude, the Quadrature Response, the Maximum Quadrature Component, the Kennedy-Pancu, the inverse and Dobson's methods (Maia *et al.* 1997, pp. 217-231), also exist. A comparative study of a number of alternative modal estimation techniques, including the Rational Fraction Polynomial, Prony or Complex Exponential, Ibrahim Time Domain, and Hilbert Envelope methods, was undertaken by Iglesias (2000). Iglesias suggests that the Rational Fraction Polynomial method yields the most accurate and reliable estimates of the damping ratio. Garcia-Romeu-Martinez (*et al.* 2007) suggested that, for SDof systems, the Rational Fraction Polynomial technique and the least-squares regression curve-fit of the FRF magnitude do not produce significant differences and that the least-squares regression method yields reliable results. Based on the successful, practical, application of the least squares technique by Garcia-Romeu-Martinez (*et al.* 2007), and later by Rouillard (*et al.* 2007), it will be used as the basis of analysis in the remaining sections.

In order to establish an appropriate model of the FRF used for curve-fitting it is necessary to determine the equation of motion of the system under analysis. As discussed in chapter 4, the configuration used for evaluating the performance of protective packaging elements subjected to random excitation can be represented as a lumped parameter system consisting of a guided load (with mass  $m$ ), a spring (with stiffness  $k$ ) and a damper (with a damping coefficient  $c$ ), with displacement as both the excitation and response. If this configuration is approximated using an assumption of linearity and stationarity its equation of motion is defined as:

$$m \ddot{y}(t) + c \dot{y}(t) + ky(t) = c \dot{x}(t) + kx(t) \quad (5-15)$$

The FRF of a system is the Fourier transform of its response due to a unit impulse (Bendat & Piersol 2000, pp. 31-32). In this instance the response is the displacement  $y(t)$  to a unit impulse of the displacement  $x(t) = \delta(t)$  whose Fourier transforms are given by:

$$Y(f) = \int_0^{\infty} y(t)e^{-j2\pi ft} \cdot dt = H(f) \quad (5-16)$$

and unity, respectively.

Therefore it follows that:

$$\mathcal{F} \left[ \dot{y}(t) \right] = j2\pi f Y(f) \quad (5-17)$$

$$\mathcal{F} \left[ \ddot{y}(t) \right] = -j(2\pi f)^2 Y(f) \quad (5-18)$$

$$\mathcal{F} \left[ \dot{x}(t) \right] = j2\pi f \quad (5-19)$$

By substituting Equations 5-17 to 5-19 into Equation 5-15 the equation of motion becomes:

$$\left[ m(-2\pi f)^2 + c(j2\pi f) + k \right] Y(f) = \left[ k + c(j2\pi f) \right], \quad (5-20)$$

which can be rearranged to give:

$$Y(f) = H(f) = \frac{\left[ k + c(j2\pi f) \right]}{\left[ m(-2\pi f)^2 + c(j2\pi f) + k \right]} \quad (5-21)$$

Noting that:

$$f_n = \text{the system's undamped natural frequency} = \frac{1}{2\pi} \sqrt{\frac{k}{m}} \quad (5-22)$$

and

$$\zeta = \text{the system's damping ratio} = \frac{c}{2\sqrt{km}} \quad (5-23)$$

Equation 5-21 can be written as (Crandall 1958, p. 5):

$$Y(f) = H(f) = \frac{\left[ 1 + j2\zeta \left( \frac{f}{f_n} \right) \right]}{\left[ 1 - \left( \frac{f}{f_n} \right)^2 + j2\zeta \left( \frac{f}{f_n} \right) \right]} \quad (5-24)$$

Equation 5-24 is the complex FRF the system. In most cases it is desirable to describe the FRF using its magnitude and phase separately. The magnitude and phase of the complex FRF are given in Equations 5-25 and 5-26, respectively (Rao 2005, p.239-240).

$$|H(f)| = \left( \frac{1 + \left[ 2\zeta \left( \frac{f}{f_n} \right) \right]^2}{\left[ 1 - \left( \frac{f}{f_n} \right)^2 \right]^2 + \left[ 2\zeta \left( \frac{f}{f_n} \right) \right]^2} \right)^{1/2} \quad (5-25)$$

$$\phi(f) = \arctan \left[ \frac{2\zeta \left( \frac{f}{f_n} \right)^3}{1 - \left( \frac{f}{f_n} \right)^2 + 4\zeta^2 \left( \frac{f}{f_n} \right)^2} \right] \quad (5-26)$$

### 5.2.1. Modal Parameter Estimation From Nonstationary Signals

So far discussions related to the Fourier transform based modal parameter extraction technique have been limited to the analysis of stationary signals (since the FRFs obtained have been derived using a constant parameter system). In order to make the technique applicable to continuous structural integrity assessment the short-time or “instantaneous” FRFs of the system, which evolve with the induction of damage (changes in modal parameters), need to be estimated. The short-time FRFs may be determined using the ratio of the excitation and response spectrograms obtained using the STFT. However, since the excitation and response signals are random in nature, and contain extraneous noise, the results will contain statistical uncertainty.

Newland (1993, pp. 137-138) demonstrates that, when using the Fourier transform, the only way to improve the accuracy of frequency domain estimates is to average adjacent frequency spectra. Bendat & Piersol (2000, pp 306-308.) show that the level of spectral uncertainty  $\varepsilon_r$  is equal to the inverse of the square root of the number of independent (distinct) averages  $n_d$  performed, as given in Equation 5-27:

$$\varepsilon_r = \frac{1}{\sqrt{n_d}} \quad (5-27)$$

The need for averaging means that a compromise needs to be made between the temporal resolution and the level of spectral uncertainty (from both a lack of resolution and uncertainty in terms of magnitude).

With the introduction of averaging the temporal resolution  $T_r$  becomes:

$$T_r = n_d T_{sr} \quad (5-28)$$

If the sub-record length is substituted into Equation 5-28 in terms of spectral resolution it follows that:

$$T_r = \frac{n_d}{\Delta f} = \frac{1}{\Delta f \cdot \epsilon_r^2} \quad (5-29)$$

Now that a basis for the development of the short-time FRF has been established it is a matter of using it to determine the variations in the modal parameters of the system as a function of time. Again, since the level or type of nonlinearity and damping of packaging cannot be accurately established a priori, the system's modal properties can only be approximated using the least-squares regression curve-fit of the linear model described by Equations 5-25 and 5-26. This approximation will not always perfectly represent the system's true FRF over a broad frequency range. This means that the appropriate data for curve-fitting needs to be selected. In almost all cases curve-fitting data is selected to ensure an accurate fit of the FRF in the region of resonance. The data used for curve-fitting can be selected by the operator who is able to discern true modes from false perturbations. However, in many applications, particularly those which require the fitting of multiple FRFs (as is the case for continuous structural integrity assessment), curve-fitting data is selected automatically using a set number of points either side of the maximum FRF transmission (Ewins 1995, p. 190). For modal parameter estimation it has been suggested that the data used for curve-fitting should not comprise of less than six points (Ewins 1995, p. 190).

## 5.2.2. Fourier Analysis Enhancement Techniques

In an attempt to limit the compromises described in Equation 5-29, various techniques designed to enhance the evaluation of the FRFs, obtained using the discrete Fourier transform, are often introduced. Two commonly applied techniques are data overlapping and zero-padding. In addition, spectral enhancement can also be achieved using what is known as windowing or time history tapering. The following sections (5.2.2.1 to 5.2.2.3) will briefly describe the function of each of these techniques.

### 5.2.2.1. Windowing

The discrete Fourier transform can be viewed as the Fourier transform of an unlimited data record multiplied by a rectangular window, which is equal to unity over the sub-record length and zero elsewhere. This rectangular windowing function generates large side lobes in its Fourier transform which allow for the leakage of power at frequencies well separated from the main lobe. This leakage of power often introduces significant distortions of estimated frequency spectra. To help alleviate this problem it is necessary to introduce time-history tapering, which is often referred to as windowing, to eliminate discontinuities at the ends of the sub-records. Any smooth rounded window function can be used to help suppress side-lobe leakage; however, the most commonly applied function is the Hanning window. The side lobe decay rate of the Hanning window is 60dB/decade as opposed to 20dB/decade for a rectangular window (Randall 1987, pp. 157-159). This increase in side lobe suppression significantly reduces the distortion of frequency domain estimates. There are a number of windowing functions  $u(t)$  available. A summary of the characteristics of the most common windowing functions is given in *Table 5-1* and by illustration in *Figure 5-4*.

*Table 5-1: Properties of various windowing functions (Randall 1987, p. 159).*

Windowing Function	Highest Side-lobe (dB)	Side-lobe Decay rate (dB/decade)	Maximum Amplitude Error (dB)
Rectangular (None)	-13	-20	3,9
Hanning	-32	-60	1,4
Hamming	-43	-20	1,8
Flat-top	-93	0	<0,001

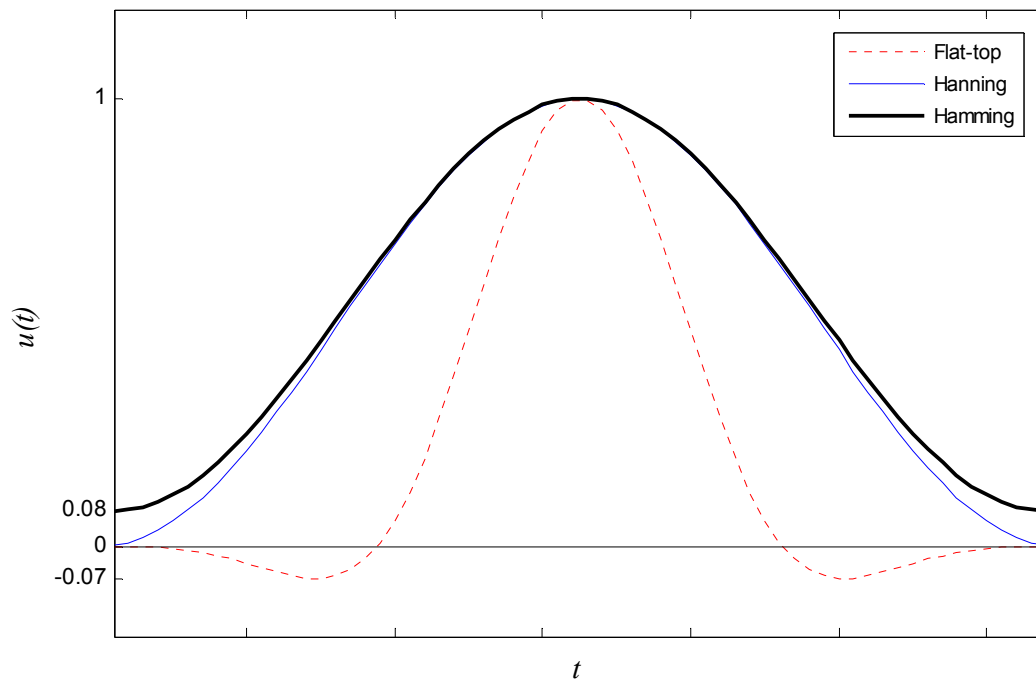


Figure 5-4: Common windowing functions.

The benefits provided by the application of the windowing are most easily demonstrated by presenting an example of the improvement in the results obtained with their application. Figure 5-5 gives a comparison between the spectral estimates obtained using three different windowing functions, the rectangular window (or no window), the Hanning window and the flat-top window. The signal consists of two sinusoids the first sinusoid has an amplitude of 1 and a frequency of 59Hz and the second has an amplitude of  $5 \times 10^{-4}$  with a frequency of 66Hz. As can be seen without the implementation of windowing the low amplitude sinusoid becomes buried by the higher amplitude sinusoid. With the introduction of windowing the smaller amplitude signal can be detected.

When windowing functions are used to determine individual spectra it is important to note that multiplication factors are required to correct the magnitudes in the spectra. However, this thesis only evaluates FRFs where response spectra are divided by excitation spectra. Since the same windowing function is applied to the excitation and response signals, the corrective factors will cancel one another out and therefore do not need to be considered herein.

It is also worth noting that flat-top windows are generally applied to harmonic signals, not the random signals discussed in the remainder of the thesis.

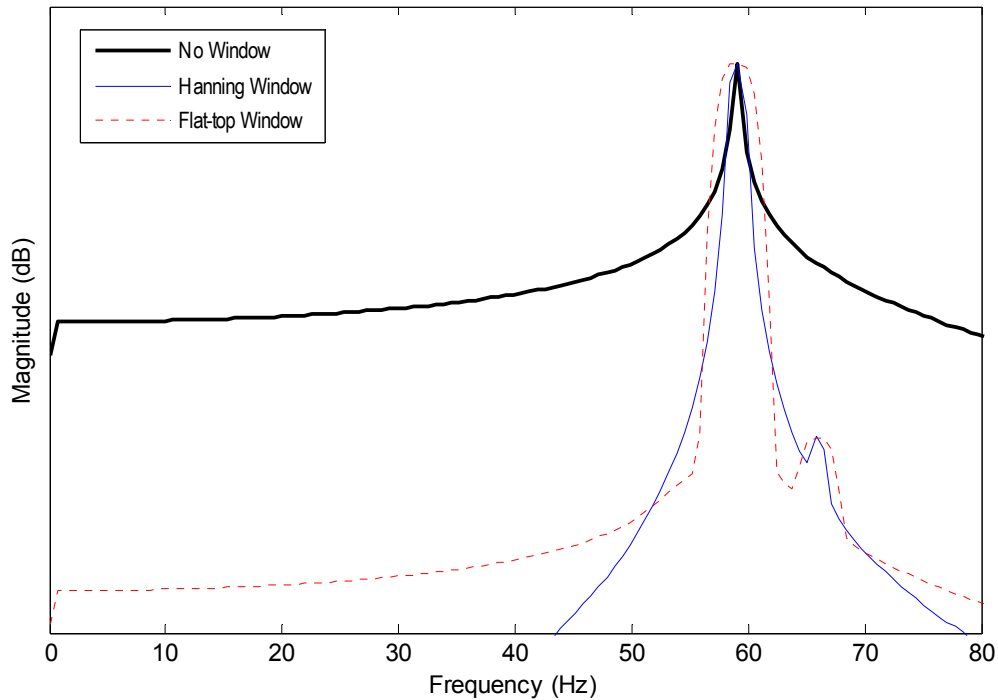


Figure 5-5: Reduced leakage by the application of windowing functions.

#### 5.2.2.2. Overlap

With the introduction of windowing a portion of the available data is disregarded, which is not desirable. For stationary processes this problem can be overcome by increasing the analysis sub-record length. However, this is not possible when analysing nonstationary processes such as structural integrity assessment applications, since the frequency structure of the response signal is expected to vary. Such applications require that the time taken to capture spectral estimates be limited to ensure that the stationary condition is achieved. The need to maintain fine temporal resolution with an increased sub-record length means that averaging is compromised and this increases spectral uncertainty. To overcome this problem the data record can be divided into equal segments which overlap one another, as depicted in *Figure 5-6*, as opposed to dividing the record into segments that are independent. In a statistical sense this overlapping operation is capable of retrieving most of the information lost due to the application of windowing (Bendat & Piersol 2000, p. 430; Randall 1987, p175).

When analysing nonstationary signals it is also necessary to carefully select the desired temporal interval between spectral estimates. Generally, it is desired to capture as much information as possible. Therefore, the interval will almost never be greater than the temporal resolution shown in *Figure 5-6*. Randall (1987, p. 212-213) suggests that for STFT displays

(which include no spectral averaging), which are used to display arbitrarily varying signals, each spectral estimate should overlap one another by at least 75% to aid visual interpretation. If this reasoning is adopted for the spectral estimation procedure shown in *Figure 5-6* each averaged FRF estimate would overlap its predecessor by at least 75% of the individual sub-record length, as opposed to 75% of the total time taken to capture the estimate, as depicted *Figure 5-7*. This is spectral estimate overlap and should not be confused with averaging overlap.

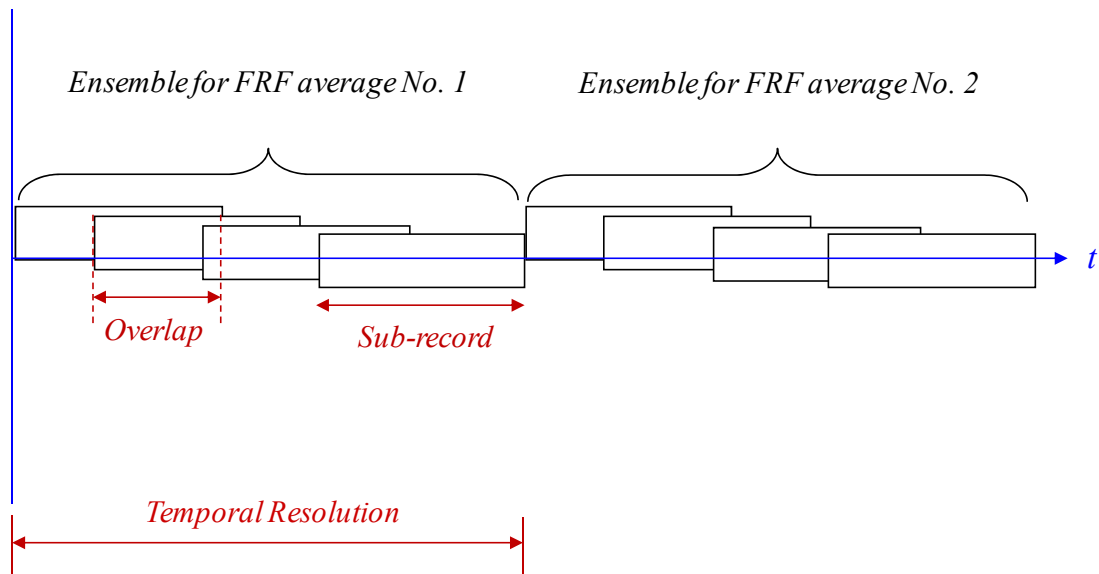


*Figure 5-6: Schematic of spectral analysis identifying overlap.*

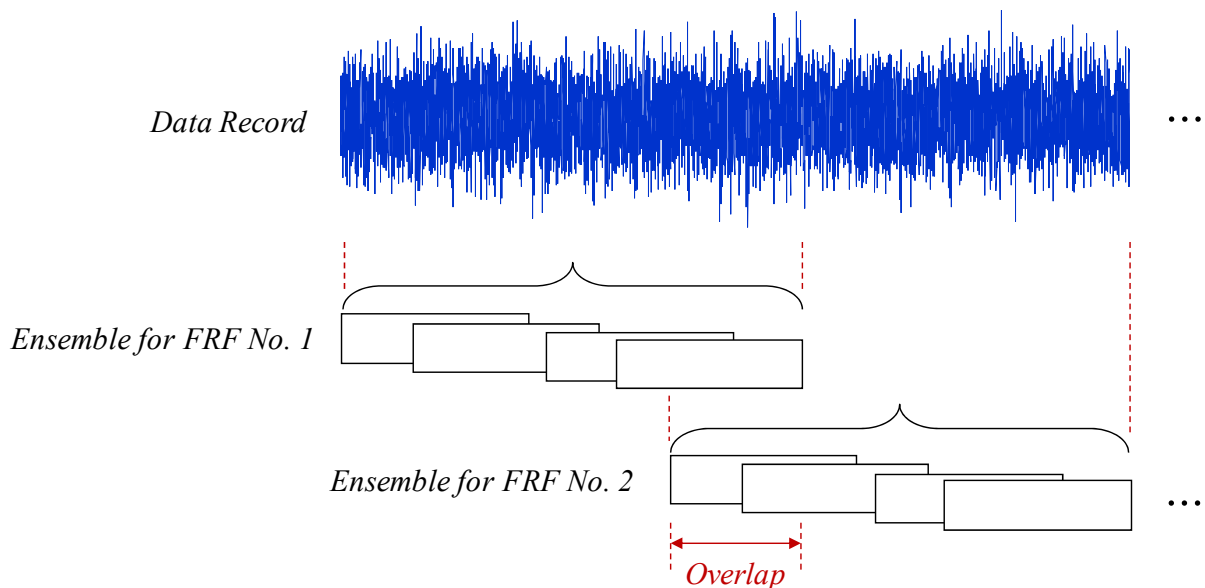


*Figure 5-7: Spectral estimate overlap.*

### 5.2.2.3. Zero-Padding

Zero-padding is a technique that is often used in an attempt to improve the evaluation of spectral estimates by artificially increasing their spectral resolution. This artificial increase in resolution is achieved by adding a sequence of zeros to each sub-record (thereby increasing the sub-record length) as shown in *Figure 5-8*.

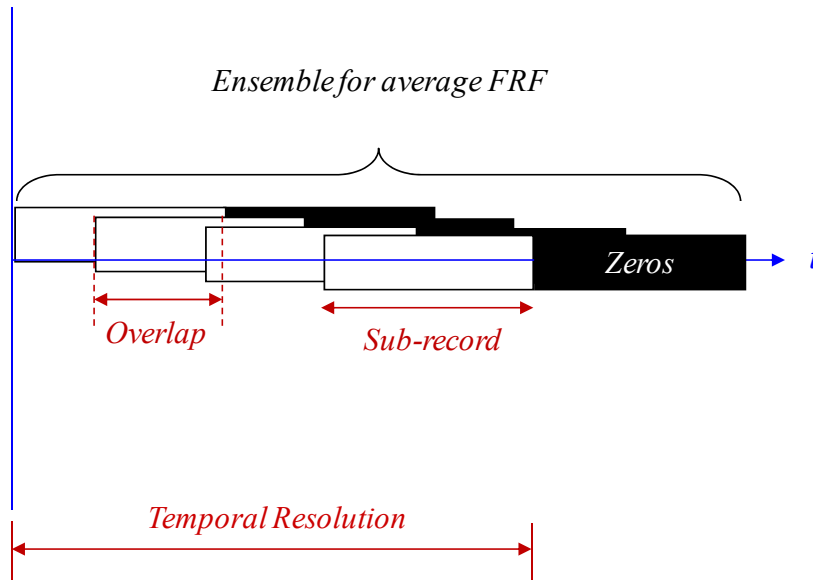


*Figure 5-8: Zero-padding.*

Zero-padding is under-pinned by the assumption that the signal is zero outside of the data segment under analysis and its application is justified mathematically as follows (Weeks 2007):

Starting with the continuous Fourier transform we have:

$$X(f) = \int_{-\infty}^{\infty} x(t)e^{-j(2\pi ft)} \quad (5-4)$$

Now suppose  $x(t)$  is non-zero over the interval  $[a, b]$  and is zero over the interval  $[b, c]$ .

Equation 5-4 can be separated into two components as follows:

$$\begin{aligned} X(f) &= \int_a^c x(t)e^{-j(2\pi ft)} \\ &= \int_a^b x(t)e^{-j(2\pi ft)} + \int_b^c x(t)e^{-j(2\pi ft)} \end{aligned} \quad (5-4a)$$

Now substitute 0 for  $x(t)$  over the interval  $[b, c]$  to obtain:

$$X(f) = \int_a^b x(t)e^{-j(2\pi ft)} + 0 \quad (5-4b)$$

Therefore for continuous signals  $X(f)$  is the same whether or not the zero component of the signal is considered.

An alternate justification of zero-padding can be made by considering it as nothing more than the application of a windowing function which forces a region of the signal to zero.

### **5.3. INFLUENCE OF SPECTRAL (STFT) ANALYSIS PARAMETERS AND ENHANCEMENT TECHNIQUES**

With the various parameters and enhancement techniques used to obtain modal parameter estimates via the Fourier transform, it is important to understand their influence on the variability of the estimates obtained. Such an understanding will assist analysts with the development of optimal modal parameter extraction procedures, especially for systems with nonstationary characteristics.

The following sections discuss the effect of various parameters and enhancement techniques on the previously described modal parameter extraction method.

Excitation and response data was generated using the procedure described in Chapter 4 (Methodology).

Post-processing was achieved with purposely designed software that used a modified, STFT based, Welch method to extract average  $H_l$  FRF estimates using ensembles as shown in *Figure 5-6*. This technique allows for the configuration of various parameters namely, zero-padding, spectral averaging overlap and changes to the analysis sub-record length, all of which are often manipulated in an attempt to improve spectral estimates.

Time history tapering was achieved using a Tukey windowing function (Harris 1978), which was adjusted to minimise data suppression whilst still allowing for a reduction in spectral leakage. It must be noted that when zero-padding was used, in conjunction with time history tapering, the Tukey window was only applied to the original signal in order to avoid distorting the window, which leads to extraneous errors (Kay 1988, pp. 78-79).

In order to enable the statistical nature of the results to be assessed, a large number of independent band-limited Gaussian excitation signals were used. The corresponding independent signal pairs (excitation and response) were subjected to short-time FRF analysis (including least mean squares modal parameter extraction) with variations in the parameters of interest. As well as examining the consistency (variability) of the results using a statistical

analysis, the robustness of the potential improvements to extraneous noise, in both the excitation and response signals, was also evaluated.

The results obtained from a simulated SDoF system are given in the remaining sections for illustrative purposes. The system was configured with a natural frequency of 20Hz and a viscous damping ratio of 11% (although arbitrary these parameters lie within a practical range for packaging systems). Excitation was achieved with a random Gaussian signal band limited between 0 and 100Hz. It is important to note that the actual values of the system's natural frequency and damping ratio have no influence on the nature of the results to be discussed in this chapter. However, for completeness, numerically simulated experiments that are found to be of particular importance will be repeated using physical systems which exhibit different modal characteristics to the simulated systems used in this chapter (refer to chapter 8). The remainder of this chapter does not discuss the effectiveness of the chosen modal parameter extraction technique, which may be influenced by the nominal natural frequency and damping ratio, but rather potential improvements in the FRF for parameter extraction purposes.

### **5.3.1. Influence of Spectral Averaging and Sub-record Length**

Most authors agree that spectral estimation using random signals requires some degree of averaging to minimise statistical uncertainty. However, in many applications, the time available to capture data is limited, thus restricting the amount of data available for averaging. This limited window means that a compromise needs to be made between the number of spectral averages and the analysis sub-record length. For the purposes of modal parameter extraction it is unclear which is more important. Frequency resolution, hence the sub-record length, is important as it affects the sensitivity of the frequency estimates (although it is not the limiting factor in this instance as curve-fitting is applied). However, it is not clear how much spectral averaging can be compromised.

An initial set of numerically simulated experiments (experiment 1) was developed to evaluate the influence of various amounts of averaging, in conjunction with varying sub-record lengths (with the combination of the two varying parameters resulting in a constant analysis window size, or temporal resolution), on modal parameter extraction. As mentioned above, since the time available to capture the modal estimate is limited, the sub-record length and the number of averages are a function of each other. This means an increase in the number of averages results in a reduction in the sub-record length and vice-versa. *Table 5-2* contains the parameters used for analysis.

Table 5-2: Experiment 1 analysis parameters.

Group No.	No. Averages	Sub-Record Length (s)
1	480	0.25
2	240	0.5
3	120	1
4	60	2
5	30	4
6	15	8
7	8	15
8	4	30
Excitation	Band-Limited (0-100Hz) Gaussian	
Natural Frequency	20Hz	
Damping Ratio	11%	

The results gathered from experiment 1, for systems with a natural frequency of 20Hz and 11% damping (for excitation response signal pairs containing 0% and 10% extraneous noise), are presented in *Figure 5-9*, as the mean natural frequency extracted from 50 independent signal pairs (excitation and response) along with error bars indicating  $\pm$  one population standard deviation,  $\sigma$ . It must be noted that during experiment 1 no spectral overlapping or zero-padding was applied.

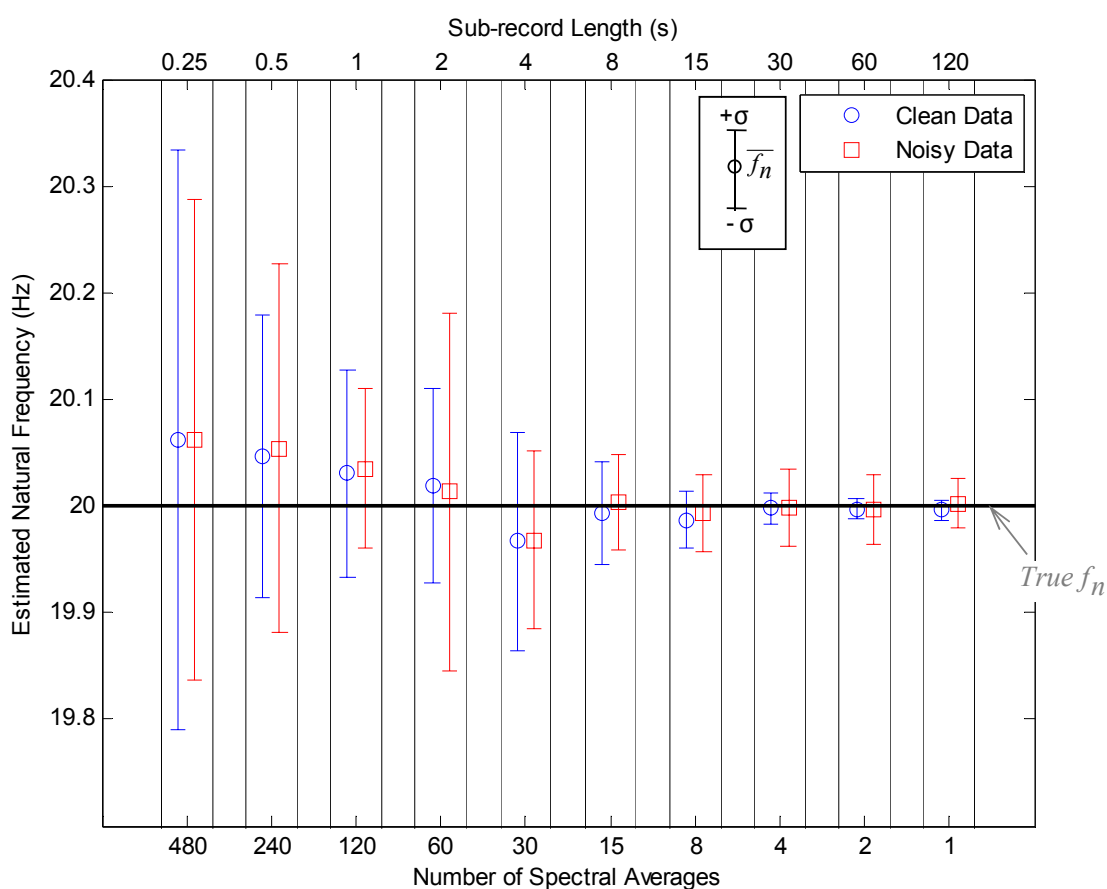


Figure 5-9: Experiment 1 - Spectral resolution and uncertainty.

The results from this series of numerically simulated experiments indicate that, for the purposes of modal parameter extraction, spectral resolution, hence sub-record length, has a more significant influence on the extracted natural frequencies than reduced spectral uncertainty via spectral averaging. This is made most evident by the small variance of the results obtained using the 120 second sub-record, which provides fine spectral resolution (0.0083Hz) but does not allow for any spectral averaging (100% theoretical uncertainty). This finding is attributed to the fact that spectral uncertainty only creates variability in the magnitude of frequency estimates, which, due to its random nature, has a limited effect when curve-fitting using least squares regression. Conversely, coarse spectral resolution limits the amount of data available within the bandwidth appropriate for curve-fitting, thereby creating uncertainties in terms of both magnitude and spectral locality (spectral frequency bin).

In *Figure 5-9* some of the natural frequency estimates obtained from noise-contaminated data appear to be more accurate than those obtained from noise-free data. This is not the case. The standard deviation indicated on the figure is an estimate based on a population of 50 samples. The statistical uncertainty of this estimate conforms to the  $\chi^2$  (Chi-squared) distribution and is larger than the difference between the values for the noise-free and noise-contaminated results (Ott & Mendenhall 1990, pp. 374-377). What is important here is the trend that shows a decrease in the variance of the natural frequency estimate as the sub-record length increases.

### **5.3.2. Influence of Zero-Padding on Modal Parameter Estimation**

Since the frequency content of response signals captured during random fatigue test is likely to vary as a function of time (with the introduction of damage), it is necessary to obtain estimates of the system whilst consuming the least possible amount of temporal data. Accurate estimates of the system's properties using limited temporal data can only be achieved by improving the evaluation of spectral estimates with relatively coarse spectral resolution. This improved evaluation is often attempted by artificially refining the spectral resolution of coarse frequency spectra using zero-padding to extend the duration of the sub-records. However, it is uncertain whether or not zero-padding actually helps. Most agree that zero-padding does not improve true spectral resolution; however, many authors are unclear about what it does achieve (Kay 1988, pp. 78-79; Lyons 2004, p.87, Manolakis *et al.* 2005, p.202, Andreas 2006, p. 328, Roberts 2004, pp. 541-542, Baher 1990, pp. 365-367, Douglas 1987, pp. 722-723).

Some examples of the influence of zero-padding according to various published works include:

- Kay (1988): “No extra resolution is afforded by zero padding, but we achieve a better evaluation of the periodogram”
- Lyons (2004): “...zero-padding does not improve our ability to resolve, to distinguish between, two closely spaced signals in the frequency domain”
- Manolakis (et al. 2005): “...zero-padding does not increase the resolution of the spectrum...[it just provides] a better display of available information”
- Andreas (2006): “...by increasing the number of zeros...a higher density of sample points can be achieved”

An attempt to determine whether or not zero-padding can improve modal parameter extraction from spectra with relatively coarse resolution was made by conducting a second set of numerically simulated experiments (experiment 2). The signals used in the previous numerical experiment were again analysed using the parameters listed in *Table 5-3* (notice that the number of spectral averages was proportional to the inverse of the sub-record length, which resulted in a constant temporal resolution for each of the sub-records analysed).

The results for numerically simulated experiments with no extraneous noise are given in *Figure 5-10* and those obtained from numerically simulated experiments containing 10% extraneous noise are given in *Figure 5-11*.

*Table 5-3: Experiment 2 analysis parameters.*

Sub-Record Length (s)	No. of Averages	Zero-padding (X Sub-record )	Artificial Frequency Resolution (Hz)
0.25	480	0, 0.25, 1, 2, 4, 8, 16	4, 3.2, 2, 1.333, 0.8, 0.444, 0.235
1	120	0, 0.25, 1, 2, 4, 8, 16	1, 0.8, 0.5, 0.333, 0.2, 0.111, 0.059
2	60	0, 0.25, 1, 2, 4, 8, 16	0.5, 0.4, 0.25, 0.167, 0.1, 0.056, 0.029
8	15	0, 0.25, 1, 2, 4, 8, 16	0.1, 0.063, 0.042, 0.025, 0.014, 0.007
Excitation		Band-Limited (0-100 Hz) Gaussian	
Natural Frequency		20 Hz	
Damping Ratio		11%	

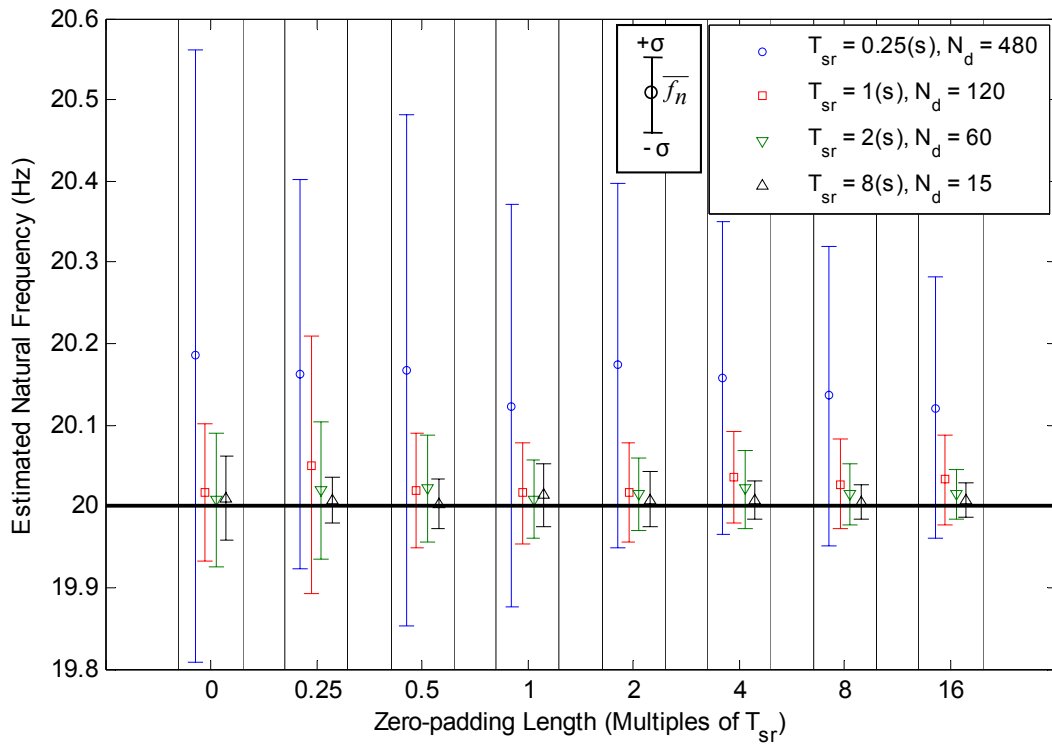


Figure 5-10: Experiment 2 - Results of increased zero-padding.

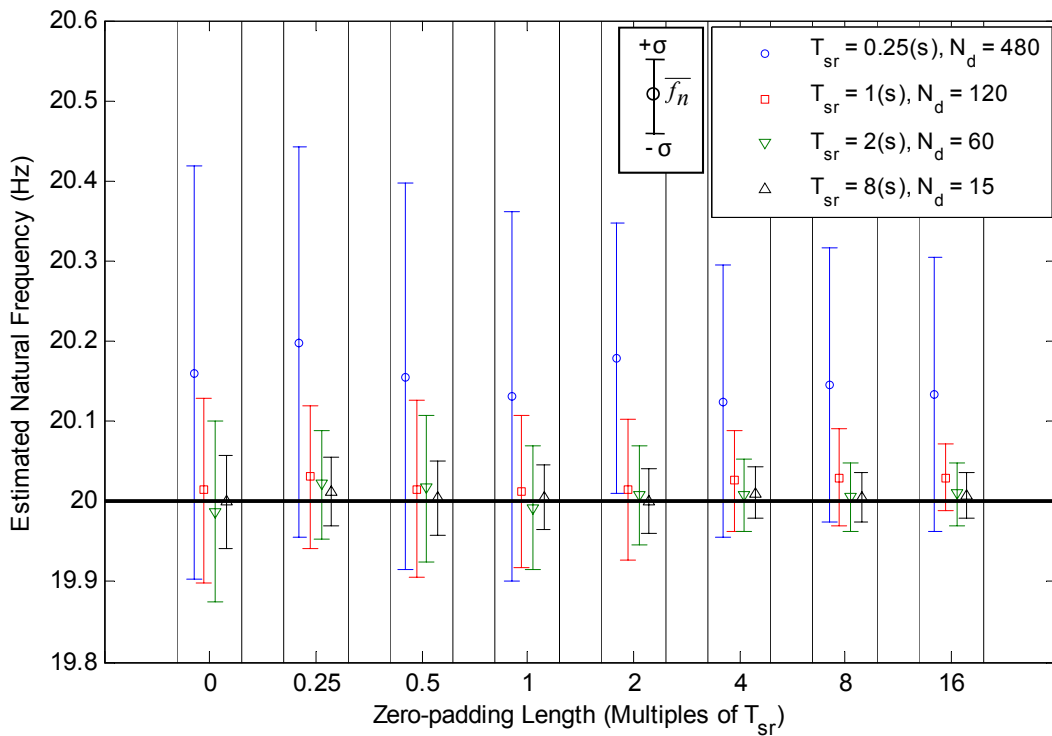
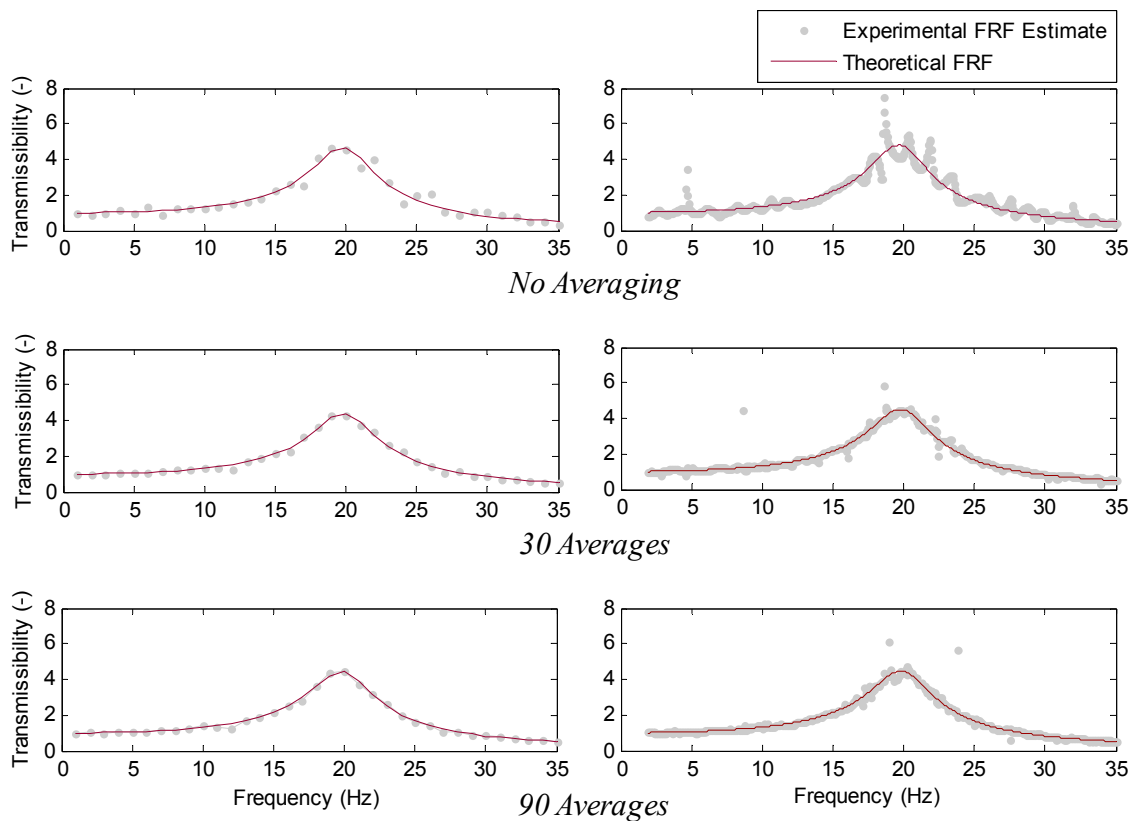


Figure 5-11: Experiment 2 - Results of increased zero-padding (10% noise).

The findings from experiment 2 indicate that, for signals containing as much as 10% extraneous noise, the introduction of up to 16 times zero-padding significantly reduces the variability of the frequency estimates obtained using least squares regression modal parameter extraction, irrespective of the sub-record length used. The finding that the introduction of zeros will not degrade results is significant in that it enables analysts to apply zero-padding with confidence. In saying this, it must also be noted that the value of zero-padding should not be overstated and that where possible increases in spectral resolution should always be obtained by increasing the analysis sub-record length.

In order to provide an illustrative example of the influence of zero-padding the magnitude of a typical, noise contaminated (10%), low spectral resolution (1Hz) FRF, at three stages in the averaging process, is presented alongside its theoretical equivalent in *Figure 5-12*.



*Figure 5-12: FRF estimates and zero-padding: Left – No zero-padding, Right – Zero-padding ( $T_{sr} \times 16$ ).*

The improvements obtained by implementing zero-padding are attributed to the fact that it provides estimates of the system’s response at otherwise non-described frequencies, which with the implementation of averaging, effectively increases the portion of data which describes the theoretical model of the FRF, without distorting its shape. This suggestion follows Semmlow’s (2005) description of zero-padding: “Zero padding provides an interpolation of the points in the unpadded signal”.

Experiment 2 also indicates that, with the implementation of zero-padding, sub-record length continues to be more influential than spectral averaging. However, since zero-padding provides additional data points for curve-fitting, it was thought that at some point spectral averaging may become more significant. Therefore, experiment 1 was repeated with the application of 16 times zero-padding. The results from this repeat experiment are given in *Figure 5-13*. As can be seen, the findings from experiment 1 remain true after the application of zero-padding. However, a limit to the potential improvements made by increasing the sub-record length at the expense of averaging is also evident.

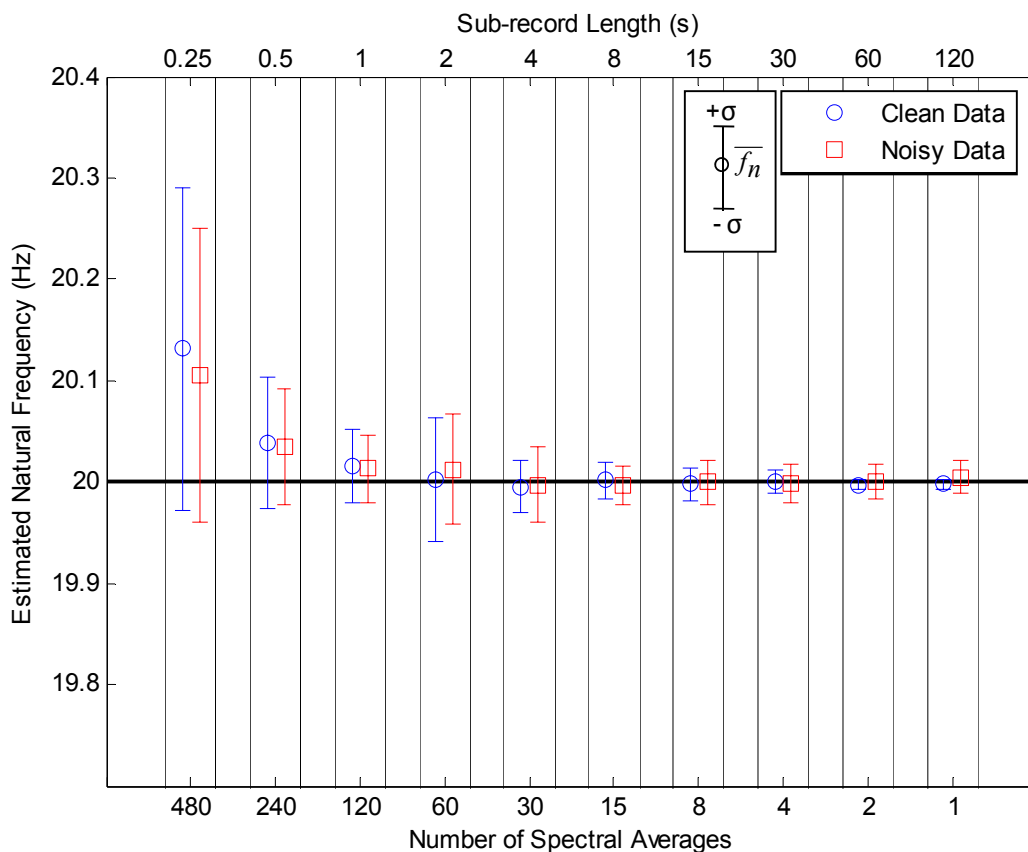


*Figure 5-13: Spectral resolution and uncertainty with zero-padding.*

In order to demonstrate the effectiveness of zero-padding in improving the relationship between temporal and spectral resolution, a third series of numerically simulated experiments (experiment 3) was carried out. During this series of experiments the sub-record length, used to analyse the above mentioned signal pairs, was progressively shortened to create a finer temporal resolution. This reduction in sub-record-length was matched by a corresponding increase in zero-padding in order to achieve a constant apparent spectral resolution. Experiment 3 was conducted using the above mention 50 independent signal pairs and the analysis parameters listed in *Table 5-4*.

*Table 5-4: Experiment 3 analysis parameters.*

Sub-Record Length (s)	Zero-padding (s)	True Frequency Resolution (Hz)	Artificial Frequency Resolution (Hz)
30	0	0.033	0.033
15	15	0.067	0.033
8	22	0.125	0.033
4	26	0.25	0.033
2	28	0.5	0.033
1	29	1	0.033
0.5	29.5	2	0.033
0.25	29.75	4	0.033
Excitation		Band Limited (0-100 Hz) Gaussian	
Natural Frequency		20 Hz	
Damping Ratio		11%	
Number of Spectral Averages ( $N_d$ )		4	

The results obtained from experiment 3 are depicted, along side of the results obtained without zero-padding, in *Figure 5-14*, for clean signals and *Figure 5-15* for signals containing 10% extraneous noise. As can be seen zero-padding can significantly improve the spectral uncertainty of results obtained with fine temporal sensitivity. This means that, if zero-padding is introduced, estimates of the system's natural frequency can be made at more regular intervals with less impact on the accuracy of the estimates.

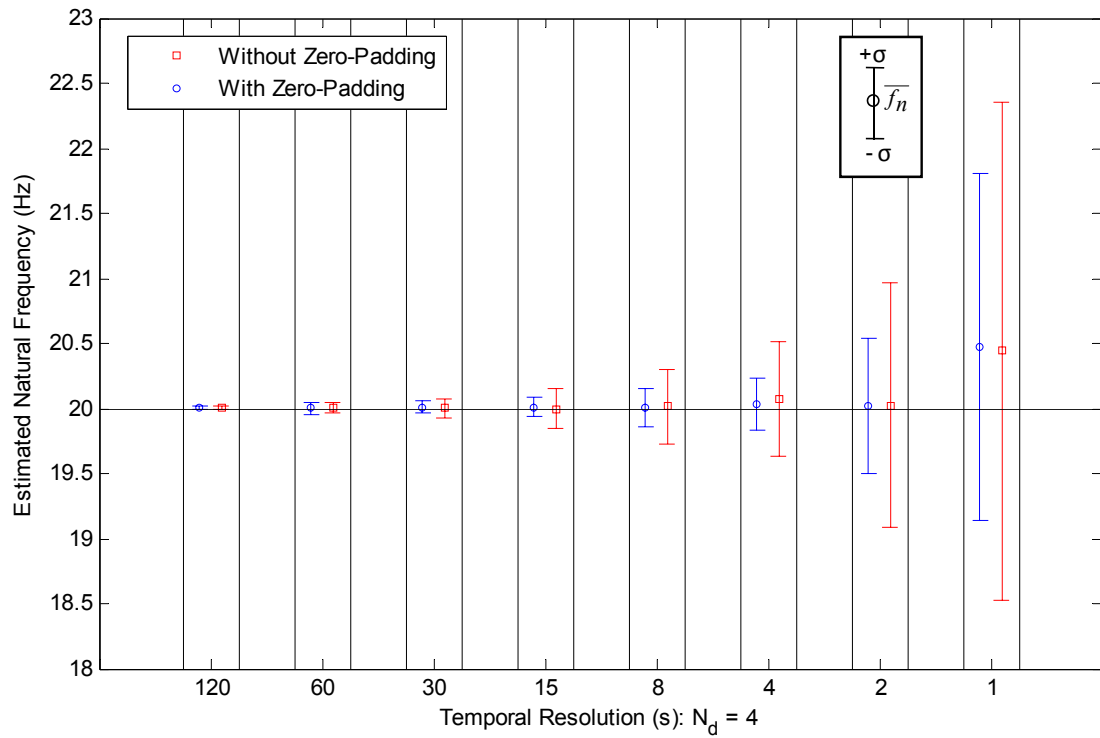


Figure 5-14: Experiment 3 - Results from improved temporal resolution using zero-padding.

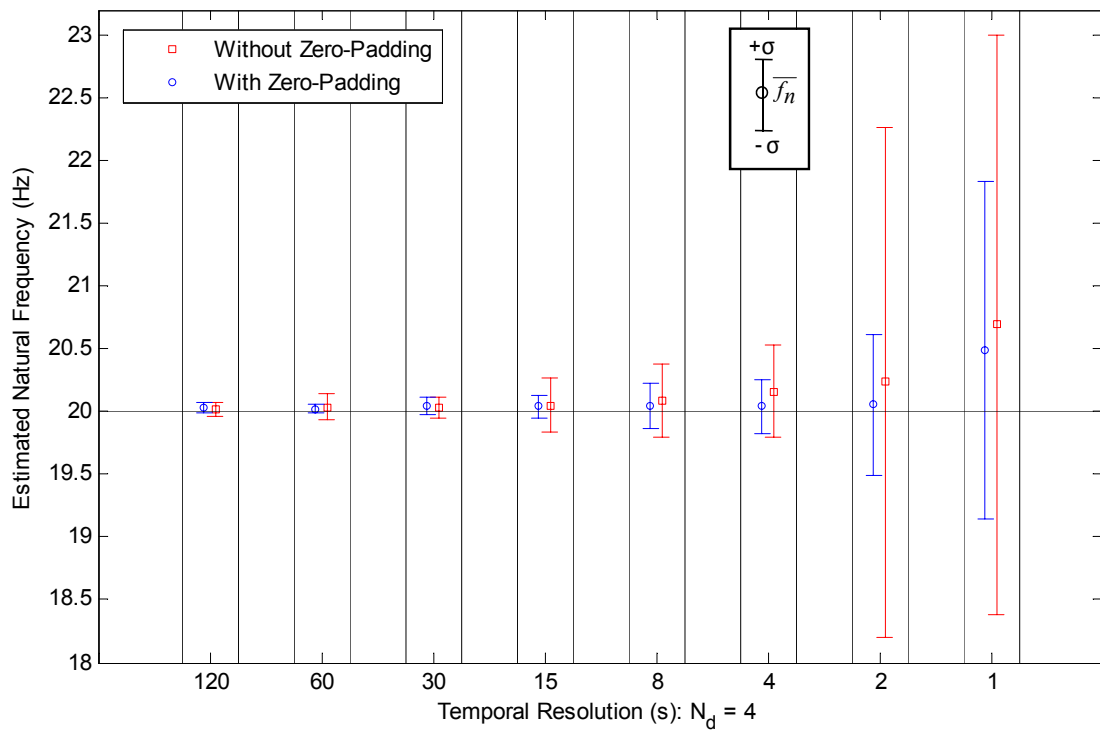


Figure 5-15: Experiment 3 – Results of improved temporal resolution using zero-padding from signals (10% noise).

### 5.3.3. Influence of Overlapped Averages on Modal Parameter Estimation

It is understood that overlapped spectral averaging can be used to retrieve the statistical stability lost due to windowing. Bendat & Piersol (2000, p. 430) state that if 50% overlap is used with the application of the Hanning window, approximately 90% of the stability lost, due to the window, can be retrieved. Randall (1987, p.175) suggests that, for the Hanning window, overlaps of greater than 50% provide no appreciable improvement in statistical uncertainty. However, the ability to apply greater values of overlap exists when using common frequency analysers. For modal parameter extraction purposes overlap values as high as 90% have been used to allow for additional averaging without the use of additional temporal data (Garcia-Romeu-Martinez *et al.* 2007). While these additional spectral averages may not improve the statistical uncertainty of the spectral estimates, it is possible that the resulting FRFs will be better suited for parameter extraction.

Overall, for the purposes of modal parameter extraction from time-varying systems it is uncertain if large amounts of spectral overlapping can be used to enhance results. Therefore, to gain a better understanding of the influence of overlapped spectral averaging, on modal parameter extraction, a fourth set of numerically simulated experiments (experiment 4) was undertaken. During experiment 4 varying amounts of averaging overlap (0% to maximum, all but one point overlapped) were used in conjunction with the Tukey window to analyse 50 constant parameter signal pairs. The variables used for analysis are given in *Table 5-5* below as can be seen with the increased number of overlapped averages no additional temporal data was consumed.

The results obtained from experiment 4, for a system with a natural frequency of 20Hz and a damping ratio of 11%, at a temporal resolution of 10 seconds (5 second sub-records, 2 independent averages and no zero-padding), are given in *Figure 5-16*. As can be seen, for signals containing as much as 10% noise, data overlapping can generate a significant reduction in the level of variance in the extracted natural frequencies obtained using least squares regression modal parameter extraction.

Table 5-5: Experiment 4 analysis parameters (Maximum: Represents maximum overlap, where all but one sample point are overlapped).

Sub-Record Length (s)	No. Independent Averages	No. Overlapped Averages	Averaging Overlap (%)
5	2	2	0
5	2	3	50
5	2	5	75
5	2	11	90
5	2	101	99
5	2	10241	Maximum
Excitation		Band-Limited (0-100 Hz) Gaussian	
Natural Frequency		20 Hz	
Damping Ratio		11%	

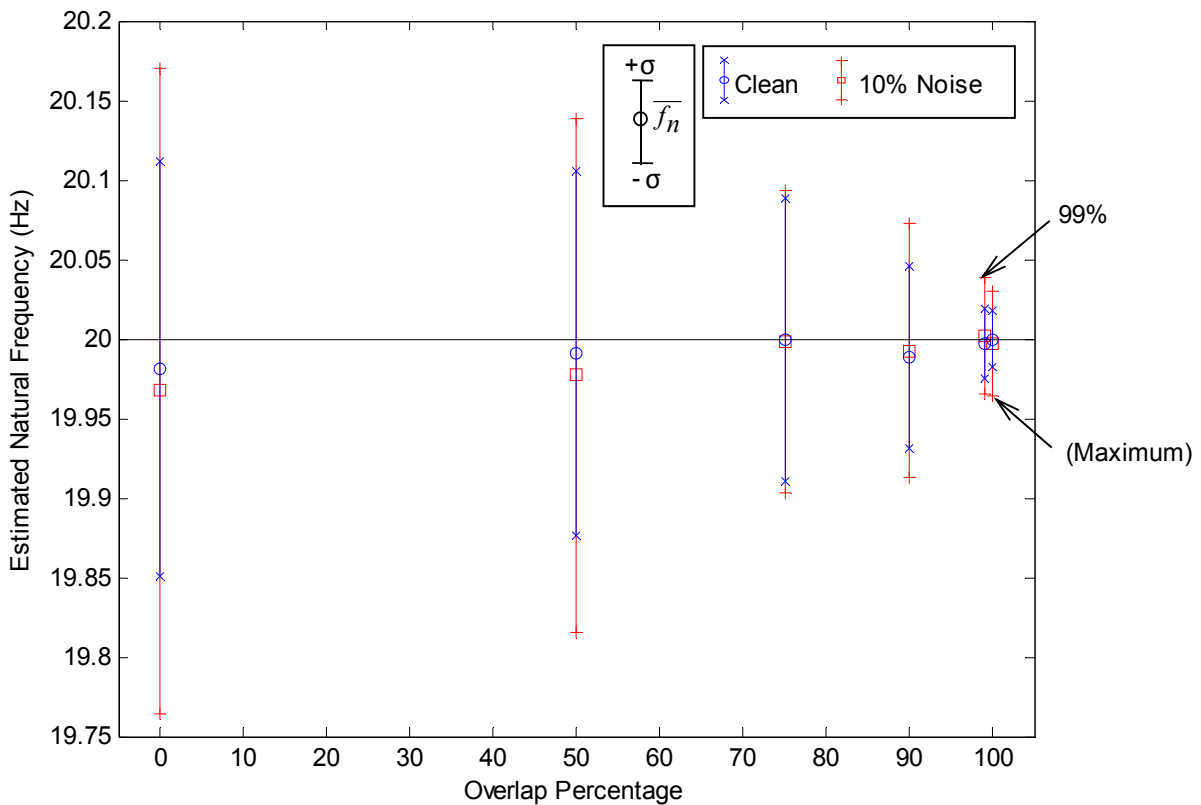


Figure 5-16: Experiment 4 - Effect of overlapped averages.

Since the frequency resolution was kept constant with the addition of increased spectral overlap, it is reasonable to expect that the effect on the estimates must result from a reduction in the spectral variation of the FRF estimates. Harris (1978, pp. 55-57) provides equations to determine the variance of spectral estimates obtained using correlated overlapped segments.

Equation 5-30 is used for 50% overlap and Equation 5-31 for 75%, where  $n_d$  now represents the number of overlapped (correlated) averages.

$$\frac{\sigma_{avg.}^2}{\sigma_{meas.}^2} = \frac{1}{n_d} (1 + 2c^2_{50\%}) - \frac{1}{n_d^2} (2c^2_{50\%}) \quad (5-30)$$

$$\frac{\sigma_{avg.}^2}{\sigma_{meas.}^2} = \frac{1}{n_d} (1 + 2c^2_{75\%} + 2c^2_{50\%} + 2c^2_{25\%}) - \frac{2}{n_d^2} (c^2_{75\%} + 2c^2_{50\%} + 3c^2_{25\%}), \quad (5-31)$$

where  $c_r$  is the correlation coefficient and can be calculated using Equation 5-32.

$$c_r = \frac{\int_0^{T_{sr}} w(t) \cdot w(t + [1-r]T_{sr}) \cdot dt}{\int_0^{T_{sr}} w^2(t) \cdot dt}, \quad (5-32)$$

where  $w$  is the applied windowing function and  $r$  is the percentage overlap.

Values of correlation coefficients for typical windowing functions are given in *Table 5-6*.

*Table 5-6: Correlation coefficients for typical windowing functions (Based on windowing functions available in Matlab®).*

Window	25% Overlap	50% Overlap	75% Overlap
Tukey $\alpha=0.25$	0.1481	0.4444	0.7407
Tukey $\alpha=0.5$	0.0454	0.3636	0.7272
Hamming	0.0268	0.2337	0.7069
Hanning	0.0075	0.1667	0.6592
Rectangular	0.25	0.5	0.75

Equations 5-30 and 5-31 predict a reduction in estimate variance of 11% and 10%, for 50% and 75% overlap respectively, when compared to the results obtained using no overlap. Clearly, these values do not reflect the improvements shown in *Figure 5-16*, particularly those obtained using 75% overlap.

According to the formulation provided Naidu (1996, p192) the variance of Welch spectral estimates is inversely proportional to the number of uncorrelated overlapped spectral averages. *Figure 5-17* presents the variance of the natural frequency estimates obtained from experiment 4 against the number of overlapped spectral averages. The closest inverse relationship of each set of results is also included. As can be seen the extracted natural frequency variance has a strong correlation with the fitted trend, thereby suggesting that, within certain bounds, such a relationship may also exist when extracting estimates of natural frequency using FRF magnitude data calculated from correlated, overlapped segments. This finding does not suggest that a more accurate FRF has been obtained, but rather the FRF estimate has improved for modal parameter extraction purposes.

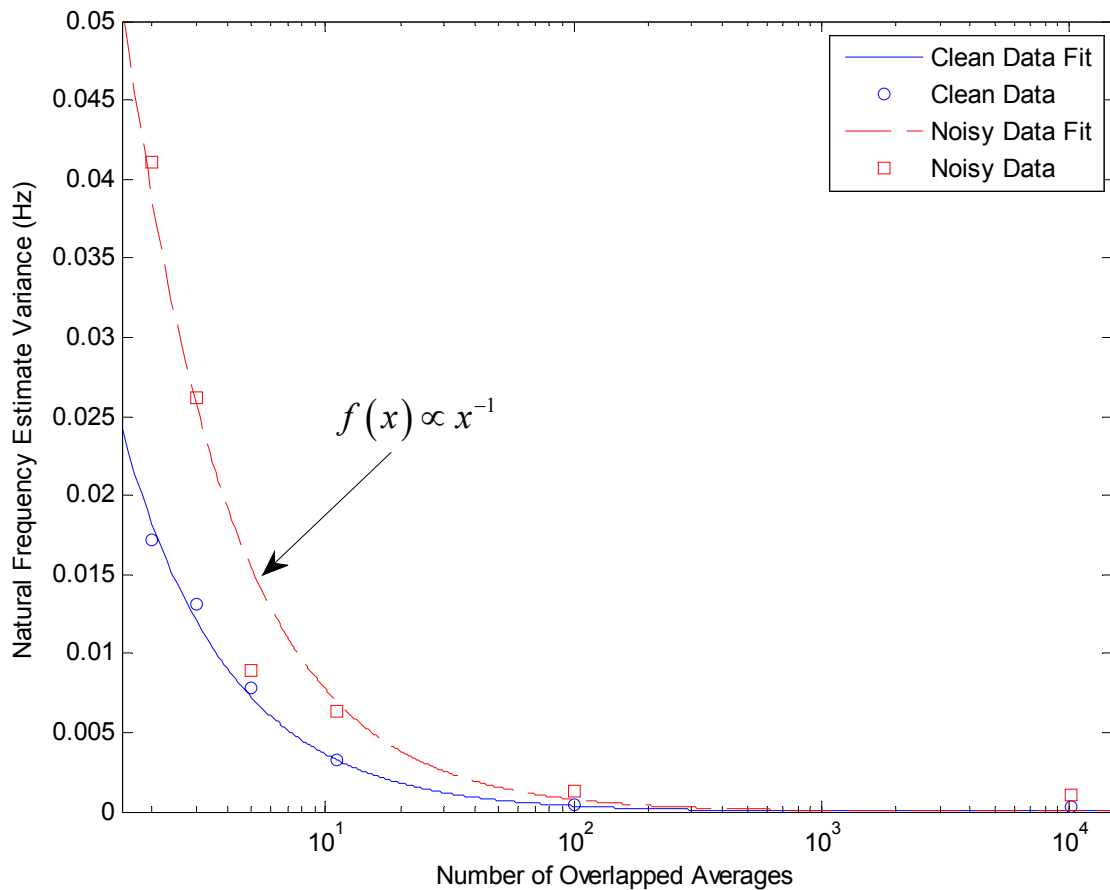


*Figure 5-17: Experiment 4 - Estimated natural frequency variance versus increased spectral overlapping (where  $x$  is the number of overlapped averages).*

The results in *Figure 5-16* and *Figure 5-17* clearly demonstrate that increased spectral overlapping can significantly improve modal parameter extraction results. These figures also clearly demonstrate a diminishing return when using in excess of approximately 100 overlapped averages. The use of overlapped averaging in excess of this point should be avoided in order to allow for the largest possible sub-record length, hence finest spectral resolution.

In order to illustrate how the improvements depicted in *Figure 5-16* and *Figure 5-17* are achieved, typical noise-contaminated (10%) moderately high resolution (0.1Hz) FRFs, obtained from the same the data set, with various amounts of averaging overlap, are presented in *Figure 5-18*. As can be seen, the introduction of increased overlapped averaging results in a significant reduction in the random deviation from the actual FRF, even though no additional data is analysed.

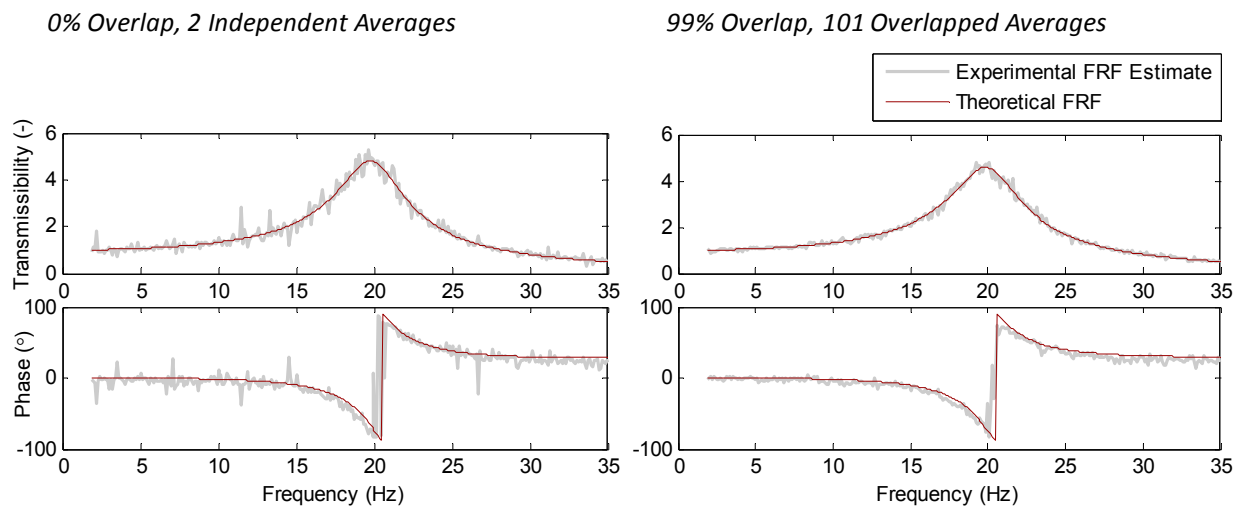


*Figure 5-18: Enhancement of FRF estimates using overlapped averaging.*

Experiment 4 was repeated with the application of zero-padding (16 times), at various temporal resolutions, in order to ensure that the effectiveness of overlapped averaging remained, after zero-padding was applied. *Figure 5-19* contains typical results obtained from the repeat experiment (particular results obtain at a temporal resolution of 8 seconds with 4 second sub-records). As can be seen, the estimated natural frequency variance continues to decrease inversely as the number of overlapped spectral averages is increased.

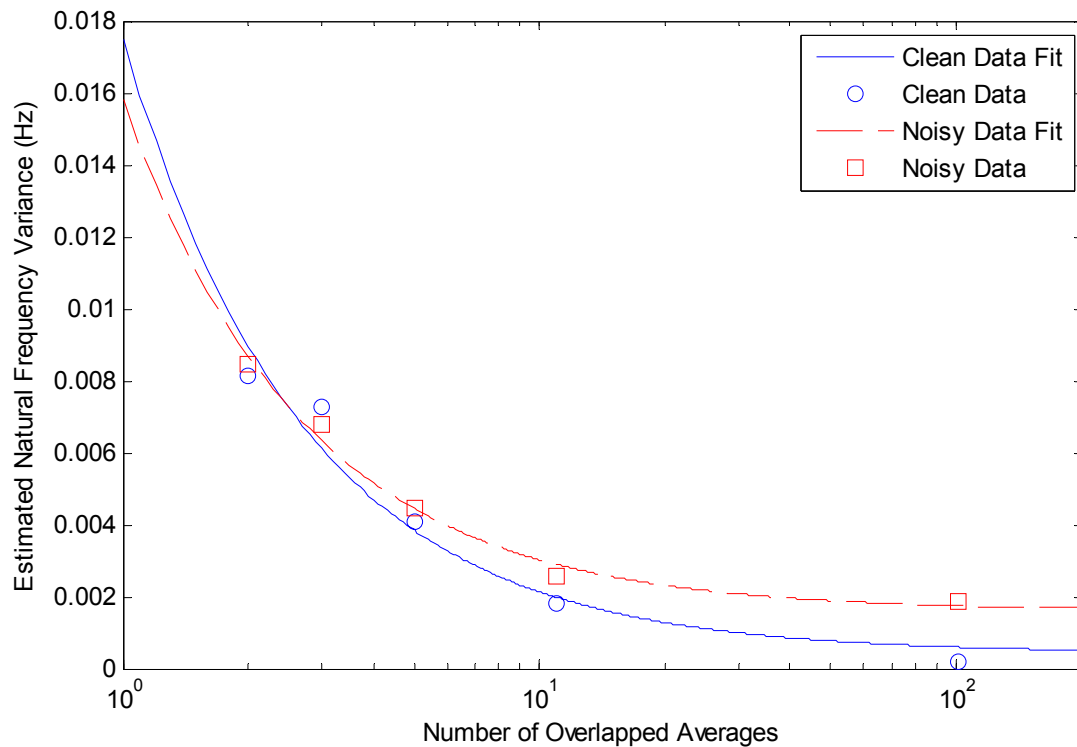


Figure 5-19: Influence of overlapped averaging on the natural frequency estimate variance with zero-applied ( $T_{sr} \times 16$ ).

## 5.4. CONCLUSIONS

When using FRFs to extract modal parameters, such as the natural frequency, with least-squares techniques, any variation in the FRF estimates can have a significant influence on the results. This is especially the case when small variations in the natural frequency need to be discerned continually, since the amount of data available to compute an accurate estimate of the system's FRF is limited. The variation in the FRF estimates can be significantly reduced by selecting suitable values for the analysis parameters, mainly sub-record length and number of averages. Further improvements can also be expected by making use of spectral enhancement techniques, specifically overlapped averaging and zero-padding.

This chapter presented results obtained from numerically simulated experiments aimed at evaluating the influence of several common analysis parameters and enhancement techniques including spectral averaging, sub-record length, averaging overlap percentage and zero-padding. The results show that these parameters and techniques have a significant influence on the extraction of natural frequency estimates from SDoF systems subjected to random excitation. It was found that, for records containing up to 10% extraneous noise, sub-record length, hence spectral resolution, has a more pronounced influence on the accuracy of modal parameter extraction than the level of spectral averaging, therefore spectral uncertainty.

It was also found that while zero-padding may not increase true spectral resolution, it does allow for improved natural frequency estimates with the introduction of interpolated estimates at the non-described frequencies. This enhancement can be exploited to maintain temporal resolution whilst minimising the level of natural frequency estimation uncertainty.

Finally, it was found that for modal parameter extraction purposes (in this case natural frequency), increased amounts of overlapped averaging can significantly reduce the variance of estimates obtained from curve-fitting FRF magnitude data. This is particularly useful as it allows for increased spectral accuracy without compromising temporal resolution.

Based on the findings of this research, it is recommended that, if the data available for analysis is random and limited, zero-padding and maximum overlap should always be applied when using FRF magnitude data (obtained using Fourier analysis) to extract estimates of natural frequency.

It was also found that, beyond a certain value, overlapped averaging has a diminishing return and should be limited in order to allow for a suitable sub-record length.

## REFERENCES

- Andreas, A 2006, *Digital signal processing: Signals, systems, and filters*, McGraw-Hill Professional, New York
- Avitabile, P 2006, '101 ways to extract modal parameters – which one is for me?', *Experimental techniques*, September/October, Society for Experimental Mechanics
- Baher, H 1990, *Analog & digital signal processing*, Wiley, Chichester, pp. 365-367.
- Bendat, J & Piersol, A 2000, *Random Data: Analysis and measurement procedures*, 3<sup>rd</sup> Edition, John Wiley & Sons, New York
- Burke-Hubbard, B 1998, *The world according to wavelets*, A. K. Peters, Natick
- Cannon, J & Dostrovsky, S 1981, *The evolution of dynamics: Vibration theory 1687 to 1742*, Springer-Verlag, New York
- Cooley, J & Tukey, J 1965, 'An algorithm for the machine computation of the complex Fourier series', *Mathematics of Computation*, vol. 19, pp. 297-301

- Crandall, S 1958, 'Mechanical vibrations with deterministic excitation', in S Crandall (ed), *Random vibration*, Wiley, London
- Douglas, E 1987, *Handbook of digital signal processing*, Elsevier Academic Press, pp. 722-723.
- Ewins, D 1995, *Modal testing theory and practice*, Research Studies Press, Taunton
- Gabor, D 1946, 'Theory of communication', *Journal of the Institution of Electrical Engineers 1889-1948*, Part 3, vol. 93, London, pp.429-457
- Garcia-Romeu-Martinez, M.A, Rouillard, V, Sek, M & Cloquell-Ballester, V.A. 2007, 'Monitoring the evolution of fatigue in corrugated paperboard under random loads', *Proceedings of the 5<sup>th</sup> BSSM international conference on advances in experimental mechanics*
- Harris, F 1978, 'On the use of windows for harmonic analysis with the discrete Fourier transform', *Proceedings of the IEEE*, vol. 66, no. 1, pp. 51-83
- Huang, N, Shen, Z, Long, S, Wu, M, Shih, H, Zheng, Q, Yen, N, Tung, C & Liu, H 1998, 'The empirical mode decomposition and the Hilbert spectrum for non-linear and non-stationary time series analysis', *Proceedings of the Royal Society*, The Royal Society, London, pp. 903-995
- Iglesias, A 2000, *Investigating various modal analysis extraction techniques to estimate damping ratio*, Mechanical engineering thesis, Virginia Polytechnic Institute and State University.
- Kay, S 1988, 'Spectral estimation', in J Lim & A Oppenheim (eds), *Advanced Topics in Signal Processing*, Prentice Hall, Englewood Cliffs
- Lyons, R 2004, *Understanding digital signal processing*, 2<sup>nd</sup> Edition, Prentice Hall, Upper Saddle River
- Manolakis, D, Ingle, V & Kogon, S 2005, *Statistical and adaptive signal processing: Spectral estimation, signal modeling, adaptive filtering, and array processing*, Artech House, Boston

- Maia, N, Silva, J, He, J, Lieven, N, Lin, R, Skingle, G, To, W & Urgueria, A 1997, 'Theoretical and Experimental Modal Analysis', Research studies press, Taunton
- Naidu, P 1996, *Modern spectrum analysis of time Series: Fast algorithms and error control techniques*, CRC Press, pp. 173-192
- Newland 1993, *An introduction to random vibrations, spectral and wavelet analysis*, 3<sup>rd</sup> Edition, Longman Scientific & Technical
- Norwood, C 1990, 'The use of vibration techniques in non-destructive testing', *Proceedings of the vibration and noise conference, 1990*, no. 90, The Institute of Engineers Australia, Barton, pp. 270-275
- Ott, L & Mendenhall, W 1990, *Understanding Statistics*, ed. 5, PWS-KENT Publishing, Boston
- Randall, R.B 1987, *Frequency analysis*, 3<sup>rd</sup> Edition, Brüel & Kjaer, Denmark, K Larson & Son
- Rao, S 2005, *Mechanical vibrations*, SI Edition, Prentice Hall
- Roberts, M 2004, *Signals and systems: analysis using transform methods and MATLAB*, McGraw-Hill Higher Education, London, pp. 541-542.
- Rouillard, V, Lamb, M & Sek, M 2007, 'Determining fatigue progression in corrugated paperboard containers subjected to dynamic compression', *Proceedings of the 5th Australasian congress on applied mechanics, ACAM 2007*, vol. 1, Engineers Australia, Brisbane, pp. 331-336
- Sek, M 2007, 'Numerical simulation of impacts involving a collapsible nonlinear multilayer structure', *Proceedings of the world conference of engineering*, London, pp. 1367-1372
- Semmlow, J 2005, *Circuits, signals and systems for bioengineers: A Matlab based introduction*, Academic Press, pp. 96-97
- Trethewey, M 2000, 'Window and overlap processing effects on power estimates from spectra', *Mechanical systems and signal processing*, vol. 14, no. 2, pp. 267-278

University of St. Andrews 1997, *Jean Baptiste Joseph Fourier*, viewed 7 August 2008, <  
<http://www-groups.dcs.st-and.ac.uk/~history/Printonly/Fourier.html>>

Weeks, M 2007, *Digital signal processing using Matlab and wavelets*, Infinity science press,  
Hingham, pp. 202-203

## Chapter 6 ADAPTIVE CONDITION ASSESSMENT

As demonstrated in the previous chapter, the Fourier transform requires a significant compromise between the accuracy of modal estimates and the rate at which they are made. This chapter discusses the development of a multi-resolution technique, which is designed to eliminate this compromise. The technique uses stochastic excitation and response data to continually determine the system's instantaneous impulse response function. The instantaneous impulse response functions are established using the coefficients of an adaptive digital filter and are used to continuously monitor shifts in the system's natural frequency.

### 6.1. MODAL PARAMETER EXTRACTION: FREE-RESPONSE

A system is said to undergo free vibrations when it oscillates under no external force other than an initial disturbance. Free vibrations are particularly useful in modal analysis applications where their transient decay and oscillation frequency can be used to extract the fundamental modal parameters, natural frequency and damping ratio. Many practical vibratory arrangements, such as that used during the evaluation of protective packaging systems (as discussed in Chapter 2), can be modelled as an equivalent viscously damped, single degree-of-freedom (SDoF) system (Rao 2005, 106-132). When subjected to an initial disturbance viscously damped systems return one of three different forms of transient response, each of which is dependent of the level of damping within the system. A system is said to be underdamped if its damping ratio is less than 1 (Rao 2005, p. 141), critically damped if its damping ratio is equal to 1 or overdamped if it is greater than 1 (Jackson 1991, pp. 243-246; Rao 2005, pp. 142-146). The response for each level of damping is illustrated in *Figure 6-1*. As most protective packaging systems are underdamped, the research presented herein will only discuss viscously, underdamped linear SDoF systems.

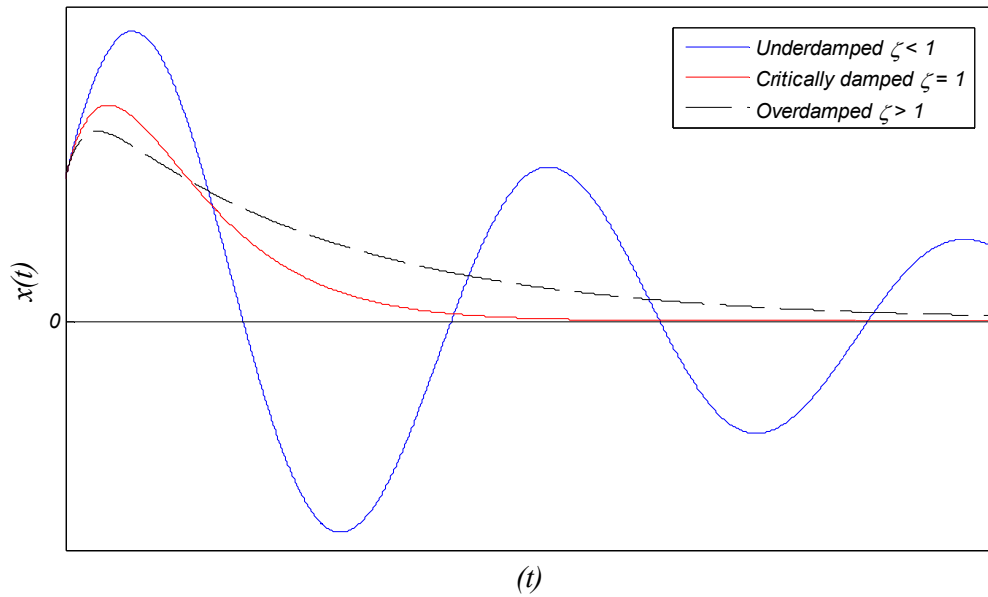


Figure 6-1: Comparison of overdamped, critical and underdamped response (Rao 2005, p.145).

Before discussing the modal parameter extraction techniques available for viscous, underdamped free-response systems, it is necessary to understand their transient decay. Starting with the free-body diagram of a free-response system in Figure 6-2 it can be seen that the motion of the system can be described using Equation 6-1.

$$m\ddot{x} + c\dot{x} + kx = 0 \tag{6-1}$$

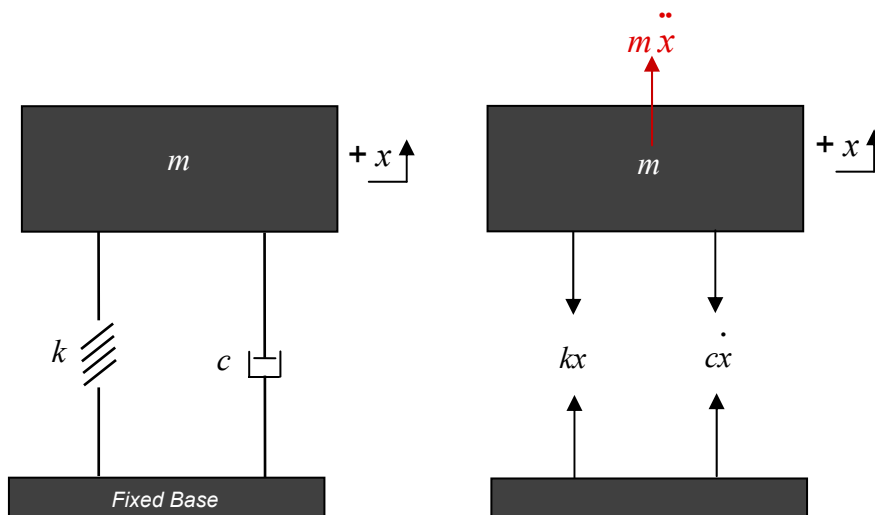


Figure 6-2: Free vibration free-body diagram.

If it is assumed that the solution to Equation 6-1 is of the form  $x(t) = Ce^{st}$  it becomes

$$\begin{aligned} ms^2Ce^{st} + csCe^{st} + kCe^{st} &= 0 \\ \rightarrow ms^2 + cs + k &= 0, \end{aligned} \quad (6-2)$$

the roots of which are

$$s_{1,2} = \frac{-c \pm \sqrt{c^2 - 4mk}}{2m} \quad (6-3)$$

These roots lead to the following solutions of Equation 6-2 (Rao 2005, p. 140):

$$x_1(t) = C_1e^{s_1t} \text{ and } x_2(t) = C_2e^{s_2t}, \quad (6-4)$$

which give the general equation of motion

$$x(t) = C_1e^{s_1t} + C_2e^{s_2t}, \quad (6-5)$$

where  $s_1$  and  $s_2$  are known from Equation 6-3 and  $C_1$  and  $C_2$  can be determined from the initial conditions of the system.

If the damping ratio  $\zeta$  and natural frequency  $\omega_n$  are substituted into Equation 6-5 in place of the mass, stiffness and damping ( $m$ ,  $k$  and  $c$ ) the equation becomes (Rao 2005, p. 141)

$$x(t) = C_1e^{(-\zeta + \sqrt{\zeta^2 - 1})\omega_n t} + C_2e^{(-\zeta - \sqrt{\zeta^2 - 1})\omega_n t} \quad (6-6)$$

For underdamped systems the roots become complex and Equation 6-6 is written as

$$\begin{aligned} x(t) &= C_1e^{(-\zeta + i\sqrt{1-\zeta^2})\omega_n t} + C_2e^{(-\zeta - i\sqrt{1-\zeta^2})\omega_n t} \\ &= e^{-\zeta\omega_n t} \left[ (C_1 + C_2) \cos \sqrt{1-\zeta^2} \omega_n t + (C_1 - C_2) \sin \sqrt{1-\zeta^2} \omega_n t \right] \\ &= e^{-\zeta\omega_n t} \left[ C'_1 \cos \sqrt{1-\zeta^2} \omega_n t + C'_2 \sin \sqrt{1-\zeta^2} \omega_n t \right] \end{aligned} \quad (6-7)$$

By entering the initial conditions  $x(t=0) = x_0$  and  $\dot{x}(t=0) = \dot{x}_0$  Equation 6-7 becomes

$$x(t) = e^{-\zeta\omega_n t} \left[ x_0 \cos \sqrt{1-\zeta^2} \omega_n t + \frac{\dot{x}_0 + \zeta\omega_n x_0}{\sqrt{1-\zeta^2} \omega_n} \sin \sqrt{1-\zeta^2} \omega_n t \right] \quad (6-8)$$

The main properties of the free-response described by Equation 6-8 are illustrated in *Figure 6-3*. In sections 6.1.1 and 6.1.2 it will be shown how these properties can be manipulated to extract the desired modal information.

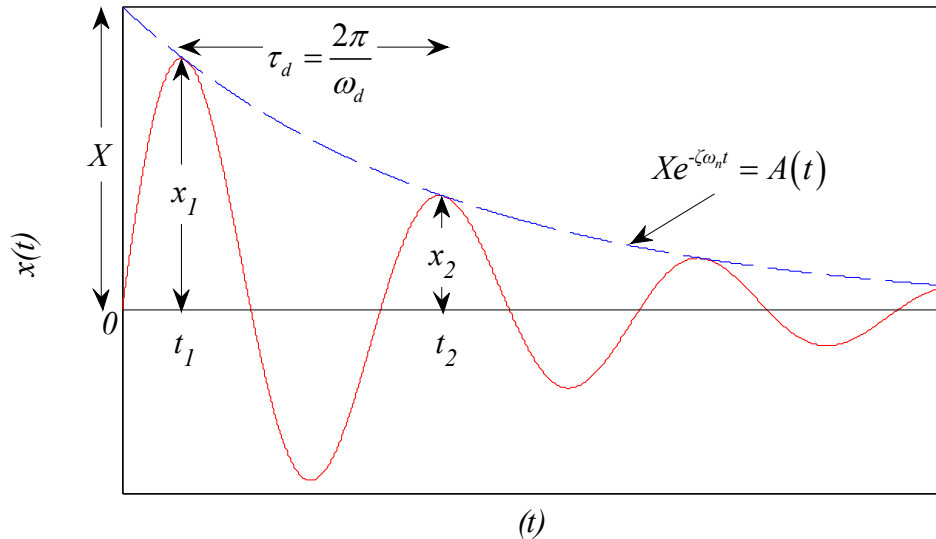


*Figure 6-3: Free vibration response of a viscously underdamped SDoF system (Reproduced from: Rao 2005, p. 143).*

### 6.1.1. Logarithmic Decrement Technique

The logarithmic decrement technique is possibly the most commonly used method for extracting damping estimates from time domain free-response data. Logarithmic decrement,  $\delta$  is the rate at which the amplitude of vibration decreases and is defined as the natural logarithm of two successive peaks (Rao 2005, p. 146). Often it is desirable to estimate an average logarithmic decrement over  $m$  cycles, which can be achieved by implementing Equation 6-9 (Rao 2005, p. 148; Smith & Wereley 1997).

$$\delta = \ln\left(\frac{x_i}{x_{i+1}}\right) = \frac{1}{m} \ln\left(\frac{x_i}{x_{i+m}}\right) \quad (6-9)$$

Using Equation 6-9 the damping ratio can be calculated as (Rao 2005, p. 147; Smith & Wereley 1997)

$$\zeta = \frac{\delta}{\sqrt{\delta^2 + 4\pi^2}} \quad (6-10)$$

The system's natural frequency can be determined using its damping ratio and damped natural frequency  $\omega_d$  (obtained using zero crossings in the free-response signal) and Equation 6-11.

$$\omega_n = \frac{\omega_d}{\sqrt{1-\zeta^2}} \quad (6-11)$$

### 6.1.2. Hilbert Envelope Technique

An alternative to the logarithmic decrement technique is the Hilbert envelope technique, which makes use of the instantaneous properties of the free-response data.

In contrast to the logarithmic decrement damping estimation procedure, the Hilbert envelope technique makes use of the entire transient signal using the Hilbert transform.

The Hilbert transform of a real-valued time signal, such as the free-vibration response  $x(t)$  is defined as (Bendat & Piersol 2000, p. 518; Thrane 1984, p. 5).

$$\mathcal{H}[x(t)] = \tilde{x}(t) = \frac{1}{\pi} \int_{-\infty}^{\infty} \frac{x(\tau)}{t-\tau} d\tau = \frac{1}{\pi} x(t) * \frac{1}{t} \quad (6-12)$$

The application of Equation 6-12 creates 90° phase shift in the signal under analysis. This phase shift is used to create a complex analytic signal  $z(t)$ , which is defined as follows:

$$z(t) = x(t) + j\tilde{x}(t) = A(t)e^{j\phi(t)}, \quad (6-13)$$

where  $A(t)$  and  $\phi(t)$  are the signal's envelope and instantaneous phase, respectively.

These parameters can be determined using Equations 6-14 and 6-15, respectively.

$$A(t) = \sqrt{x^2(t) + \tilde{x}^2(t)} \quad (6-14)$$

$$\phi(t) = \arctan \left[ \frac{\tilde{x}(t)}{x(t)} \right] \quad (6-15)$$

The system's "instantaneous natural frequency",  $\omega_0$  (Bendat & Piersol 2000, p. 512; Huang *et al.* 1998; Thrane 1984, p. 10) can be determined using Equation 6-16.

$$\omega_0(t) = \frac{d\phi(t)}{dt} \quad (6-16)$$

Given that, for a constant parameter system  $\omega_0$  is constant, the damped natural frequency of a time invariant SDoF system can be determined by calculating the gradient of the unwrapped instantaneous phase vector  $\phi(t)$ .

Now that the damped natural frequency has been determined it is a matter of calculating the damping ratio and, hence, the natural frequency.

It is known that the envelope of the analytic signal is defined by

$$Xe^{-\zeta\omega_n t} = A(t) \quad (6-17)$$

By taking the natural logarithm of both sides of Equation 6-17 it becomes

$$\ln(X) - \zeta\omega_n t = \ln[A(t)], \quad (6-18)$$

which is a linear equation with a maximum value of  $X$  and gradient of  $-\zeta\omega_n$ .

Given that

$$\frac{d}{dt}(\ln[A(t)]) = -\zeta\omega_n = -\zeta \frac{\omega_d}{\sqrt{1-\zeta^2}} \quad (6-19)$$

$$\zeta = \pm \frac{\sqrt{\left[\frac{d}{dt}(\ln[A(t)])\right]^2}}{\sqrt{\omega_d^2 + \left[\frac{d}{dt}(\ln[A(t)])\right]^2}} \quad (6-20)$$

Since negative values of damping are illogical,

$$\zeta = \frac{\sqrt{\left[\frac{d}{dt}(\ln[A(t)])\right]^2}}{\sqrt{\omega_d^2 + \left[\frac{d}{dt}(\ln[A(t)])\right]^2}} \quad (6-21)$$

Once the damping ratio is obtained, the natural frequency can be estimated using Equation 6-6-19 or using the system's damped natural frequency (Equation 6-11).

The Hilbert envelope technique has a significant benefit over the logarithmic decrement/zero-crossings technique in that it allows the entire transient response to be used as opposed to a select group of points. This attribute is particularly useful when analysing noise contaminated signals which have peaks and zero crossings that are difficult to locate.

A further advantage of the technique is that it leaves the signal in the time domain as opposed to converting it to the frequency domain. This means that fine spectral resolution can be achieved irrespective of the length of data analysed, a feature which is not shared by parameter extraction techniques which rely on the Fourier transform.

## 6.2. NONSTATIONARY FORCED EXCITATION/RESPONSE

The modal parameter extraction techniques discussed so far are only suitable for the analysis of free-response data obtained from time invariant systems. Therefore, for these methods to be applicable to the continuous structural integrity assessment of systems subjected to random loads (excitation), a technique for converting nonstationary forced excitation and response data into a series of stationary free-response signals is required. The following sections (6.2.1 and 6.2.2) discuss the development of such a technique.

### 6.2.1. Impulse Response Functions and Finite-Impulse-Response Filters

The dynamic characteristics of a time-invariant linear system can be described using its impulse response function  $h(\tau)$ . Impulse response functions can be used to determine a system's response  $y(t)$  for any arbitrary excitation  $x(t)$  using the convolution integral shown in Equation 6-22 (Refer to section 5-2 for greater detail).

$$y(t) = \int_0^{\infty} h(\tau)x(t-\tau)d\tau \quad (6-22)$$

In most practical applications, only a finite portion ( $t - T_{IR} \rightarrow t$ ) of the impulse response function is seen as significant in terms of magnitude (Smith & Wereley 1997). Therefore, as a result of their insignificant influence, the contribution of inputs older than  $t - T_{IR}$  can be approximated to zero.

This means that, for discretely sampled time signals Equation 6-22 can be estimated using

$$y(t) = \sum_{k=1}^M h_k x \left[ t - \left( \frac{k-1}{f_s} \right) \right], \quad (6-23)$$

where  $k$  represents the number of each discretely sampled point of the impulse response function and  $M$  represents the total number of points required to span the interval  $t - T_{IR} \rightarrow t$ .

From Equation 6-23 it becomes apparent that the relationship between excitation and response can be established using a digital finite-impulse-response (FIR) filter. With the implementation of an FIR filter, the system's discretely sampled FIR function is represented by a vector of constants called filter tap coefficients. FIR filters work by multiplying a vector of the most recent  $M$  data samples by the filter tap coefficients, and summing the elements of the resulting vector, as illustrated in *Figure 6-4*. The calculation of the present value of the response sequence requires the current value and the previous  $M - 1$  values of the excitation sequence. The calculation of each consecutive response point requires the values of the excitation sequence from the proceeding step to be shifted one space to the right, with the oldest value being discarded at each update.

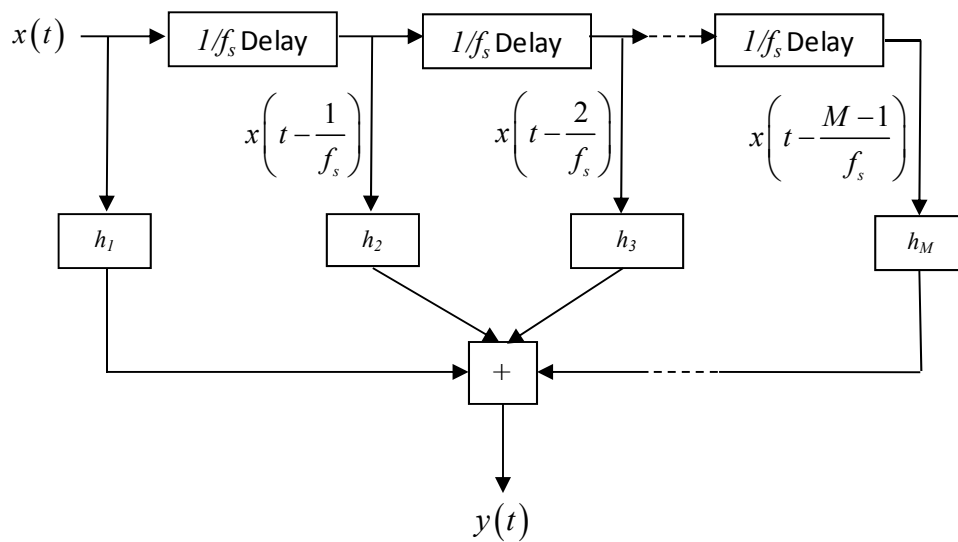


*Figure 6-4: FIR filter schematic.*

With an understanding of digital FIR filters it becomes apparent that, if the excitation and response are both known, a form of adaptation can be implemented to track the filter tap coefficients and, hence, the instantaneous FIR functions of either time variant or invariant systems.

## 6.2.2. Least-Mean-Square Adaptive Filters

Adaptive filters were first established in the late 1950s, when numerous researchers were working independently on the development and implementation of a number of adaption algorithms (Haykin 2003, p. xi). One of these techniques is the least-mean-square (LMS) algorithm of Widrow & Hoff (1960), which can be described as a stochastic gradient algorithm in that its adaptation is dependent on the instantaneous gradient of an error signal (Haykin 2003, p. xi).

A description of the LMS algorithm is achieved by first considering the adaptive filter in *Figure 6-5*. As can be seen the adaptive filter consists of two parts: 1) an FIR filter with adjustable tap coefficients, whose values at time  $n$  are denoted by  $h_1(n)$ ,  $h_2(n)$ , ...,  $h_M(n)$ , and 2) an LMS adaptation mechanism for adjusting the filter tap coefficients to minimise the difference  $e(n)$  between the actual response  $y(n)$  and its filtered estimate  $\hat{y}(n|\mathcal{X}_n)$ , where  $\mathcal{X}_n$  is the space spanned by the tap input vector (system excitation)  $x(n)$  to  $x(n-M+1)$ . This adaptation is achieved by minimising the mean squared error  $J(n)$ .

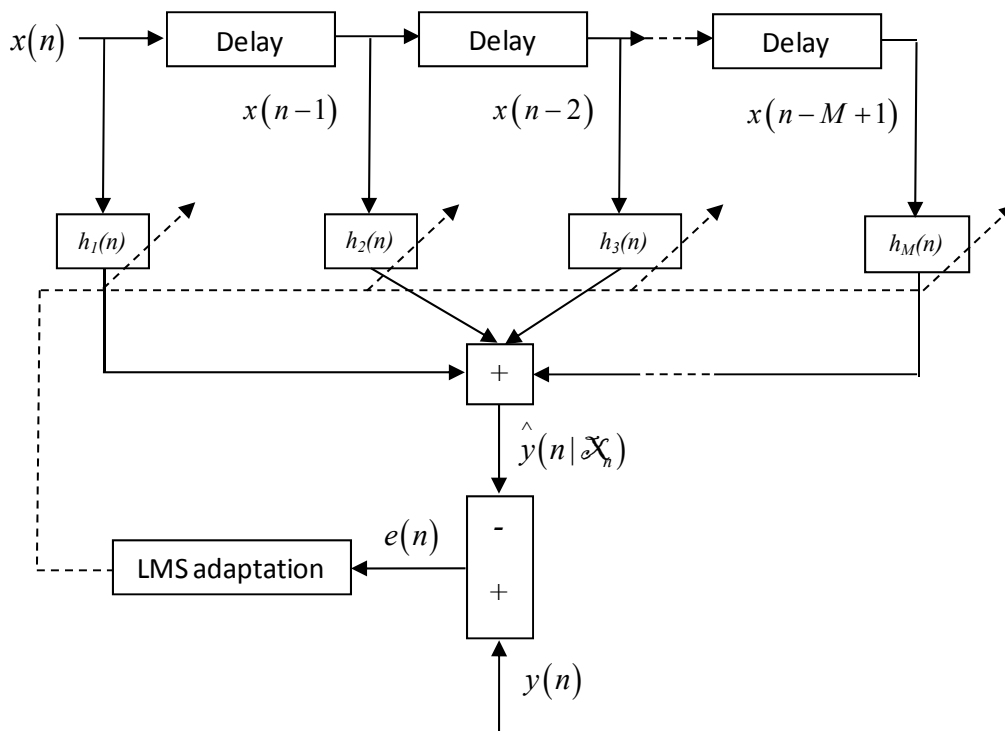


*Figure 6-5: Adaptive FIR filter schematic.*

Haykin (1986, p. 196) shows that, when the input tap and the desired response vectors are jointly stationary the mean squared error can be represented as

$$J(n) = \sigma_y^2 - \mathbf{h}^H(n) \mathbf{p} - \mathbf{p}^H \mathbf{h}(n) + \mathbf{h}^H(n) \mathbf{R} \mathbf{h}(n), \quad (6-24)$$

*Note: Bold face used to indicate vectors*

where  $\sigma_y^2 = \text{variance of } y(n)$

$\mathbf{p}$  = cross-correlation vector between the tap input vector  $\mathbf{x}(n)$  and the desired response  $y(n)$

$\mathbf{R}$  = correlation matrix of the tap input vector  $\mathbf{x}(n)$

Equation 6-24 returns a parabolic bowl shaped surface, commonly known as the error performance surface. The error performance surface has a single minimum which the adaptation process continually searches for in order to find the optimum filter tap coefficient vector  $\mathbf{h}_0$ . This vector can be determined by setting the derivative of Equation 6-24 to zero. Widrow & Stearns (1985, p. 21) and Haykin (1986, pp. 107 – 108) show that the derivative of Equation 6-24 is

$$\nabla = \frac{dJ(\mathbf{h})}{d\mathbf{h}} = 2\mathbf{R}\mathbf{h} - 2\mathbf{p} \quad (6-25)$$

If  $\nabla$  is set to zero, it is evident that the optimum filter tap vector can be determined using

$$\mathbf{h}_0 = \mathbf{R}^{-1} \mathbf{p} \quad (6-26)$$

Solving Equation 6-26 using an analytical method is known to present computational difficulties when the number of filter tap coefficients is large and the data sampling rate is high (Haykin 1986, p. 197). An approach which reduces these difficulties is the method of steepest decent. This method employs the following four steps (Haykin 1986, p. 197-199):

1. Make an arbitrary initial estimate of the optimum filter tap coefficient vector (generally zeros)
2. Calculate the gradient of the mean squared error at the initial estimate
3. Compute the next estimate by making a change in the initial or present estimate in the opposite direction to the gradient vector from step 2
4. Repeat steps 2 to 4 until the optimum is found

The method of steepest decent calculates the updated filter tap coefficients at time  $n + 1$  using the following recursion equation (Haykin 1986, p. 198):

$$\mathbf{h}(n+1) = \mathbf{h}(n) + \frac{1}{2} \mu [-\nabla(n)], \quad (6-27)$$

where  $\mu$  is a real valued constant known as either the step-size parameter or the weighting constant.

When the right hand side of Equation 6-25 is substituted into Equation 6-27 the equation becomes

$$\mathbf{h}(n+1) = \mathbf{h}(n) + \mu [\mathbf{p} - \mathbf{R}\mathbf{h}(n)] \quad (6-28)$$

If exact measurements of the gradient vector could be made at each iteration, the method of steepest decent could be used to determine the optimum solution. However, in practice exact measurements of the gradient vector are not available. Therefore, a technique which allows for the estimation of the gradient vector is required. The LMS algorithm is such a technique. The LMS technique estimates the gradient vector using instantaneous values of  $\mathbf{R}$  and  $\mathbf{p}$ , which Haykin (1986, p. 216) defines as follows:

$$\hat{\mathbf{R}}(n) = \mathbf{x}(n) \mathbf{x}^H(n) \quad (6-29)$$

$$\hat{\mathbf{p}}(n) = \mathbf{x}(n) y^*(n) \quad (6-30)$$

These values, when substituted into Equation 6-28, give the LMS filter tap coefficient algorithm

$$\hat{\mathbf{h}}(n+1) = \hat{\mathbf{h}}(n) + \mu \mathbf{x}(n) \left[ y^*(n) - \mathbf{x}^H(n) \hat{\mathbf{h}}(n) \right], \quad (6-31)$$

where the hat over symbol,  $\hat{\mathbf{h}}$ , is used to distinguish the LMS algorithm from the method of steepest decent.

Through the observation of Equation 6-31 it becomes apparent that the step-size parameter controls the size of the incremental correction applied to the filter tap coefficients. As may be expected, the use of small step-sizes means that the rate of convergence is reduced. However, the converged solution will have a small excess mean-squared (steady-state) error as a result of the large amount of data used to estimate the gradient vector provided that the system is stationary. Conversely, when the step-size is large the rate of convergence is increased at the expense of precision (Haykin 1986, p. 238). As well as the increased steady-state error introduced with the application of large step-sizes, the stability of the LMS algorithm may also be compromised.

According to Haykin (1986, p. 239), in order to ensure stability, the step-size must conform to the following condition:

$$0 < \mu < \frac{2}{\sum_{i=1}^M \lambda_i}, \quad (6-32)$$

where  $\lambda_i$  represents the  $i^{\text{th}}$  eigenvalue of the correlation matrix

### 6.2.2.1. LMS algorithm for nonstationary systems

In the case of continuous structural integrity assessment, a technique which can provide instantaneous estimates of a system's continuously changing characteristics is required.

If the system varies continuously the adaptive filter needs to not only seek the minimum point on the error performance surface, but also track the continually changing position of this point. The LMS algorithm is capable of performing such a task; however, the shifting of the optimal filter coefficients sees the introduction of a coefficient vector lag. This lag increases what is known as the misadjustment.

Misadjustment is a dimensionless measure of how far, on average, the optimal finite solution deviates from the true optimal (Weiner) solution (Widrow & Kamenetsky 2003, p. 8). For stationary systems the misadjustment results purely from gradient noise during adaptation

and can be reduced by adapting more slowly (Widrow & Kamenetsky 2003, p. 16). However, in a nonstationary environment the total misadjustment becomes the sum of the misadjustment due to gradient noise and the misadjustment due to lag, with the later being a result of adapting too slowly (Widrow & Kamenetsky 2003, p. 16; Haykin 1986, pp. 251-254). According to Haykin (1986, p. 254) and Widrow & Kamenetsky (2003, p. 17), the misadjustment due to gradient noise is directly proportional to the step-size whereas the misadjustment due to lag is inversely proportional to the step-size. This means that for nonstationary processes, the optimum step-size occurs when the contribution of the misadjustments are equal as shown in *Figure 6-6*. This optimum shows the importance of choosing the correct step-size when analysing nonstationary systems.

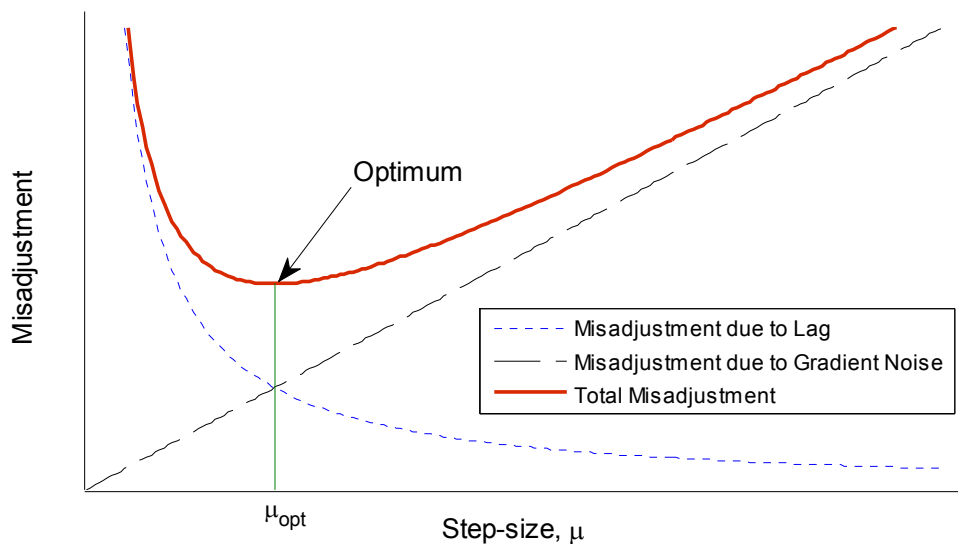


*Figure 6-6: Total misadjustment and the optimum step-size (Reproduced from Haykin 1986, p. 254).*

### 6.2.2.2. Normalised LMS (NLMS) algorithm

In its standard form the corrections applied by the LMS algorithm during adaptation are directly proportional to the tap input vector from the preceding iteration. As a result of this dependency, large tap input vectors cause the LMS algorithm to suffer from gradient noise amplification (Haykin 1996, pp.432-433), which in turn limits the robustness and convergence capabilities of the algorithm. In order to limit the effect of gradient noise amplification a modification to the LMS algorithm, commonly known as the normalised LMS (NLMS) algorithm, is often applied. The NLMS algorithm normalises the corrections applied with respect to the Euclidean norm of the preceding tap input vector. This is, effectively, achieved by dividing the corrections by the square of the Euclidean norm of the preceding tap input vector (Refer to Haykin 1996, p.433-436 for a rigorous derivation), which results in the following algorithm:

$$\hat{\mathbf{h}}(n+1) = \hat{\mathbf{h}}(n) + \frac{\mu_N \mathbf{x}(n)}{\|\mathbf{x}(n)\|^2} \left[ y^*(n) - \mathbf{x}^H(n) \hat{\mathbf{h}}(n) \right], \quad (6-33)$$

where the subscript,  $N$ , is used to distinguish the dimensionless adaptation constant,  $\mu_N$ , of the NLMS algorithm from the inverse power step-size,  $\mu$ , of the standard LMS algorithm.

Interestingly, in overcoming the gradient noise amplification problem the NLMS technique introduces difficulties when the input tap vector is small. These difficulties are purely a result of dividing by near zero (or zero) squared norm values and are generally overcome by adding a small positive constant  $a$  to the denominator of Equation 6-33 (Haykin 1996, p. 437). With this addition Equation 6-33 becomes

$$\hat{\mathbf{h}}(n+1) = \hat{\mathbf{h}}(n) + \frac{\mu_N \mathbf{x}(n)}{a + \|\mathbf{x}(n)\|^2} \left[ y^*(n) - \mathbf{x}^H(n) \hat{\mathbf{h}}(n) \right] \quad (6-34)$$

The introduction of the squared norm term effectively creates an LMS adaptation with a time varying step-size of

$$\mu = \frac{\mu_N \mathbf{x}(n)}{a + \|\mathbf{x}(n)\|^2} \quad (6-35)$$

Through the implementation of this normalised step-size the NLMS algorithm allows for the updated weight vector to be determined using a minimum change (minimal disturbance) in relation to the Euclidean norm and most importantly provides the potential for improvements to the rate of convergence.

With the changes to the step-size parameter a corresponding change in stability conditions is also introduced. According to Haykin (1996, p. 437) the stability condition of the NLMS algorithm is as follows:

$$0 < \mu_N < 2 \quad (6-36)$$

### 6.2.2.3. Leaky LMS Algorithm

In some applications, the implementation of the standard LMS algorithm can be problematic (Mayyas & Aboulnasr 1997; Hakansson 2004). Therefore, in order to improve the applicability of the LMS adaptation, a modified version of the algorithm known as the leaky LMS algorithm was introduced (Widrow & Stearns 1985, pp. 376-379). The modification introduced is a leakage factor,  $(1 - \mu\alpha)$ . With the introduction of this factor the standard and normalised LMS algorithms become Equations 6-37 and 6-38, respectively.

$$\hat{\mathbf{h}}(n+1) = \hat{\mathbf{h}}(n)(1 - \mu\alpha) + \mu\mathbf{x}(n) \left[ y^*(n) - \mathbf{x}^H(n)\hat{\mathbf{h}}(n) \right] \quad (6-37)$$

$$\hat{\mathbf{h}}(n+1) = \hat{\mathbf{h}}(n)(1 - \mu_N\alpha) + \frac{\mu_N\mathbf{x}(n)}{a + \|\mathbf{x}(n)\|^2} \left[ y^*(n) - \mathbf{x}^H(n)\hat{\mathbf{h}}(n) \right] \quad (6-38)$$

Hassibi (2003, p.137-143) shows that the inclusion of the leakage term in the LMS algorithm makes the adaptation technique particularly well suited to tracking nonstationaries. This potential increase in tracking ability may prove to be particularly significant when using LMS adaptation for continuous structural integrity assessment, which requires the continuous monitoring of variations in modal parameters and, hence, nonstationaries.

### 6.2.3. SUMMARY OF LEAKY, NLMS ADAPTATION FOR MODAL PARAMETER ESTIMATION

The preceding sections have discussed how adaptive filters can be used to extract instantaneous impulse response functions from systems with time varying characteristics. Modal parameter estimation from free-response data using the Hilbert transform was also briefly mentioned.

A summary of the process developed for extracting instantaneous estimates of natural frequency and damping using the described adaptive FIR approach is given in *Figure 6-7*.

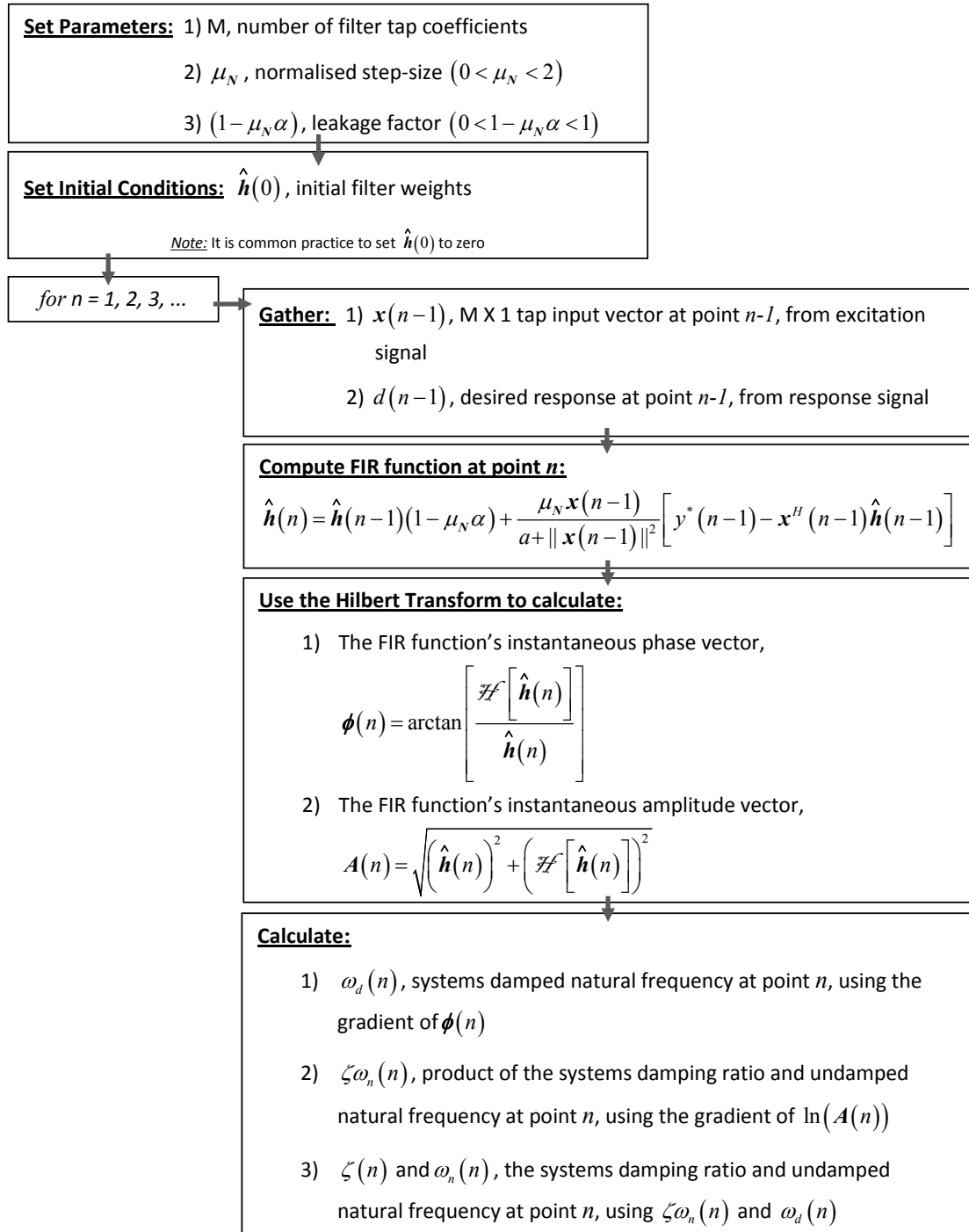


Figure 6-7: NLMS adaptive modal parameter estimation algorithm.

One noteworthy point is that, when extracting the damped natural frequency, large noise amplification is introduced if the instantaneous phase vector is differentiated directly. This problem can be avoided by fitting a linear trend directly to the unwrapped instantaneous phase vector and using the gradient of the trend to estimate the damped natural frequency. Figure 6-8 and Figure 6-9 present the results obtained from data (gathered from the analysis of a numerically simulated SDoF system) containing 10% extraneous noise by directly

differentiating the instantaneous phase vector and utilising a linear fit to obtain estimates of damped natural frequency, respectively.

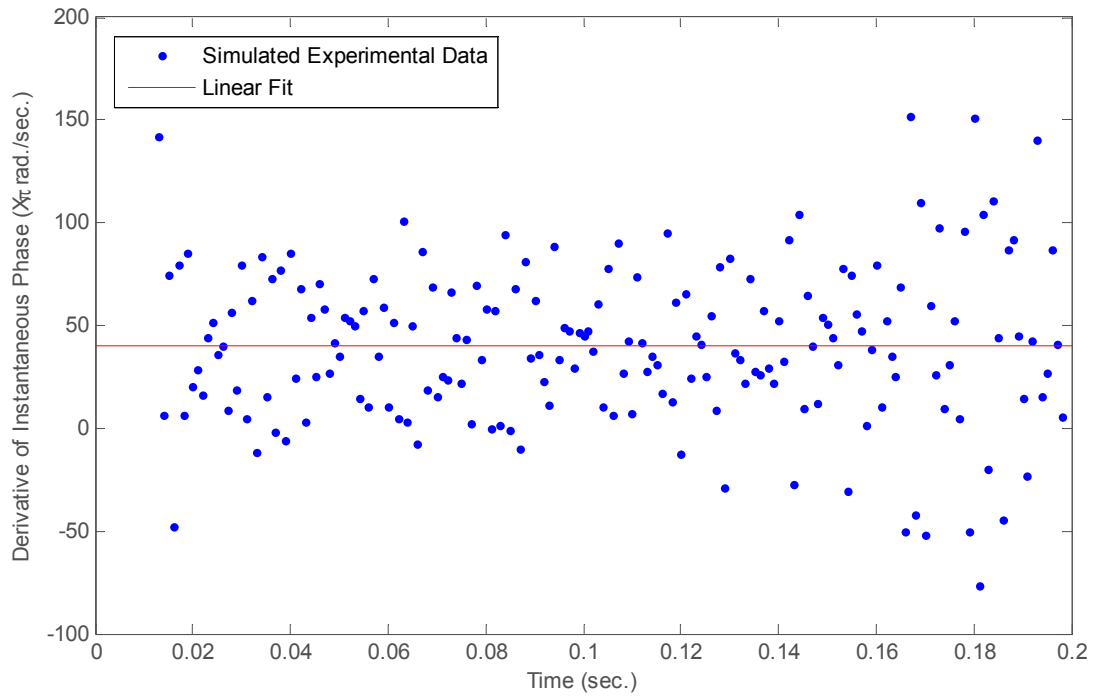


Figure 6-8: Technique one, mean of the derivative of the  $n^{\text{th}}$  instantaneous phase vector.

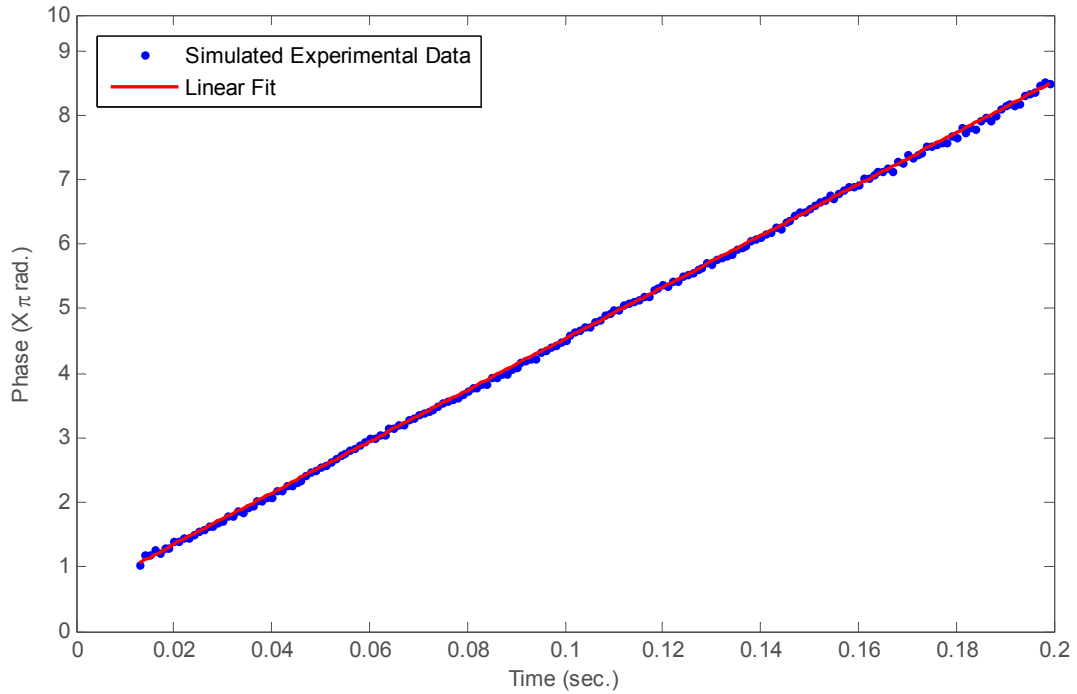


Figure 6-9: Technique two, polynomial fit of the  $n^{\text{th}}$  instantaneous phase vector.

### 6.2.3.1. Further Enhanced Curve-fitting

Two different parameter extraction techniques have so far been discussed; one technique uses zero crossings and logarithmic decrement while the other makes use of the Hilbert transform. In this section the development of a third technique, which allows for parameters to be estimated using the curve-fit of a sinusoidal wave is introduced. The technique starts by normalising the system's  $n^{th}$  FIR function (by dividing it by its instantaneous amplitude, which is obtained using the Hilbert transform) which results in a sinusoid with an amplitude of unity. Once the sinusoid is obtained, a least-squares regression technique can be applied to estimate the system's damped natural frequency by means of curve-fitting. The 'nlinfit' function available in the Matlab® Statistics Toolbox™ was used as the curve-fitting algorithm throughout this study. This algorithm is a nonlinear regression technique which iteratively reweights response values and recomputes a least-squares fit. Preliminary experiments showed that the technique is robust and insensitive to appropriate variations to the regression parameters (the default values work quite well, however, the author increased the maximum number of iterations allowed from 100 to 500 and reduced the termination tolerances from  $1 \times 10^{-8}$  to  $1 \times 10^{-20}$ ). In order to avoid aliasing of the curve-fit, the sinusoid technique requires an initial estimate of natural frequency. Such an estimate can be obtained using the value of damped natural frequency obtained using the instantaneous phase vector. The sinusoid approach provides benefits over the linear fit of the instantaneous phase vector when noise contaminated (or corrupt) data is present. *Figure 6-10* and *Figure 6-11*, which present the results obtained from a FIR function with an exaggerated percentage of noise contaminated (data with a low signal to noise ratio) data, show how the sinusoid approach is able to correctly fit the non-contaminated portion of the data while the instantaneous phase technique is not. This type of noise contaminated data can be avoided by narrowing the range of data used for curve-fitting; however, since continuous structural health monitoring techniques rely on the automated fitting of experimental data (in which the range appropriate for curve-fitting may vary), the sinusoid approach may provide significant benefits. Throughout this study both the sinusoidal and linear curve-fitting techniques will be applied and the results with the least variance will be presented. This is because the sinusoid approach may be limited when analysing FIR signals which have limited data available for curve-fitting, such as those obtained from signals with high damping.

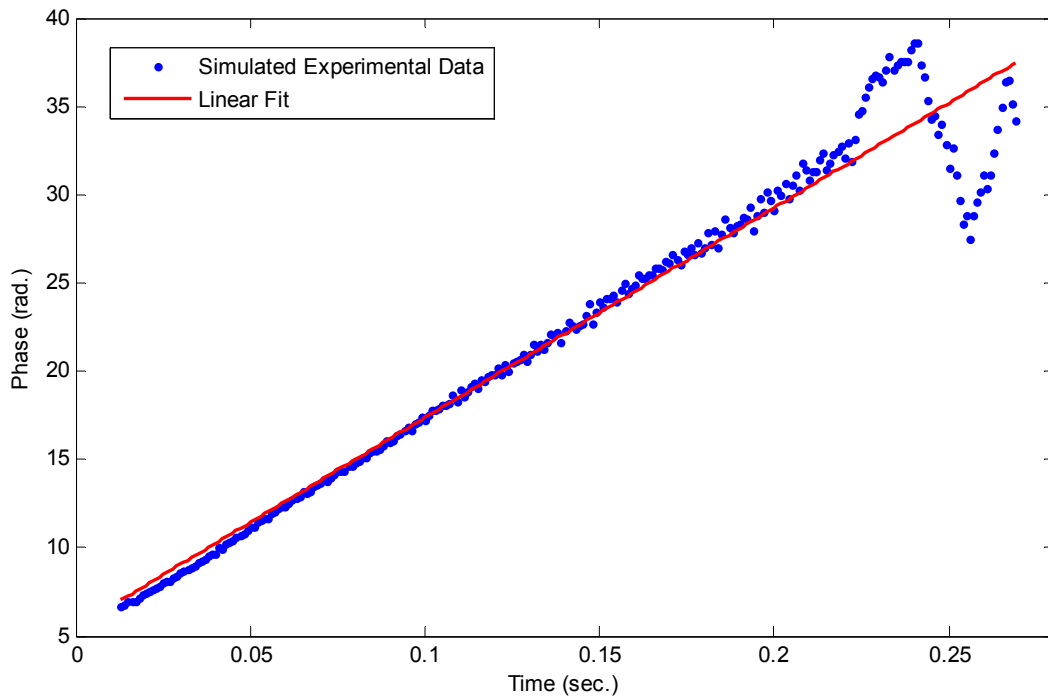


Figure 6-10: Phase curve-fit with contaminated data.

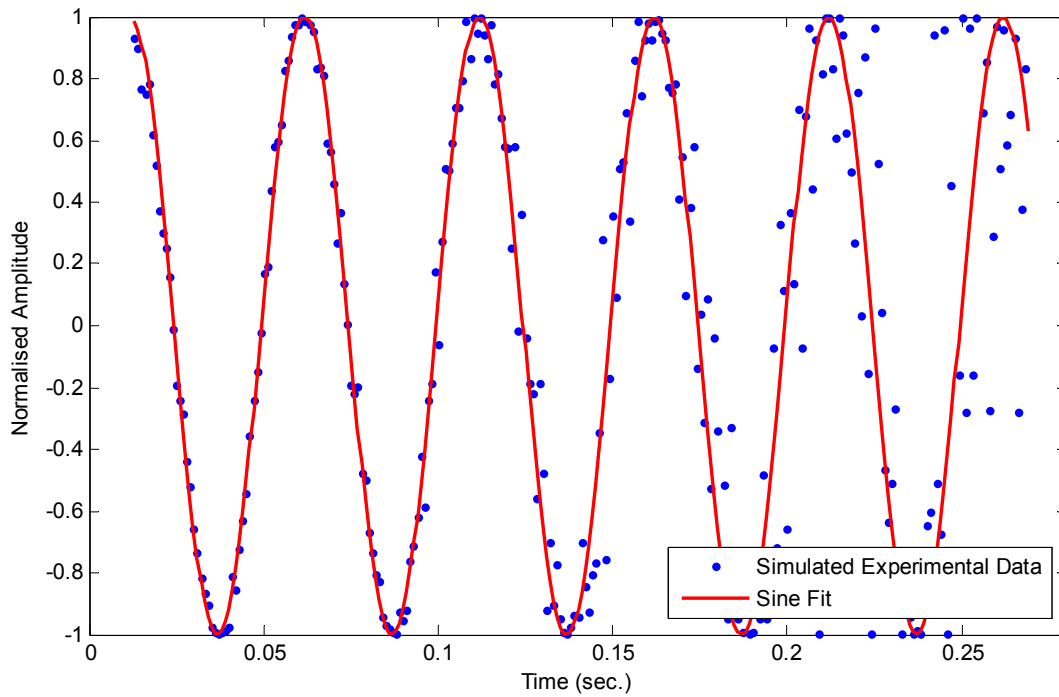


Figure 6-11: Sinusoidal curve-fit with contaminated data.

## 6.2.4. EXPERIMENTAL EVALUATION OF ADAPTIVE FINITE-IMPULSE-RESPONSE PARAMETERS

The selection of optimum analysis parameters for modal parameter extraction using the aforementioned adaptive algorithm is far from trivial. It requires a thorough understanding of each parameter in order to ensure that the correct choices have been made. This section discusses the influence of the parameters required when implementing the leaky, NLMS modal parameter extraction algorithm. These parameters include:

- Normalised step-size  $\mu_N$
- Leakage factor  $(1 - \mu\alpha)$
- Initial filter weights  $\hat{\mathbf{h}}(0)$
- Number of required filter tap coefficients

Each section will include numerically simulated experiments which make use of the simulation tool described in chapter 4 (Methodology) of this study.

### 6.2.4.1. Evaluation of the normalised step-size and leakage factor

In order to evaluate the performance and limitations of the adaptive FIR technique, for monitoring variations in the modal characteristics of systems, numerical SDoF systems, with their mass, stiffness and damping configured to achieve an arbitrary undamped natural frequency of 20Hz and a damping ratio of 11% prior to damage (resulting in a damped natural frequency of 19.88 Hz), were analysed. Damage was simulated by introducing a sudden reduction in stiffness at an arbitrary time (10% at 15 seconds in this instance). Step changes are used as they represent the most rapid variation in a system's properties and are therefore the most difficult to monitor. The leakage factor was initially set to 1 (i.e. no leakage) and the initial filter tap coefficients were all set to zero (which is common practice, Haykin 1986, p. 237). The length of the filter tap coefficient vector was set so as to cover the duration of the FIR function which was of significant amplitude (data above the background noise). Results from the experiments, using various values of normalised step-size are shown in *Figure 6-12* and *Figure 6-13*. *Figure 6-12* contains all of the results obtained and *Figure 6-13* highlights the effect of the normalised step-size on the rate of convergence and steady-state error. As can be seen for small values of normalised step-size, convergence is slow while the steady-state error is small. Conversely, for moderate values of normalised step-size the rate of convergence is improved at the expense of increased steady-state error. With the

introduction of normalised step-size values in excess of 1.5, problems in terms of the stability of the algorithm, due to excess gradient noise, begin to appear. These results conform to the theory of misadjustment (Haykin 1986, p. 254) for the simple LMS algorithm. This finding suggests that for the analysis of nonstationary signals an optimum step-size, which allows for a compromise between the rate of convergence and the steady-state error, exists.

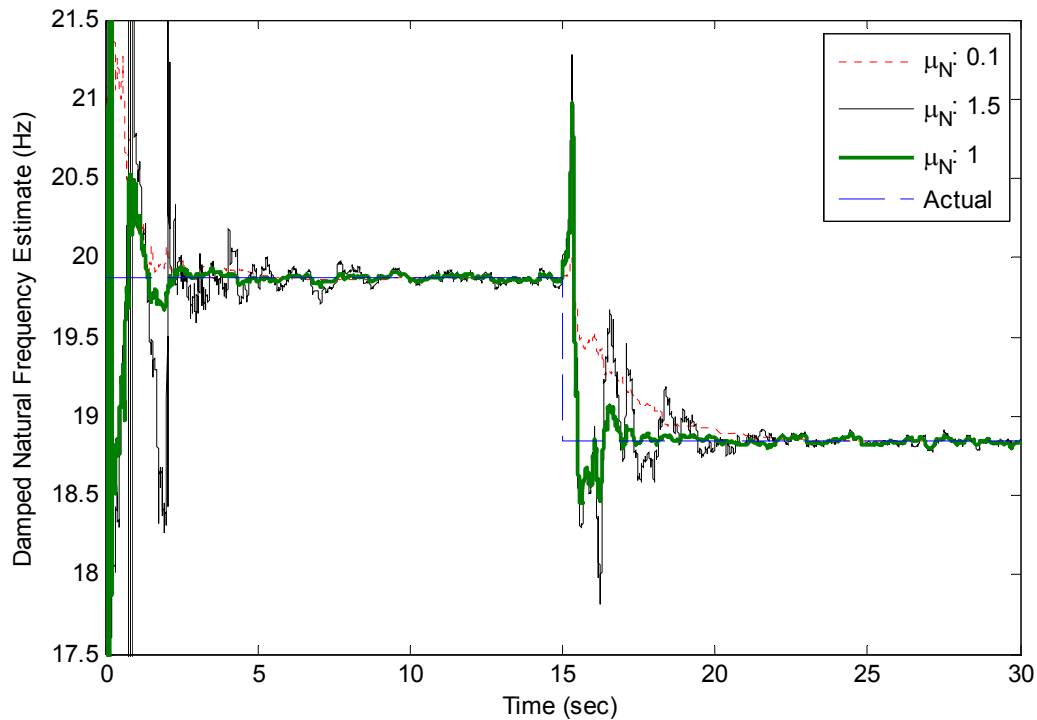


Figure 6-12: Effect of normalised step-size  $\mu_N$  on nonstationary parameter extraction.

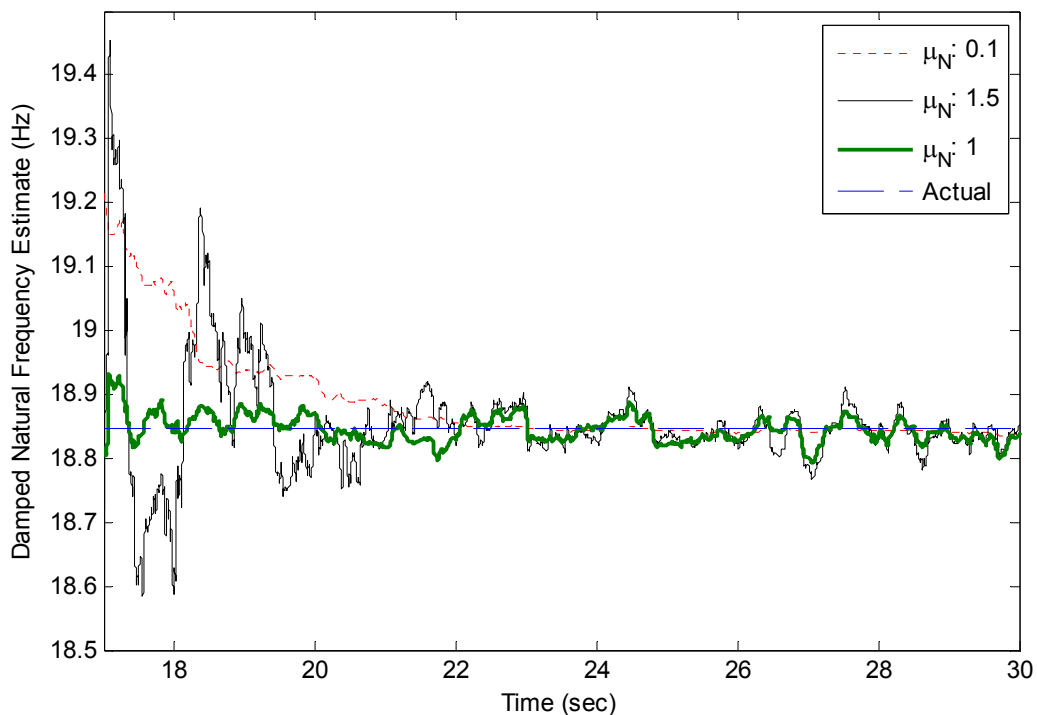
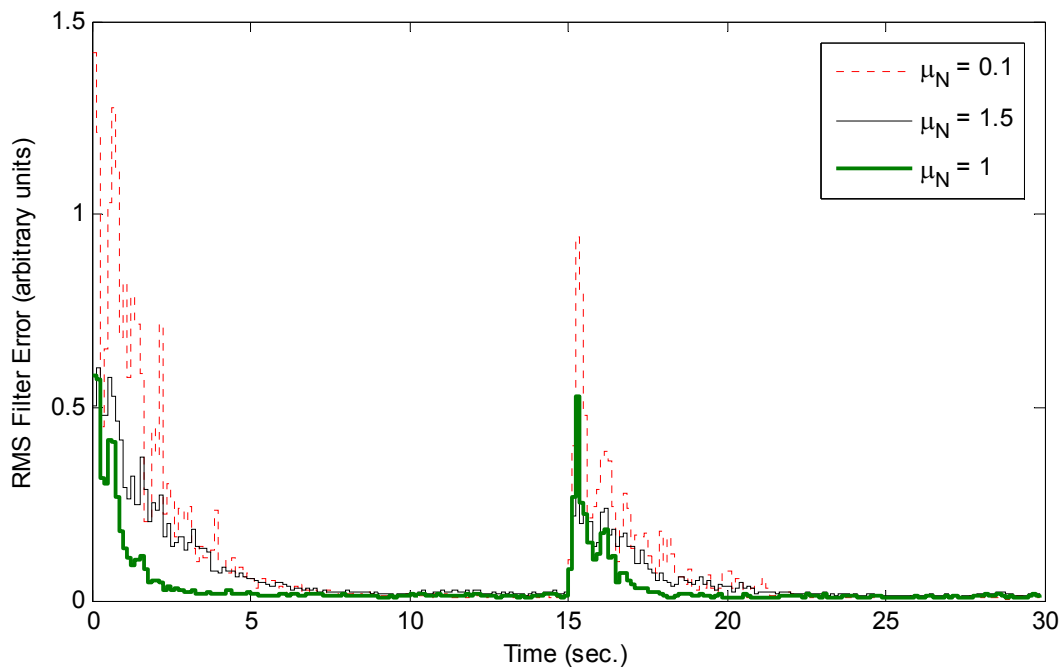


Figure 6-13: Zoomed section from Figure 6-12 showing steady-state error.

During physical experiments, the true damped natural frequency estimates are unknown. This makes it impossible to identify the optimum step-size using the error in the damped natural frequency estimates. However, the filter error  $e(n)$  is available. This parameter contains no external influence (other than instrument noise) since it is simply the difference between the actual (measured) response and the filters estimate of the response at any time  $n$ . Therefore, in principle, minimising the filter's error signal should be effectively the same as minimising the error in the extracted modal parameters. The root-mean-square (RMS) filter error corresponding to the previously depicted damped natural frequency estimates is given in *Figure 6-14* and *Figure 6-15*. These figures show that the normalised step-size has the same influence on the RMS filter error as it does the damped natural frequency estimates. This finding suggests that it is likely that, if the RMS filter error is minimised, so too will the error corresponding to the modal parameter estimates.



*Figure 6-14: Effect of normalised step-size  $\mu_N$  on RMS filter error.*

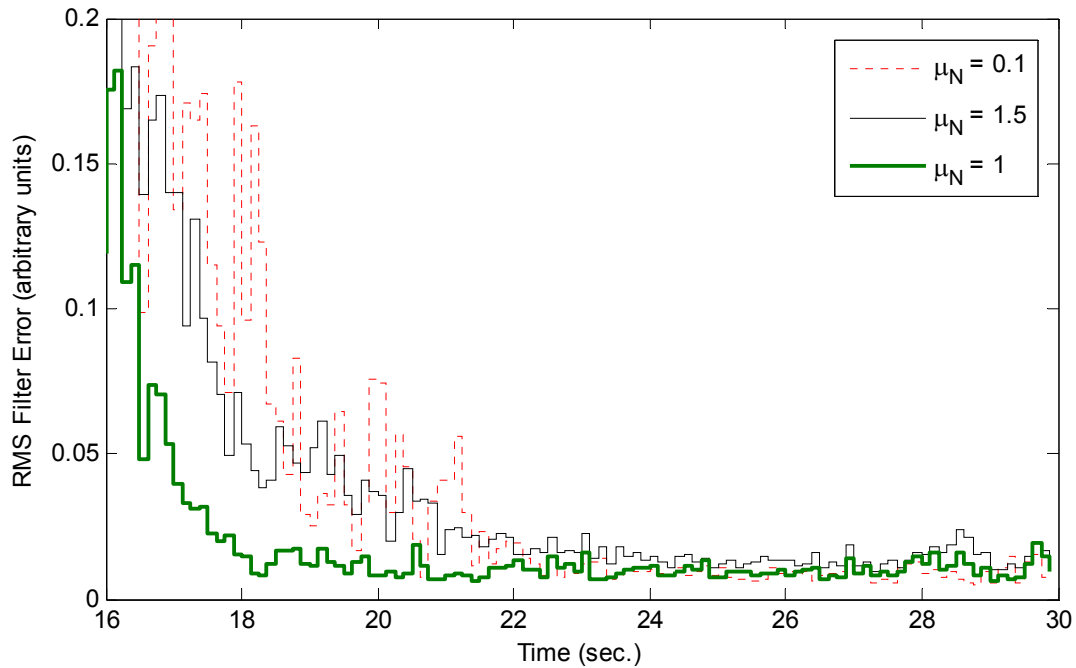


Figure 6-15: Zoomed section of Figure 6-14 showing convergence and steady-state error.

In order to establish the feasibility of minimising the filter error for nonstationary systems, a series of numerically simulated experiments (experiment 5) consisting of the analysis of several simulated SDoF systems, with various rates of linear stiffness decay (0.5%, 1% and 2% per second) was carried out for simulations including with and without extraneous noise. During this series of experiments each of the simulated systems were analysed using the full range of possible normalised step-size values (between zero and two) and the RMS error of the entire duration of the simulation was taken for each of these values. Since these experiments were aimed at the minimisation of the RMS filter error obtained from the analysis of nonstationary systems, and that leakage is, in theory, capable of improving the tracking ability of the NLMS algorithm, it is also helpful at this point to evaluate the influence of leakage. The evaluation of leakage was based on its ability to reduce the RMS filter error obtained without its inclusion. The results obtained for a leakage factor of 1 (no leakage) and 0.9 (10% leakage), are summarised in *Figure 6-16*, for no extraneous noise, and in *Figure 6-17*, for 10% extraneous noise. As can be seen, for linear stiffness decay rates of up to 2% per second the introduction of leakage exacerbates the error. The results also indicate that, for linear decay, a single optimum value for the normalised step-size can be obtained.

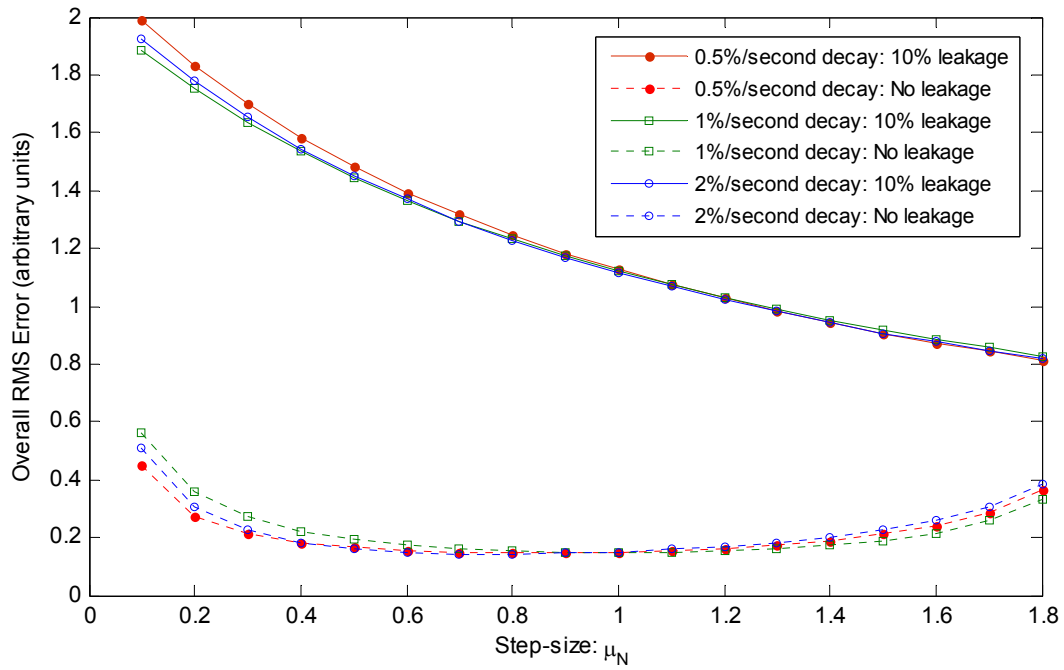


Figure 6-16: Experiment 5 - Effect of normalised step-size  $\mu_N$  on overall RMS filter error, linear decay.

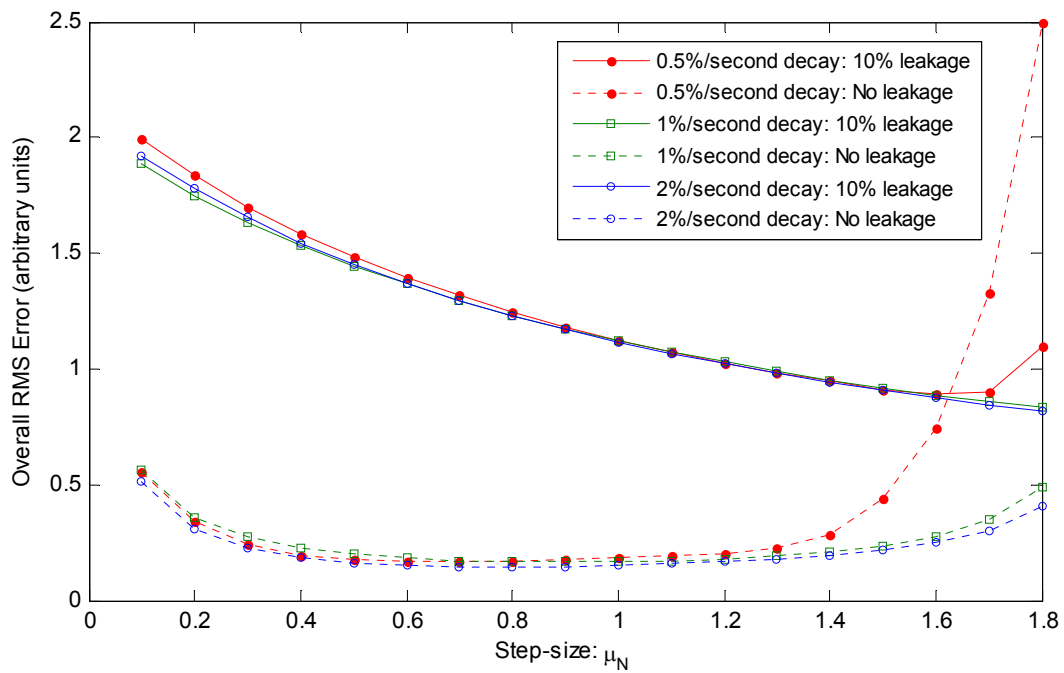
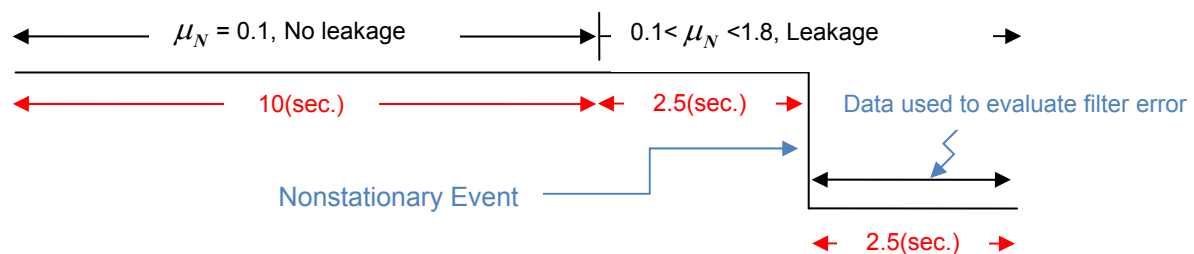


Figure 6-17: Experiment 5 - Effect of normalised step-size  $\mu_N$  on overall RMS filter error, linear decay (10% noise).

The results in *Figure 6-16* and *Figure 6-17* indicate that, for linear decay, when leakage is applied, the RMS filter error is reduced at large values of normalised step-size. This occurrence suggests that the results suffered as a result of slow convergence. Since, it is well documented that leakage can improve the tracking ability of the NLMS algorithm, an extension of experiment 5 (experiment 6) will be undertaken. During experiment 6, the effect of convergence will be minimised by allowing the system to converge over a stationary period with no leakage applied (the normalised step-size value will also remain constant during this time) and to enable leakage to occur just before the nonstationary event (the effect of various step-sizes will also be evaluated from this point). Also, since the principle of leakage works by suppressing the influence of the filter estimate at time  $n-1$ , its effectiveness requires that the filter tap coefficients before a nonstationary event do not closely reflect the system subsequent to the event. Therefore, the nonstationaries for experiment 6 will be in the form of sudden changes in stiffness of various magnitudes. This form of damage will maximise the potential improvements of the leaky algorithm.

The damage sequence, leakage parameters and normalised step-size values for experiment 6 are summarised in *Figure 6-18*. The parameters for the filter tap coefficients were selected using the same principles as those from experiment 5.



*Figure 6-18: Experiment 6 parameter summary.*

The results obtained from experiment 6 for a leakage factor of 1 (no leakage) and 0.9 (10% leakage) are summarised in *Figure 6-19*, for no extraneous noise, and in *Figure 6-20*, for signals containing 10% extraneous noise. As can be seen, by reducing the effect of convergence and simulating sudden damage, the introduction of leakage can help to minimise the RMS error of the filter estimates. However, it can also be seen that, for this damage pattern, the improvements as a result of the introduction of leakage only occur for sudden changes in stiffness which are in excess of approximately 50%.

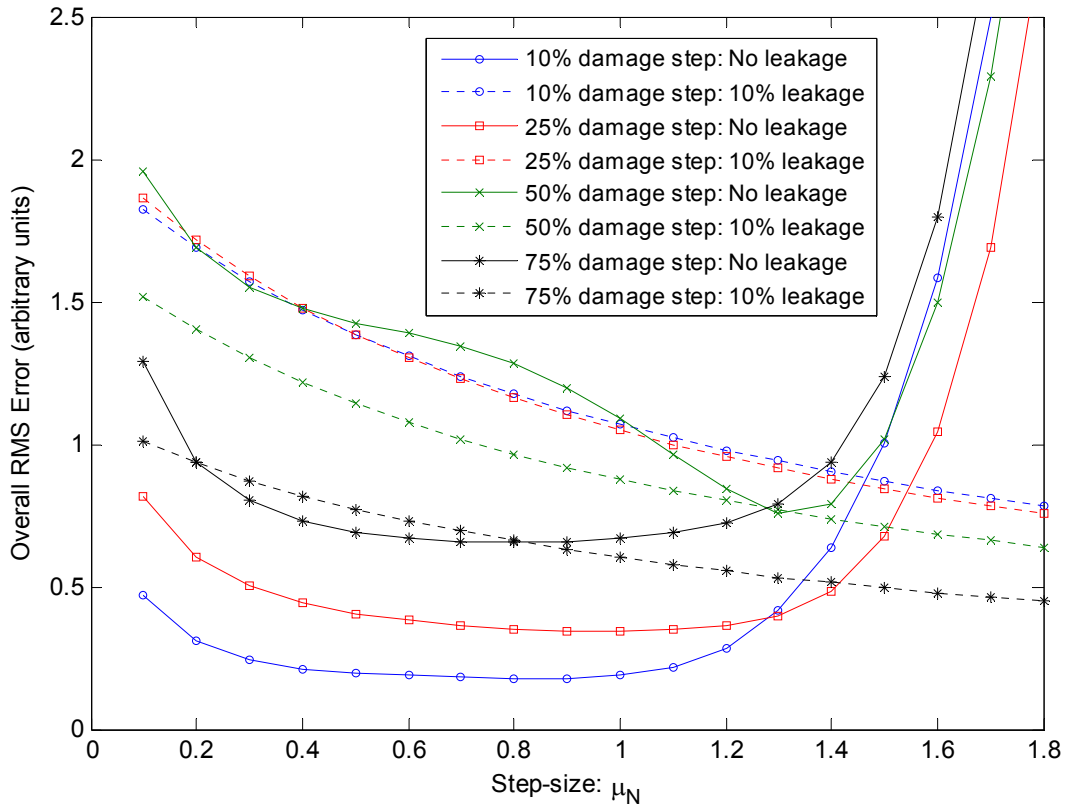


Figure 6-19: Experiment 6 - Effect of normalised step-size  $\mu_N$  on final RMS filter error, sudden damage.

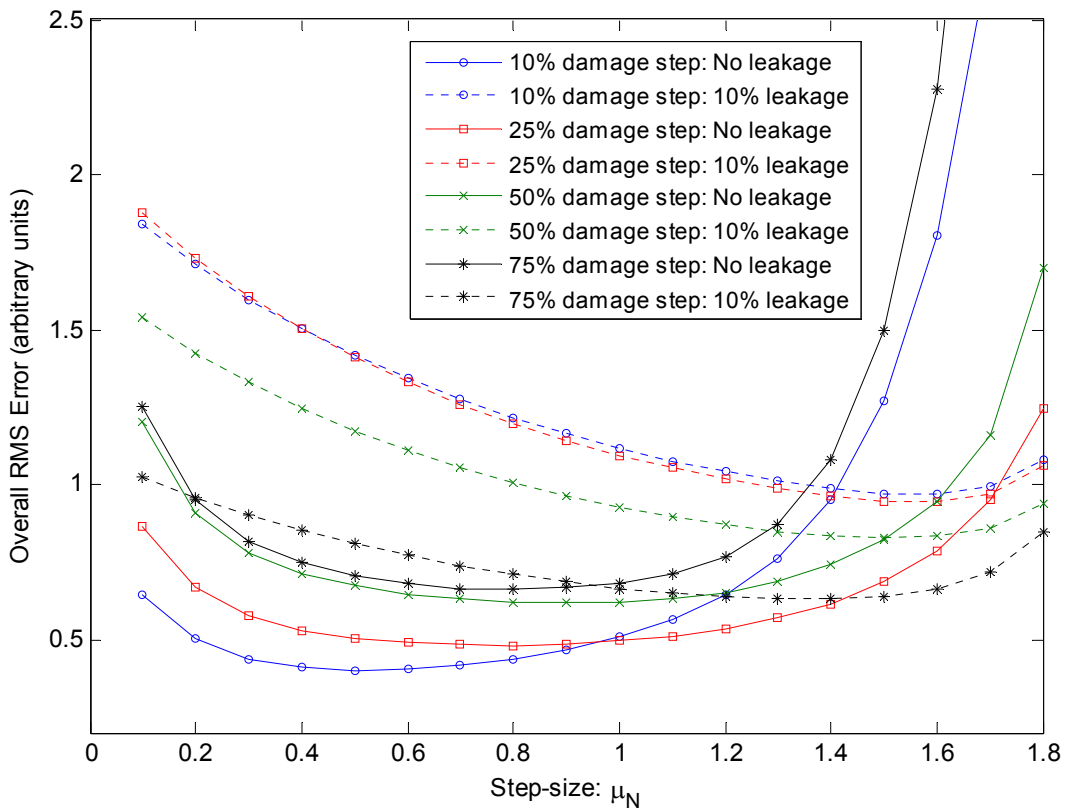
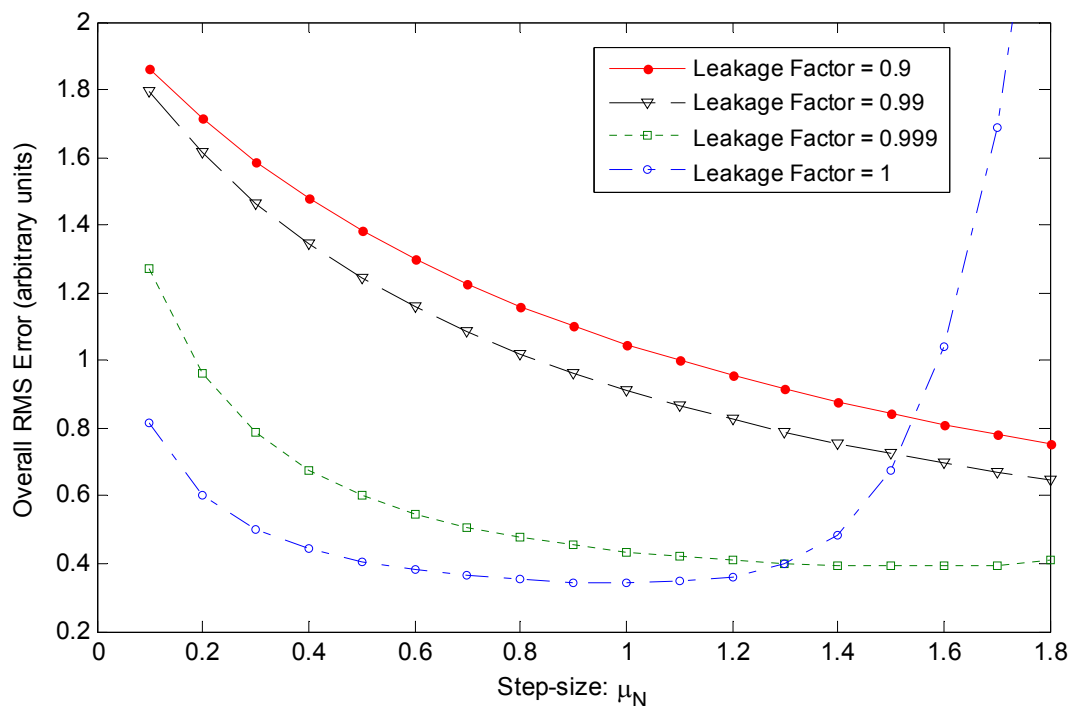


Figure 6-20: Experiment 6 - Effect of normalised step-size  $\mu_N$  on final RMS filter error, sudden damage (10% noise).

It is not unreasonable to suggest that 10% leakage is just too much and that a lesser amount may prove beneficial; however, this is not the case. The results obtained from a system subjected to 25% damage, for leakage factors between 1 (no leakage) and 0.9 (10% leakage) are summarised in *Figure 6-21*, for no extraneous noise, and in *Figure 6-22*, for signals containing 10% extraneous noise. As can be seen, even with the introduction of such a large amount of damage, the inclusion of any level of leakage was unable to improve the results obtained.

Given that such large amounts of damage are required for leakage to provide any improvement, and that it can have a detrimental effect on the rate of convergence, it is suggested that, for the purposes of evaluating damage in physical systems, leakage should not be applied. Based on the curves obtained for no leakage, shown in *Figure 6-19* to *Figure 6-22*, it is possible to suggest that, for sudden damage, a single optimum value for the normalised step-size can be obtained.



*Figure 6-21: Experiment 6 - Effect of normalised step-size  $\mu_N$  and leakage on final RMS filter error, 25% sudden damage.*

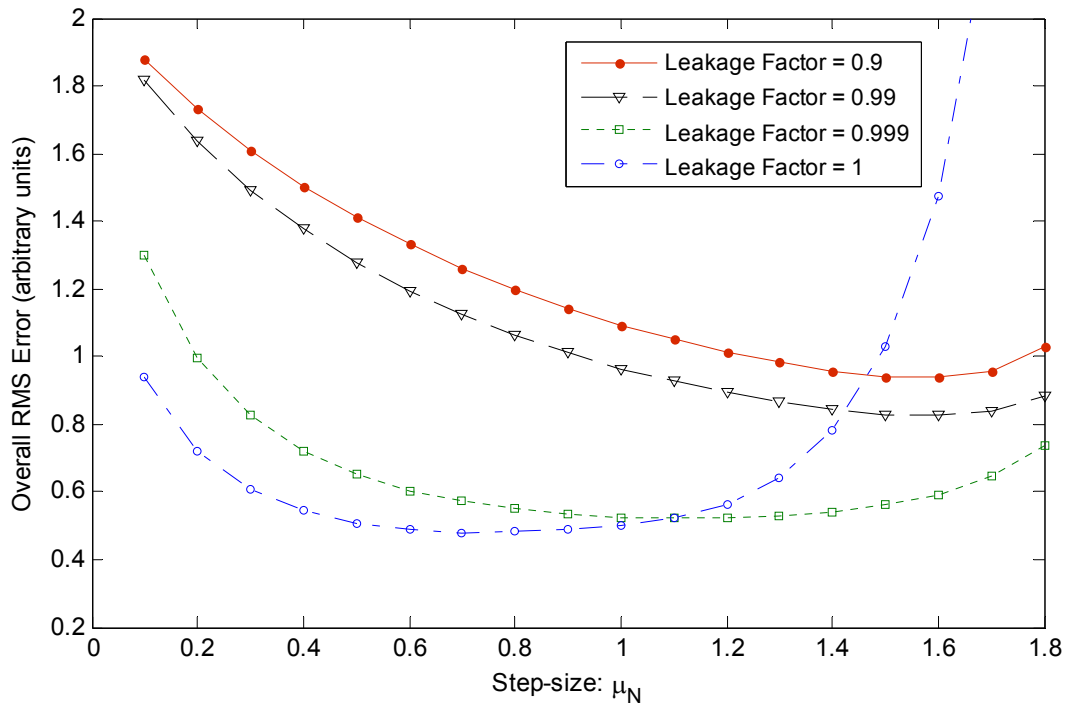


Figure 6-22: Experiment 6 - Effect of normalised step-size  $\mu_N$  and leakage on final RMS filter error, 25% sudden damage (10% noise).

The results from the preceding numerically simulated experiments suggest that, irrespective of the type of damage (progressive or sudden), the evaluation of the overall RMS filter error for various values of normalised step-size results in a curved trend with a clearly defined single minimum from which the optimum step-size can be selected. This finding means that the normalised step-size can now be selected using the minimised RMS filter error as opposed to relying on subjective estimates. Some readers may notice that the results for the 50% damage scenario presented in *Figure 6-19* differ slightly from the other results presented (slight distortion in the curve). However, this is of no concern at this stage, as the curve still has a well defined single minimum. Also, the 50% damage scenario represents less than 3% of the total results set for this series of experiments. If the optimisation technique only failed to find an optimum step-size 3% of the time, it is of the author's opinion that the technique would still provide a significant advantage. In order to reduce the required number of computations, the optimum normalised step-size can be found using a simple optimisation algorithm which searches for the minimum RMS filter error; for this study the sequential dichotomy (method of bisection) optimisation technique (Dieter 1986, p. 135) is used. An example of the function of the algorithm is given in *Figure 6-23*. As can be seen, the optimisation algorithm significantly reduces the number of calculations required to accurately locate the optimum step-size.

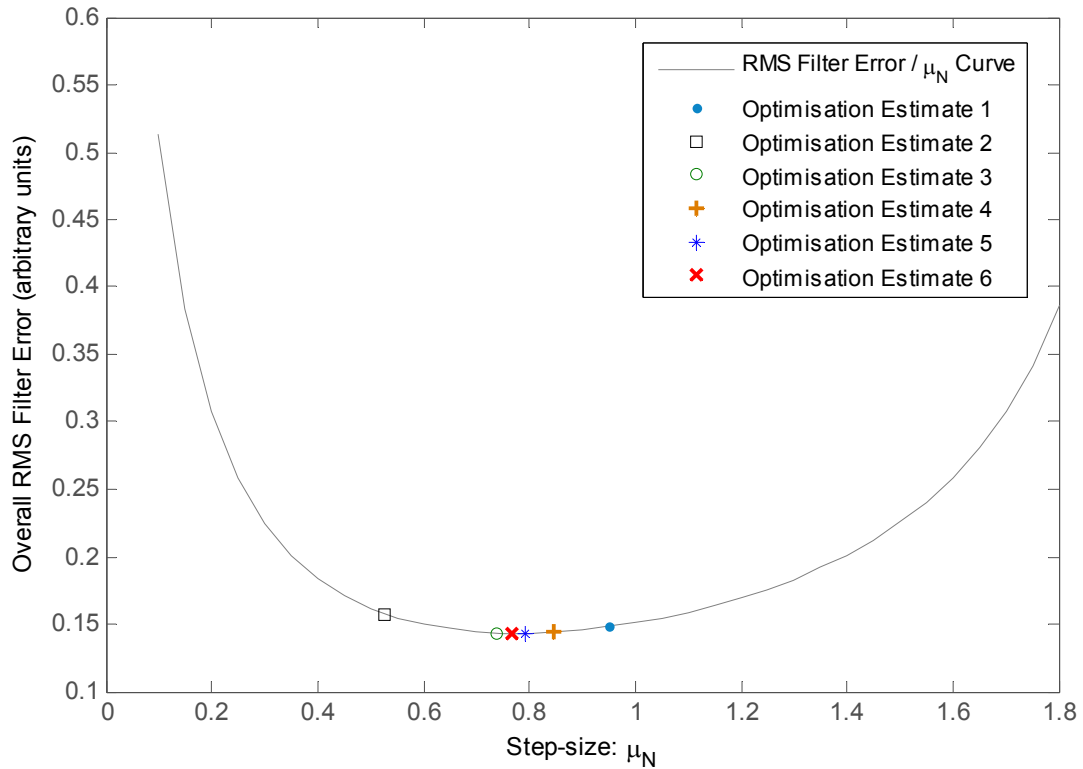
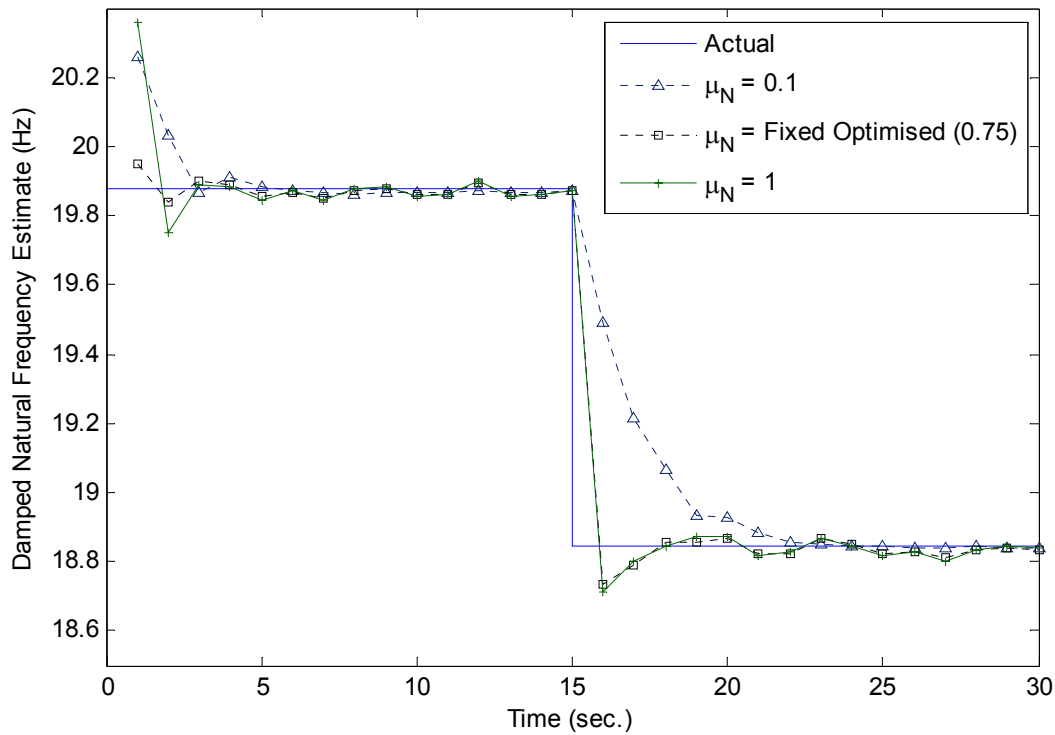


Figure 6-23: Reduction in the required calculations for determining the optimum normalised step-size by implementing the sequential dichotomy technique.

The use of this optimum reduces the overall RMS value of the filter's error signal, thereby resulting in best possible compromise between the rate of convergence and the steady-state error obtainable using a single value of step-size.

The ability to select an optimised normalised step-size, which produces the lowest overall RMS error, is not influenced by variations in modal parameters such as damping (this will be shown in section 8.1.3.2). At higher levels of damping (>11%) the effectiveness of leakage may be improved since the rate of convergence could increase as the number of coefficients required to describe the systems impulse response function is likely to reduce (to be discussed in section 6.2.4.3). However, considering that such a large amount of damage was required for leakage to be effective when evaluating systems with 11% damping, it is unlikely that its introduction will ever be beneficial when tracking small changes in a systems characteristics (which is the topic of discussion). Furthermore, if the damping ratio of the system is less than 11%, the addition of leakage will be even less appropriate than suggested above. Therefore, considering the space limitations in this study and the unlikely event that leakage will be beneficial, the author believes that further analysis of the influence of leakage is unwarranted. Conversely, further discussions on the optimised normalised step-size technique are required. Therefore, in order to demonstrate the potential of the optimised normalised step-size

technique, the signals used in the initial evaluation of normalised step-size will be re-analysed with its application. *Figure 6-24* and *Figure 6-25* contain the results obtained by the application of the technique. *Figure 6-24* contains the results obtained for the entire length of data and *Figure 6-25* shows how the technique is able to select the normalised step-size value (0.75) which gives the best compromise between the rate of convergence and steady-state error.



*Figure 6-24: Introduction of a fixed optimised normalised step-size.*

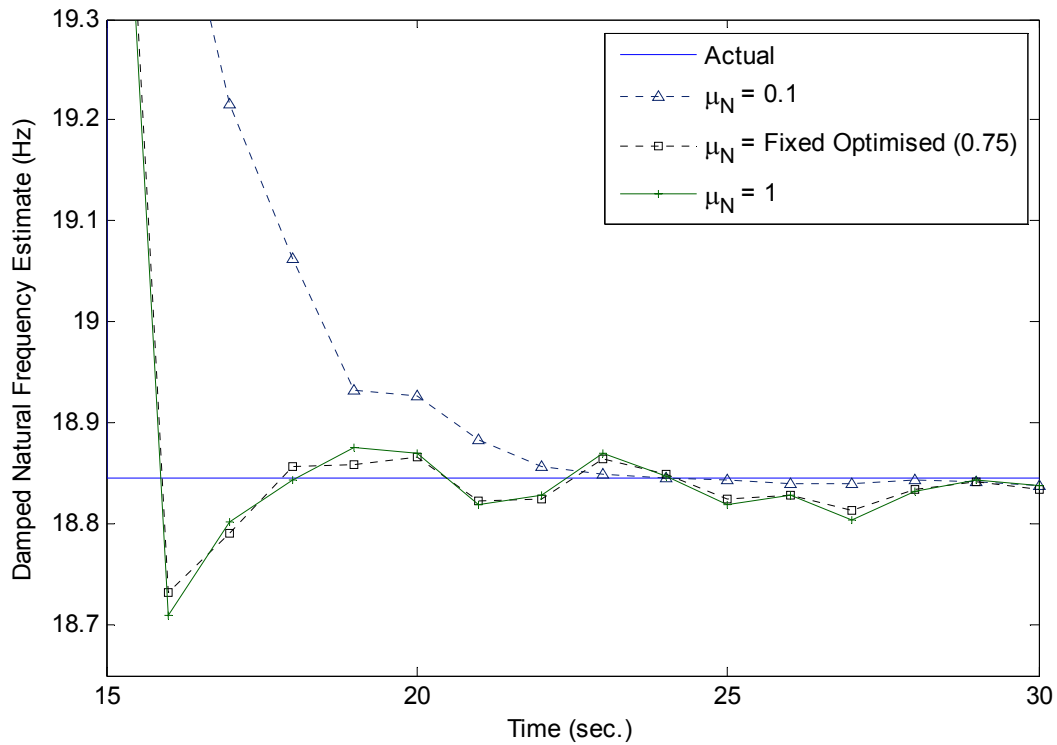


Figure 6-25: Compromise between convergence and steady-state error when using a fixed optimised normalised step-size.

With the introduction of any new technique questions of its robustness need to be addressed. Therefore, the evaluation was repeated with the introduction of extraneous noise. Figure 6-26 and Figure 6-27 contain the results obtained with the application of 10% (RMS) extraneous noise to the excitation and response signal pair. As can be seen the technique is equally effective in selecting the appropriate normalised step-size (0.33) with the introduction of noise.

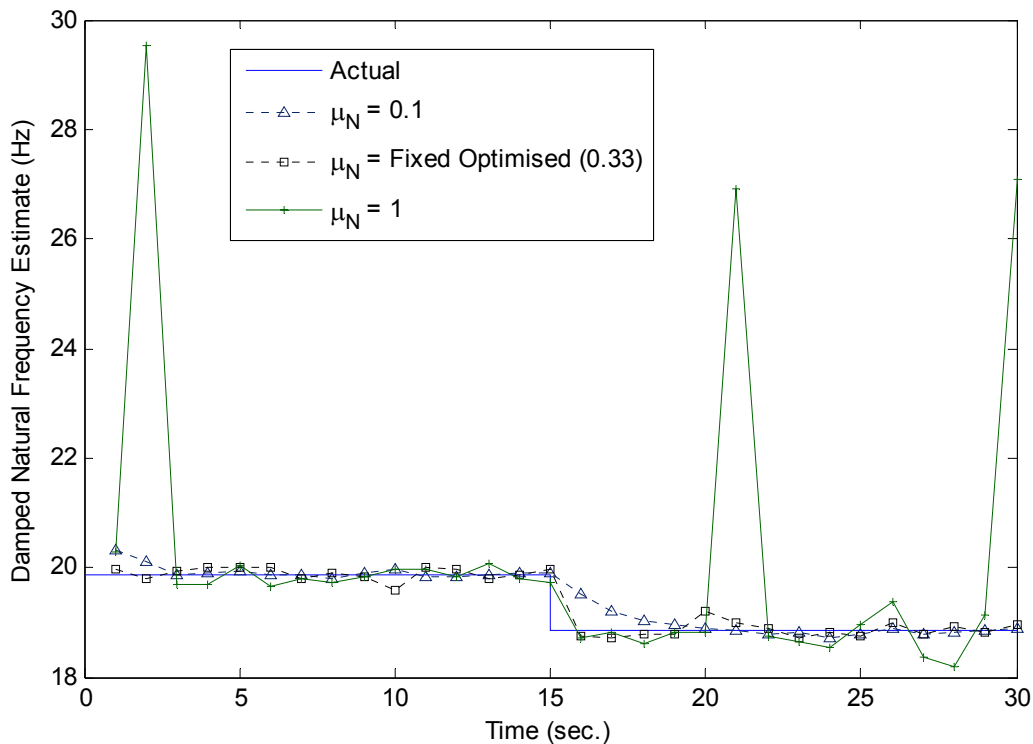


Figure 6-26: Introduction of a fixed optimised normalised step-size (10% noise).

The selection of normalised step-size has so far been based on an optimum which reduces the overall RMS value of the filter's error signal, thereby resulting in the best possible compromise between the rate of convergence and the steady-state error obtainable using a single value of step-size. In order to further improve the filter's performance, a method by which the step-size is allowed to be re-optimised at regular intervals was implemented. The variable optimised step-size technique is based on updating the step-size, to a value that minimises the RMS filter error between each update. The results obtained using the optimum step-size techniques to analyse the nonstationary SDoF system are given in *Figure 6-28* and *Figure 6-29*, for signals containing no extraneous noise, and *Figure 6-30*, for signals containing 10% extraneous noise. As can be seen, the variable optimised step-size technique provides further improvements over the fixed optimised step-size approach in that the compromise between the steady-state error and rate of convergence is all but eliminated.

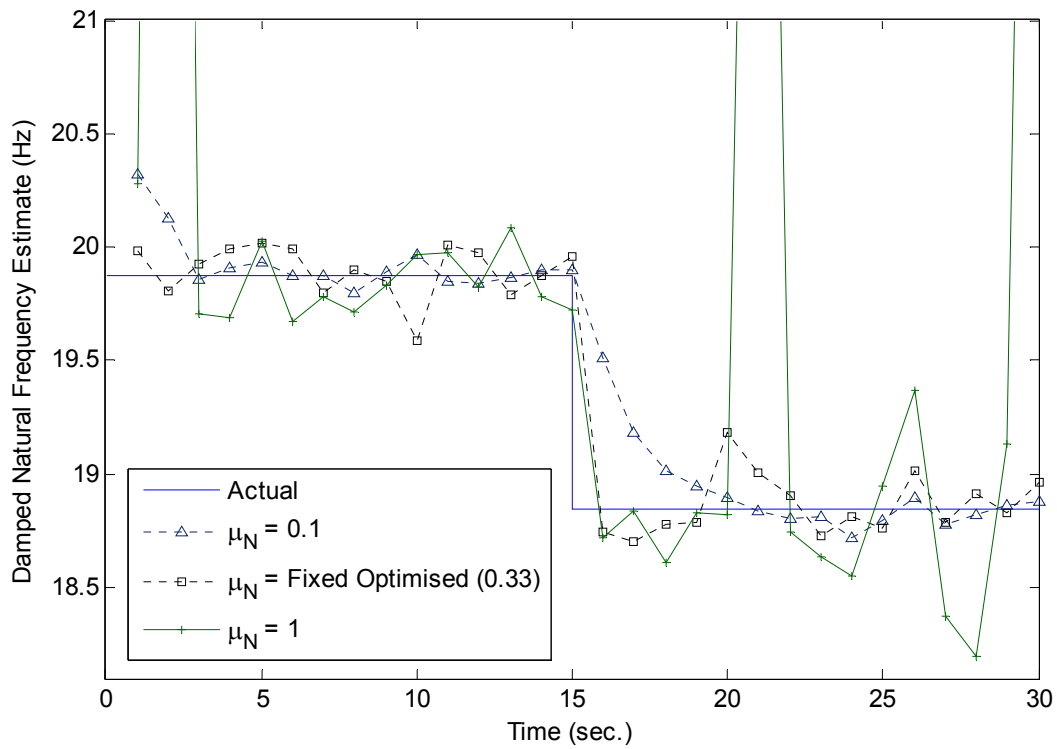


Figure 6-27: Compromise between convergence and steady-state error when using a fixed optimised normalised step-size (10% noise).

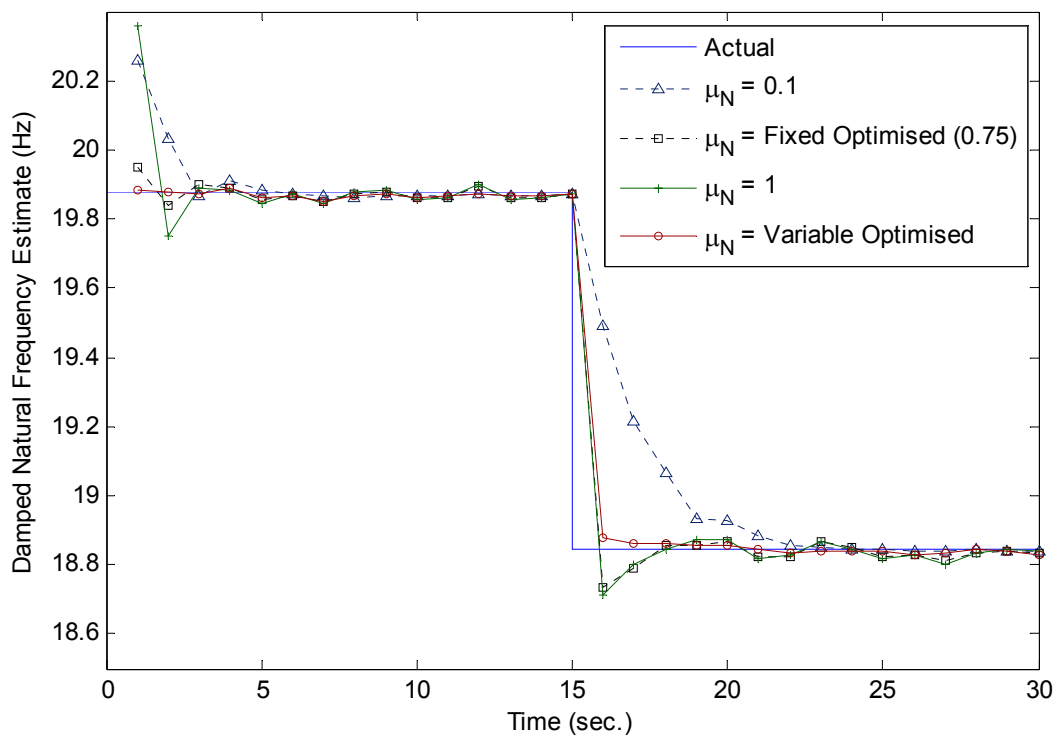


Figure 6-28: Introduction of a variable optimised normalised step-size.

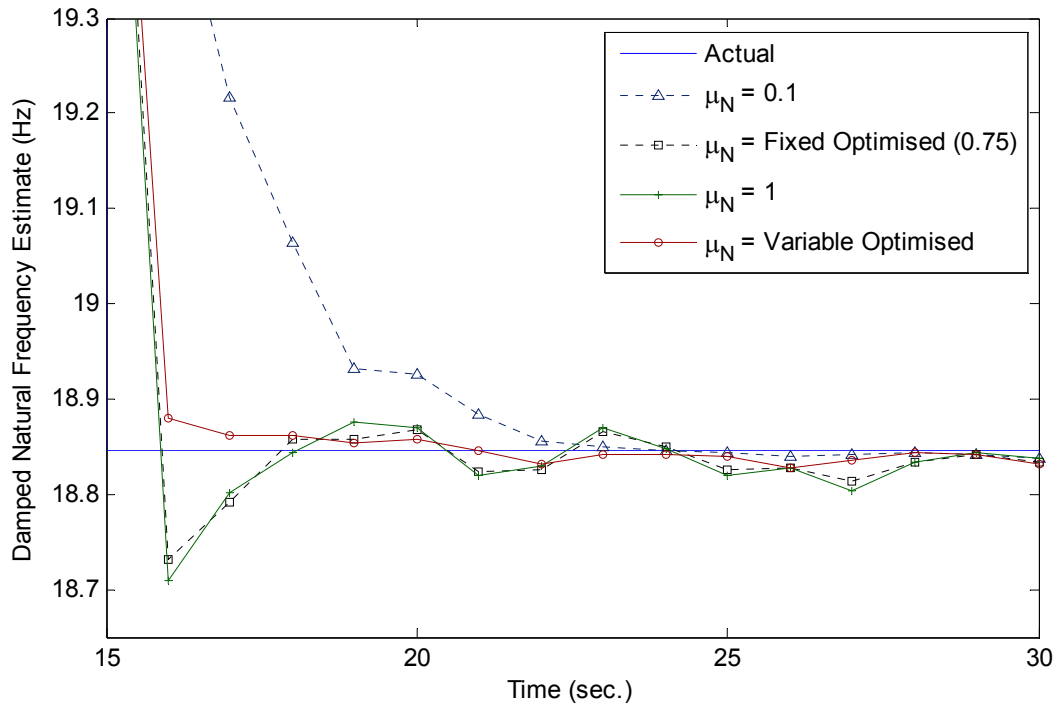


Figure 6-29: Reduced compromise between convergence and steady-state error when using a variable optimised normalised step-size.

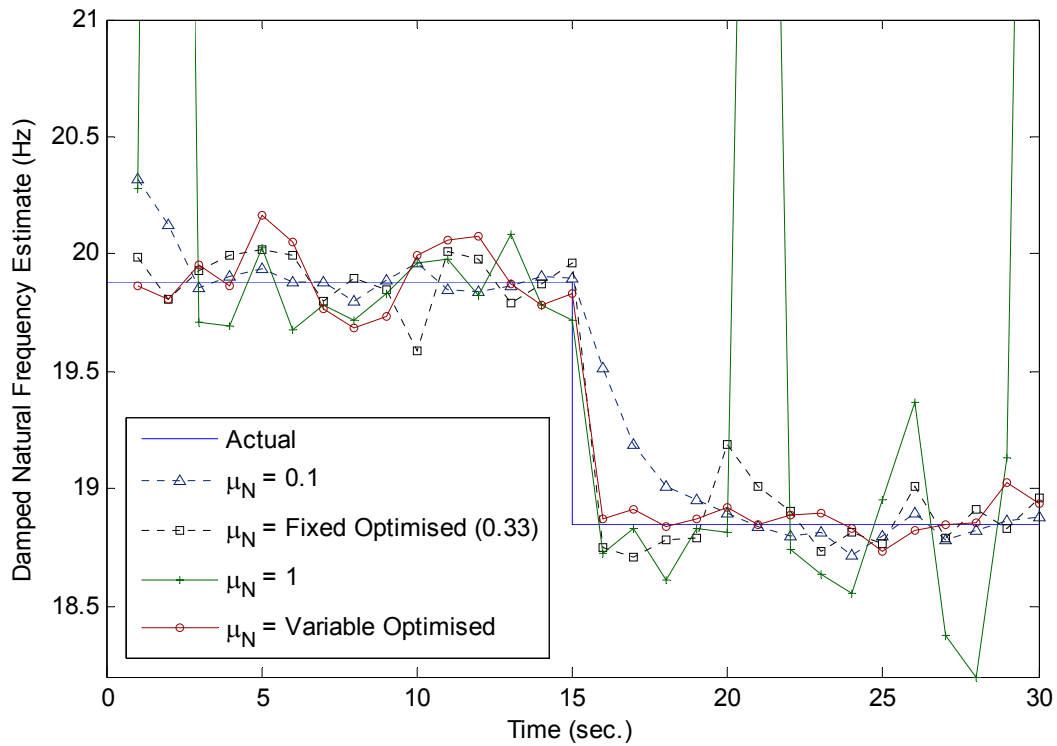
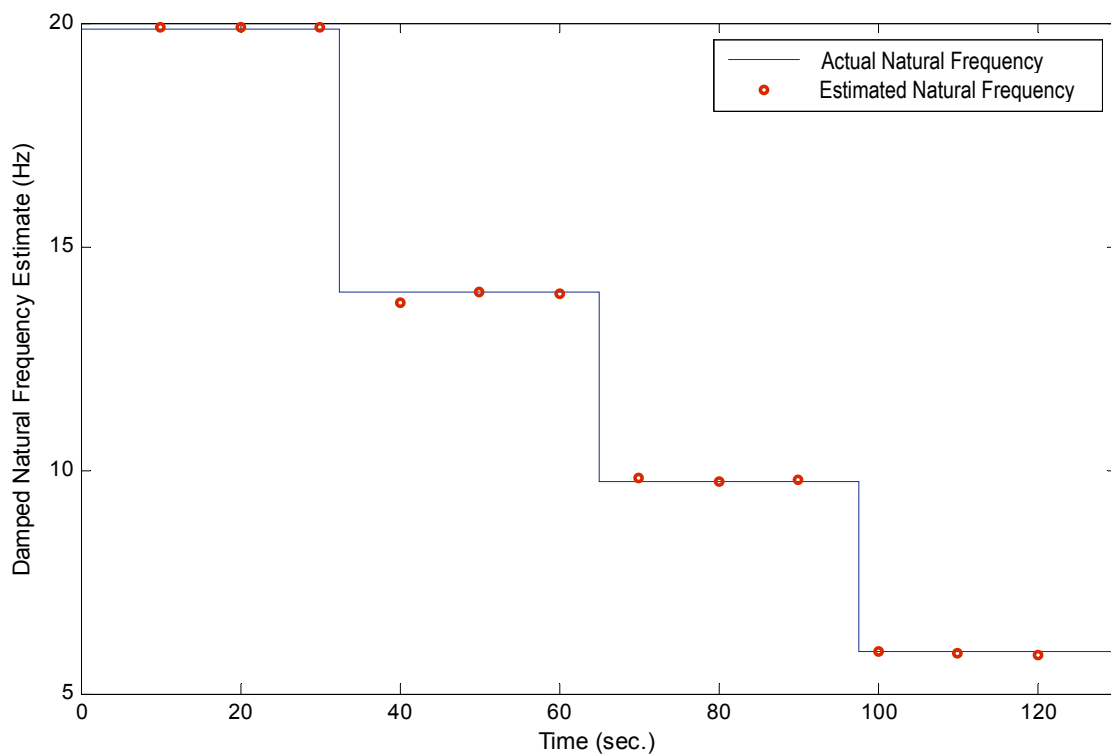


Figure 6-30: Reduced compromise between convergence and steady-state error when using a variable optimised normalised step-size (10% noise).

The method by which the variable optimised normalised step-step technique reduces the required compromise between the rate of convergence and steady-state error is best explained by example. Consider the damage pattern given in *Figure 6-31* and the corresponding filter error signal and step-size updates in *Figure 6-32* and *Figure 6-33*, respectively. As can be seen, subsequent to each nonstationary event there is a rapid increase in the magnitude of the error signal (this is less evident for signals which contain extraneous noise) which needs to be reduced quickly. This requires a higher rate of convergence, hence a higher normalised step-size. Conversely, during the time-invariant segments of the damage pattern the filter error is settled and requires a decrease in gradient noise to reduce its magnitude further. A reduction of gradient noise can only be obtained by adapting more slowly, hence a smaller normalised step-size. *Figure 6-33* shows that, for the most part, the variable optimised normalised step-size technique is capable of fulfilling these requirements. This ability is identified by the higher values of normalised step-size in the vicinity of each nonstationary event.



*Figure 6-31: Example damage pattern.*

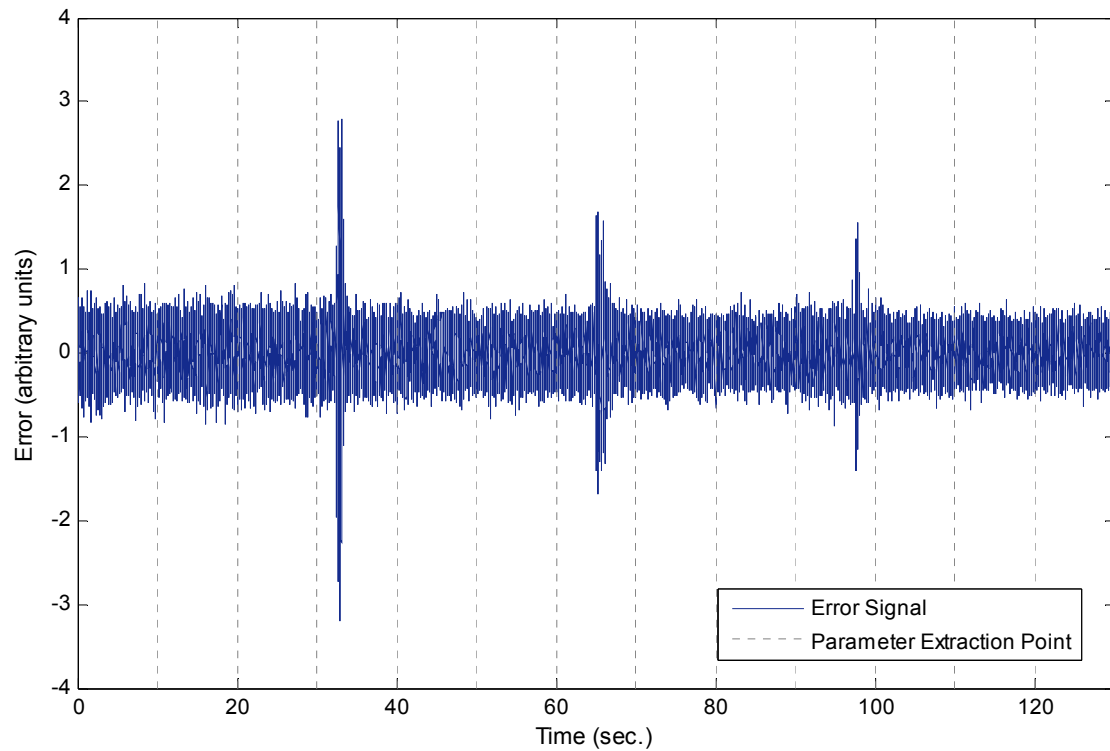


Figure 6-32: Filter error corresponding to the damage pattern in Figure 6-31.

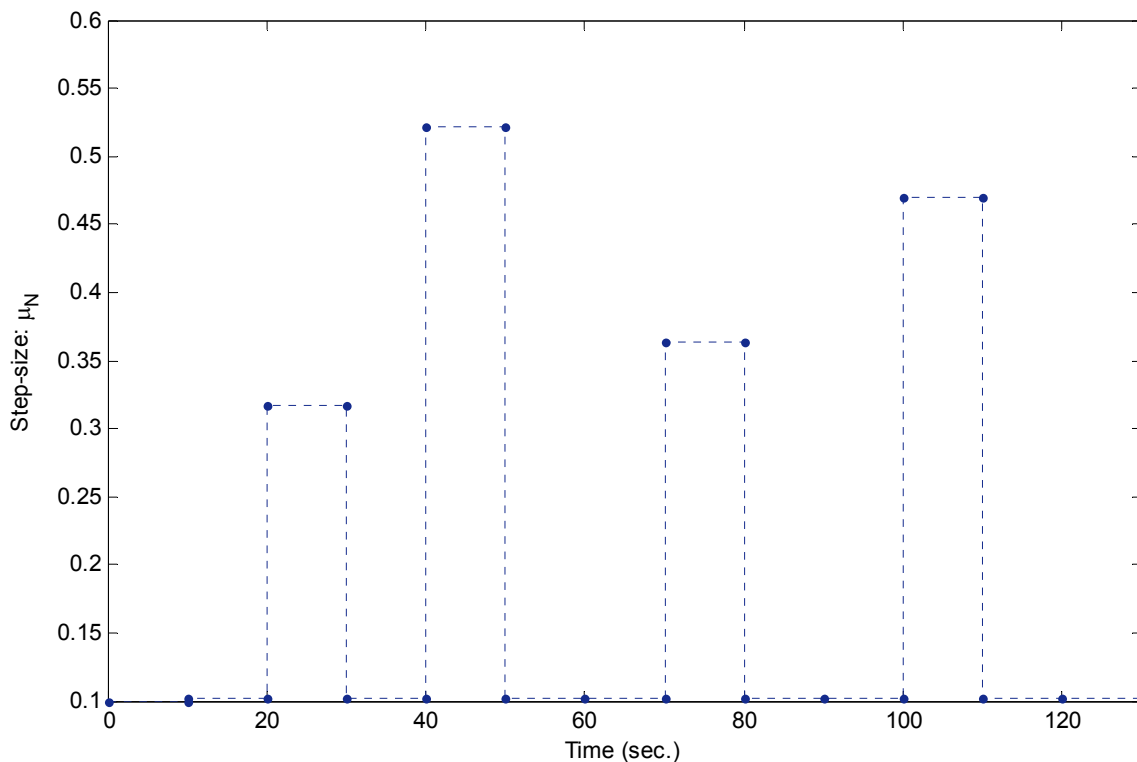


Figure 6-33: Variable normalised step-size corresponding to the damage pattern in Figure 6-31.

While the variable optimised normalised step-size technique provides significant improvements over those which use a fixed step-size, there is a limit to the rate at which the updates in the normalised step-size can be made. Preliminary numerically simulated experiments, which considered the system's natural frequency, the magnitude of the damage event (or nonstationary) and the sampling frequency, suggest that no fewer than 500 and in the order of 1000-2000 sample points are required between each update in order to ensure stability and reliability of the technique. This value was established by comparing the convergence times and steady-state error values obtained using various normalised step-size update rates with the results obtained using a fixed optimum normalised step-size. This comparison was completed for vibration records captured over a range of sampling frequencies (500Hz – 4000Hz) from systems containing a single nonstationary event. These systems had a range of natural frequencies (20Hz – 45Hz) and the magnitude of the nonstationary events was also varied (5% - 80% damage). An optimum rate for the step-size updates is expected to be dependent on a range of parameters with the most obvious parameters being the magnitude and frequency of the nonstationary events within the signal. For example, if the system under analysis is stationary the optimum step-size will remain low throughout the analysis. Also, if the system contains consistent nonstationary events which exist for a similar, or equal, amount of time, the optimum step-size will remain consistent throughout the analysis. This means that the best results may be obtained using the fixed optimised step-size technique for both stationary systems and those containing consistent nonstationary events. Conversely, if the system includes nonstationary events that exist for an irregular period of time, the step-size will need to be updated on a more regular basis in order to minimise both steady-state and convergence error. Extraneous noise is also expected to have some influence. The development of a technique which is able to select an optimum update rate is expected to be far from trivial while the improvements it can provide are expected to be limited. As a result the development of such a technique will not be included in this study. Until further research provides a technique to select the optimum rate for re-optimisation it is recommended to update the normalised step-size values at a rate which does not exceed the desired temporal resolution and insures that each update is separated by at least 1000 sample points.

Because of the improvements achievable using the variable optimum normalised step-size technique, it will be used with the re-optimisation rate set at every 1000 points, for the evaluation of each of the parameters in the remaining sections of this chapter.

#### 6.2.4.2. Evaluation of the Initial Filter Tap Coefficients

The previous numerically simulated experiments made use of an initial filter tap coefficient vector which consisted entirely of zeros as the starting point of adaptation, as is common practice (Haykin 1986, p. 237). For modal parameter extraction purposes, it is not unreasonable to expect that the best initial filter coefficients will not be zeros. The effect of non-zero initial filter tap coefficients was evaluated for a short (3 second) noise-free stationary SDoF signal pair using three different initial conditions for the filter tap coefficient vector:

1. Zeros
2. Converged coefficients (from an initial condition of zeros) after 0.1 seconds
3. Converged coefficients (from an initial condition of zeros) after 0.1 seconds reiterated 1000 times.

Reiteration involves taking the filter tap coefficients converged from zero after 0.1 seconds (100 sample points in this instance) and setting them as the initial condition for the next iteration. This feedback loop is repeated a number of times (1000 in this case). In doing this, the only cost is computation time (i.e. no data is consumed).

The results obtained from the numerically simulated experiment are given in *Figure 6-34*, which shows that the iteration of the initial filter tap coefficients, even over a period as short as 0.1 seconds, creates a significant reduction in both the filter error during convergence and the time taken for the filter to converge. This is significant as it allows for the establishment of the system's characteristics during the early stages of analysis which would not otherwise be possible. *Figure 6-35* demonstrates how this improvement is achieved by comparing each of the three initial filter tap conditions with the final converged filter tap coefficients. Based on these improvements it is recommended that, prior to the initiation of parameter extraction, the initial filter tap coefficients be estimated using this iteration process, with the only limitation being the amount of affordable computation time. Note that, in order for each filter coefficient to be adjusted from its initial estimate, reiteration must be performed on a portion of the signal pair no shorter than the filter tap coefficient vector length. The effect of reiterating using too little data is demonstrated in *Figure 6-34*, where it can be seen that the filter tap coefficient values between 0.1 seconds and 0.15 seconds remain at their initial value of zero. This occurs because the duration over which reiteration is performed is too short to

fill the digital FIR. For this reason, it is recommended that the reiteration process is performed over an interval which matches the duration of the FIR function.

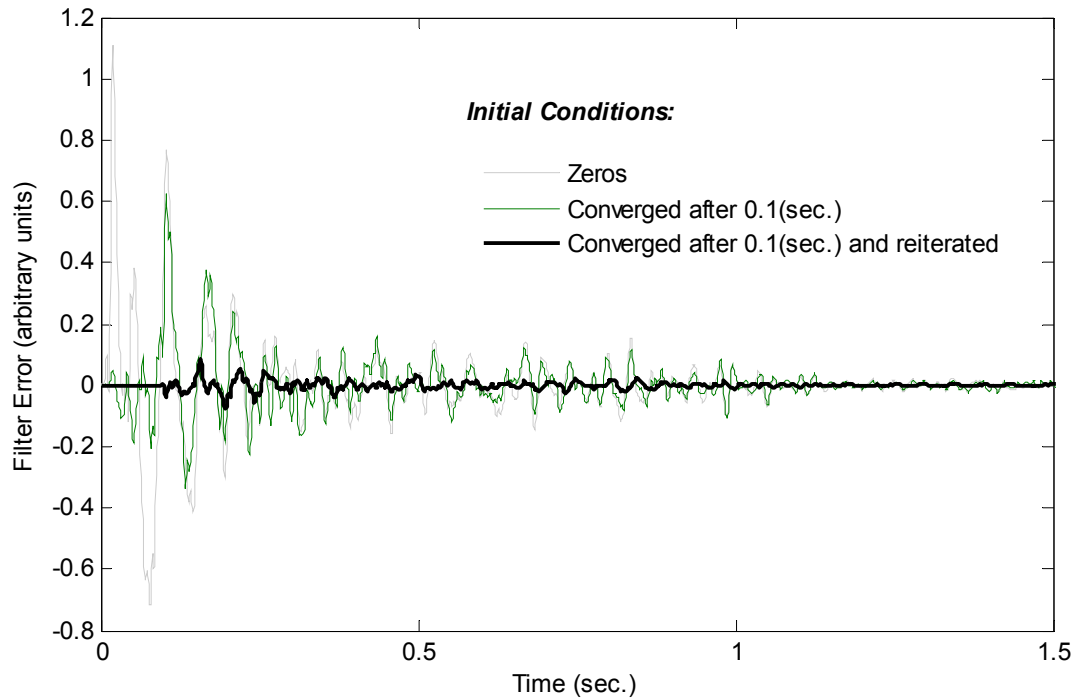


Figure 6-34: Reduction of filter error by improving the initial filter tap coefficients.

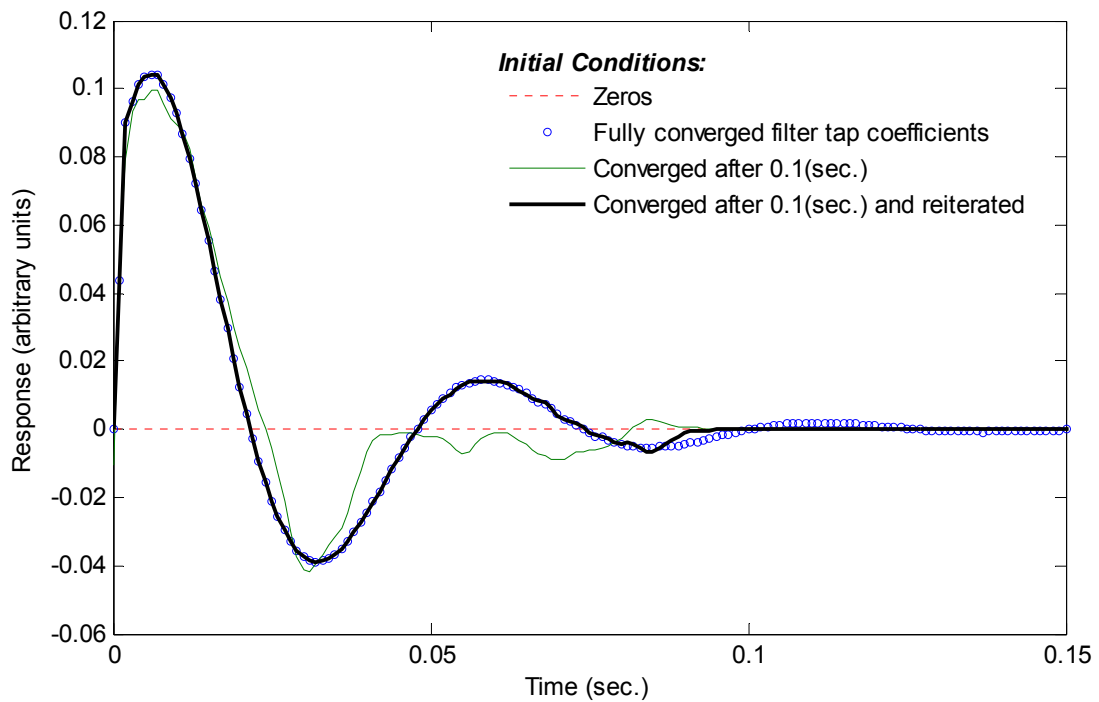
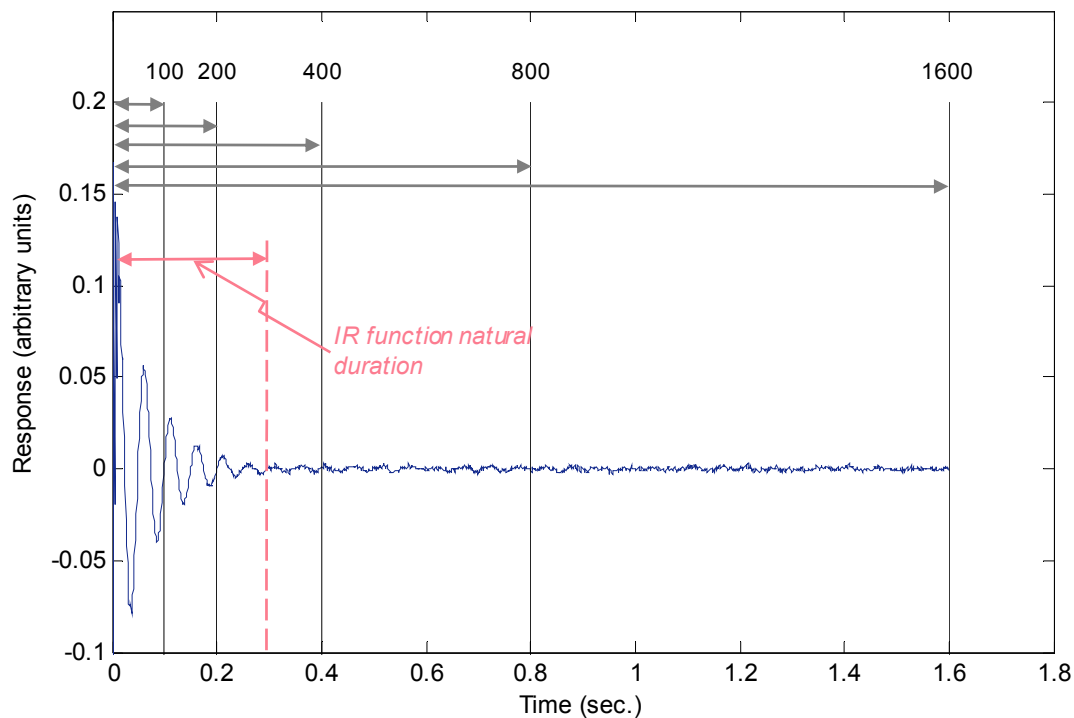


Figure 6-35: Convergence of the initial filter tap coefficients through iteration.

### 6.2.4.3. Evaluation of the Number of Filter Tap Coefficients

It is well documented that the number of filter tap coefficients is directly proportional to the misadjustment of the optimum finite data filter tap coefficients when analysing signals using LMS adaptation (Widrow & Kamenetsky 2003; Hassbi 2003). This relationship suggests that with an increase in the number of filter tap coefficients comes an increased difference between the optimal and estimated coefficients for that particular solution, provided that the number of training samples is unchanged. The effect of increased misadjustment suggests that it may be beneficial to limit the number of filter tap coefficients. However, it is also expected that minimising the number of filter tap coefficients will limit the filters ability to fully describe the system under analysis, particularly in terms of parameter extraction (potential for curve-fitting). In order to evaluate the influence of the filter tap vector length, a series of numerically simulated experiments (experiment 7) was carried out using both clean and noise-contaminated (10%) signal pairs for an SDoF system. During experiment 7 the length of the filter tap coefficient vector was varied to represent various proportions of the system's impulse response function as shown in *Figure 6-36*, where the vertical lines highlight the proportion of the signal covered by the filter tap coefficient vector using their corresponding number of coefficients.



*Figure 6-36: Experiment 7 - Portion of the system's impulse response function described by the given number of filter tap coefficients.*

In order to avoid the influence of end effects in the instantaneous phase vector, only a portion of the impulse response function was used. An example of the range of data used is given in *Figure 6-37*. *Table 6-1* gives a summary of the portions used for each of the variations in the filter tap coefficient vector length.

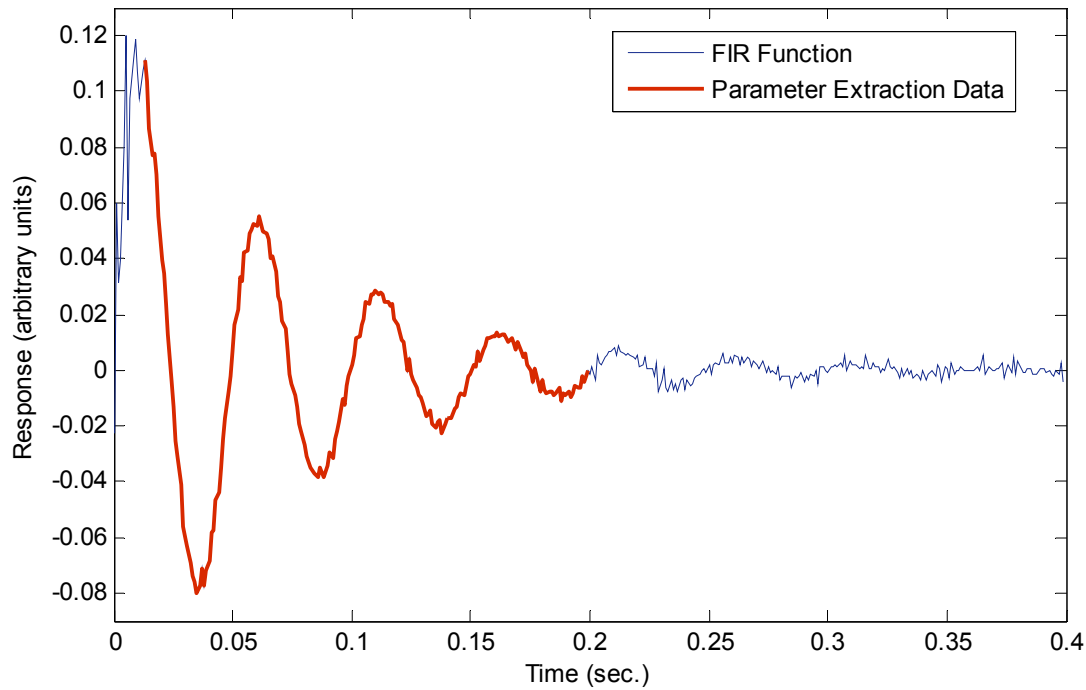


*Figure 6-37: Experiment 7 - Portion of the system's impulse response function used for parameter extraction.*

*Table 6-1: Experiment 7 - Range of impulse response function used for parameter extraction.*

Filter Tap Coefficient Vector Length	Lower Extent of Range (ms)	Upper Extent of Range (ms)
100	12.5	80
200	12.5	150
400	12.5	200
800	12.5	200
1600	12.5	200

The results obtained from experiment 7 are summarised in *Figure 6-38* and *Figure 6-39*, for no extraneous noise, and *Figure 6-38* and *Figure 6-40*, for 10% extraneous noise. *Figure 6-38* shows the converged natural frequencies extracted for each variation in the filter tap coefficient vector length, with  $\pm$  one standard deviation shown as error bars. These results suggest that the number of coefficients used must not be less than the natural duration  $T_{IR}$  of the impulse response function. It is also apparent that, for a number of coefficients well in excess of this limit, there may be a slight reduction in the variance of the extracted results (for

the noise contaminated results) although this is accompanied by a shift in the mean away from the actual damped natural frequency (dashed line).

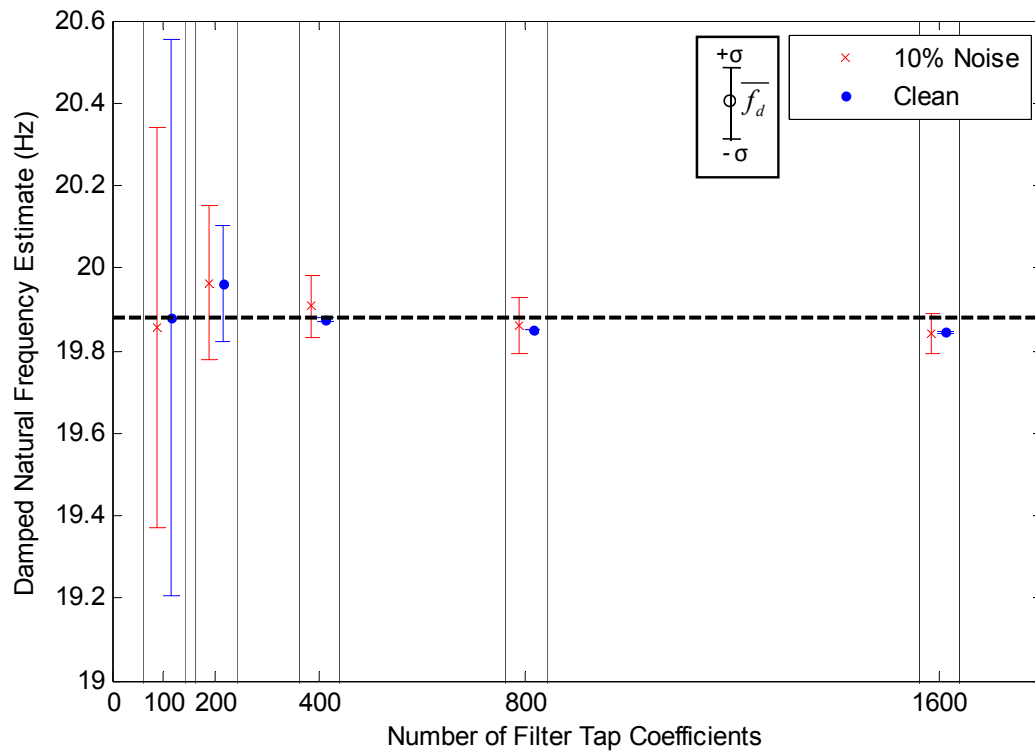


Figure 6-38: Experiment 7 - Converged damped natural frequencies (natural duration approximately 300-350 coefficients).

Figure 6-39 and Figure 6-40 show the RMS values of the error signals for each variation in the number of filter tap coefficients. There is a strong indication that increasing the number of filter tap coefficients decreases the rate of convergence (note that convergence is from an initial filter weight vector of zeros), by increasing the misadjustment due to lag (Widrow & Kamenetsky, 2003). The results also show that the reduction of convergence time (by reducing the filter vector length) is accompanied by a corresponding increase in RMS filter error. This demonstrates that there exists an optimum number of filter tap coefficients that corresponds to the natural duration of the impulse response function. This represents the best condition for parameter extraction (allows all significant data to be used for curve-fitting) without introducing any unnecessary effects of misadjustment. Therefore, it is recommended that the number of filter tap coefficients be selected prior to the extraction of modal parameters by running the adaptation, with an excessive number of filters for a short period and selecting the number of required filter coefficients using an amplitude threshold in the FIR function. This process could be executed alongside the initial filter tap coefficient iteration technique to minimise computational time.

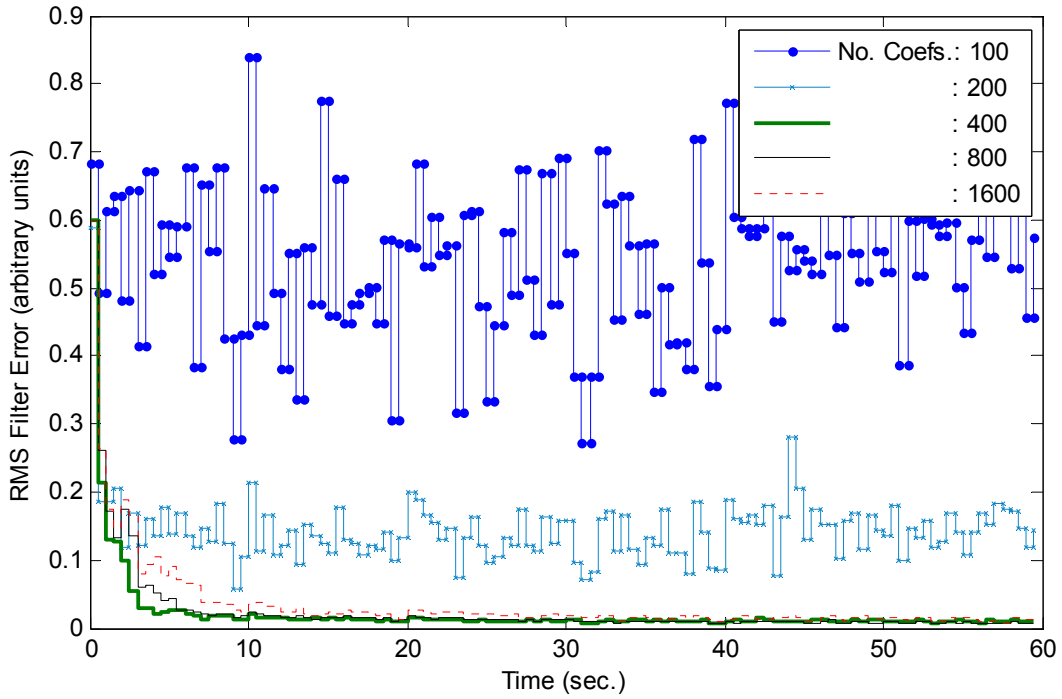


Figure 6-39: Experiment 7 - RMS Filter error signal.

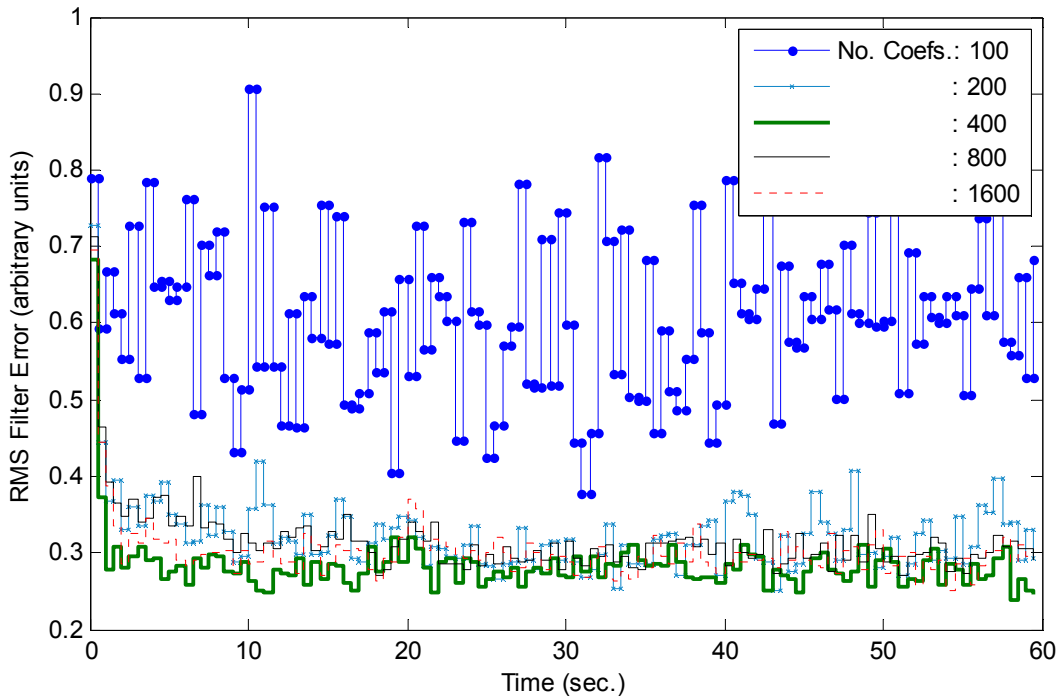


Figure 6-40: Experiment 7 - RMS Filter error signal (10% noise).

#### 6.2.4.4. Evaluation of Sampling Frequency

When using traditional, Fourier based, analysis techniques the selection of the sampling frequency is a trivial decision as the only limitation, according to Shannon's sampling theorem, is that the sample rate must be at least twice the maximum expected frequency. The lack of an upper limit for the sampling frequency means that data can be sampled as fast as possible with the available equipment, with the only limitation being data storage capacity. However, for the adaptive FIR technique the selection of the appropriate sampling frequency requires careful consideration.

In order to establish a technique for selecting the appropriate sampling frequency the modal parameters of a number of stationary, simulated, SDoF linear systems, with various natural frequencies were evaluated using a range of sampling frequencies (experiment 8). During experiment 8 a total of 50 damped natural frequency estimates were extracted from each system at each sampling frequency. The statistical mean and standard deviation of the natural frequency estimates obtained from systems with a natural frequency of 20Hz (11% damping) are shown in *Figure 6-41*, in *Figure 6-42* for a system with a natural frequency of 40Hz (11% damping) and in *Figure 6-43* for a system with a natural frequency of 80Hz (11% damping). As can be seen from these figures, the numerically simulated experiments suggest that sampling frequencies in the order of 25 times greater than the expected natural frequencies are required to minimise the variability in the results extracted, with no appreciable improvement beyond this point. For situations when high levels of extraneous noise exist, this number increases to as much as 50 times the expected natural frequency. The apparent optimum at 500Hz in *Figure 6-43* cannot be explained; however, considering the penalty for using an insufficiently high sampling rate, it is best avoided.

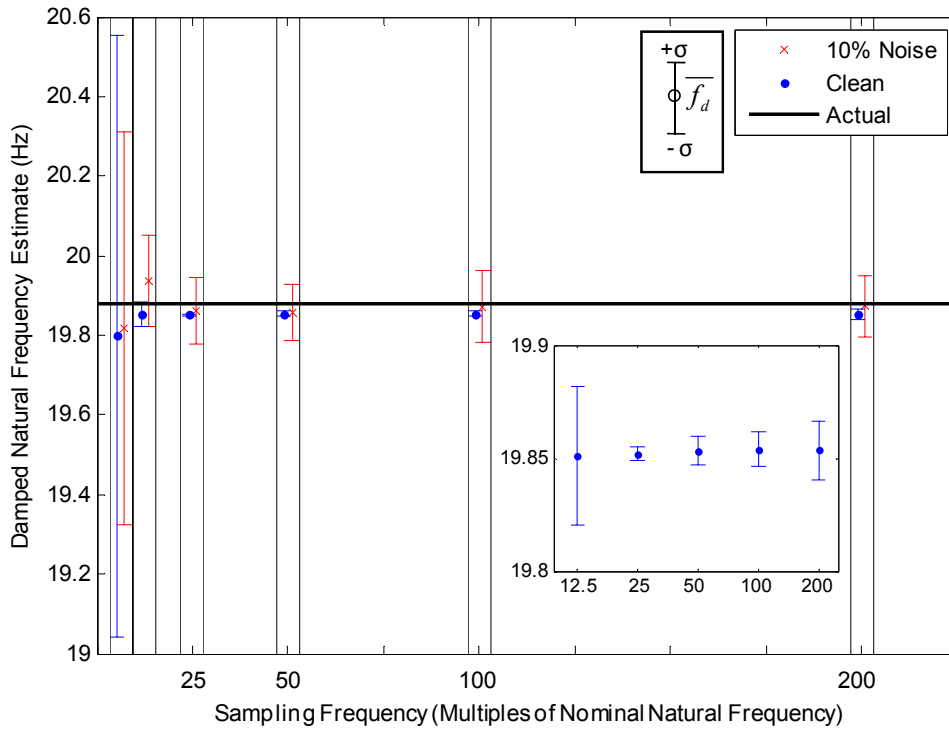


Figure 6-41: Experiment 8 - Influence of sampling frequency on results extracted from a system with 20Hz natural frequency and 11% damping (inset clean results for 500Hz-4000Hz sampling frequencies).

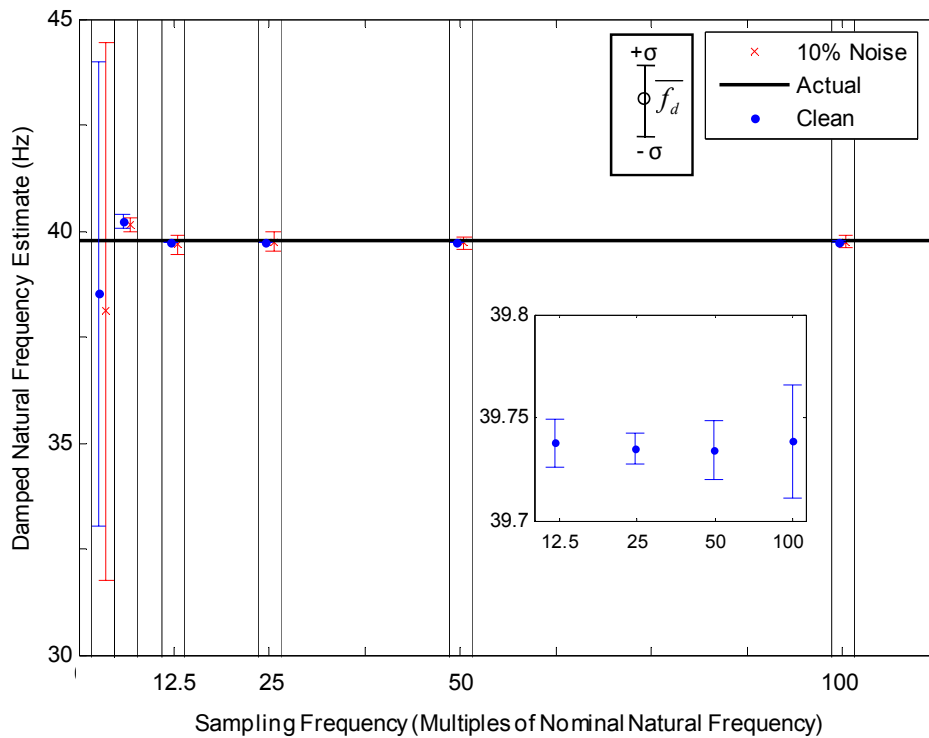


Figure 6-42: Experiment 8 - Influence of sampling frequency on results extracted from a system with 40Hz natural frequency and 11% damping (inset clean results for 500Hz-4000Hz sampling frequencies).

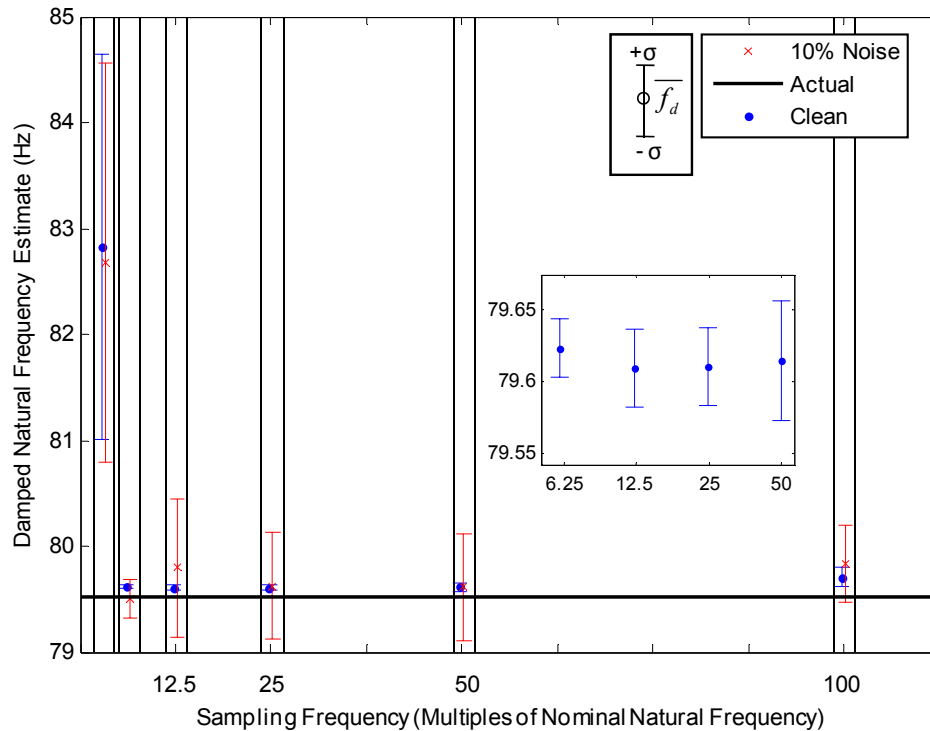


Figure 6-43: Experiment 8 - Influence of sampling frequency on results extracted from a system with 80Hz natural frequency and 11% damping (inset clean results for 500Hz-4000Hz sampling frequencies).

### 6.3. CONCLUSIONS

Free vibrations are particularly useful in modal analysis applications where their transient decay and oscillation frequency can be used to extract the fundamental modal parameters, namely natural frequency and damping ratio. Techniques which provide accurate estimates of the system's properties using limited data exist. However, materials or structures subjected to forced excitation, such as protective packaging during random fatigue testing, cannot be directly analysed using free-response techniques. This chapter discussed the development of a technique which uses a NLMS adaptive filter to convert forced excitation and response data into a series of instantaneous FIR functions to which free-response modal parameter extraction techniques can be applied. It was demonstrated that the technique is capable of extracting spectral estimates with high sensitivity without compromising temporal resolution.

A procedure which optimises the adaptation step-size using the RMS of the adaptive filter's error signal was introduced. It was shown that, for linear SDoF systems, this procedure can significantly improve the tracking ability of the adaptive FIR technique, particularly when the step-size is re-optimized at regular intervals. It was also demonstrated that significant improvements, in terms of both the spectral sensitivity and the rate of initial convergence, can

be achieved by iteratively adjusting the initial filter tap coefficients, respectively. Results which aid the selection of the appropriate values for the filter tap coefficient vector length and data sampling frequency were also presented. These results suggested that the length of the filter tap coefficient vector should be set to match, or slightly exceed, the natural duration of the impulse response function and that the sampling frequency should be in the order of 25-50 times the expected natural frequency.

## REFERENCES

- Bendat, J & Piersol, A 2000, *Random Data: Analysis and measurement procedures*, 3<sup>rd</sup> Edition, John Wiley & Sons, New York
- Dieter, G 1986, *Engineering Design: A materials and processing approach, first metric addition*, McGraw-Hill, p. 135
- Hakansson, L 2004, *Limited numerical precision and the LMS algorithm, and the leaky LMS – solution*, pp. 1 – 7
- Hassibi, B 2003, ‘On the robustness of LMS filters’, in S Haykin & B Widrow (eds), *Least-mean-squares adaptive filters*, John Wiley & Sons, New York
- Haykin, S 1986, *Adaptive filter theory*, Prentice Hall, Englewood Cliffs
- Haykin, S 1996, *Adaptive filter theory*, 3<sup>rd</sup> Edition, Prentice Hall, Upper Saddle River, pp. 432-439
- Haykin, S 2003, ‘Introduction: The LMS filter (algorithm)’, in S Haykin & B Widrow (eds), *Least-mean-squares adaptive filters*, John Wiley & Sons, New York
- Mayyas, K & Aboulnasar, T 1997, ‘Leaky LMS algorithm: MSE analysis for Gaussian data’, *IEEE transactions on signal processing*, vol. 45, no. 4, pp. 928 - 934
- Rao, S 2005, *Mechanical Vibrations*, SI Edition, Prentice Hall
- Smith, C & Wereley, N 1997, ‘Composite rotorcraft flexbeams with viscoelastic damping layers for aeromechanical stability augmentation’, *M<sup>3</sup>D III: Mechanics and mechanisms of material damping*, Wolfenden, A & Kinra, V (eds), American Society for Testing and Materials
- Thrane, N 1984, ‘The Hilbert transform’, *Technical review*, no. 3, Bruel & Kjaer, Denmark, Naerum Offset
- Widrow, B & Hoff, M 1960, *Adaptive switching circuits*, IRE WESCON convention record, vol. 4, pp. 96-104

Widrow, B & Stearns, S 1985, *Adaptive signal processing*, in Oppenheim, A (ed), Prentice Hall, Englewood Cliffs

Widrow, B & Kamenetsky, M, S 2003, 'On the efficiency of adaptive algorithms', in S Haykin & B Widrow (eds), *Least-mean-squares adaptive filters*, John Wiley & Sons, New York

## **Chapter 7 NUMERICAL COMPARATIVE STUDY**

The preceding chapters have discussed the development of two alternative continuous structural integrity assessment techniques, one which makes use of a modified short-time Fourier transform (STFT) and another which relies on adaptive digital filtering. During the development of the Fourier based technique it was shown that its application requires a compromise between the temporal and spectral resolutions. With the development of the adaptive digital filtering approach this compromise was all but eliminated. However, the adaptive filtering technique also contains inherent limitations which require further evaluation.

This chapter evaluates, compares and discusses the performance of both techniques using the results from various numerically simulated experiments.

### **7.1. SELECTION OF ANALYSIS PARAMETERS**

In order to achieve a fair comparison between the two structural integrity assessment techniques, it is necessary to ensure that they are both operating at their full potential. Therefore, the selection of the optimum analysis parameters is vital. Chapters 5 and 6 provide a detailed evaluation of the assessment techniques (chapter 5 focuses on the Fourier technique while chapter 6 covers the adaptive finite-impulse-response method), particularly the influence of variations in specific analysis parameters. The following sections (7.1.1 and 7.1.3) draw from these chapters in order to provide techniques for selecting analysis parameters which are close to the optimum values.

### 7.1.1. Fourier Based Technique

The STFT is a pseudo-stationary analysis technique. That is, the assumption must be made that the data is piecewise stationary for each ensemble length. This means that optimum parameters for the analysis of nonstationary records can be made using the results obtained from the stationary numerically simulated experiments discussed in chapter 5.

As discussed in chapter 5, when analysing random data with any Fourier based technique a compromise between resolution, both temporal and spectral, and spectral uncertainty (averaging) is unavoidable. In order to establish the correct, or best, compromise it is necessary to recall the following results (refer to chapter 5):

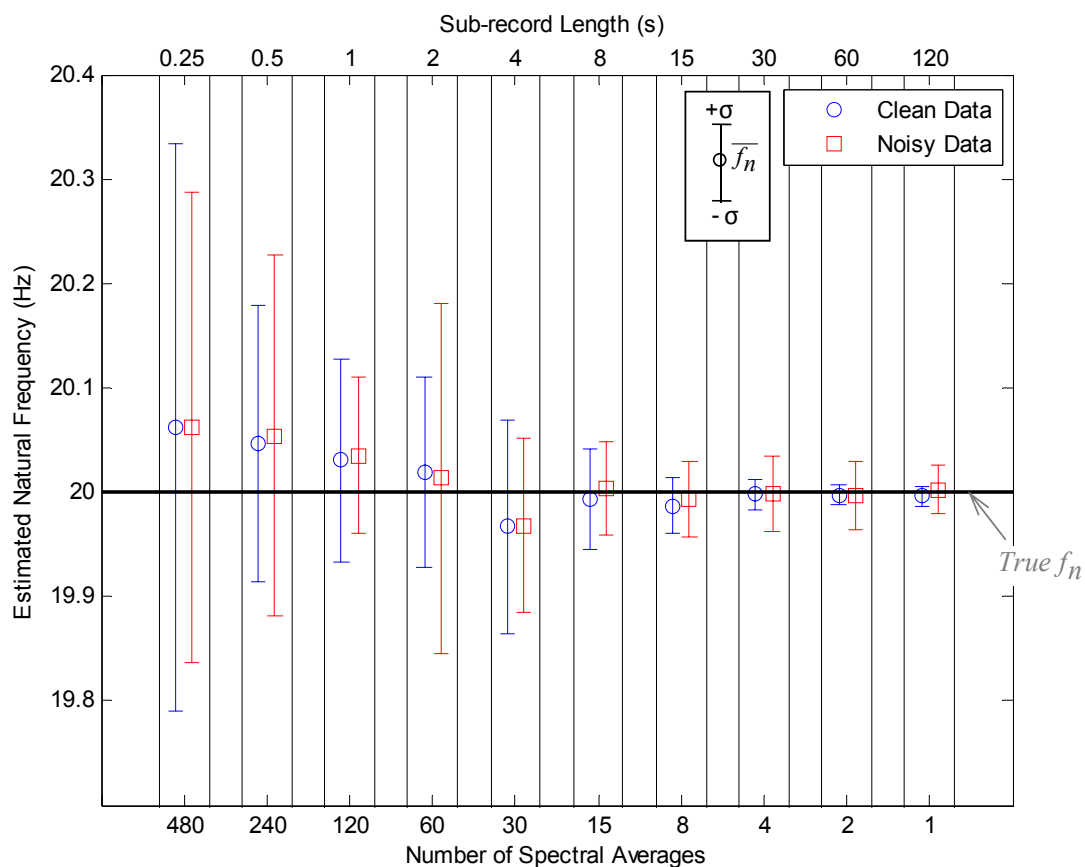


Figure 7-1: Importance of sub-record length versus spectral averaging.

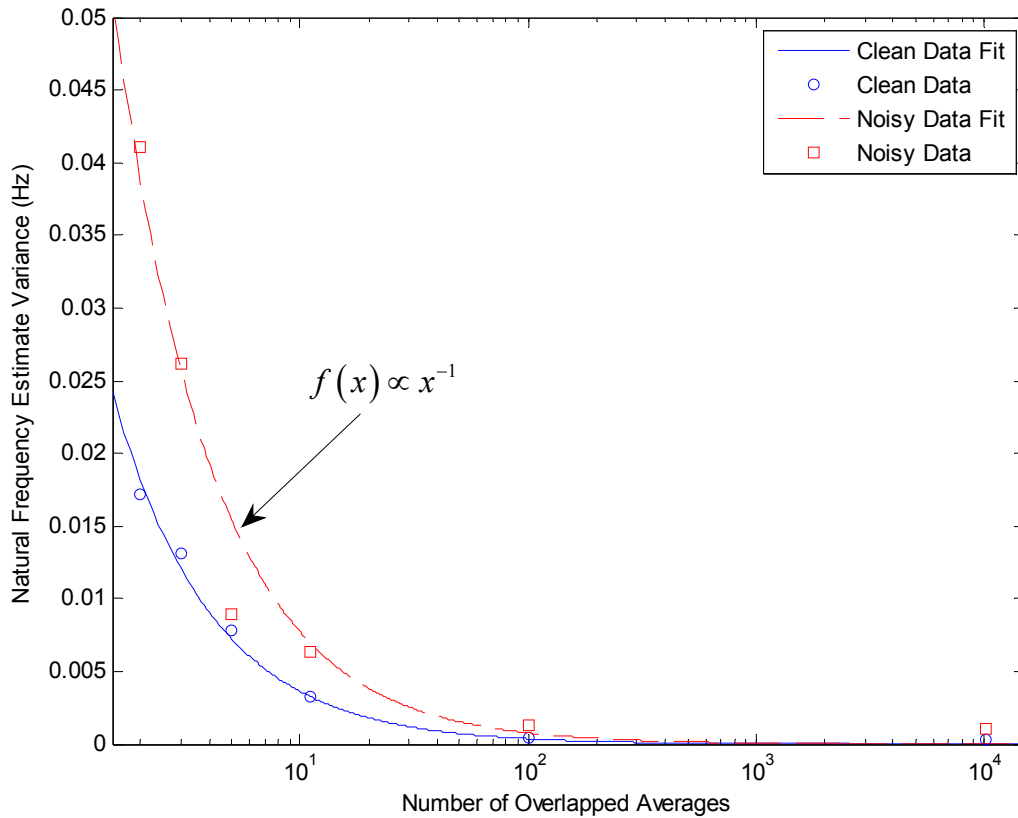


Figure 7-2: Effect of overlapped averages ( $x$ ) on estimated natural frequency variance.

Figure 7-1 shows that, when monitoring variations in natural frequency using estimates of a system's short-time frequency response function (FRF), it is better to compromise spectral averaging than it is to reduce the sub-record length. This, as stated in earlier sections, is particularly well demonstrated by the results for the 120 second sub-record, which provides fine spectral resolution (0.0083Hz) but does not allow for any spectral averaging (100% theoretical uncertainty). Also, the results given in Figure 7-2 suggests that the natural frequency estimate variance is inversely proportional to the number of overlapped spectral averages used (when extracting estimates of natural frequency using frequency response magnitude spectra obtained from limited data), as well as a depreciating return when using in excess of approximately 100 overlapped spectral averages. These findings indicate that the data overlapping should always be set to maximum (all but one point is overlapped from one sub-record to the next) and that spectral averaging should be limited to in order to achieve the highest possible spectral resolution.

The optimum value for the number of overlapped averages depends on the sampling frequency used to collect the data, the desired temporal resolution and the level of extraneous noise. The dependence on sampling frequency occurs because, when maximum overlap is applied, a higher number of averages can be afforded at higher sampling rates as the percentage overlap is increased.

Figure 7-3 and Figure 7-4 demonstrate the dependence of the optimum values for the number of overlapped averages on sampling frequency and desired temporal resolution. Figure 7-3 presents the results obtained at a temporal resolution of 5 seconds from data sampled at a rate of 2048Hz. Figure 7-4 presents the results obtained at a temporal resolution of 1 second from data sampled at a rate of 1000Hz. Both data sets contained 10% extraneous noise. As can be seen the optimum number of averages for the second data set is significantly lower than it is for the first. This demonstrates the problems associated with finding an optimum number of averages; variations in the level of extraneous noise will increase the difficulty even further.

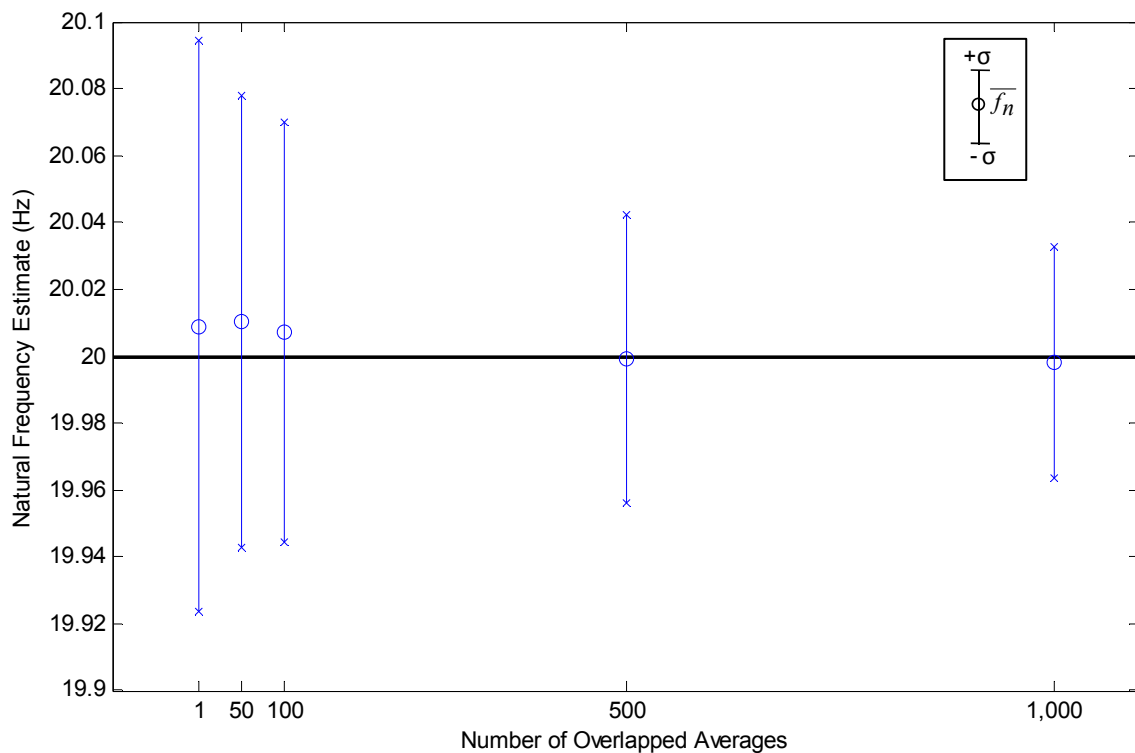


Figure 7-3: Dependence of optimum averaging amount on sampling frequency and temporal resolution (sampling frequency: 2048Hz, temporal resolution: 5 seconds).

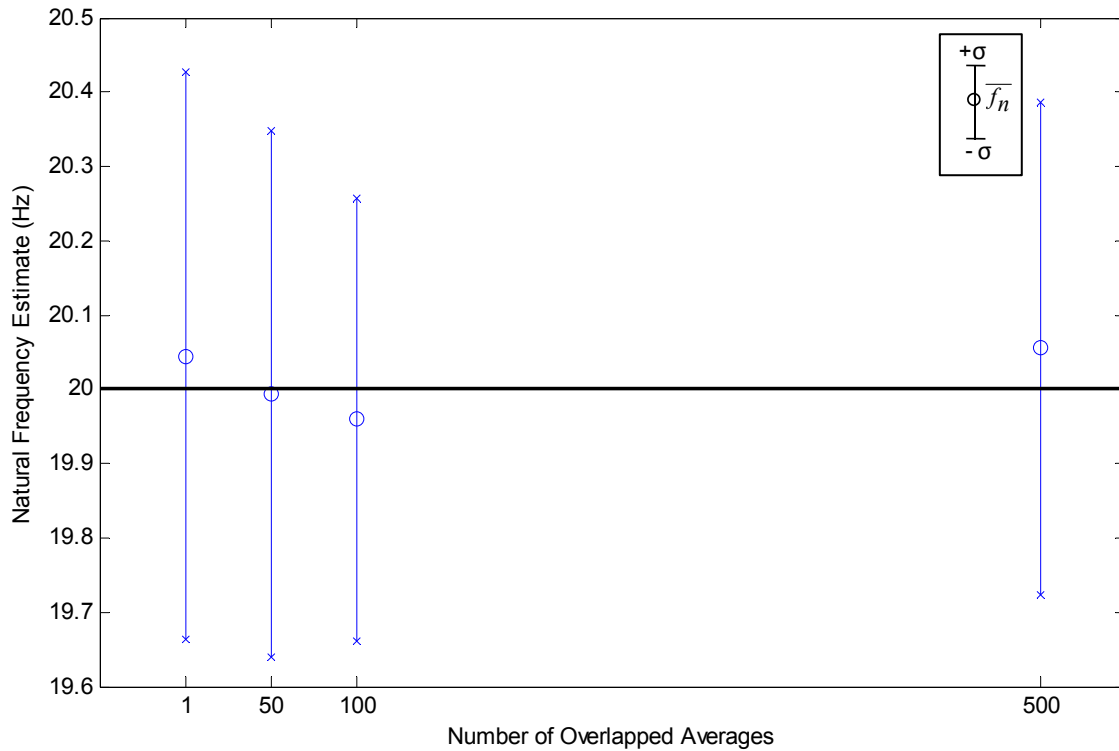


Figure 7-4: Dependence of optimum averaging amount on sampling frequency and temporal resolution (sampling frequency: 1000Hz, temporal resolution: 1 second).

When analysing data with very fine temporal resolution it becomes particularly important to maximise the analysis sub-record length. For this reason, for the results presented in the following sections, the number of overlapped spectral averages will be limited to 100. Using 100 overlapped averages the analysis sub-record length can be determined using:

$$srl = \Delta t - \frac{99}{sf} \quad (7-1)$$

, where 99 represents the number of overlapped spectral averages less one.

In addition to the selection of the optimum sub-record length, number of averages and percentage overlap, zero-padding should also be applied. Recall the follow results:

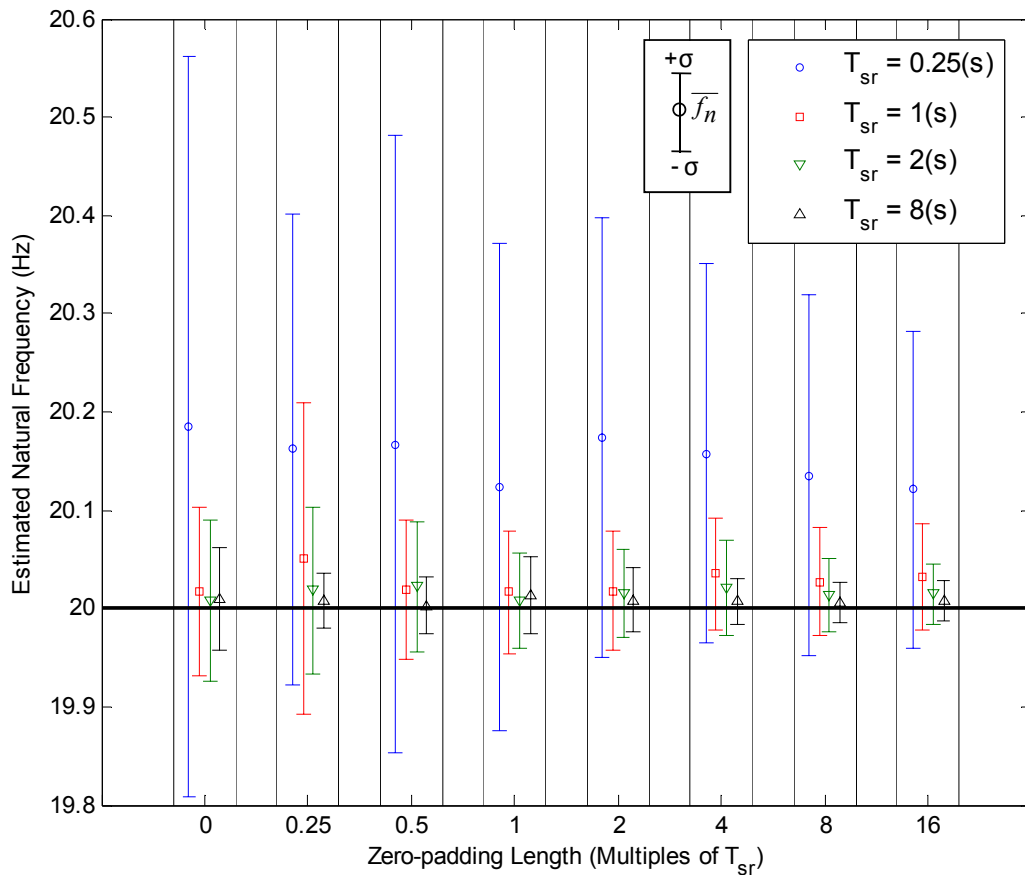


*Figure 7-5: Improvements though zero-padding*

*Figure 7-5* demonstrates that for modal parameter extraction purposes, zero-padding of up to 16 times the sub-record length can significantly reduce the variance of the extracted estimates. Therefore, in each of the following comparative experiments 16 times zero-padding will be applied.

## 7.1.2. Overview of Fourier Based Technique

A schematic representation of the algorithm used for the Fourier based continuous integrity assessment technique is given in *Figure 7-6* below. The software used for analysis was created by the author and can be made available upon request.

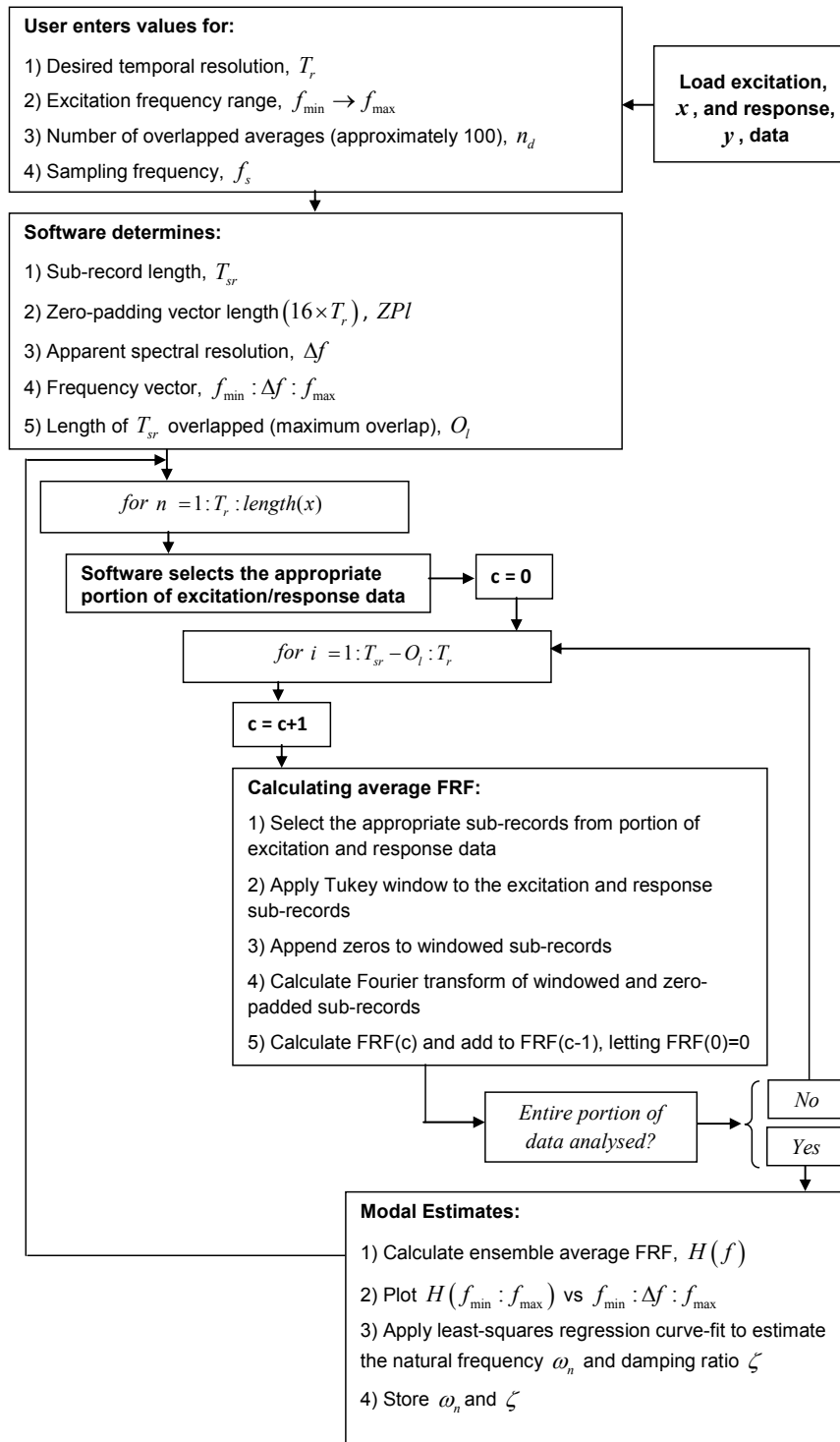


*Figure 7-6: Schematic representation of algorithm for Fourier based integrity assessment technique.*

A pictorial representation of the major steps in the aforementioned schematic is given in the following series of figures.

*Figure 7-7* and *Figure 7-8* present the evolution of the frequency response function (FRF) of a simulated linear single degree-of-freedom (SDoF) with a 10% stiffness reduction every 60 seconds. Estimates of the system's FRF were made using short, successive groups (sub-records) along the length of data. The parameters were set to achieve fine temporal and spectral resolutions (therefore limited averages).

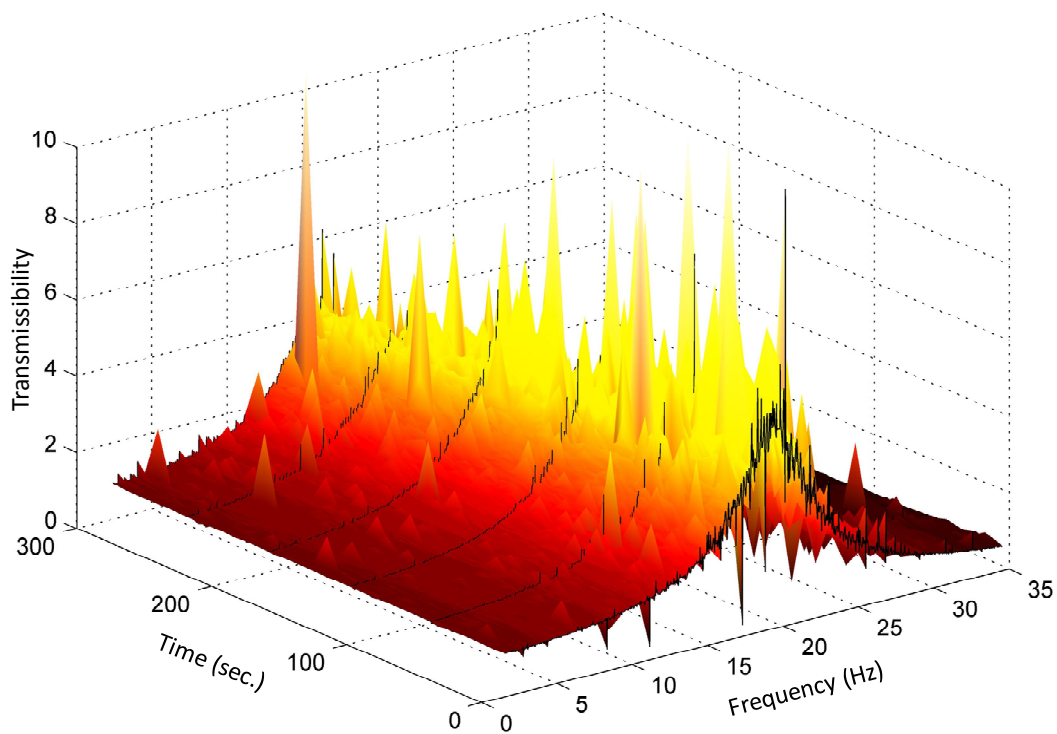


*Figure 7-7: Evolution of a system's FRF.*

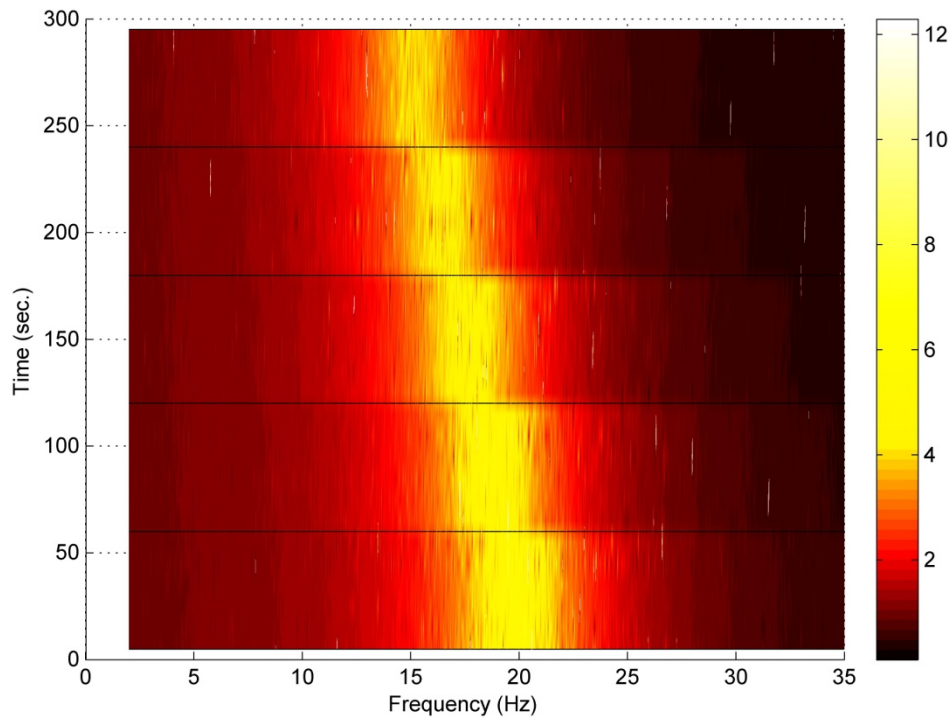


Figure 7-8: FRF spectrogram.

Using each of the average FRFs the modal properties of the system as a function of time can be estimated. This estimation is achieved using least-squares regression curve-fitting techniques to select the modal parameters of a theoretical model which closely matches the experimental results.

The results presented in *Figure 7-8 and Figure 7-9* were obtained from the acceleration records (excitation and response) of a SDoF system subjected to random base excitation and are therefore best described using Equation (7-2):

$$|H(f)| = \left( \frac{1 + \left[ 2\zeta \left( \frac{f}{f_n} \right) \right]^2}{\left[ 1 - \left( \frac{f}{f_n} \right)^2 \right]^2 + \left[ 2\zeta \left( \frac{f}{f_n} \right) \right]^2} \right)^{\frac{1}{2}} \quad (7-2)$$

*Figure 7-10* presents the fit of Equation 7-2 to the estimate of the system's final (295<sup>th</sup> second) FRF.

Finally, the parameters of the system can be plotted as a function of time, as shown in *Figure 7-10* for the system's damped natural frequency.

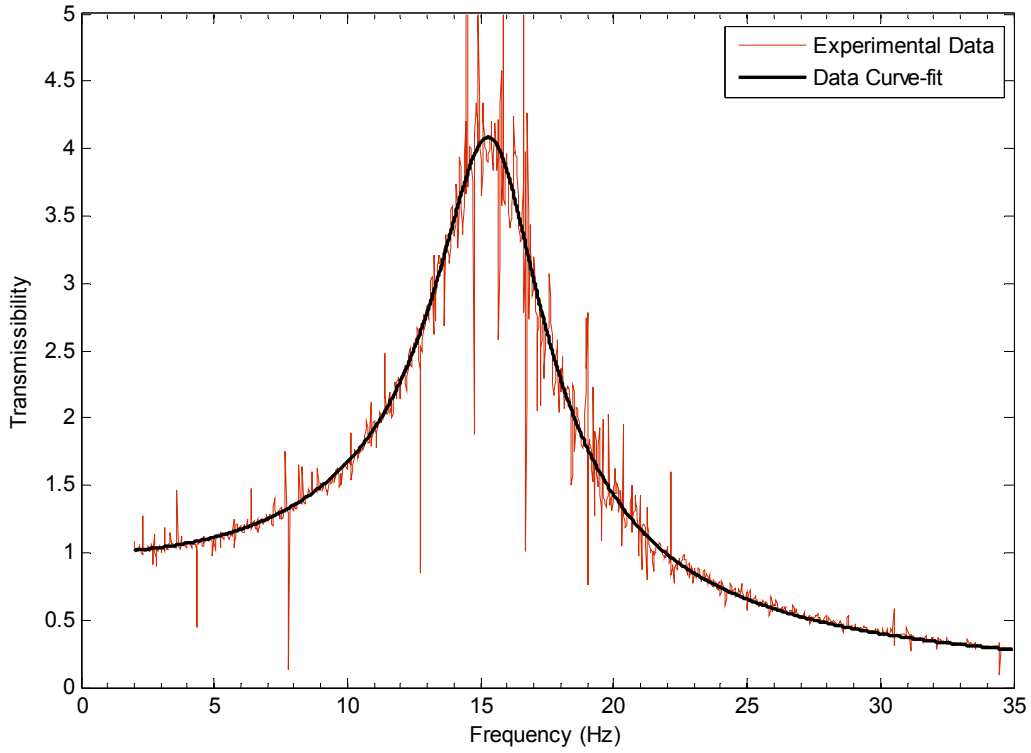


Figure 7-9: Parameter extraction from final (295<sup>th</sup> second) FRF estimate.

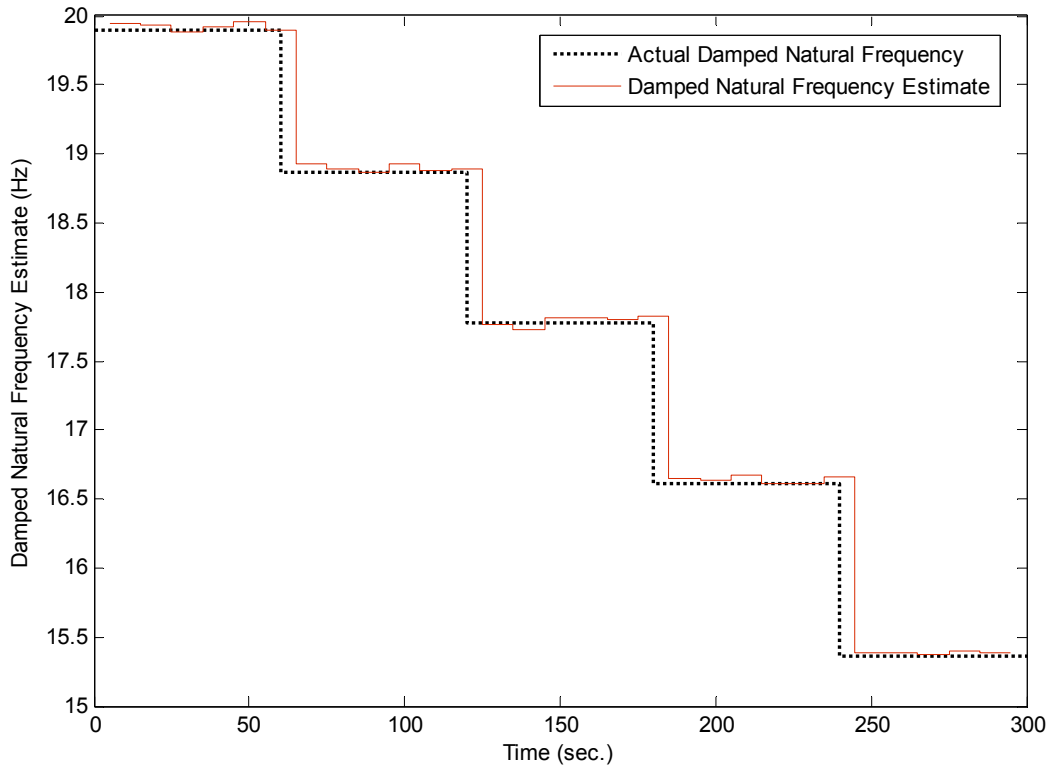


Figure 7-10: Damped natural frequency as a function of time.

### 7.1.3. Adaptive Finite Impulse Response Technique

The selection of the parameters used for the adaptive finite-impulse-response (FIR) technique is clearer, than that for the Fourier based technique, as a result of the development work presented in chapter 6.

First consider the step-size to be used. This selection is trivial provided that at least 1000 points are allowed between each step-size update as the optimisation algorithm used is capable of selecting the correct values automatically. As was suggested in chapter 6, re-optimisation should not be performed over a period shorter than the desired temporal resolution.

The adaptive FIR technique requires two entries for the filter tap coefficient vector, the vector length and the initial coefficients. In chapter 6 it was established that the number of coefficients used must be sufficient to span the natural duration of the initial FIR function, see *Figure 7-11* and *Figure 7-12*, in order to achieve sufficient accuracy.

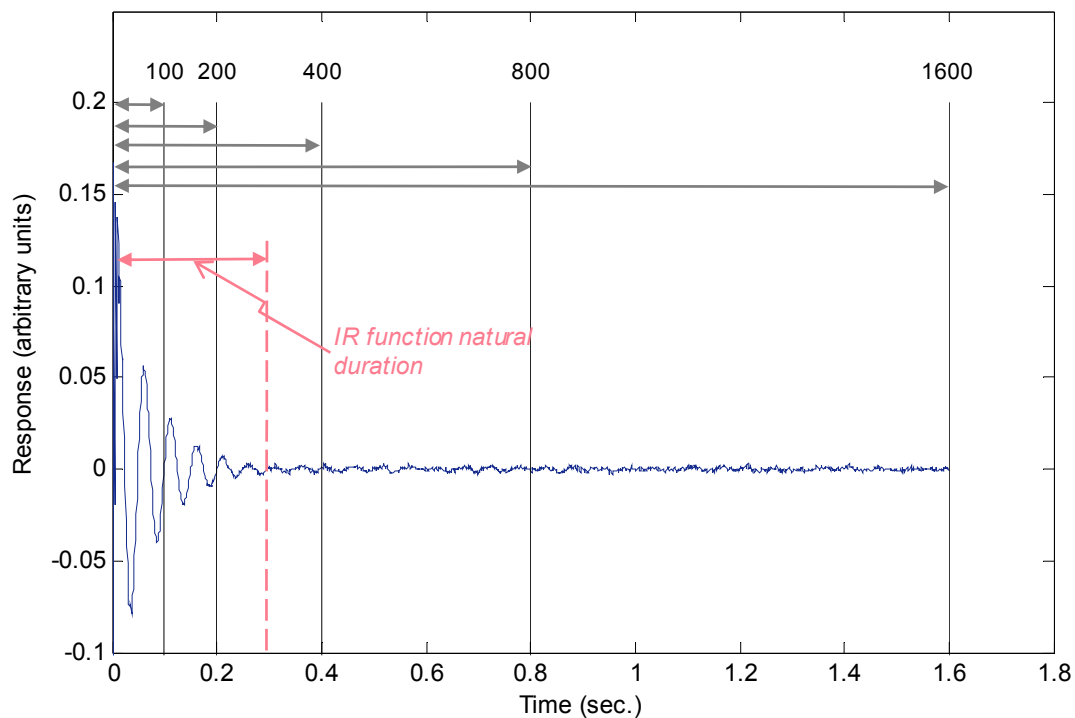


*Figure 7-11: Demonstration of filter tap coefficient vector length and impulse response natural duration.*

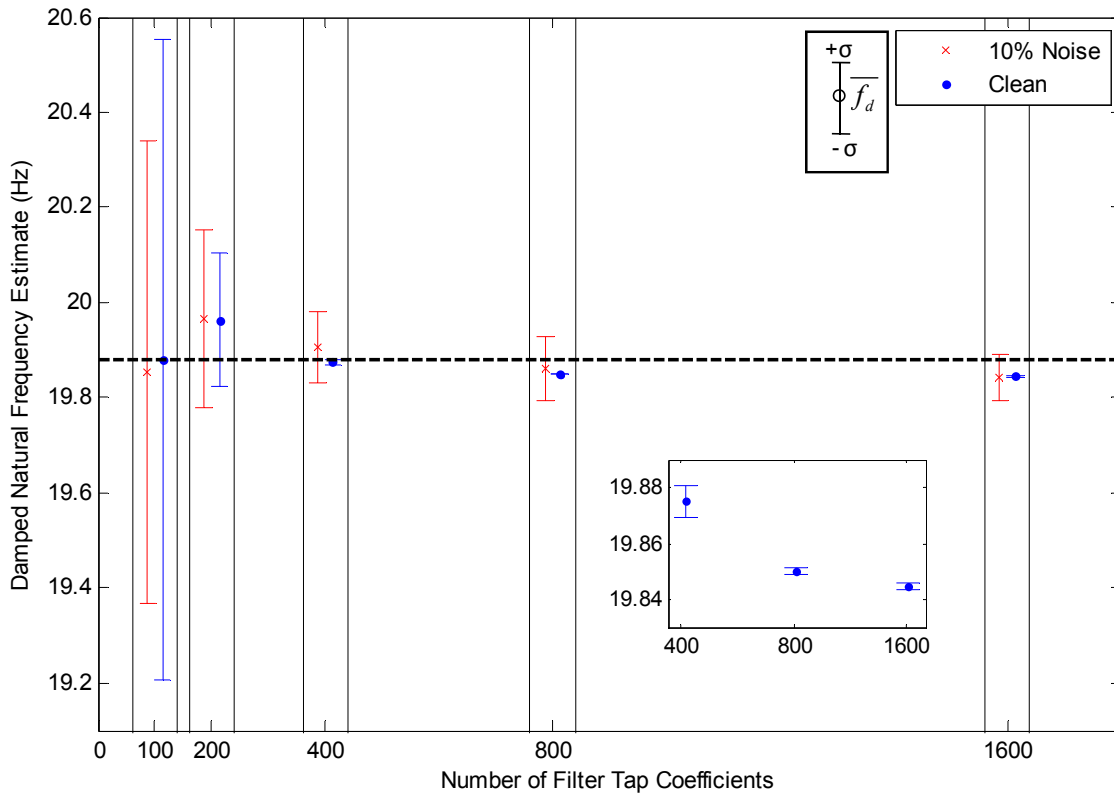
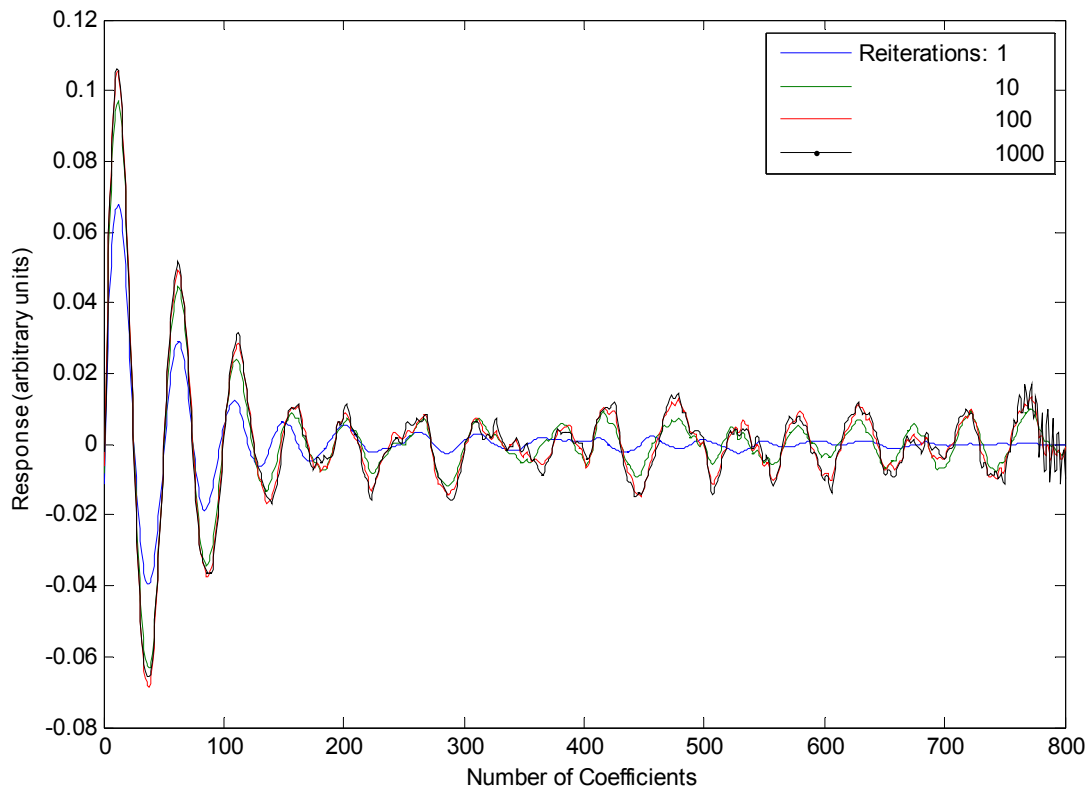


Figure 7-12: Influence of filter tap coefficient vector length on damped natural frequency estimates (inset clean results for 400-1600 filter tap coefficients).

It was also shown that filter tap coefficient vectors in excess of this length will introduce an unnecessary misadjustment due to lag. Therefore, in order to select an appropriate vector length, it is recommended that the user runs a short adaptation (short is governed by the time to converge to the initial impulse response function, from an initial estimate of zeros), with an excess number of filter tap coefficients, (excess can be estimated using the expected damping and natural frequency, or by increasing the number of coefficients incrementally) to determine the natural duration of the initial FIR function. Once the natural duration is established, the filter tap coefficient vector length should be set in order to span slightly in excess of this duration (excess allows for potential increases in natural duration as well as the influence of low amplitude oscillations which may otherwise distort the estimated FIR function). After the filter tap coefficient vector length is set, the initial filter coefficients can be estimated either by using the appropriate portion of the FIR function used to select the vector length, or the previously described reiteration technique (see section 6.2.4.2). If the signal under analysis is expected to be nonstationary in the initial stages of testing the reiteration technique should be used, as it will improve initial convergence. The only decision required when implementing the reiteration technique is the number of iterations, as the

adaptive filter will find the best possible initial estimate automatically. The only limitation on the number of reiterations is computational time. Therefore the number of iterations can be set based on the maximum desired computational time or a minimum number of iterations. Preliminary work has suggested that as little as 100 reiterations can converge to the optimum initial filter tap coefficient vector. A typical example of various stages in reiteration is given in *Figure 7-13*.



*Figure 7-13: Typical example of stages in the initial filter tap reiteration procedure.*

The final parameter to be selected is the rate at which the experimental data are sampled (the data sampling rate). Results given in chapter 6 have suggested that a sampling frequency in the order of 25-50 times greater than the expected natural frequency of the system under analysis is required, with approximately 50 times being the more stable of the two options.

### 7.1.4. Overview of Adaptive Finite-Impulse-Response Techniques

A schematic representation of the algorithm used for the adaptive FIR integrity assessment technique is given in *Figure 7-14*. The software used for analysis was written by the author and can be made available upon request.

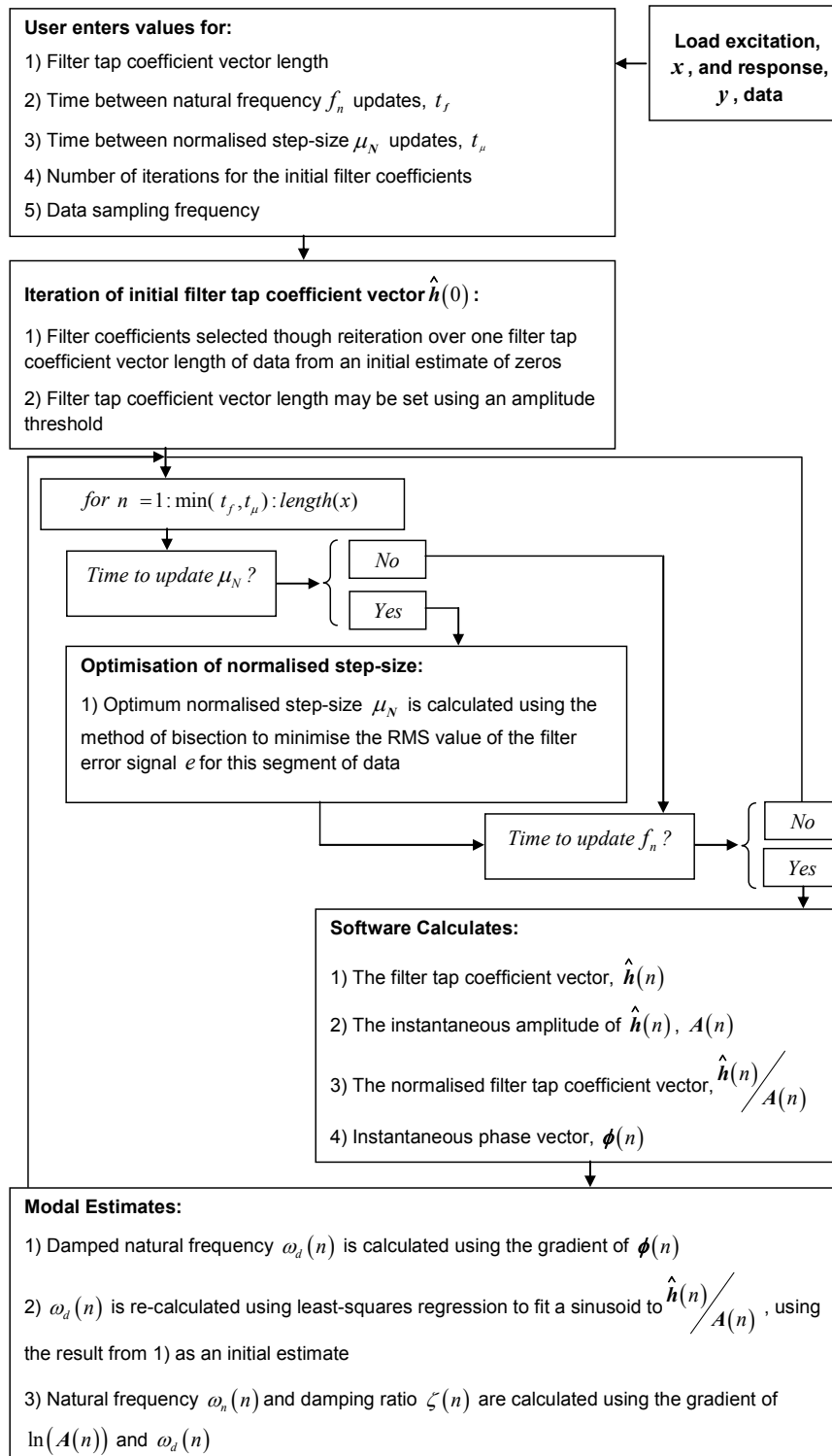


*Figure 7-14: Schematic representation of algorithm for adaptive FIR integrity assessment technique.*

A pictorial representation of the major steps in the aforementioned schematic is given in the following series of figures.

Figure 7-15 presents the evolution of the FIR function of a simulated linear SDoF with a reduction of 10% in its stiffness every 60 seconds. Estimates of the system's FIR function were made continually using an optimised step-size which was updated after processing 2000 data points (or equivalently once every 2 seconds for a sampling frequency of 1000Hz).

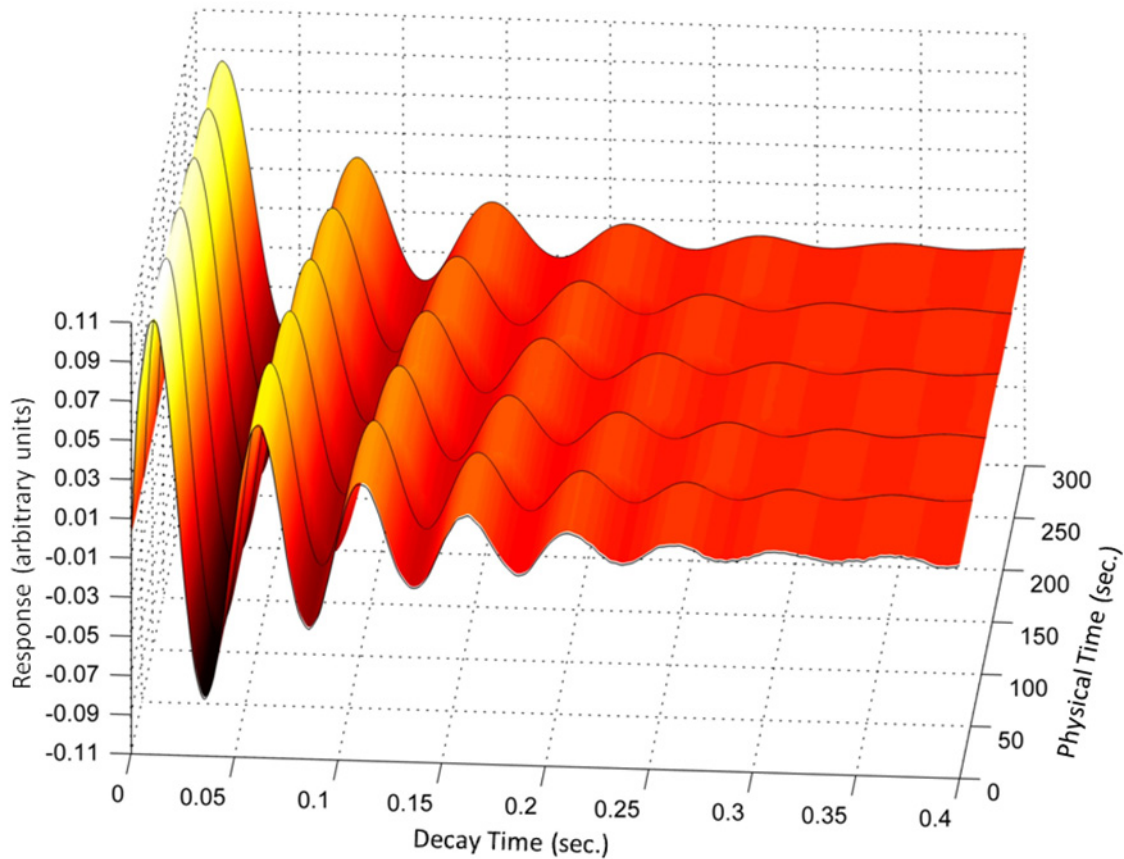
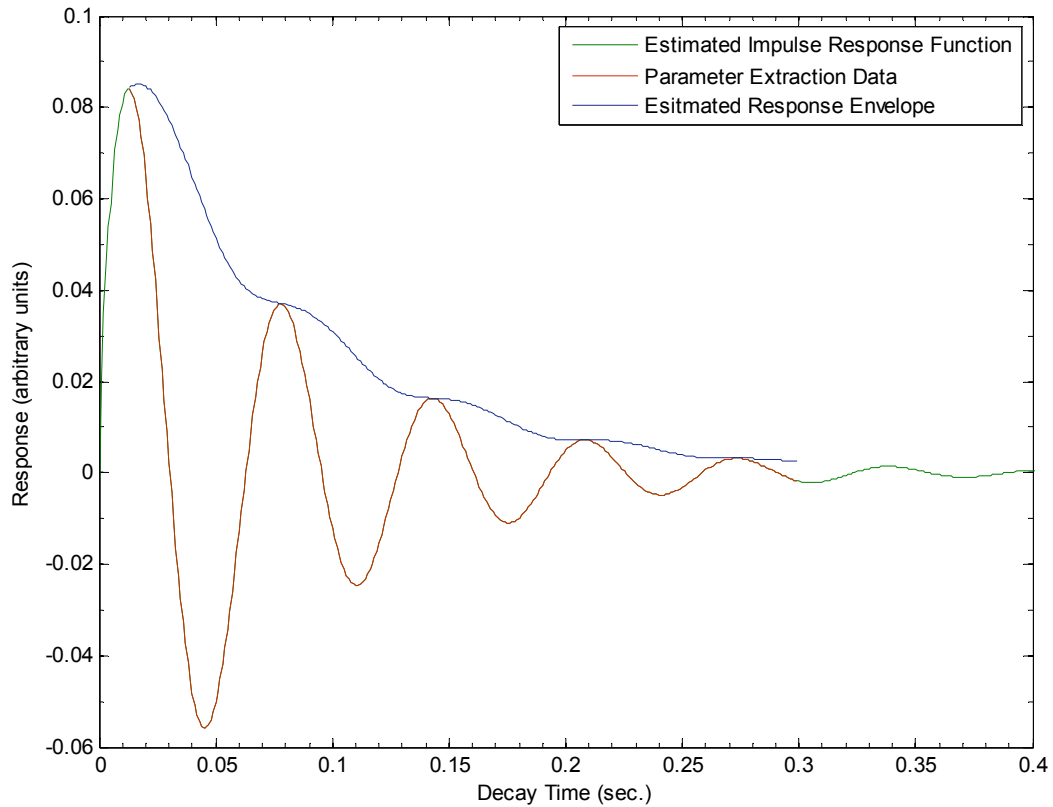


Figure 7-15: Evolution of a system's FIR function.

By performing the Hilbert transform on the appropriate portion of each of the system's instantaneous FIR functions an initial estimate of the system's damping ratios and natural frequencies (damped and undamped), for each point in time, can be obtained. Figure 7-16 shows the portion of data used for parameter extraction from the final (300<sup>th</sup> second) FIR. Also shown is the decay envelope (or instantaneous magnitude vector calculated using the Hilbert transform). If the system is viscously under-damped this envelope can be used to estimate the product of the system's viscous damping ratio and undamped natural frequency.



*Figure 7-16: Parameter extraction from final (300<sup>th</sup> second) instantaneous FIR function.*

The system's damped natural frequency is estimated using the gradient of the un-wrapped instantaneous phase vector, calculated using the Hilbert transform (which is equal to the system's damped natural frequency). This calculation is not dependant on the type of damping within the system. *Figure 7-17* presents the un-wrapped instantaneous phase vector which corresponds to the FIR function shown in *Figure 7-16*.

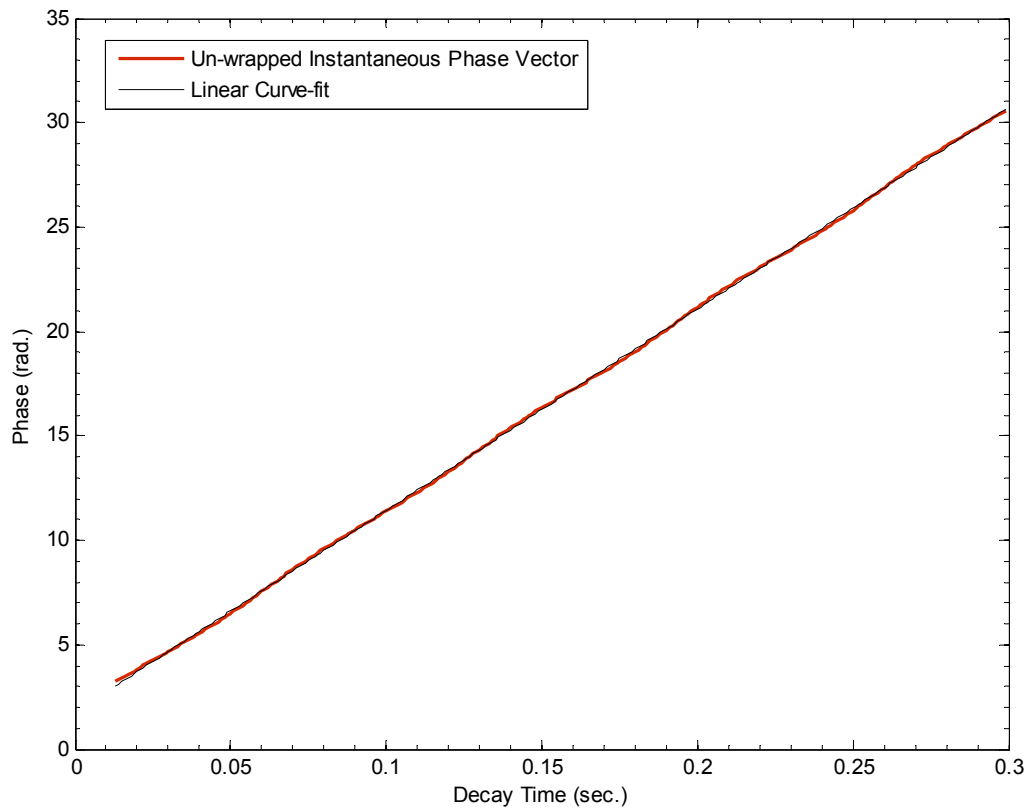


*Figure 7-17: Un-wrapped instantaneous phase vector for the final (300<sup>th</sup> second) FIR function.*

Using the instantaneous magnitude vector (as shown in *Figure 7-16*) the normalised FIR can be obtained. *Figure 7-18* and *Figure 7-19* present the evolution of the system's normalised FIR function.

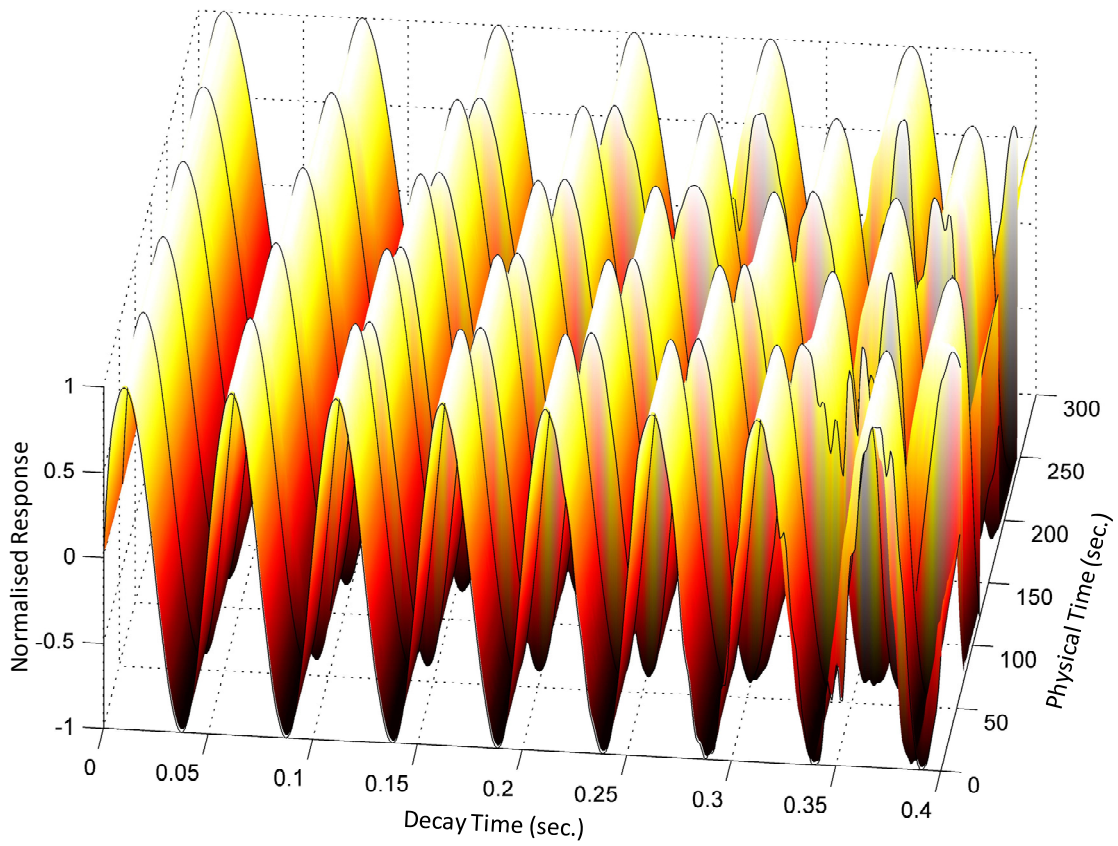


Figure 7-18: Evolution of the system's normalised FIR function.

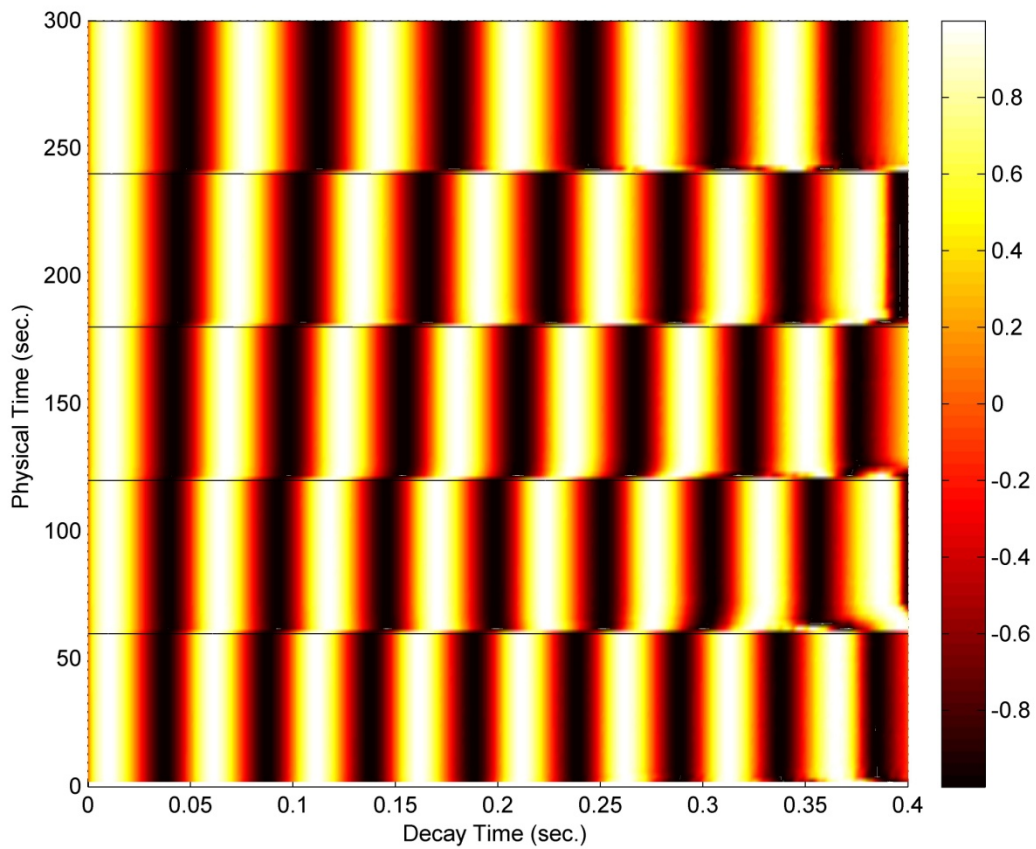


Figure 7-19: Normalised FIR function spectrogram.

Each of the normalised instantaneous impulse response functions are effectively sinusoidal waves with amplitude one. Therefore, the system's instantaneous damped natural frequency can be obtained by applying a sinusoidal curve-fit, with the value of instantaneous damped natural frequency determined using the instantaneous frequency vector as the initial estimate. This can improve the initial estimate (estimate from phase data) if contaminated data are analysed, however, if the data appropriate for curve-fitting is significantly limited (less than one period) no improvements in the results are expected.

Figure 7-20 shows the sinusoidal curve-fit of the final (300<sup>th</sup> second) normalised instantaneous impulse response function.

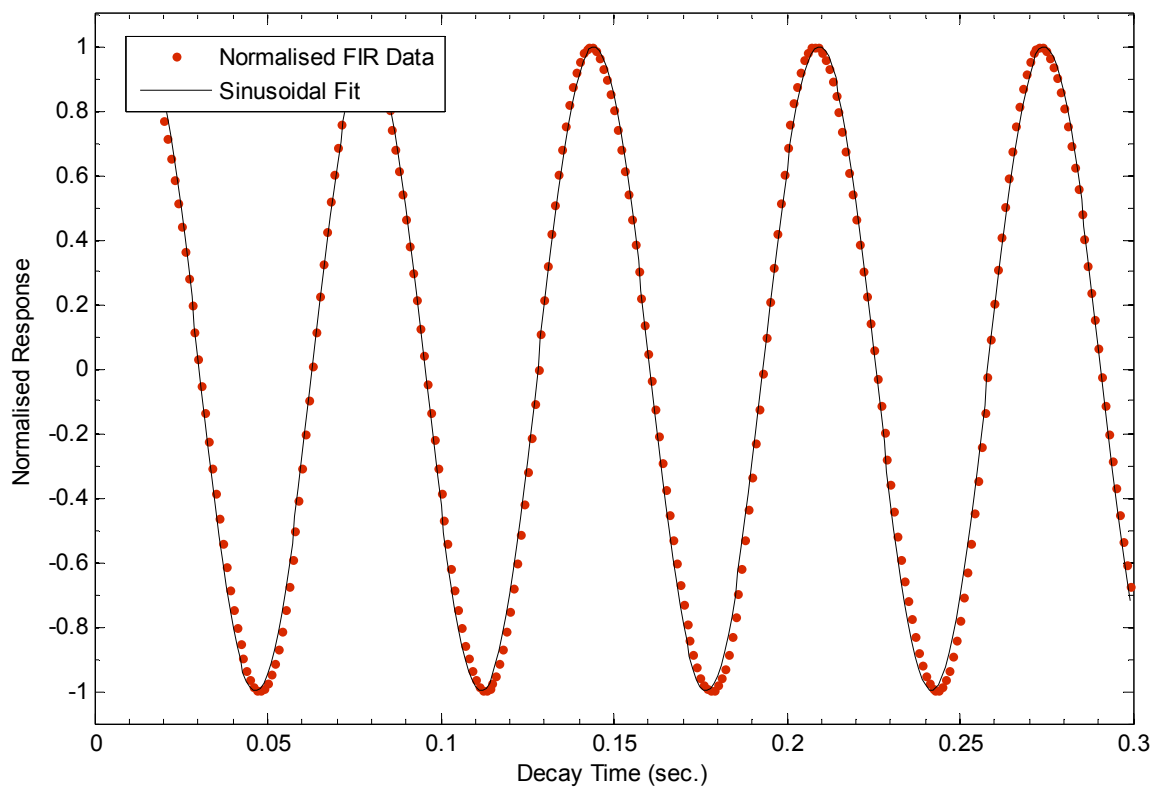
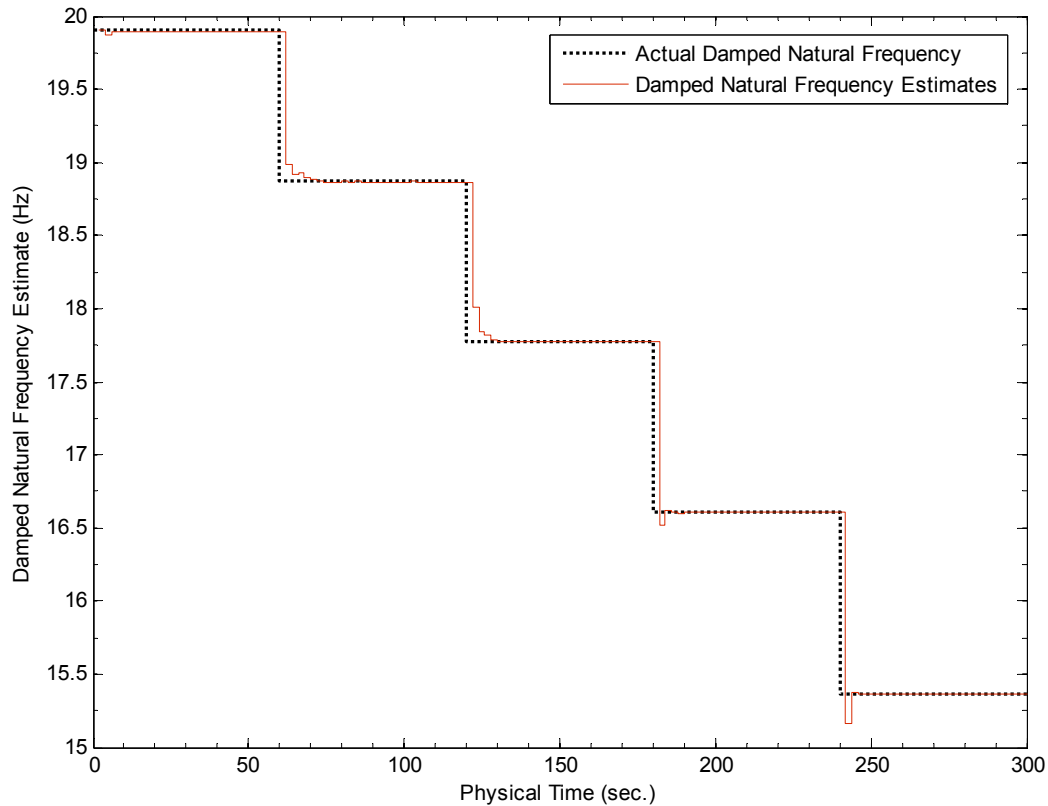


Figure 7-20: Sinusoidal curve-fit of the final (300<sup>th</sup> second) normalised instantaneous impulse response function.

Finally, the parameters of the system can be plotted as a function of time, as shown in *Figure 7-21* for the system's damped natural frequency.



*Figure 7-21: Damped natural frequency as a function of time.*

## 7.2. COMPARATIVE INFLUENCE OF NOISE

Data collected from physical experiments will contain extraneous noise to some degree of severity. Therefore, it is important to evaluate the influence of extraneous noise on the results obtained when applying both continuous structural integrity assessment techniques. In order to determine this influence, various levels of extraneous noise were added to excitation-response data obtained from a time invariant SDoF numerical model with arbitrary values for the natural frequency and damping ratio (20 Hz and 11% respectively). Both techniques were used to extract estimates of damped natural frequency, at a temporal resolution of 1 second, for each level of extraneous noise. Results from the early stages of estimation were removed to avoid issues associated with convergence. The statistical results from the 50 independent tests used in this series of experiments are presented in *Figure 7-22*. As can be seen the adaptive FIR technique is significantly more sensitive to the addition of noise than the Fourier based technique. However, the results also clearly demonstrate that, at this temporal resolution, the adaptive FIR technique is clearly the more precise of the two techniques.

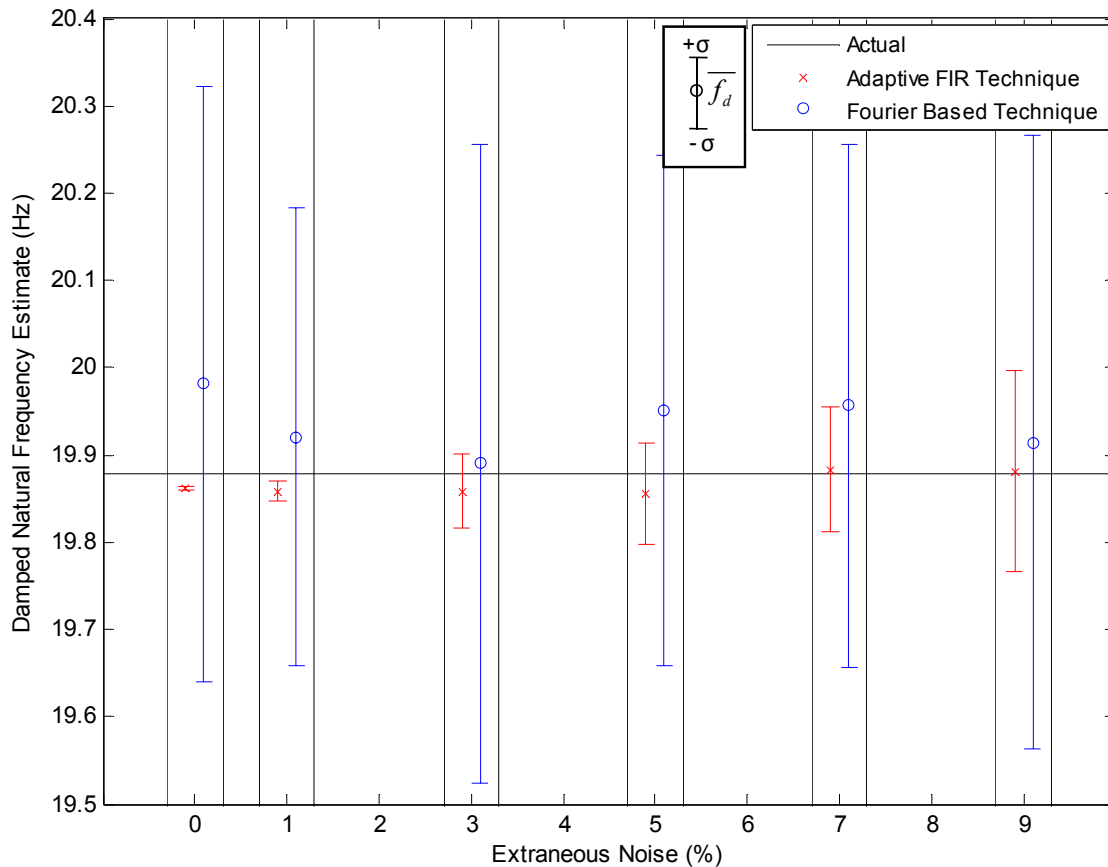


Figure 7-22: Comparison of the influence of noise on the adaptive FIR and Fourier based techniques.

Since it has been established that the impulse response technique is more sensitive to noise and that, at this time resolution, it is likely to have less estimation variance than the Fourier based technique, the following sections will only compare the results for 0% and 8% extraneous noise.

### 7.3. COMPARATIVE INFLUENCE OF DAMPING

The adaptive FIR technique will be limited at high damping ratios, since the data appropriate for curve-fitting is limited by the natural duration of the system's underdamped impulse response function (for estimates of damping it will also be limited due to the underdamped model used, that is if the system becomes critically damped or overdamped). In order to establish the range of damping ratios over which the adaptive FIR technique can extract meaningful estimates of natural frequency a second set of comparative experiments was performed. During this set of experiments time invariant numerical SDoF systems with an arbitrary natural frequency of 20Hz and damping ratios between 1% and 32% (this range of damping ratios, considered very broad from mechanical systems, was used expressly to

establish the limitations of the FIR technique) were analysed at a temporal resolution of 1 second. Results from the early stages of estimation were removed to avoid issues associated with convergence. Statistical analysis was performed on 50 estimates for each level of damping, with and without the application of extraneous noise. The results from systems containing no extraneous noise are given in *Figure 7-23*, and those from systems containing 8% extraneous noise are given in *Figure 7-24*. As can be seen, the FIR technique becomes significantly limited beyond approximately 16% damping as a result of a lack of meaningful impulse response data. In order to provide a better understanding of why this limitation exists, typical FIR functions with various levels of damping are given in *Figure 7-25*.

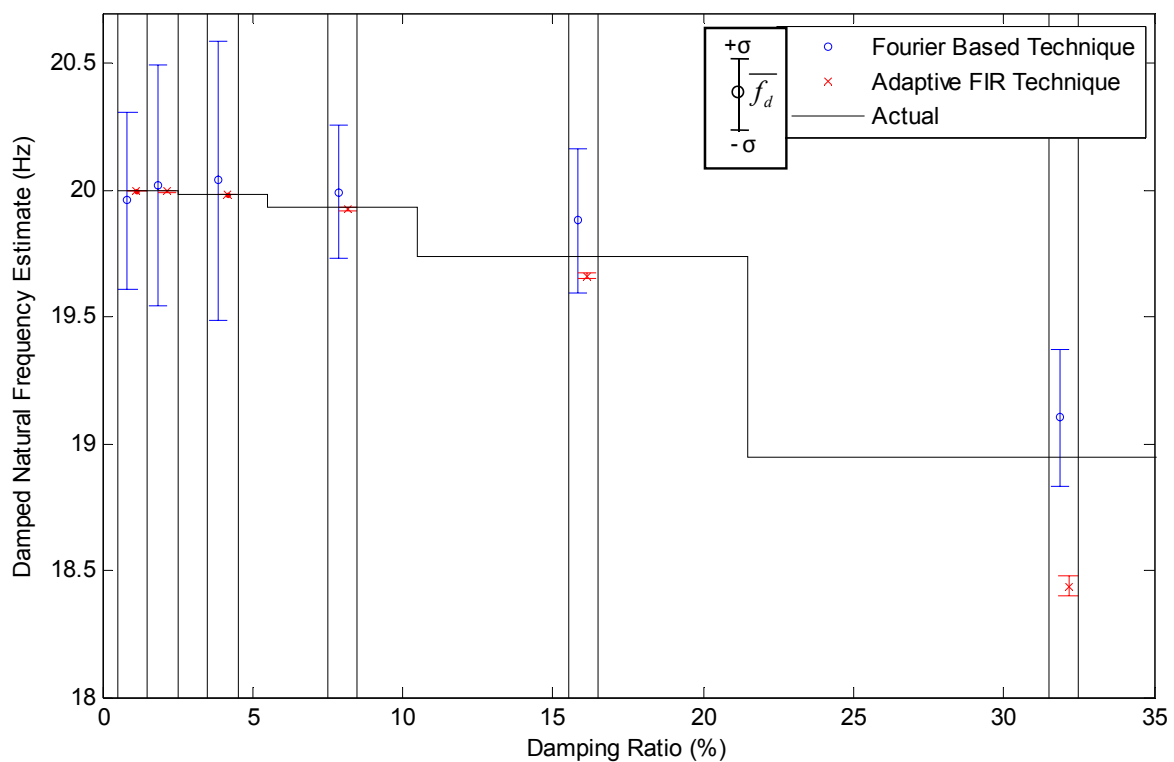


*Figure 7-23: Comparison of the influence of increased damping on the adaptive FIR and Fourier based techniques (0% noise).*

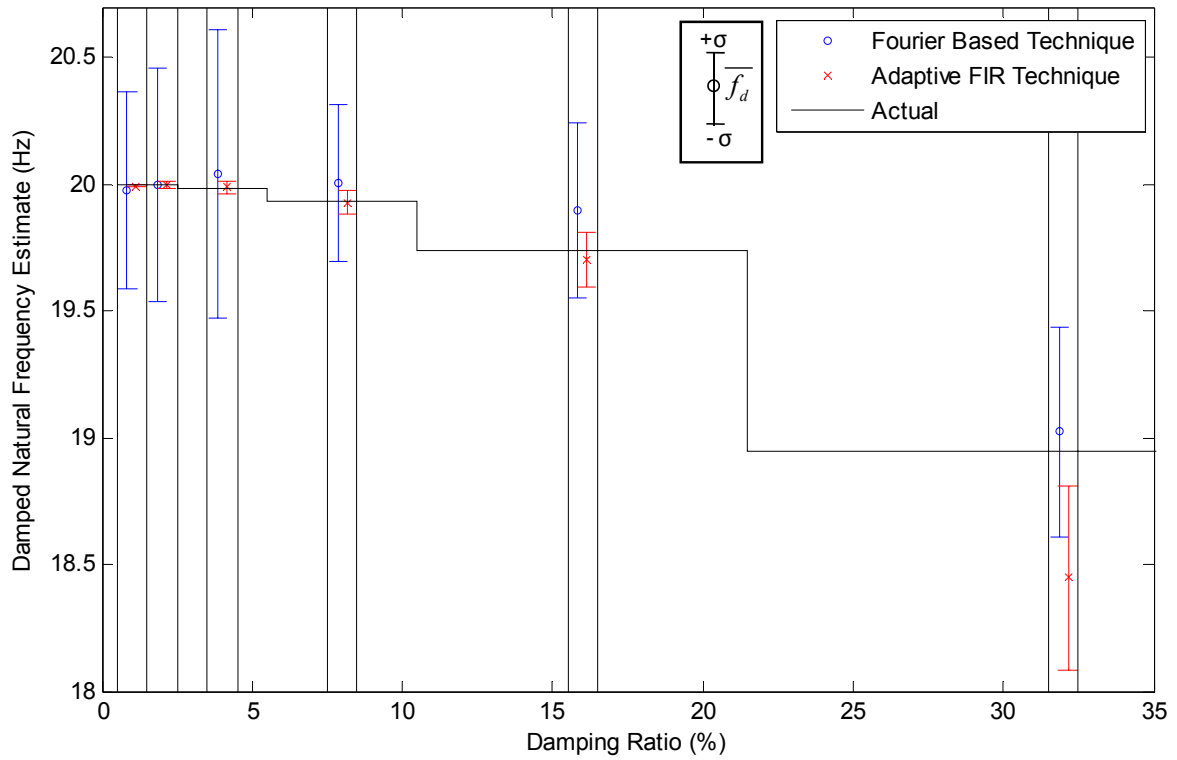


Figure 7-24: Comparison of the influence of increased damping on the adaptive FIR and Fourier based techniques (8% noise).

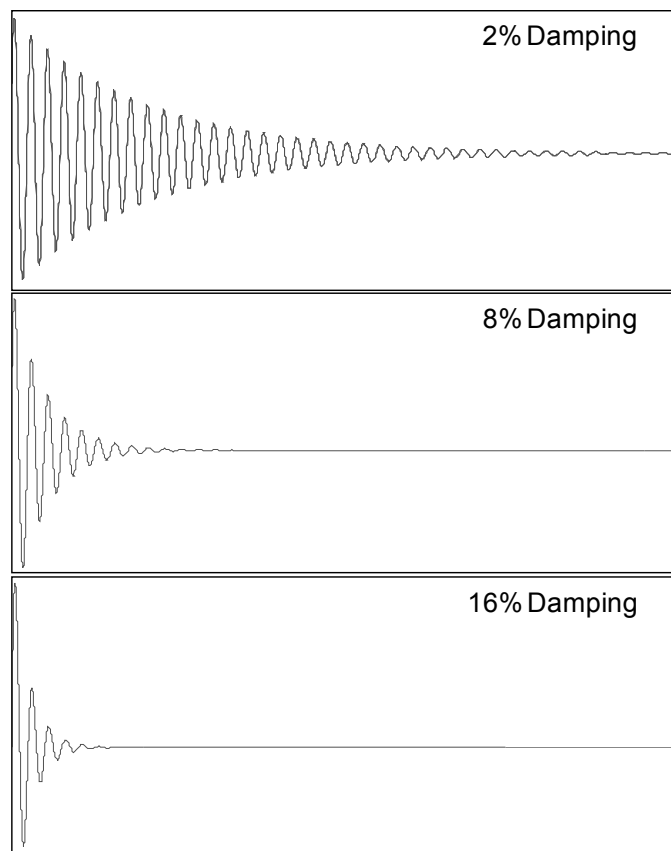


Figure 7-25: Typical filter tap coefficient vector (FIR function) for various damping ratios.

## 7.4. STEP CHANGES IN NATURAL FREQUENCY

Both integrity assessment techniques have limitations in their ability to track sudden or step changes in natural frequency. The first limitation, and one that applies to both techniques, is sensitivity, how small a step they can detect. Another limitation which applies mainly to the Fourier technique is locating the change in a temporal sense, in other words the technique's temporal resolution. The final limitation that may become apparent is the adaptive FIR technique's ability to satisfactorily track large changes in natural frequency. This final limitation is unusual as one would expect that, generally, large changes would be the easiest to identify. However, since the adaptive algorithm applied relies on preceding estimates of the system's FIR when estimating the next, large, sudden changes may create problems in terms of convergence. In order to identify the significance of these potential limitations a number of SDoF numerical systems, with a range of different damping ratios, were subjected to step changes in their natural frequency and were analysed using both structural integrity assessment techniques. The step changes in stiffness applied to the systems varied in small steps up to approximately 5%. The parameters used for the analysis were selected using the techniques described in sections 7.1.1 and 7.1.3. The following figures (*Figure 7-26 to Figure 7-36*) show the results obtained for each damping ratio, and noise level, for a system with an initial undamped natural frequency of 20Hz. Notice that the system is made to recover to its initial stiffness after each simulated damage step. While this may not be realistic in terms of physical experiments it allows large step changes to be analysed without inducing a large amount of cumulative damage, thereby limiting variations in the damping ratio (the damping constant is time invariant). Also, even though changes in the natural frequency of the systems only occur once every 60 seconds a temporal resolution of 1 second is used for both techniques, as was the case in the preceding sections. This temporal resolution was selected because the techniques are designed to detect damage events from physical systems where damage occurs at unknown intervals. Since the time that damage occurs is unknown, the only way to ensure that the timing of a damage event is not missed is to extract estimates of the system's condition at regular intervals (hence, a fine temporal resolution).

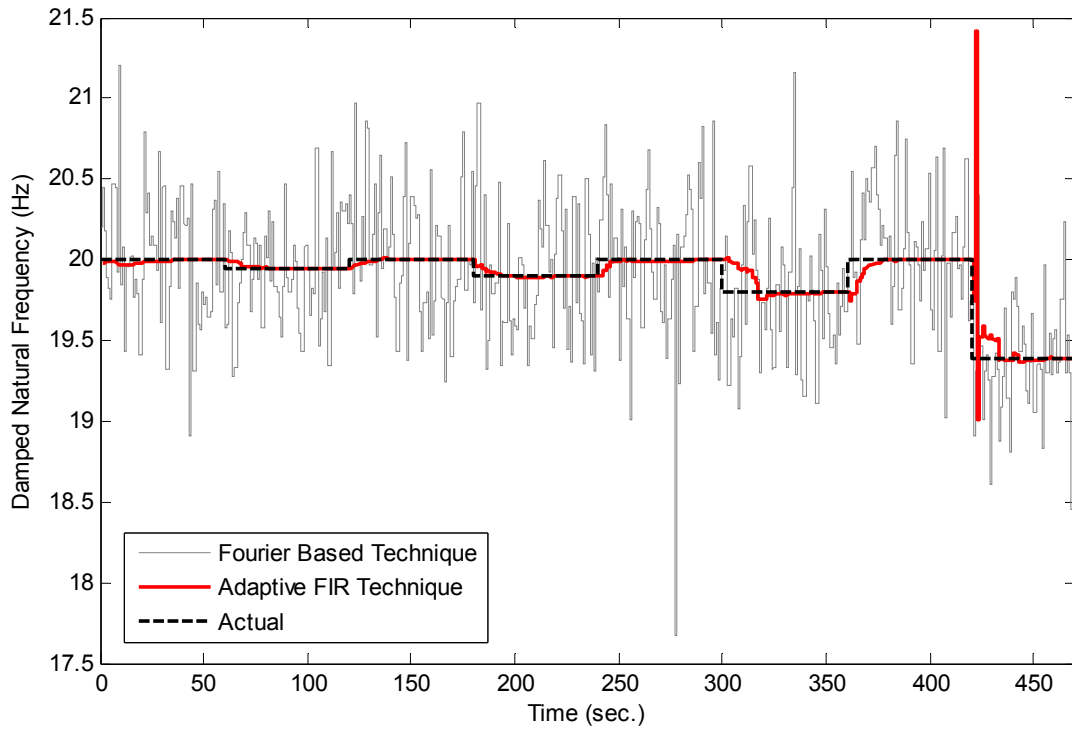


Figure 7-26: Step change results for a damping ratio of 1% (0% noise).

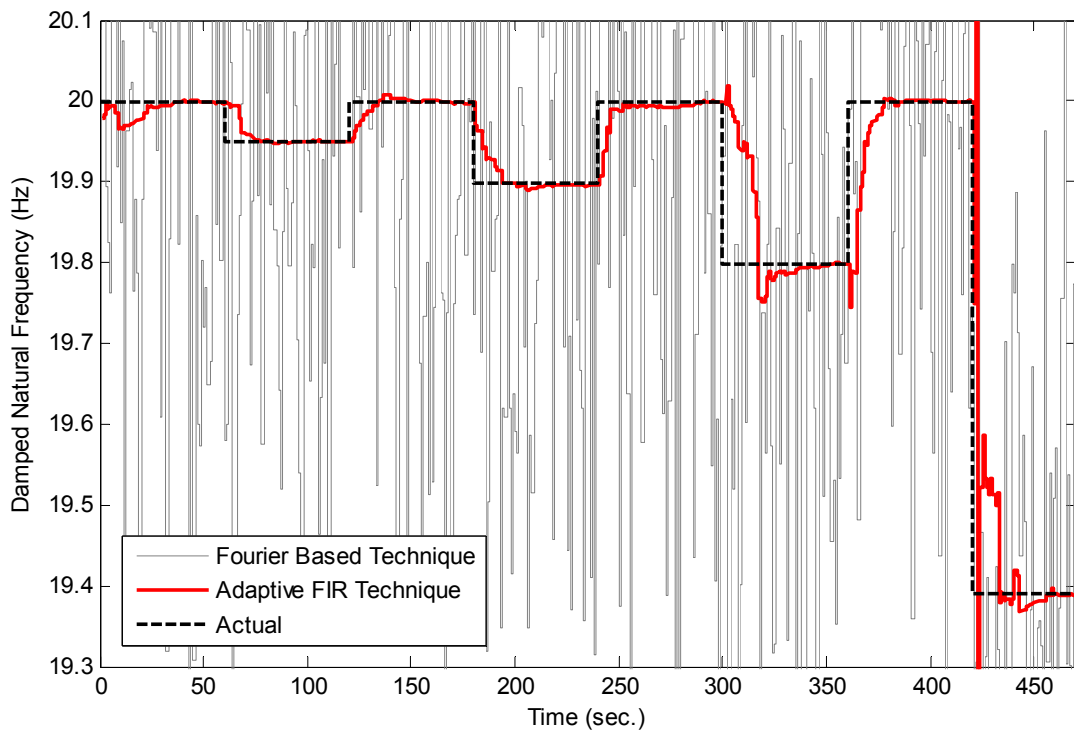


Figure 7-27: Figure 7-26 rescaled to better reveal the response of the adaptive FIR technique (0% noise).

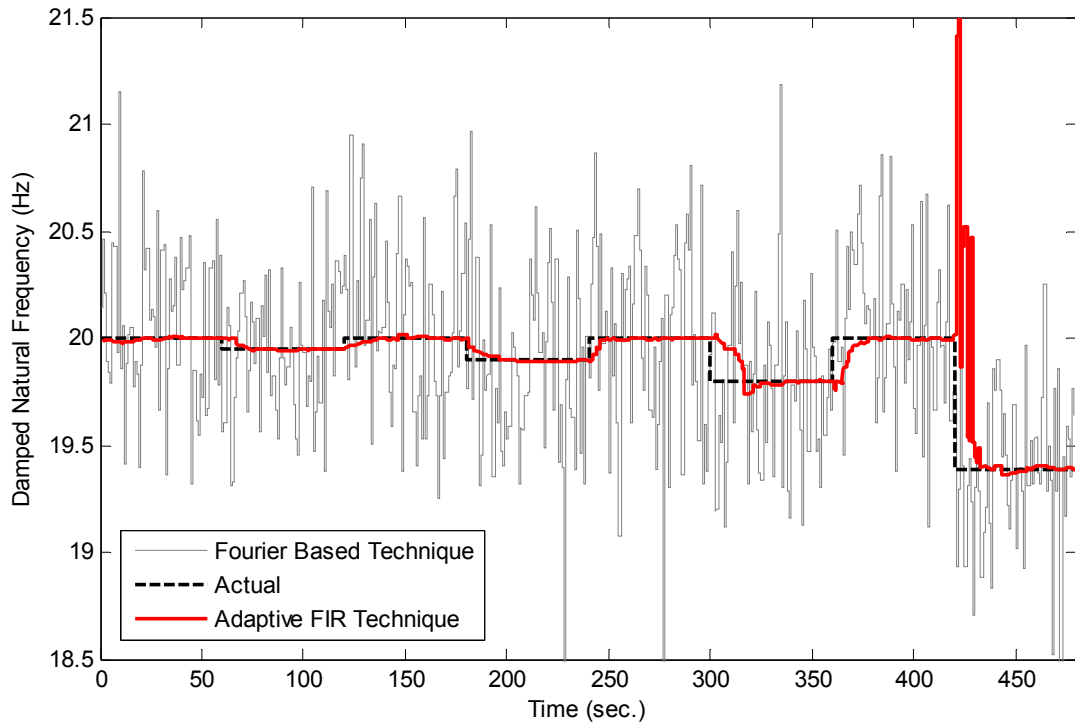


Figure 7-28: Step change results for a damping ratio of 1% (8% noise).

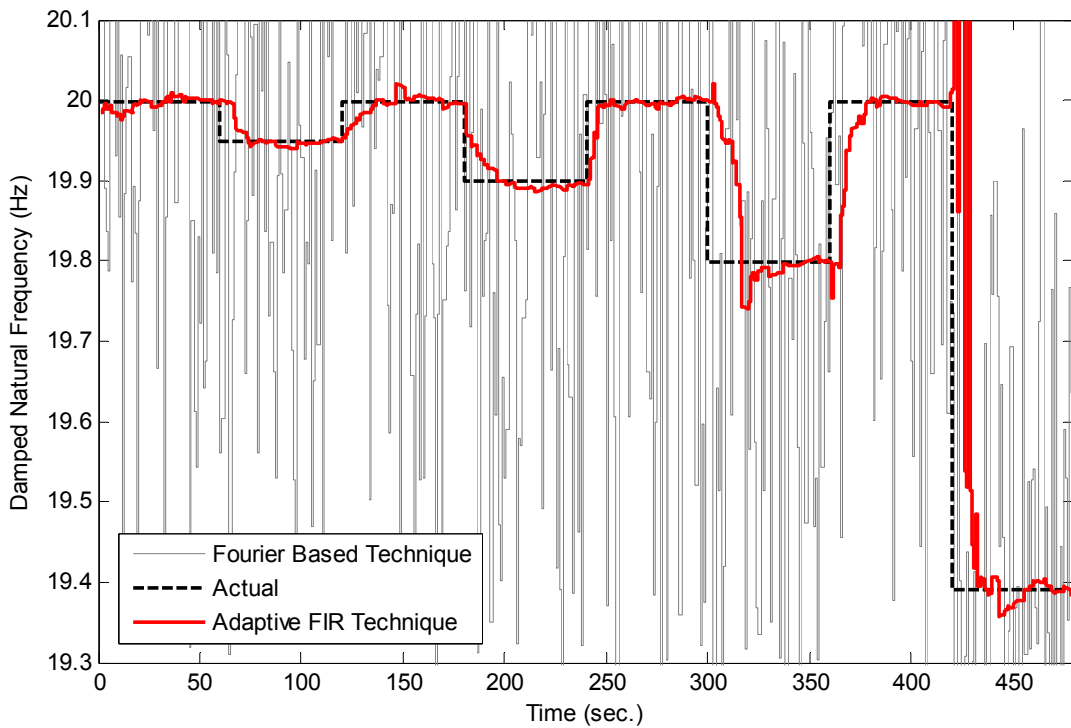


Figure 7-29: Figure 7-28 rescaled to better reveal the response of the adaptive FIR technique (8% noise).

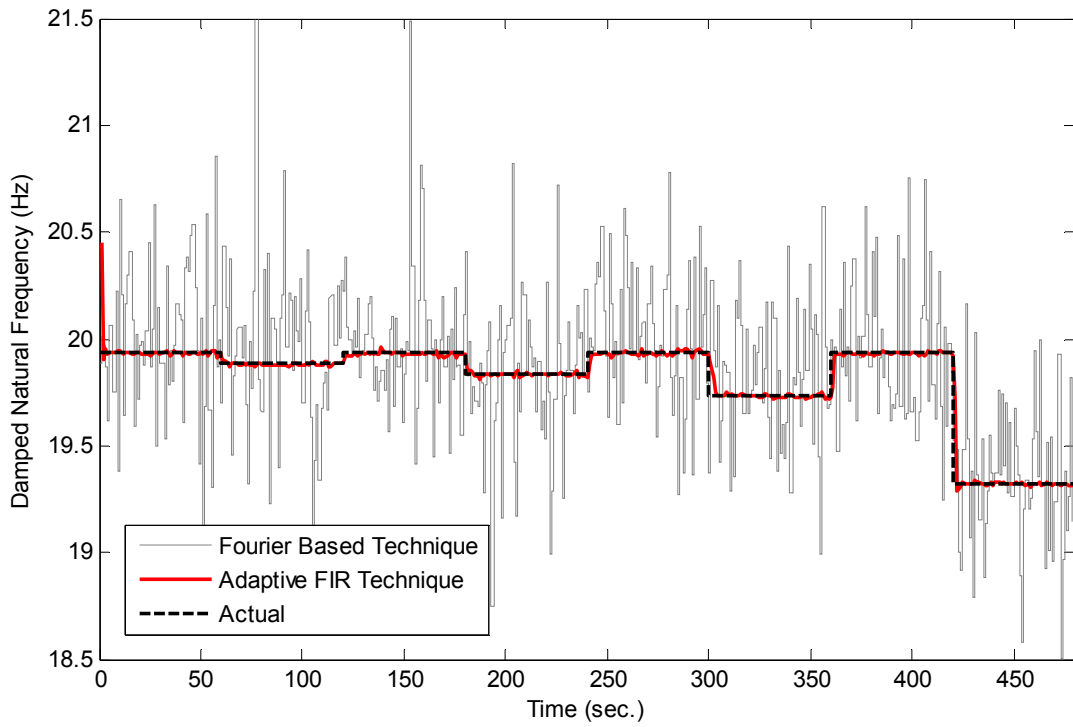


Figure 7-30: Step change results for a damping ratio of 8% (0% noise).

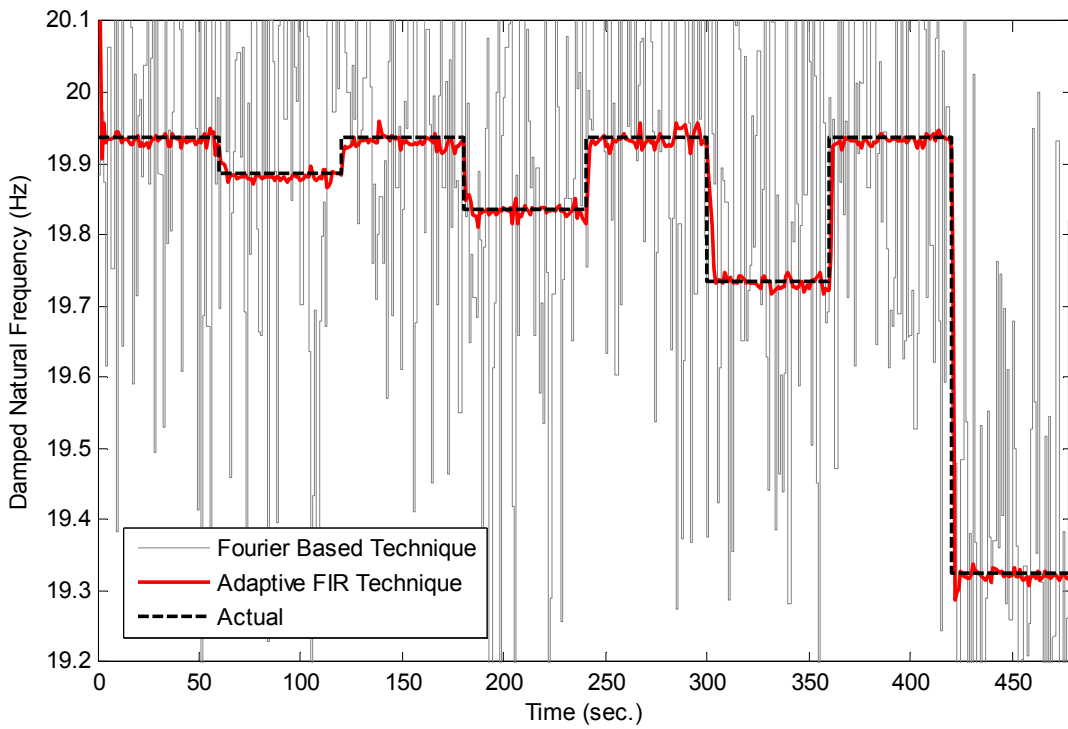


Figure 7-31: Figure 7-30 rescaled to better reveal the response of the adaptive FIR technique (0% noise).

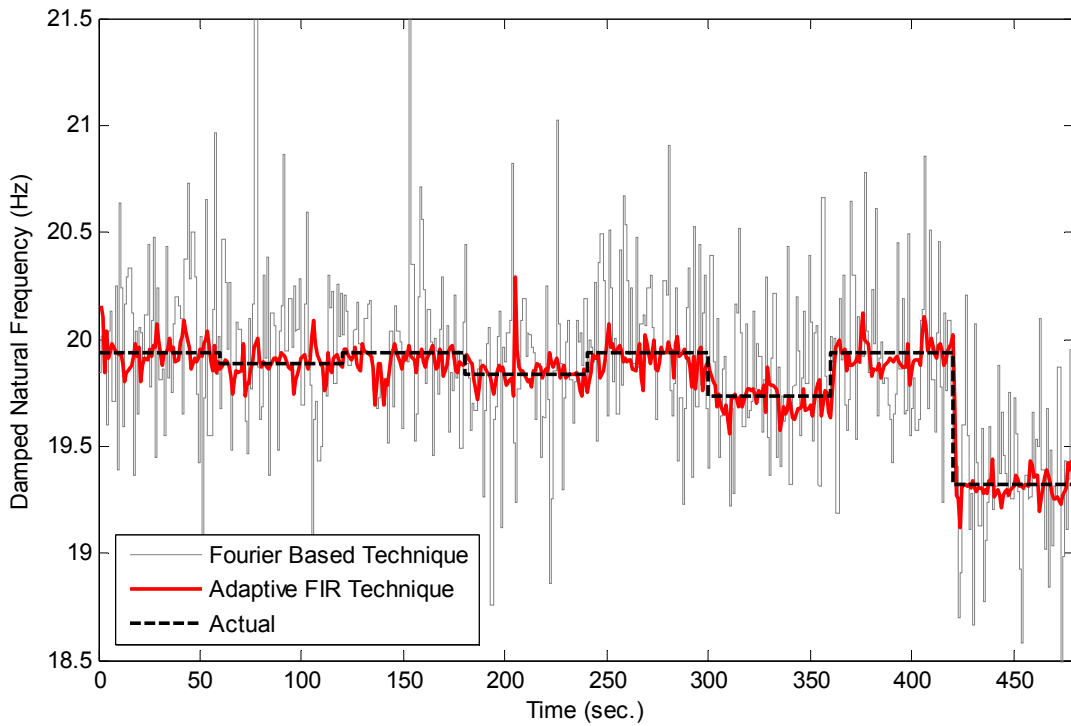


Figure 7-32: Step change results for a damping ratio of 8% (8% noise).

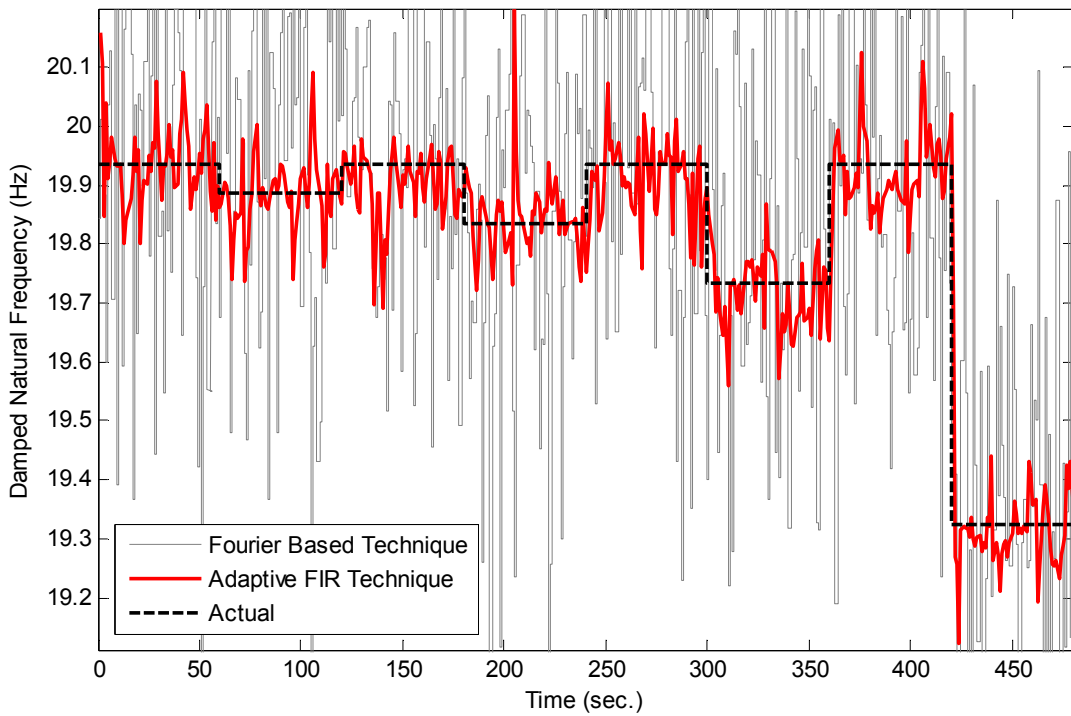


Figure 7-33: Figure 7-32 rescaled to better reveal the response of the adaptive FIR technique (8% noise).

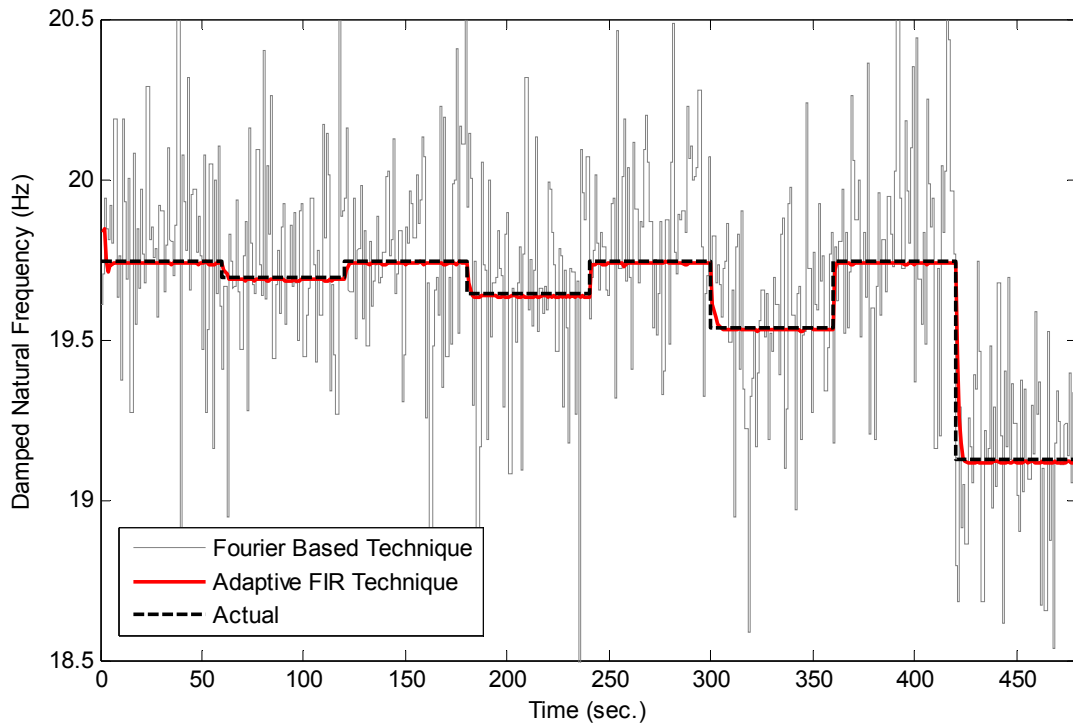


Figure 7-34: Step change results for a damping ratio of 16% (0% noise).

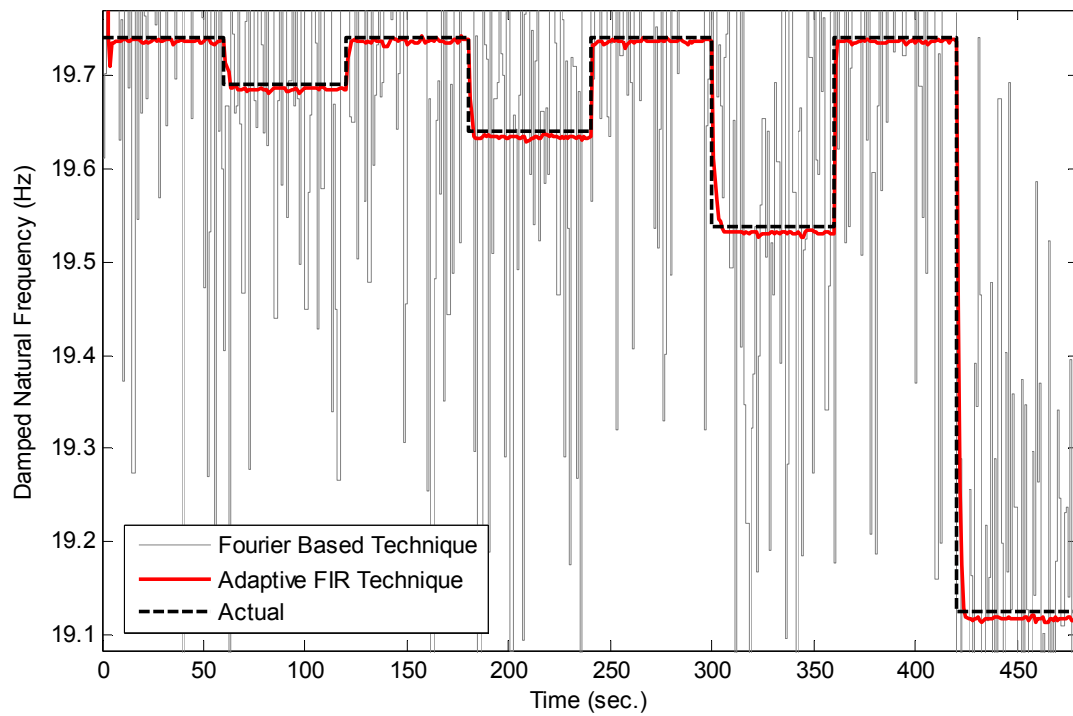
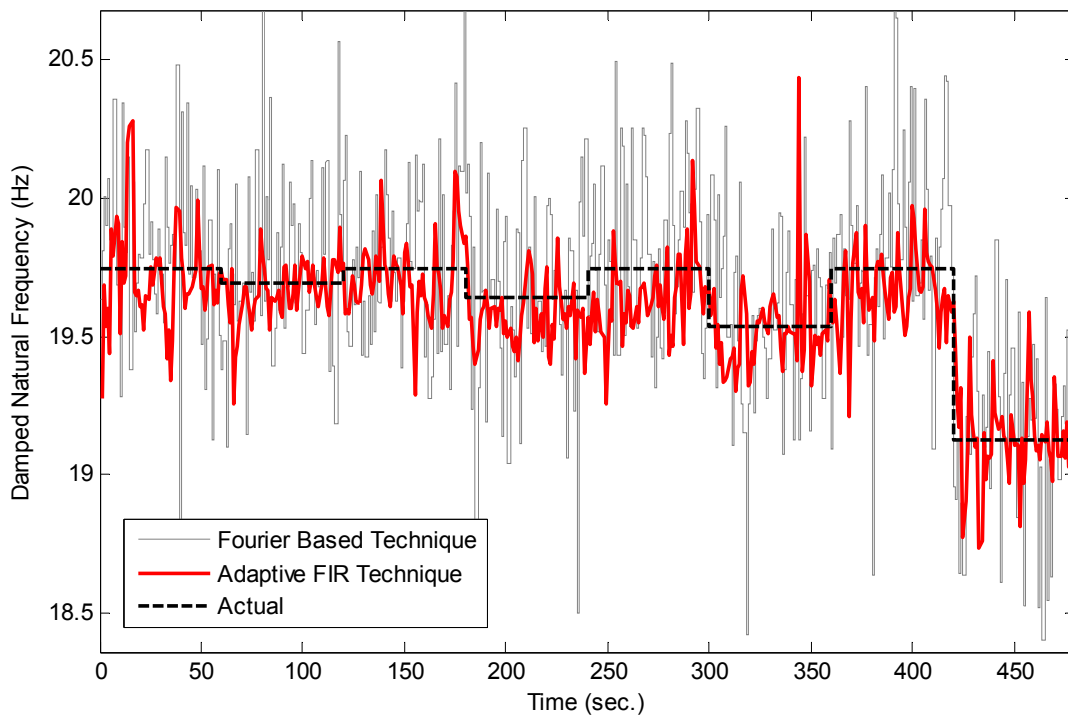


Figure 7-35: Figure 7-34 rescaled to better reveal the response of the adaptive FIR technique (0% noise).



*Figure 7-36: Step change results for a damping ratio of 16% (8% noise).*

From the observation of the preceding figures it is apparent that the combination of both high damping and extraneous noise has a noticeable effect on the results extracted using the adaptive FIR technique. However, the introduction of increased damping, without the introduction of extraneous noise had little impact. In fact, by increasing the damping ratio from 1% to 8% the results are, in a sense, improved, as the time to converge between damage instants is reduced without a significant increase in steady-state error. This reduction in convergence time can be, again, attributed to misadjustment or, more specifically, misadjustment due to lag. The higher misadjustment due to lag at low damping ratios results from the greater number of filter tap coefficients required to describe the natural duration of the FIR function. It may be possible to minimise this misadjustment by reducing the filter tap coefficient vector length; however, this will compromise steady-state precision and is not recommended.

*Figure 7-26 to Figure 7-36* are also able to suggest that for each of the systems tested, and at this temporal resolution, the adaptive FIR technique is by far superior to the Fourier based technique. However, again considering the lightly damped system (1% damping ratio), with the introduction of slow convergence at each nonstationary event, the true temporal resolution is in the order of 10-15 seconds. Since the damage pattern in this case is known to be stepped this is not an issue as the occurrence of damage is instantly apparent; however, in

practice, the damage pattern is unknown. Effectively, this means that, to present a fair comparison, the Fourier technique should be used with the temporal resolution set at approximately 10 seconds. This will significantly increase the spectral resolution of the Fourier based technique, which will, in turn considerably reduce the variation of the natural frequency estimates. Results gathered using the Fourier based technique with a temporal resolution of 10 seconds are given in *Figure 7-37*. As can be seen, at this temporal resolution, the performance of the Fourier based technique approaches that of the adaptive FIR method. It must, however, be noted that this temporal resolution closely matches a multiple of the time given between each damage step. This considered, and the fact that the variation of the Fourier based results is still in excess of that obtained using the adaptive FIR technique, the Fourier based approach provides no advantage over the adaptive FIR technique. Even though no improvement was found, this experiment is able to demonstrate that, in situations where the temporal resolution is not vital, the Fourier based technique has the potential to match the performance of the adaptive FIR method. This finding will be studied further in later sections of this chapter.

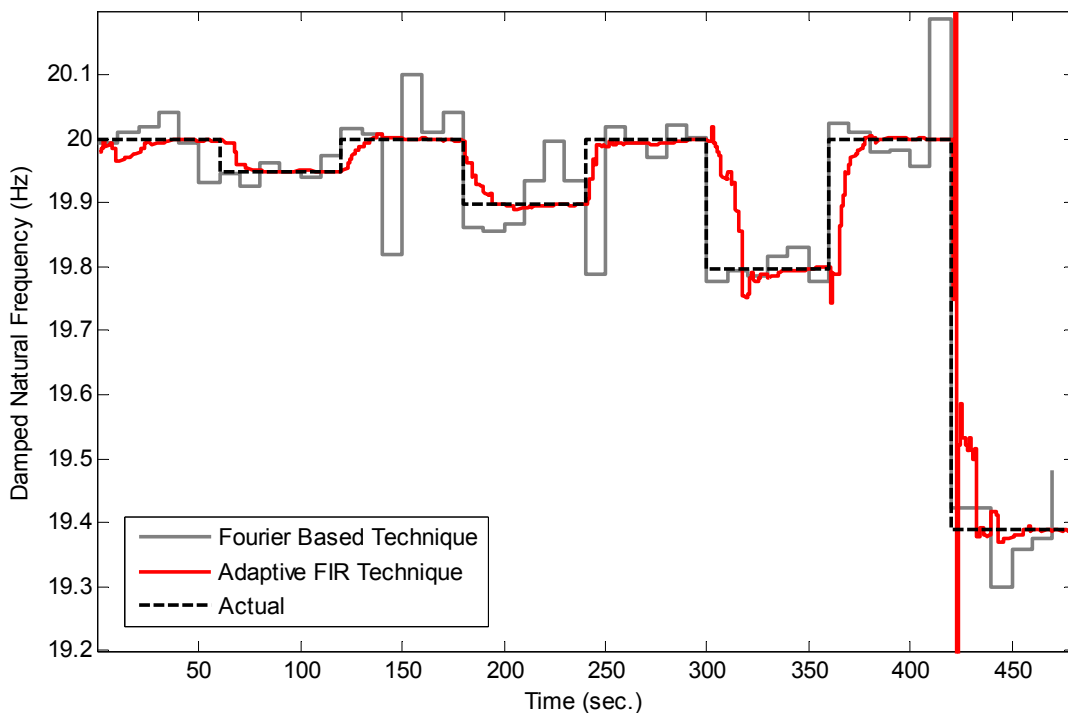


*Figure 7-37: Step change results for a damping ratio of 1%, Fourier technique with 10 second temporal resolution (0% noise).*

Improvements to the results displayed are not limited to the Fourier based technique. The results for the adaptive FIR technique presented thus far have been instantaneous values captured at 1 second time intervals. Provided that the rate at which the normalised step-size is re-optimised is not altered, results can be extracted at a much faster rate (as often as one new estimate per sample point) without loss of accuracy. This means that estimates with greater accuracy can be made by obtaining estimates at an increased rate and applying a moving average filter to achieve the desired temporal resolution. This approach significantly increases the computation time required to obtain estimates and will not be used in this chapter; however, an example of the potential improvement it provides is given in *Figure 7-38*. The instantaneous values presented in this figure were extracted from a numerical system with 4% extraneous noise once every 0.1 seconds. A moving average filter was applied to the instantaneous values to achieve a temporal resolution of 10 seconds.

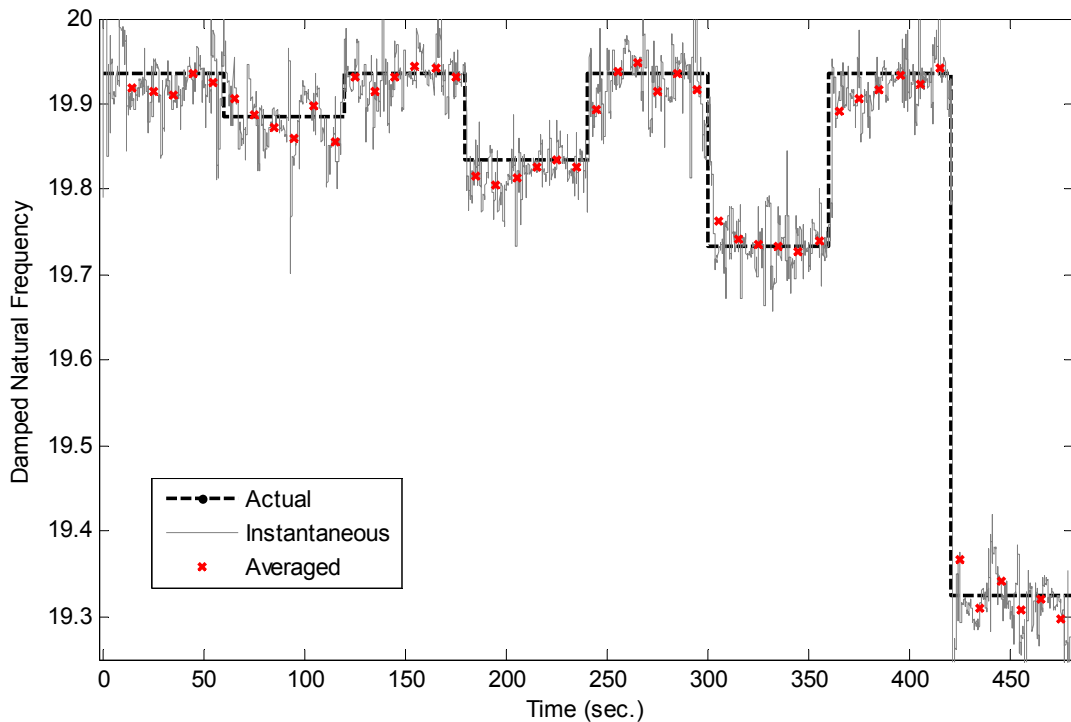


*Figure 7-38: Improved results from the adaptive FIR technique using a moving average filter.*

## 7.5. PROGRESSIVE DAMAGE

The damage patterns evaluated so far have allowed the adaptive FIR technique to converge before any significant change to the system's stiffness was made. In many cases, realistic damage patterns do not allow for adaptation to occur under constant frequency (no damage) conditions. The ability of the integrity assessment techniques to track continually varying decay rates is also yet to be established.

In order to test the limitations of the techniques for scenarios with continually varying decay rates, a series of experiments was undertaken. Two damage patterns were designed with the total change in natural frequency applied to the systems limited to 10%:

- 1) Continually varying stiffness with an increasing rate of change.
- 2) Continually varying stiffness with a decreasing rate of change.

The second case is the more aggressive scenario, particularly for the adaptive FIR technique as the filter has to immediately adapt to a system with rapidly varying stiffness.

The results obtained from systems evaluated with the first damage scenario are presented in *Figure 7-39* to *Figure 7-44* and those obtained from the second damage scenario are given in *Figure 7-45* to *Figure 7-50*. The numerical SDoF systems evaluated had an initial undamped natural frequency of 20Hz and damping ratios between 1% and 16%.

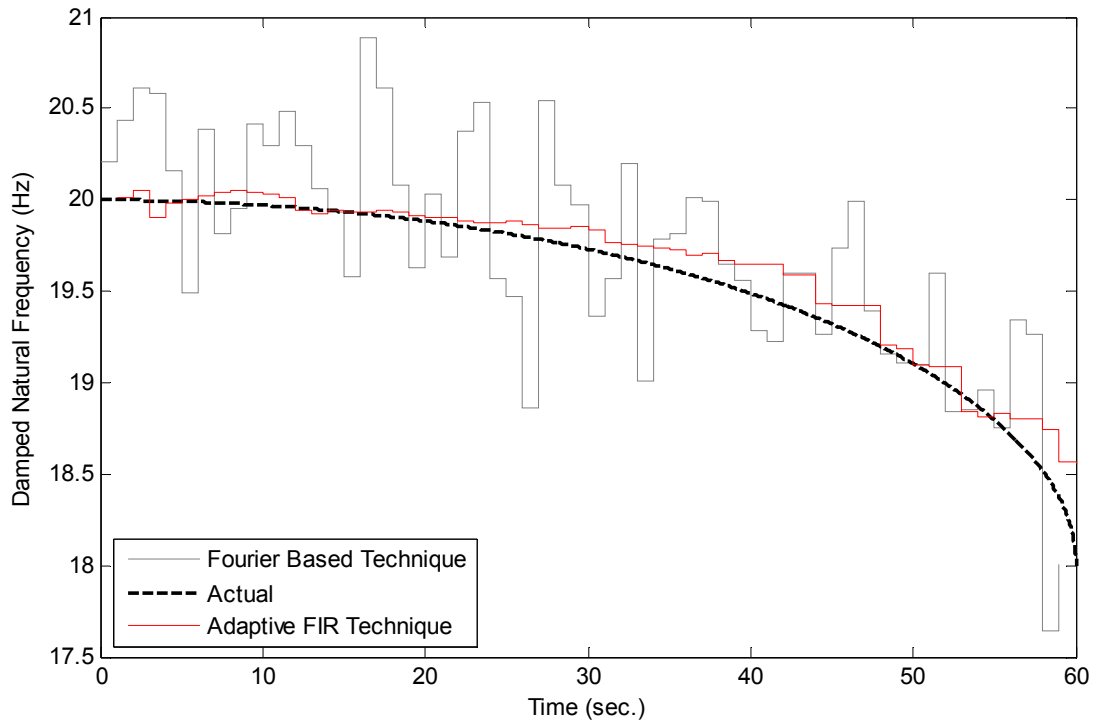


Figure 7-39: Progressive damage, increasing rate of change, 1% damping (0% noise).

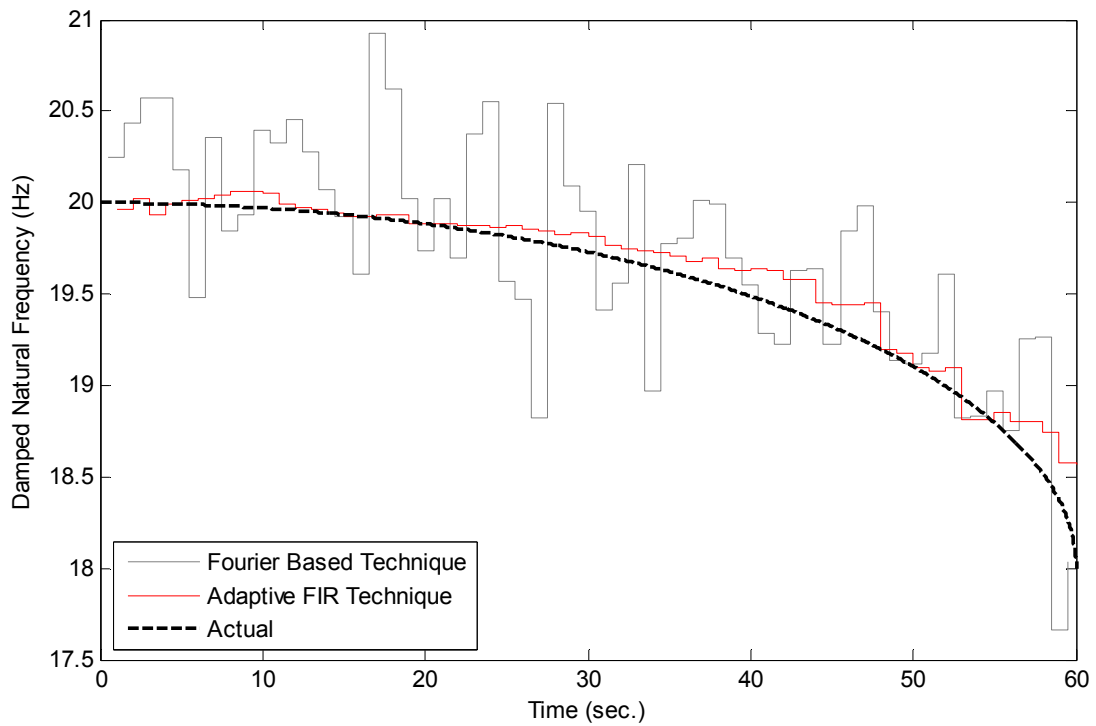


Figure 7-40: Progressive damage, increasing rate of change, 1% damping (8% noise).

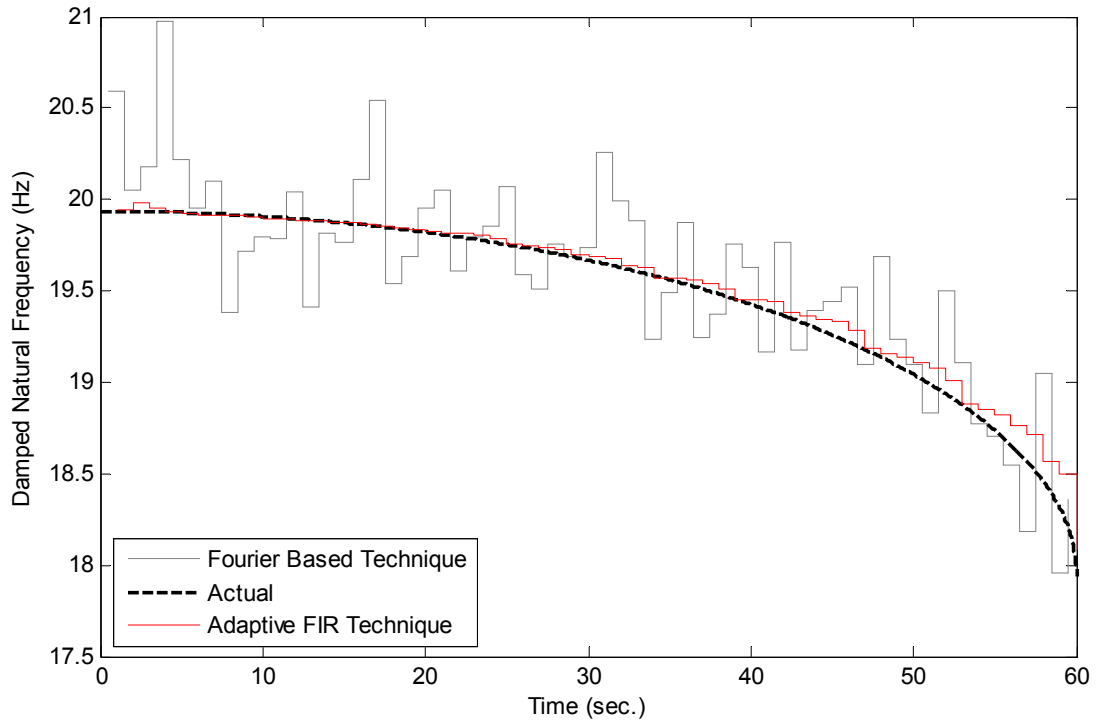


Figure 7-41: Progressive damage, increasing rate of change, 8% damping (0% noise).

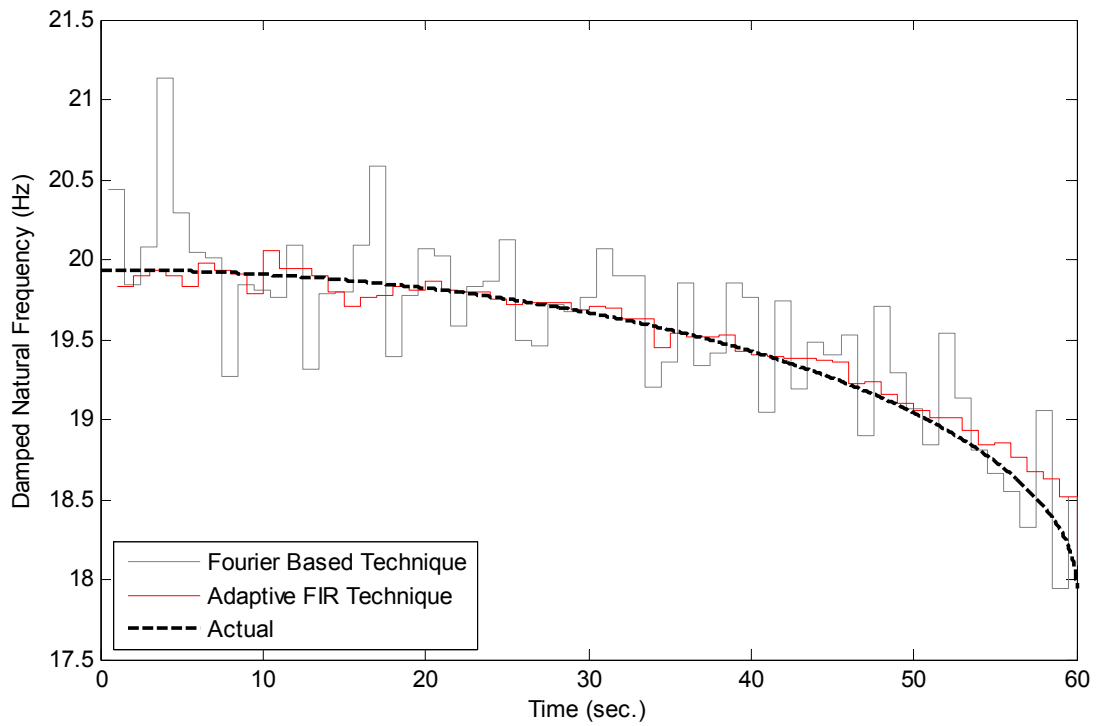


Figure 7-42: Progressive damage, increasing rate of change, 8% damping (8% noise).

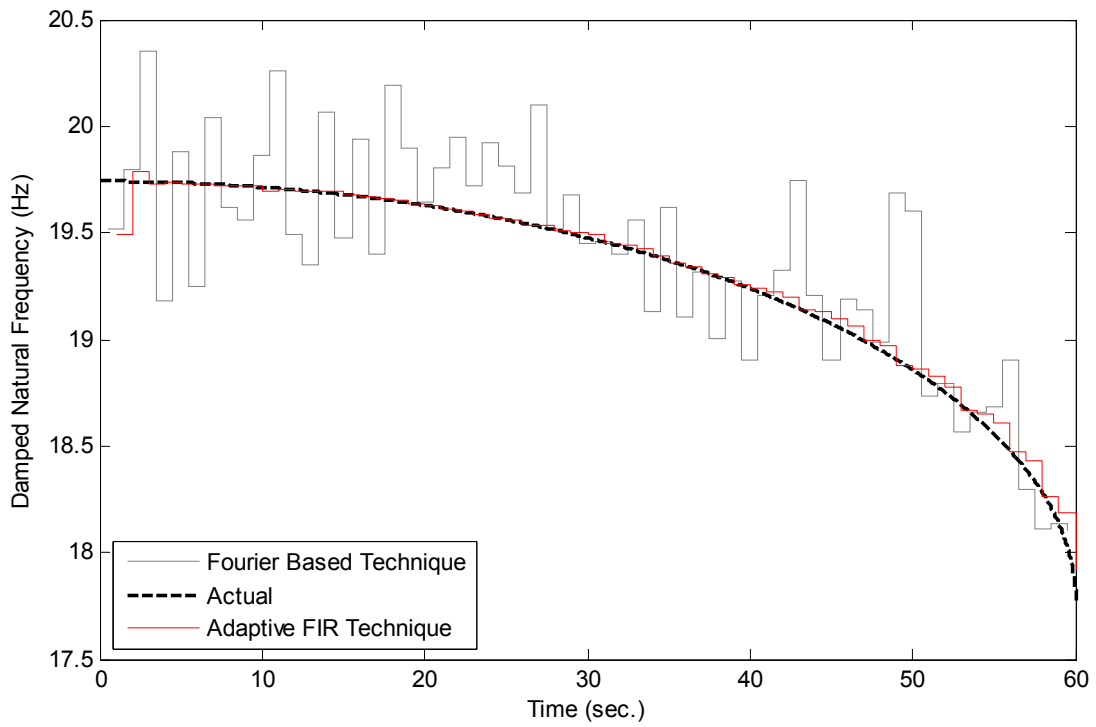


Figure 7-43: Progressive damage, increasing rate of change, 16% damping (0% noise).

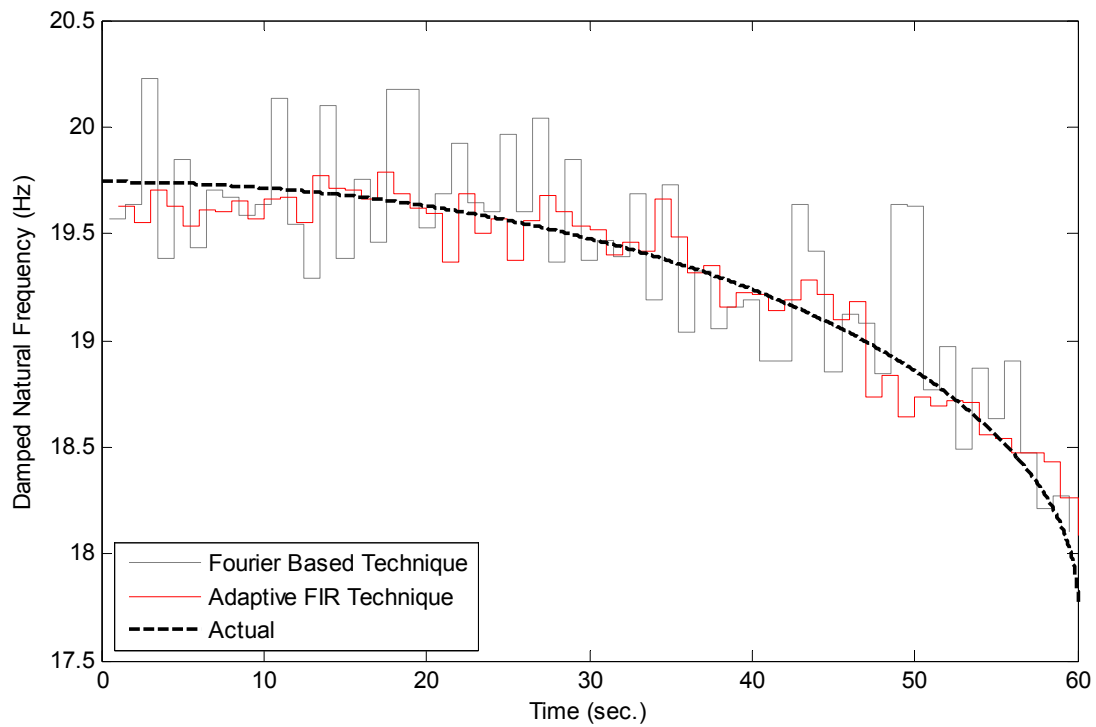


Figure 7-44: Progressive damage, increasing rate of change, 16% damping (8% noise).

The continuously decreasing rate of decay damage pattern yielded similar findings to the stepped scenario discussed in the preceding section. These findings included:

- The large filter tap coefficient vectors required at low damping create some distortion by increasing the adaptive filter's convergence time
- The influence of noise is most evident in the adaptive FIR technique's results obtained from systems with high levels of damping
- Moderate levels of damping are able to considerably improve the adaptive FIR technique's convergence times
- At a 1 second temporal resolution, the adaptive FIR technique is superior to the Fourier transform technique irrespective of damping (between 1% and 16% damping)

In addition to these findings the convergence limitations of the adaptive FIR technique were not so extreme that implementing the Fourier based technique with a coarse temporal resolution will produce estimates which are more accurate than those obtained using the adaptive FIR technique.

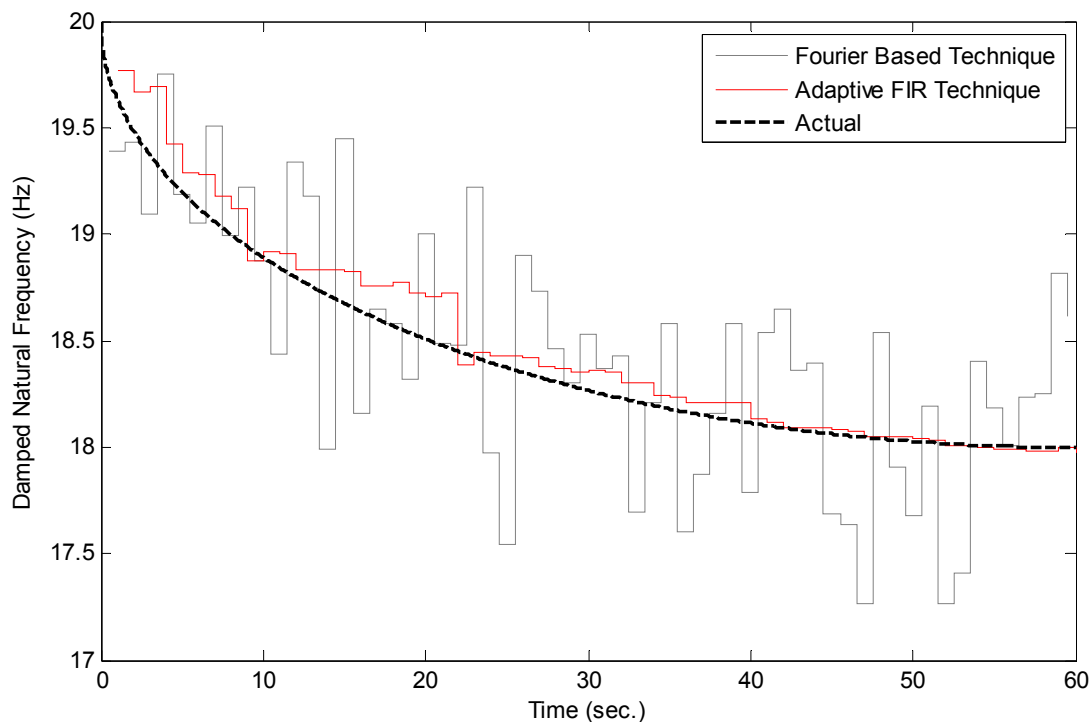


Figure 7-45: Progressive damage, decreasing rate of change, 1% damping (0% noise).

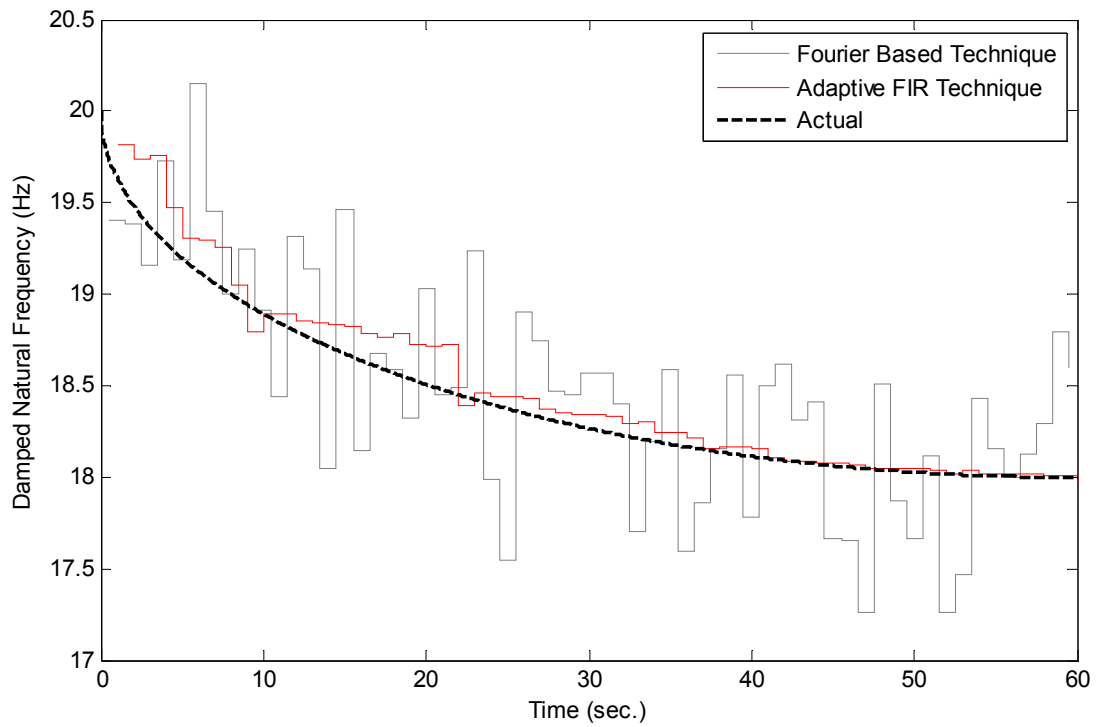


Figure 7-46: Progressive damage decreasing, rate of change, 1% damping (8% noise).

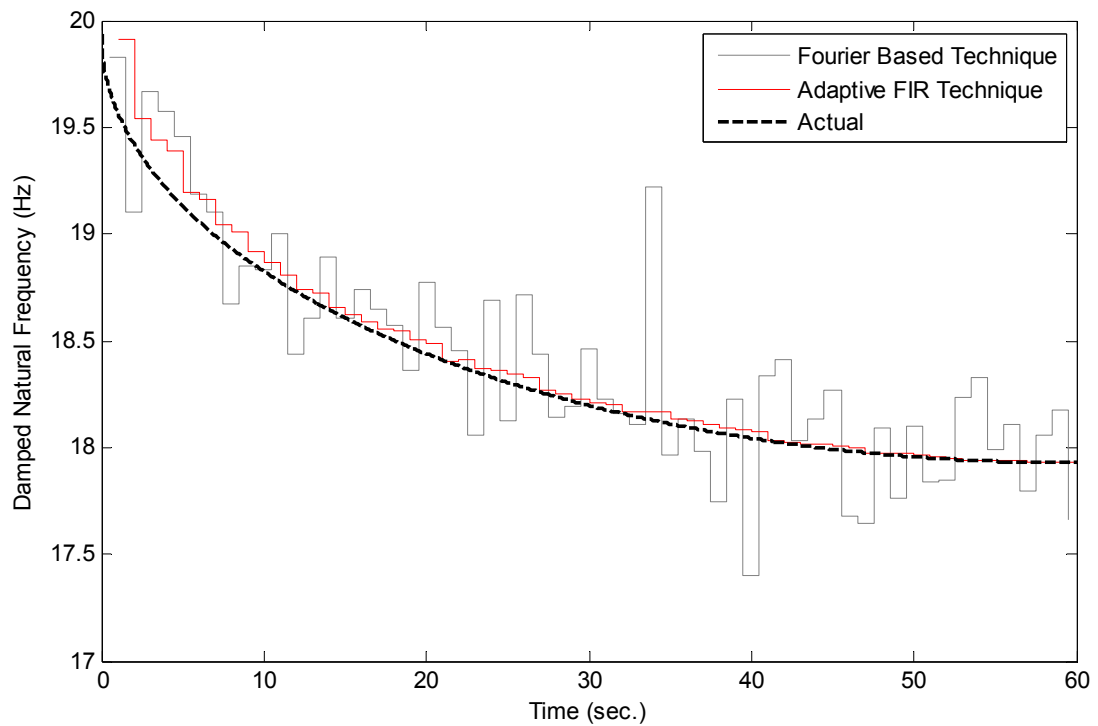


Figure 7-47: Progressive damage decreasing, rate of change, 8% damping (0% noise).

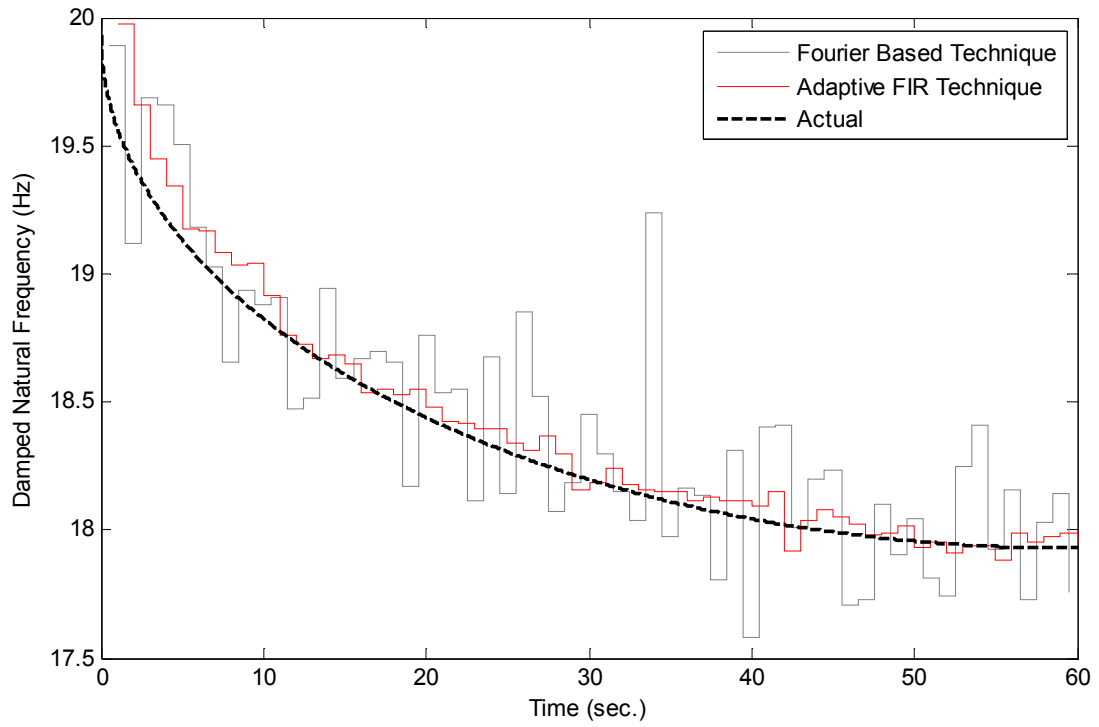


Figure 7-48: Progressive damage, decreasing rate of change, 8% damping (8% noise).

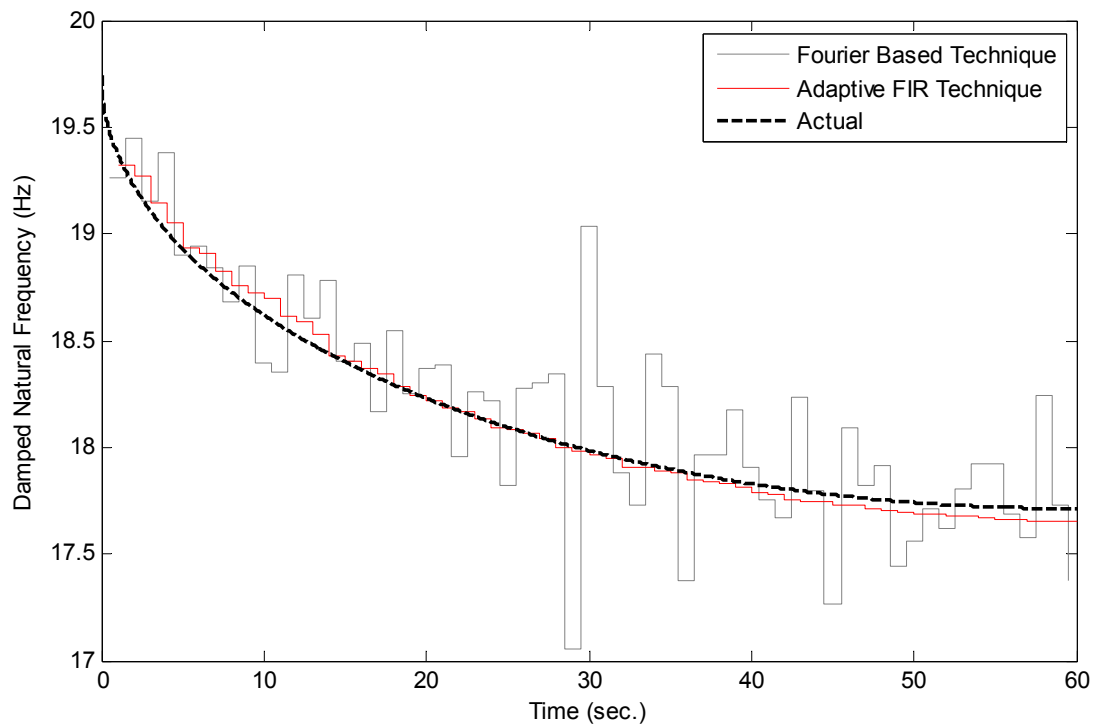


Figure 7-49: Progressive damage, decreasing rate of change, 16% damping (0% noise).

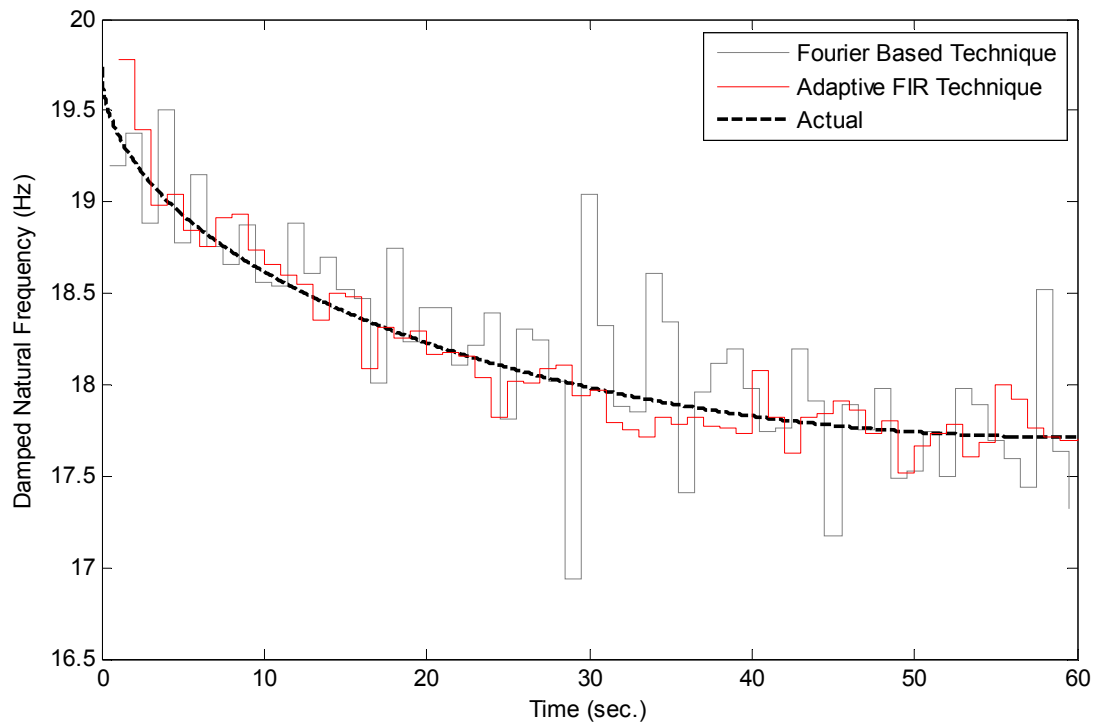


Figure 7-50: Progressive damage, decreasing rate of change, 16% damping (8% noise).

The estimates obtained using the second damage scenario resulted in similar findings to those obtained from the first and were also able to indicate that the lack of an initial settling time does not noticeably affect the adaptive FIR technique's ability to track changes in the system's natural frequency.

## 7.6. SELECTING A TECHNIQUE BASED ON TEMPORAL RESOLUTION

It was earlier shown that, when systems with low damping are subjected to sudden damage, the Fourier based technique has the potential to match the performance of the adaptive FIR technique by making adjustments to the temporal resolution. Since it has also been shown that the adaptive FIR technique is more sensitive to noise and damping, it is possible that, at elevated levels of noise and damping, the Fourier technique may be able to out-perform the adaptive FIR technique provided that coarser temporal resolution is adequate.

Figure 7-51 shows the total error (offset in the mean plus one standard deviation) obtained from a range of steady-state systems, with various damping ratios, at different temporal resolutions, for signals containing 4% extraneous noise. The results presented for the adaptive FIR technique are based on instantaneous non-averaged values.

Provided that the desired temporal resolution is known, *Figure 7-51* can be used to help determine which technique should be applied. It must be noted that these results are for a linear system at one noise level (4%). Earlier it was noted that the sensitivity of the Fourier based technique at fine temporal resolution is not significantly affected by noise, therefore the results presented in *Figure 7-51* provide a good overall representation of results obtained from linear systems when implementing the Fourier based technique. The adaptive FIR technique on the other hand varies significantly with the introduction of extraneous noise thereby making the results presented in *Figure 7-51* only suitable for one case (4% noise). For estimates of the total error expected from the adaptive FIR technique at other noise levels, namely 0% and 8%, refer to the comparative section on damping in this chapter. It is also important to note that at low levels of damping (<8%) the Fourier based technique may outperform the adaptive FIR method at finer temporal resolutions than suggested by *Figure 7-51* (as a result of reduced convergence of the adaptive FIR technique at low damping levels); however, the results of the adaptive FIR technique can also be improved by implementing a moving average filter as discussed earlier (section 7.4).

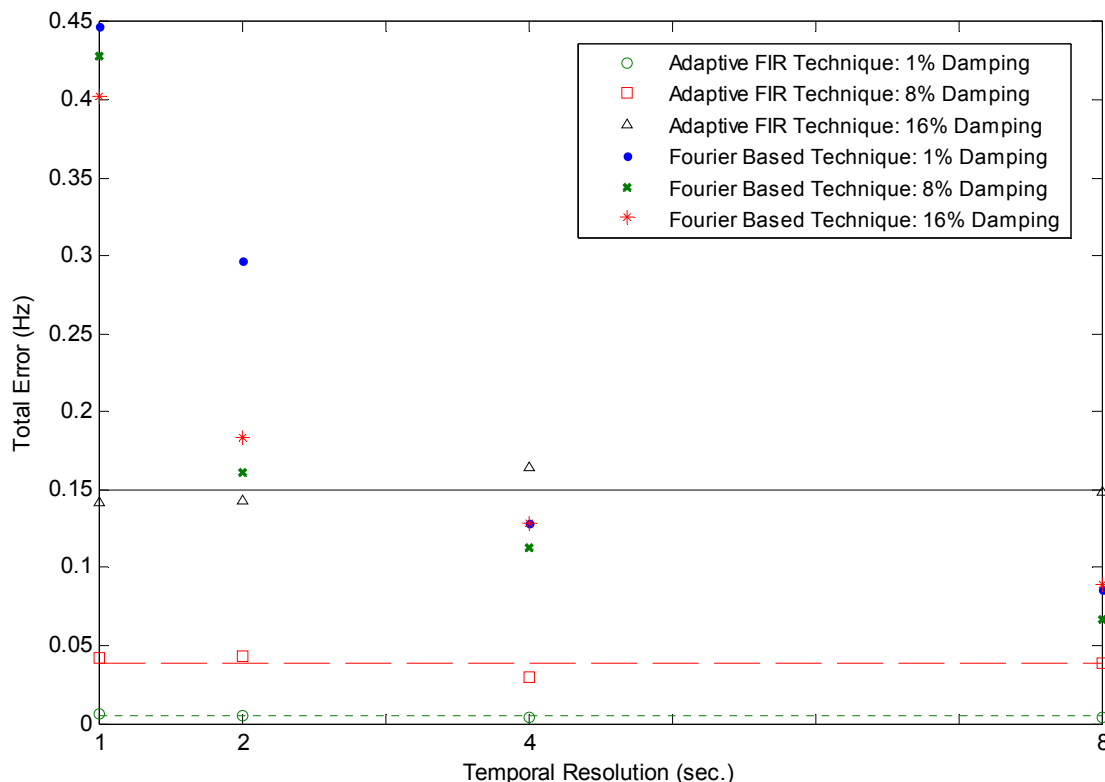


*Figure 7-51: Total error versus temporal resolution (4% noise).*

For illustrative purposes, results extracted from a system with continuous decay and 16% damping are presented in *Figure 7-52*. In this instance a temporal resolution of 3 seconds was chosen and 4% extraneous noise was added to the excitation and response signals. According to *Figure 7-51* this represents a border-line case where either technique could be selected. As can be seen there is no obvious distinction between the performance of either technique.

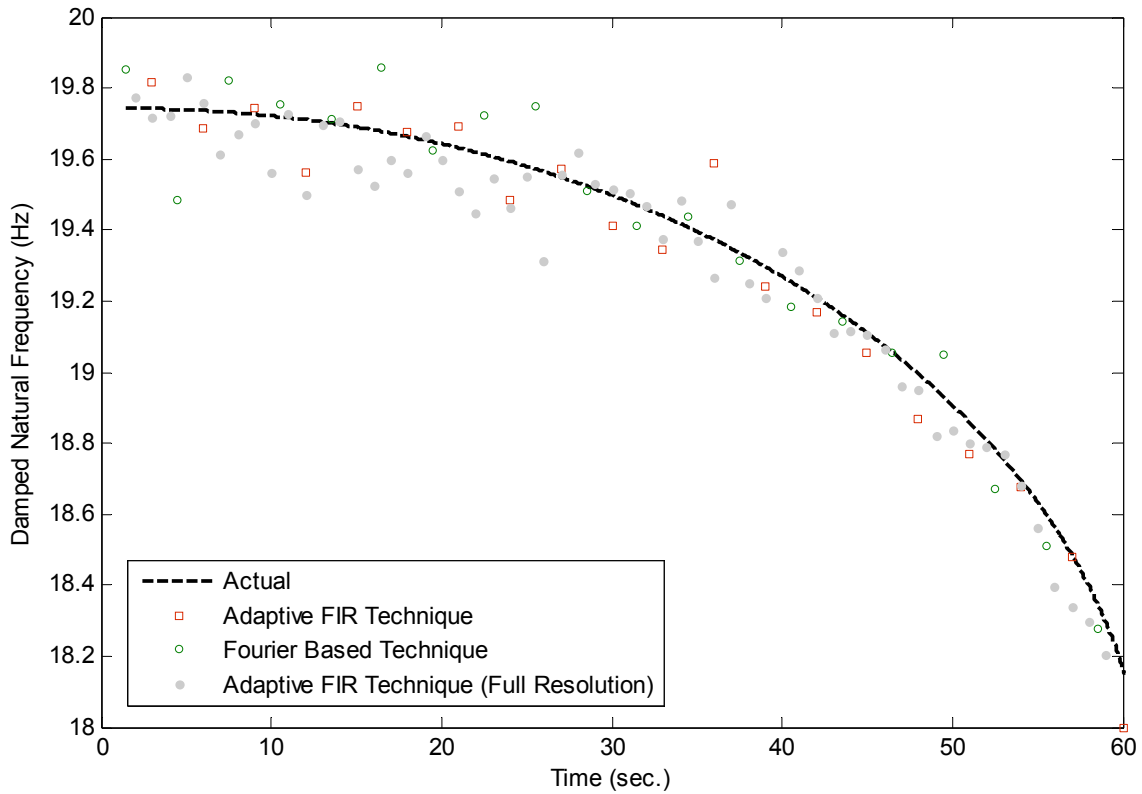


*Figure 7-52: Results obtained using a temporal resolution of 3 seconds for a system with 16% damping and signals containing 4% extraneous noise.*

## Chapter 8 PHYSICAL EXPERIMENTS

The experiments discussed so far have used well defined numerical models of linear single degree-of-freedom (SDoF) systems. These models allowed for the development of the integrity assessment techniques without the introduction of complexities (such as, nonlinearities, inconsistent extraneous noise and mixed modes), which are both difficult to define and control. The ability to control these complexities was particularly important when evaluating the influences of the analysis parameters and optimisation processes introduced.

This chapter presents the results obtained from a number of physical experiments. The experiments were divided into two groups: 1) controlled experiments, where the natural frequency of a cantilever beam was varied by a known amount; and 2) uncontrolled experiments, where actual packaging elements were allowed to deteriorate naturally. These experiments were performed to confirm the numerically simulated results, and to establish the ability of the techniques in monitoring the integrity of real material elements which are subject to fatigue testing.

### 8.1. CONTROLLABLE EXPERIMENTS

A physical experimental arrangement, which allows for controlled changes in a system's properties, is required to validate the numerically simulated experiments. This validation also requires a method for comparing the results obtained from the integrity assessment techniques with the actual properties of the system under analysis. Sections 8.1.1 and 8.1.2 discuss the development of a suitable experimental arrangement and an approach for determining the actual properties of the system, respectively. Typical results obtained from a number of samples (with differing material characteristics) are given in sections 8.1.3-8.1.4.4.

#### 8.1.1. Experimental Setup for Controlled Experiments

Given the previously discussed requirements for the controlled physical experiments, a cantilever arrangement, in which the length (hence natural frequency) of the sample under assessment can be altered during excitation, was found to be best suited. In order to assess the sensitivity of the assessment techniques for extracting natural frequency estimates from time variant systems, accurate adjustments to the cantilever's length need to be made without

affecting the motion of the cantilever or halting excitation. This requirement was fulfilled using the specifically built experimental rig depicted in *Figure 8-1*.

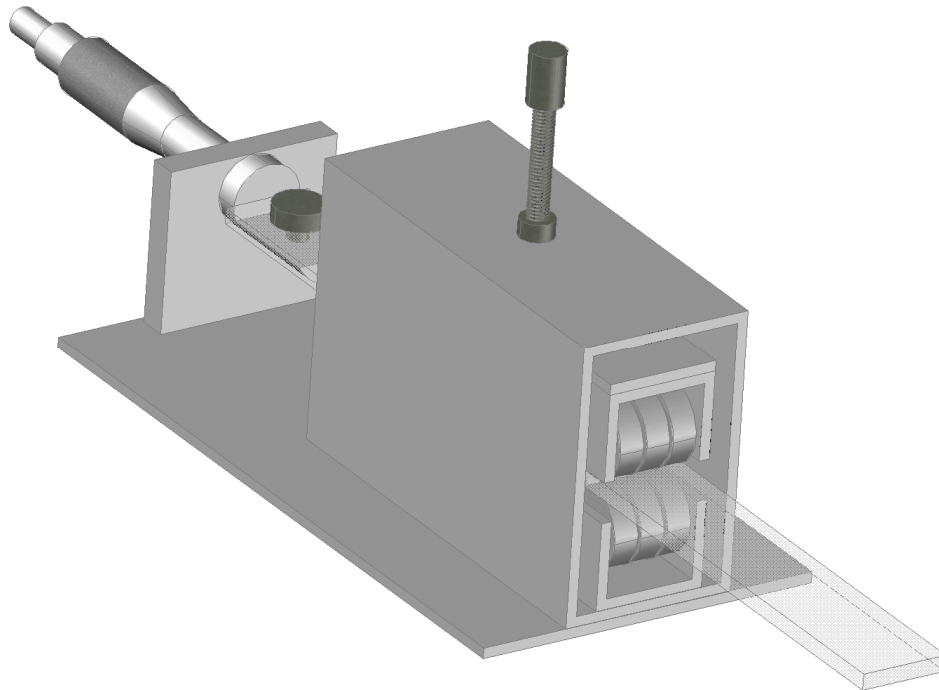


*Figure 8-1: Variable length cantilever rig.*

The rig consists of a clamp which was designed to allow for motion parallel to the supported sample and a housed micrometer (with a non-rotating spindle), driven by a stepper motor, to accurately adjust the length of the cantilever. Adjustments to the length of the cantilever were controlled using a specially developed controller to operate the stepper motor. This controller allowed for the pre-programming of any desired damage pattern. The stepper motor had a step-angle of  $7.5^\circ$ , which, when coupled to the micrometer, provided a sensitivity of approximately 0.01mm.

Excitation for the physical systems was generated using a Vibration Test Systems model 500 electro-dynamic shaker, which was controlled using Signal Calc.® software (by Data Physics) to produce a band-limited Gaussian random signal. The shaker was mounted on a 250kg seismic mass supported by pneumatic springs. The shaker was powered using a 30V DC power supply.

The excitation and response signals, along with the step sequence from the stepper motor, were recorded continuously and simultaneously using a 12 bit data acquisition module and specifically developed data capture software created using Matlab®. All post-processing was

carried out using the optimised analysis parameters discussed in sections 7.1.1 and 7.1.3 unless otherwise stated.

A schematic of the experimental arrangement is given in *Figure 8-2*.

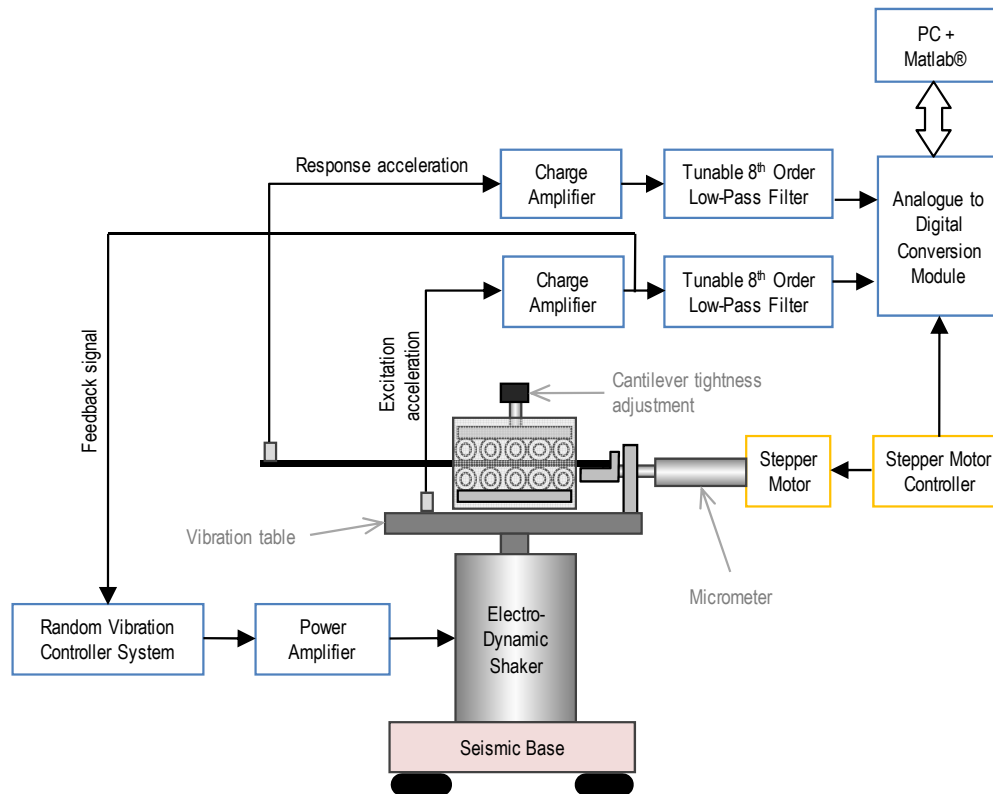


*Figure 8-2: Schematic of experimental arrangement - controllable experiments.*

### 8.1.2. Calibration of Natural Frequency

In order to establish the accuracy of the integrity assessment techniques the parameters of the system under analysis need to be established. Since the cantilever's physical properties, namely its dimensions, density and Young's modulus, can be obtained, estimates of natural frequency can be made mathematically by determining its stiffness and equivalent mass (Rao 2005, pp. 138-139). However, this introduces measurement errors which are likely to exceed the sensitivity of the assessment techniques. In order to avoid these errors, estimates of natural frequency were determined using the instantaneous phase vector (obtained using the Hilbert transform) of the system's free-vibration response. The results obtained using this approach were found to vary slightly depending on the segment of free-response data analysed. Therefore, the segment that returned the lowest coefficient of variation for the initial beam length was used. Also, the relative estimates of natural frequency (relative to the shortest beam length estimated natural frequency) were less sensitive to the segment of data analysed than the absolute values.

### 8.1.3. Preliminary Experiments

Prior to the physical experiments comparative study, several preliminary experiments were performed. These experiments were designed to establish whether or not the results obtained from the analysis of numerical systems can be used to select appropriate parameters when evaluating physical systems.

The experiments were performed using the aforementioned experimental arrangement with a steel cantilever. The cantilever was supported in its weakest axis and had a cross-section of 1X25mm and an initial length of approximately 185mm.

Excitation for the system was white noise (acceleration) band-limited between 3-50Hz while the system's natural frequency was varied between approximately 16-18Hz. The excitation and response acceleration records were captured simultaneously using a sampling frequency of 1kHz and, prior to post-processing, were band-pass filtered (3-50Hz) using a 3<sup>rd</sup> order Butterworth filter (in addition to the low pass filter shown in *Figure 8-2*).

An initial evaluation of the system revealed the presence of a higher order mode as shown in *Figure 8-3*. The mode remained present for each of the preliminary experiments performed.

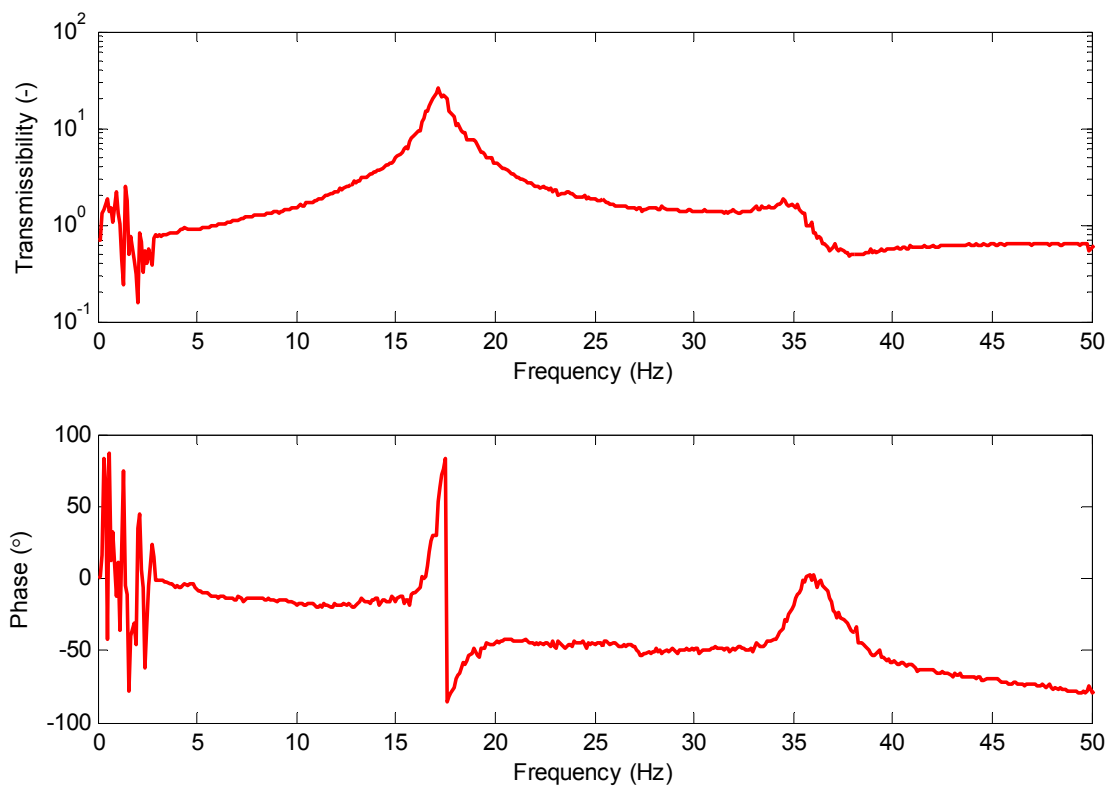


*Figure 8-3: Bode plot of physical steel cantilever arrangement.*

### 8.1.3.1. *Fourier based technique*

Chapter 5 used the results from numerous numerically simulated experiments to evaluate and discuss the influence of various analysis parameters used to obtain estimates of a system's frequency response function (FRF) via the Fourier transform. The numerical study suggested that for short-time modal parameter extraction purposes:

- Spectral resolution (or sub-record length) has a more significant influence on the natural frequency estimates than spectral uncertainty (or spectral averaging)
- Zero-padding of up to 16 times the sub-record length can significantly improve the accuracy of natural frequency estimates
- Overlapped averaging significantly reduces the variance of the natural frequency estimates

The following experiments aim to confirm or invalidate the above mentioned findings using the results from controlled physical SDoF systems. Clearly, repeating each of the numerically simulated experiments would be very time consuming; consequently, only those which provide the most useful information were repeated during this series of preliminary physical experiments.

Experiment 2 (see section 5.3.2) was repeated as it is able to examine the influence of multiple parameters, namely sub-record length, number of spectral averages, and most notably zero-padding. The results from this repeat experiment are given in *Figure 8-4*. The results reflect those presented in chapter 5 in that they are able to show that sub-record length has a more significant influence than averaging and that increased amounts of zero-padding can improve the accuracy of the estimates obtained.

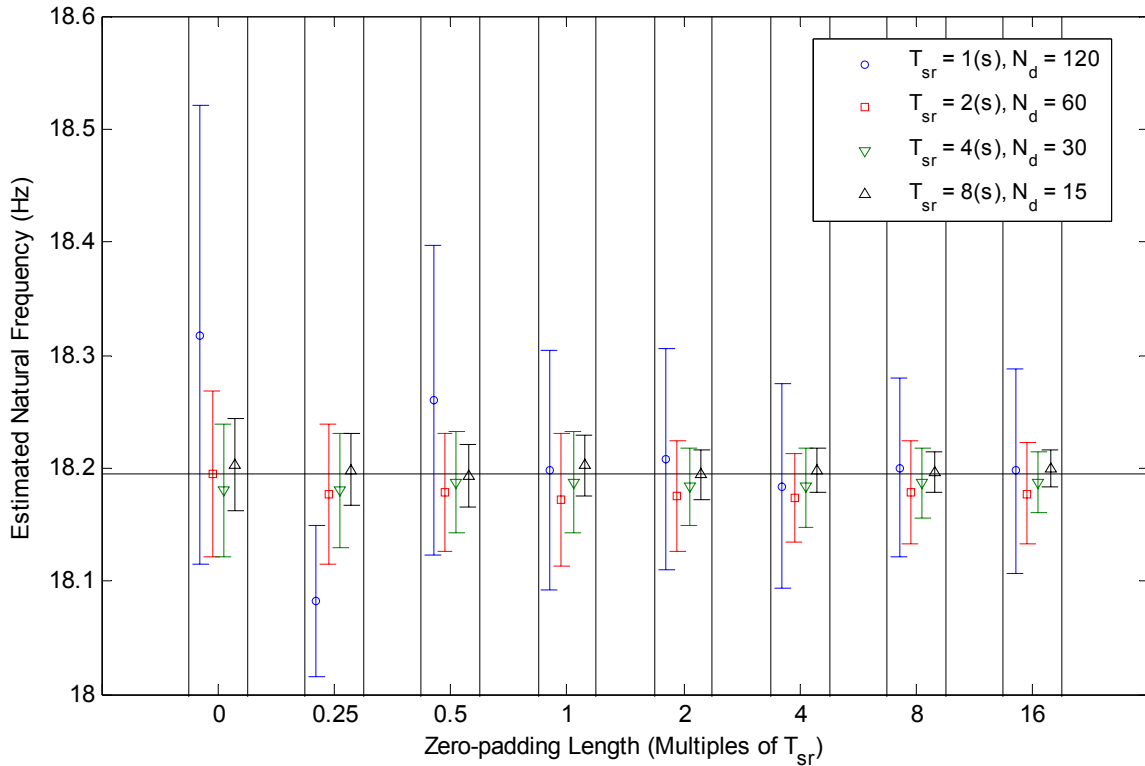


*Figure 8-4: Influence of zero-padding, sub-record length and spectral averaging.*

The influence of overlapped averages was confirmed by repeating experiment 4. The results obtained from the analysis of the physical cantilever are presented, alongside those obtained from the numerical system, in *Figure 8-5*. As can be seen the results from the physical experiments agree with those obtained from the numerical system. The results also suggest that an appropriate range of extraneous noise was evaluated during the numerical study.

*Figure 8-6* presents results obtained from the physical system, at various temporal resolutions (using maximum overlap, 16 times zero-padding and 100 spectral averages), alongside the results obtained from a numerical system with its damping ratio and natural frequency set to match the physical system. This figure is able to illustrate the required compromise between temporal resolution and uncertainty when suitable analysis parameters have been selected.

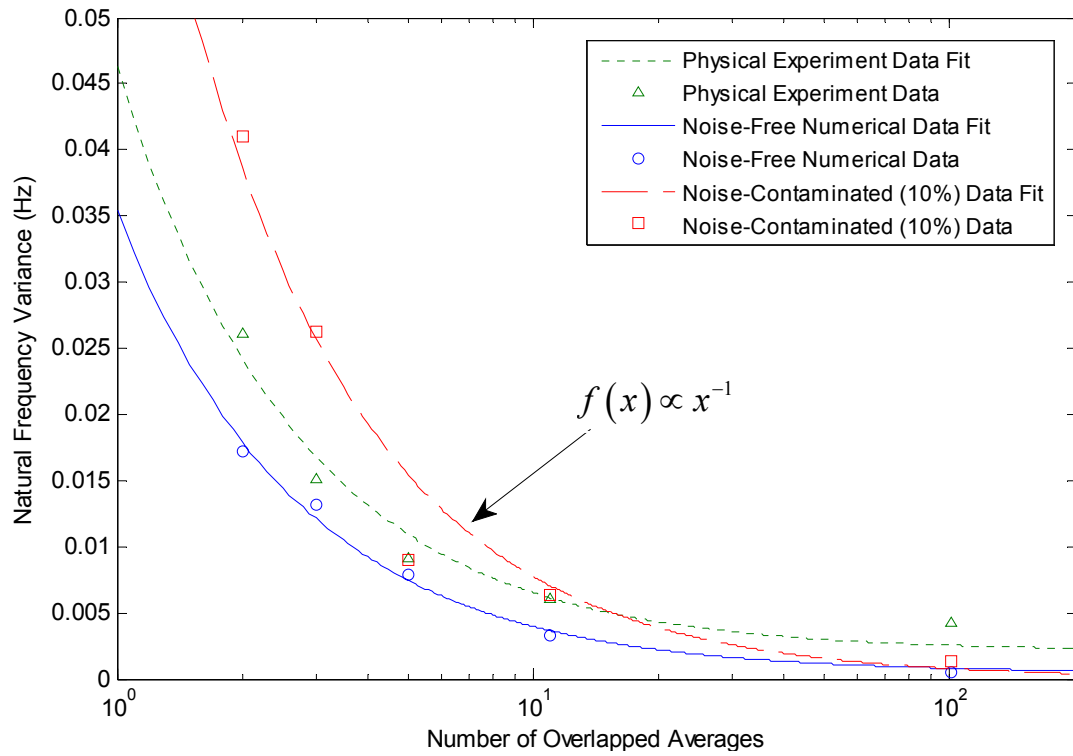


Figure 8-5: Influence of overlapped spectral averages.

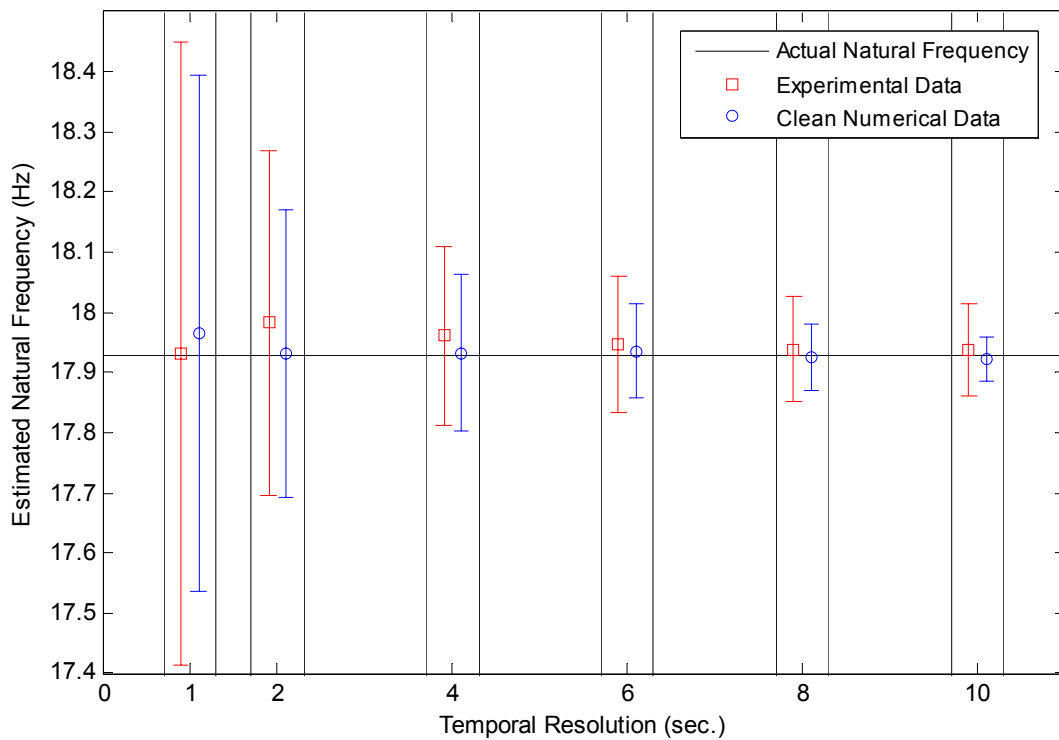


Figure 8-6: Compromise between temporal and spectral uncertainty.

### 8.1.3.2. Adaptive finite-impulse-response technique

The results obtained from the application of the Fourier based technique have suggested that:

1. The numerically simulated experiments were able to describe the influence of adjusting analysis parameters for modal parameter extraction
2. The range of extraneous noise assessed numerically exceeds the range expected during typical laboratory based modal parameter extraction experiments
3. The slight nonlinearities and presence of higher order modes did not noticeably affect the results obtained using the technique

However, it is possible that the adaptive finite-impulse-response (FIR) technique may respond differently, particularly to the presence of nonlinear behaviour and higher order modes. The results obtained using the adaptive FIR technique to monitor changes in the natural frequency of the steel cantilever, for various values of step-size  $\mu_N$ , are given in *Figure 8-7*. As can be seen the technique maintained its ability to accurately monitor shifts in natural frequency; however, the optimised step-size techniques did not function as well as previously indicated. *Figure 8-8* presents the optimisation of the fixed optimised step-size. As can be seen, the technique is clearly capable of predicting the step-size which will minimise the overall RMS filter error. However, the results presented in *Figure 8-9* indicate that the fixed optimised step-size algorithm places too much emphasis on minimising the error at the nonstationary event (due to its magnitude when compared to the steady-state error), and leaves little regard for the steady-state error (for systems with steady decay this will not as significant a limitation). When analysing the numerically simulated experimental data the limitations of the fixed optimum step-size could be avoided by updating the optimised step-size at regular intervals. However, the results presented in *Figure 8-7* show that, for this data set (which is typical), the variable optimised step-size technique is unable to select a value of step-size which will minimise the steady-state error. The results from the variable optimised step-size technique can be slightly improved by increasing the time between updates; however, increasing the re-optimisation period risks introducing the limitations of the fixed optimised step-size technique. The inability of the variable optimised step-size technique to select a suitable step-size during the time invariant stages of testing is attributed to slight nonlinear behaviour, and possibly the influence of higher order modes, which create spikes in the error signal, thereby giving a false indication of a low magnitude nonstationary event. It is possible that a technique which can determine the approximate steady state-error, isolate

potential nonstationary events (using the error signal only) and update the step-size over the time invariant and potentially time variant stages independently may provide a better means of re-optimisation. Due to space and time constraints a detailed investigation of such a technique will not be included in this study. However, for illustrative purposes, the results from an alternative variable step-size optimisation technique, which optimises the step-size for the initial convergence, clearly defined nonstationary events and the convergence from large nonstationary events separate to all other stages of testing, are given in *Figure 8-10*. The convergence and nonstationary periods were identified using the error signal obtained using a fixed step-size of 0.1. As can be seen, even at this basic level the error magnitude step-size optimisation technique is capable of providing more appropriate step-size values than the alternative optimisation techniques. *Figure 8-11* presents the error magnitude optimised step-size values for the results given in *Figure 8-10*.

All parameters other than the step-size can be set as described in chapter 6.

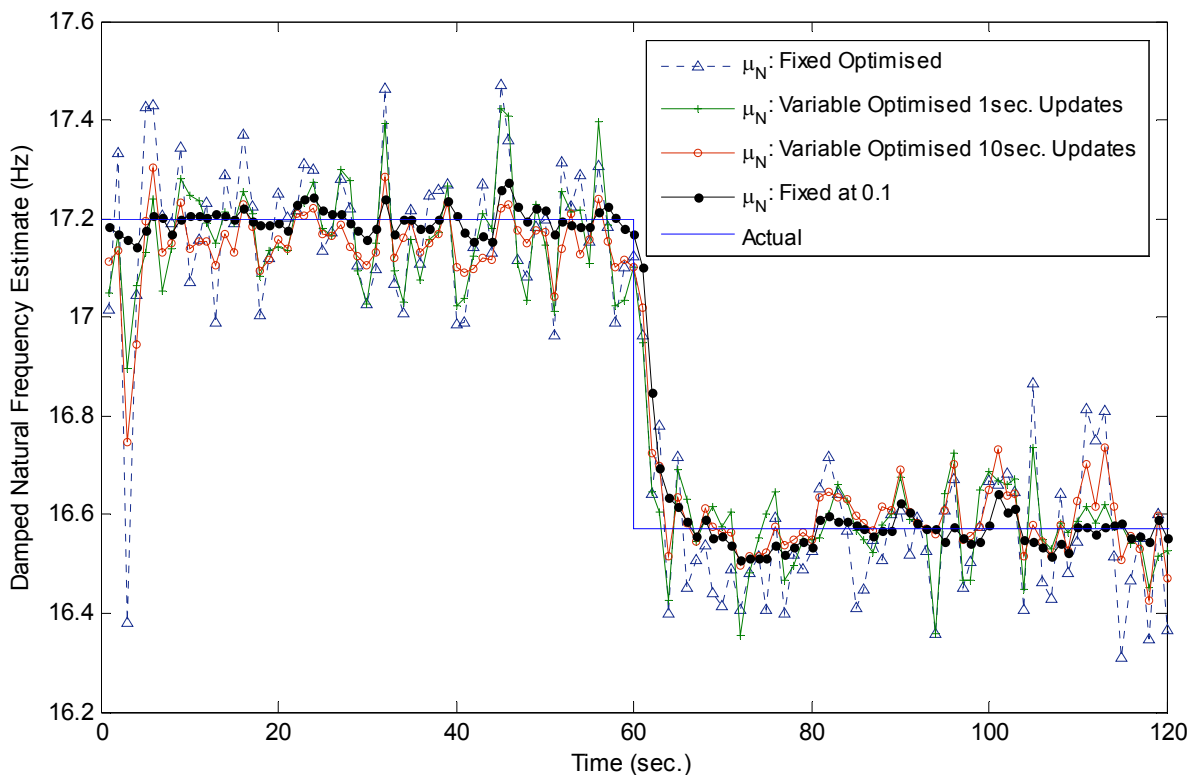


*Figure 8-7: Influence of normalised step-size on natural frequency estimates.*

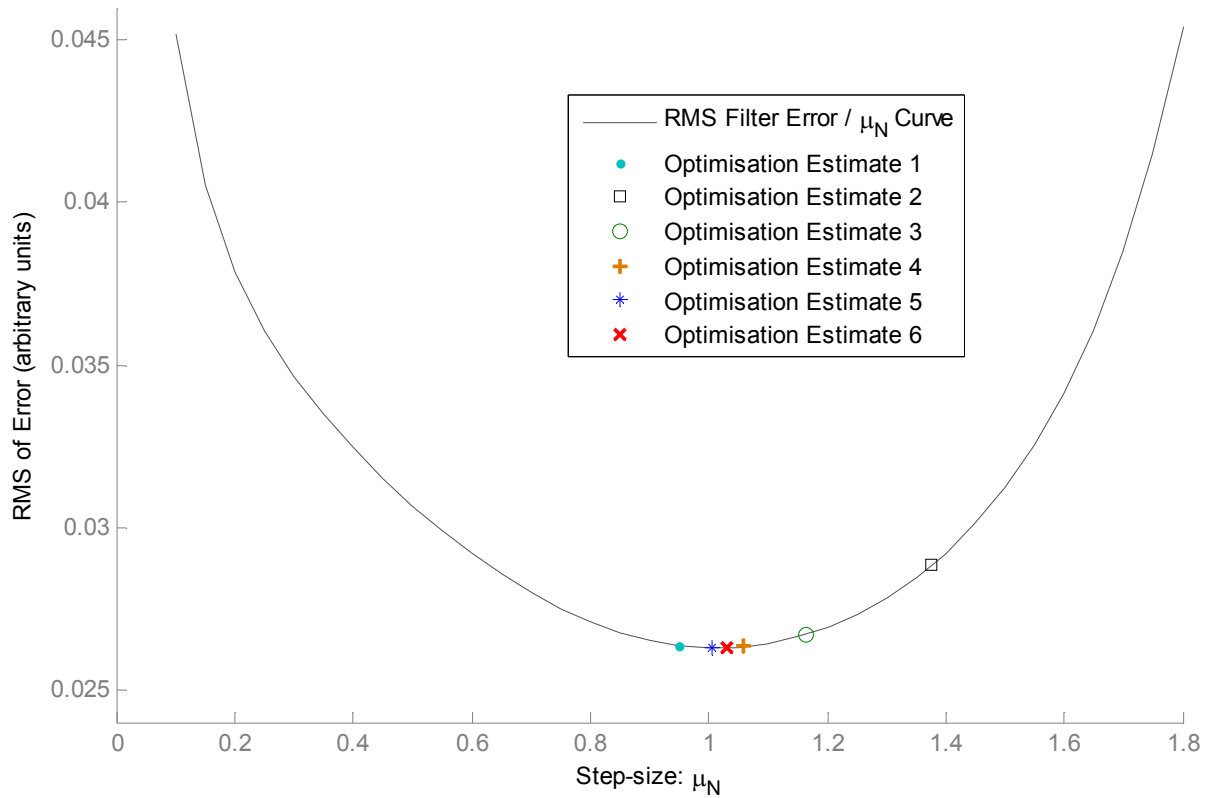


Figure 8-8: Optimisation of fixed normalised step-size.

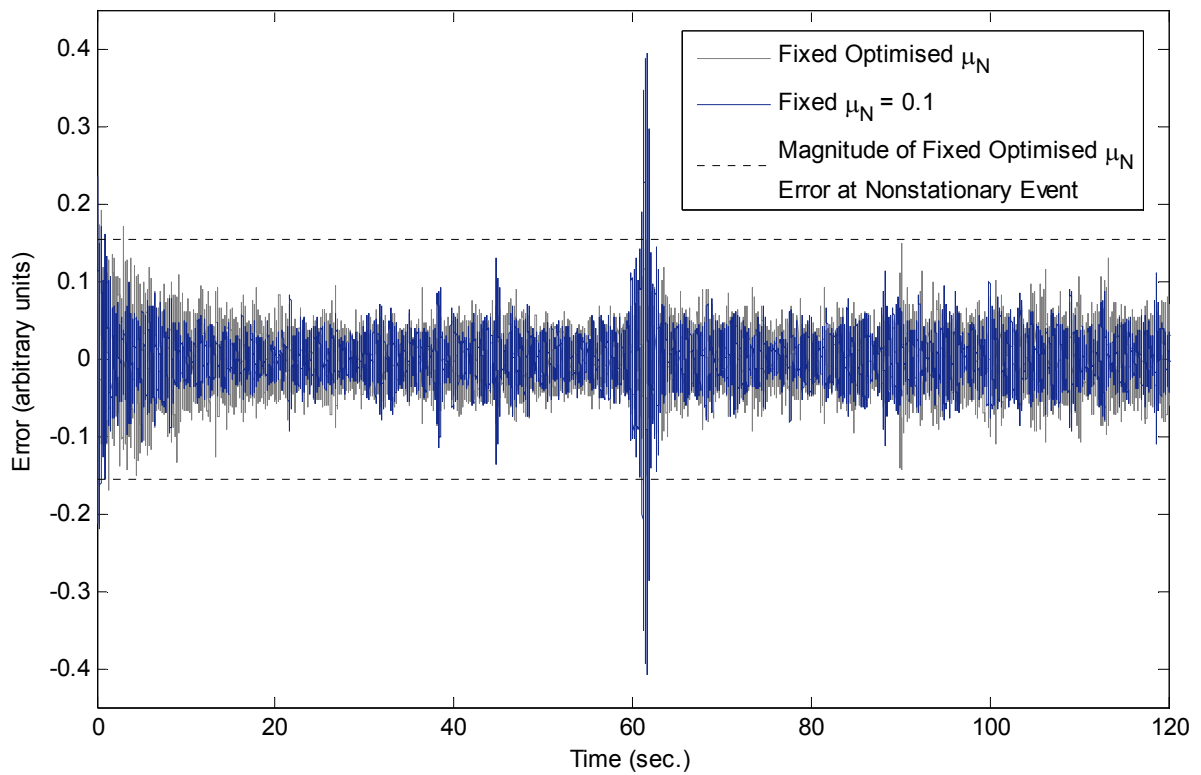


Figure 8-9: Filter error signals for a fixed optimised step-size and a fixed step-size of 0.1.

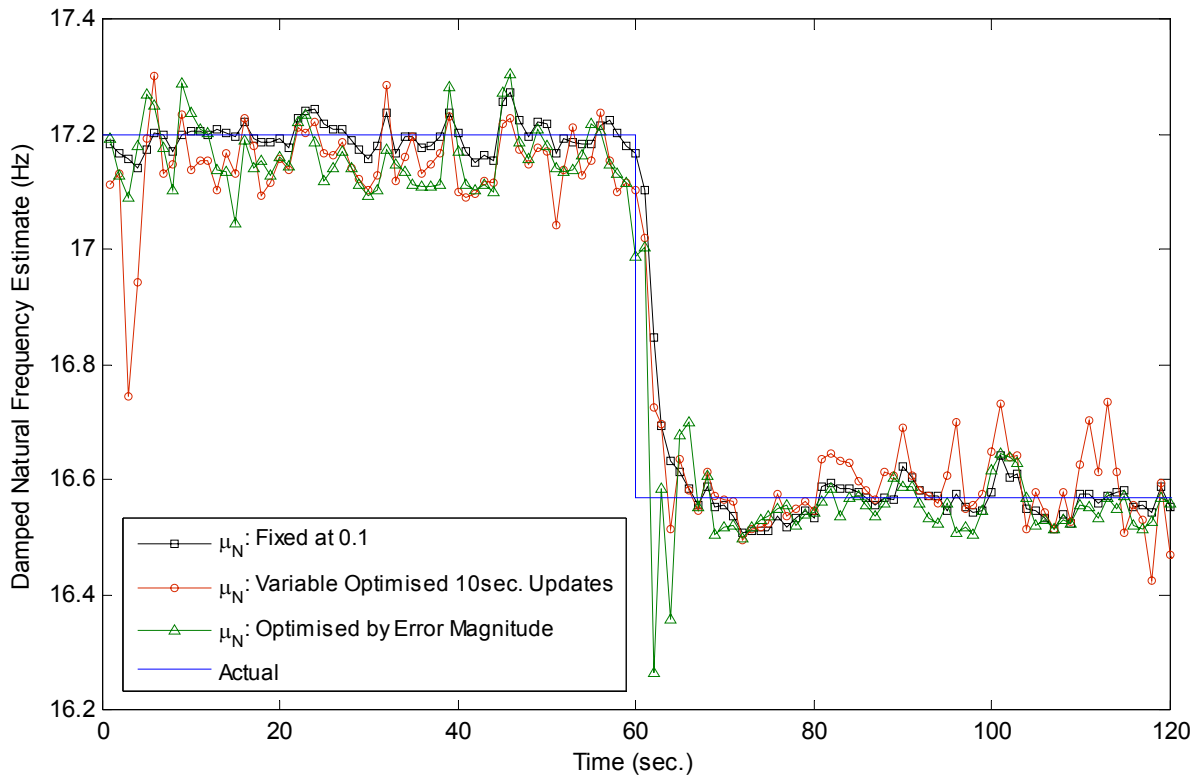


Figure 8-10: Improvement from error magnitude optimised normalised step-size.

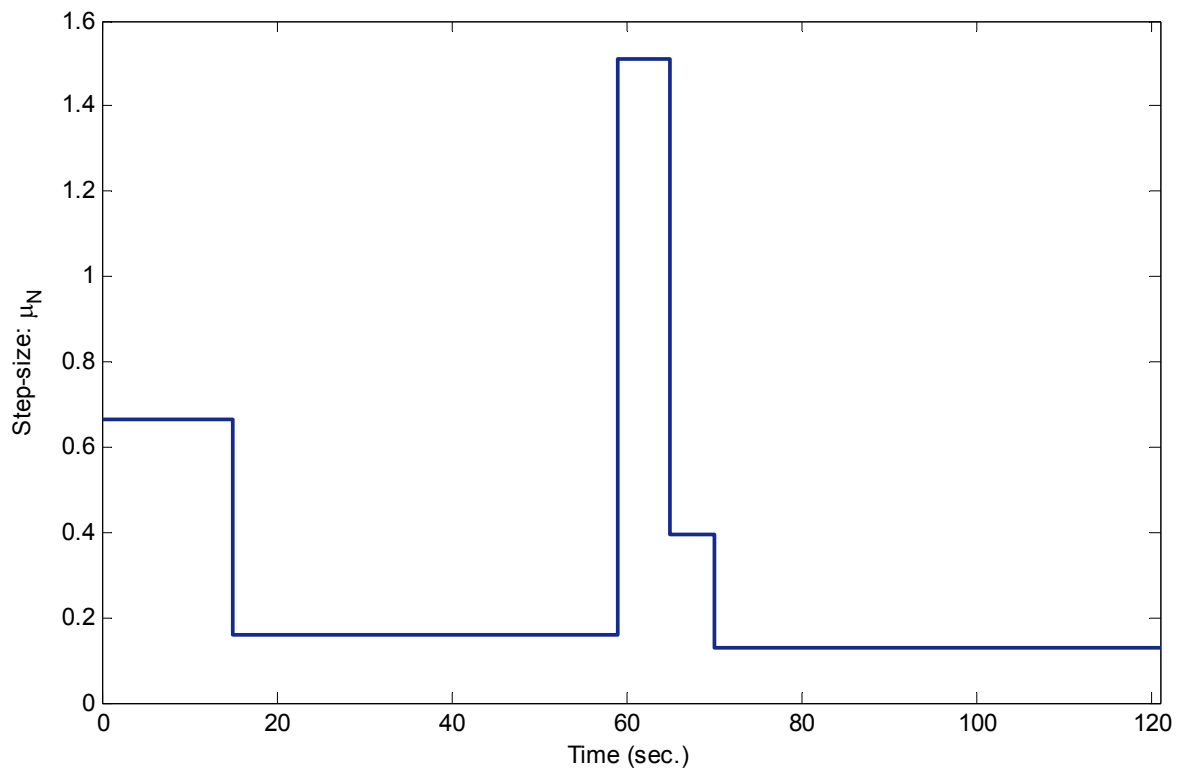


Figure 8-11: Values of step-size selected by error magnitude optimisation.

#### 8.1.4. Stepped Damage Scenarios

The following sections contain the results obtained from the analysis of various material samples configured as cantilevers. These experiments are not designed to be representative of real packaging elements. They are used to validate the numerically simulated experiments by allowing a comparison between the extracted natural frequency estimates and the known natural frequency of the cantilevers. The material types analysed are steel, aluminium, acrylic and carbon fibre. The materials were selected to determine the effectiveness of the integrity assessment techniques for a range of damping properties (and complexities such as nonlinearity). These properties were evaluated experimentally by analysing the instantaneous magnitude vector (obtained using the Hilbert transform) of the cantilever's free-response vibratory decay.

The same response accelerometer was used for each material and had a mass of 2.4g (excluding the cable).

##### 8.1.4.1. Steel cantilever results

The following results were obtained from a steel sample configured as a cantilever. The cantilever system had an equivalent viscous damping ratio of approximately 2.25%; the beam had a cross-section of 1X25mm and an initial length of approximately 185mm. The sample was orientated to allow for bending in its weakest axis. A bode plot of the system in its initial state is given in *Figure 8-3*. *Table 8-1* contains the calibration results obtained for the beam at various lengths.

*Table 8-1: Calibration results for steel cantilever.*

Increase in Length (mm)	Mean Damped Natural Frequency (Hz)	Coefficient of Variation (%)	Relative Damped Natural Frequency (%)
0±0.01	17.28	0.02	100
0.25±0.01	17.21	0.07	99.57
0.5±0.01	17.18	0.11	99.39
1±0.01	17.11	0.04	99.01
2±0.01	16.96	0.08	98.12
4±0.01	16.65	0.07	96.34

Figure 8-12 presents the results obtained using the adaptive FIR response technique for both a fixed step-size of 0.1 and a variable “optimised” step-size which was updated at one second intervals. A constant step-size of 0.1 was selected to achieve a low steady-state error with less concern for convergence time. The results were obtained at a temporal resolution of 0.01 seconds and a moving average filter was applied to achieve a temporal resolution of 1second.

Figure 8-13 presents the adaptive filter error for the results obtained using a fixed step-size of 0.1. This figure was included to demonstrate the potential of using the error signal alone to monitor changes in system properties.

Figure 8-14 compares the results obtained using the adaptive FIR technique using a fixed step-size of 0.1 with those obtained using the Fourier based technique at two different temporal resolutions (4 seconds and 8seconds).

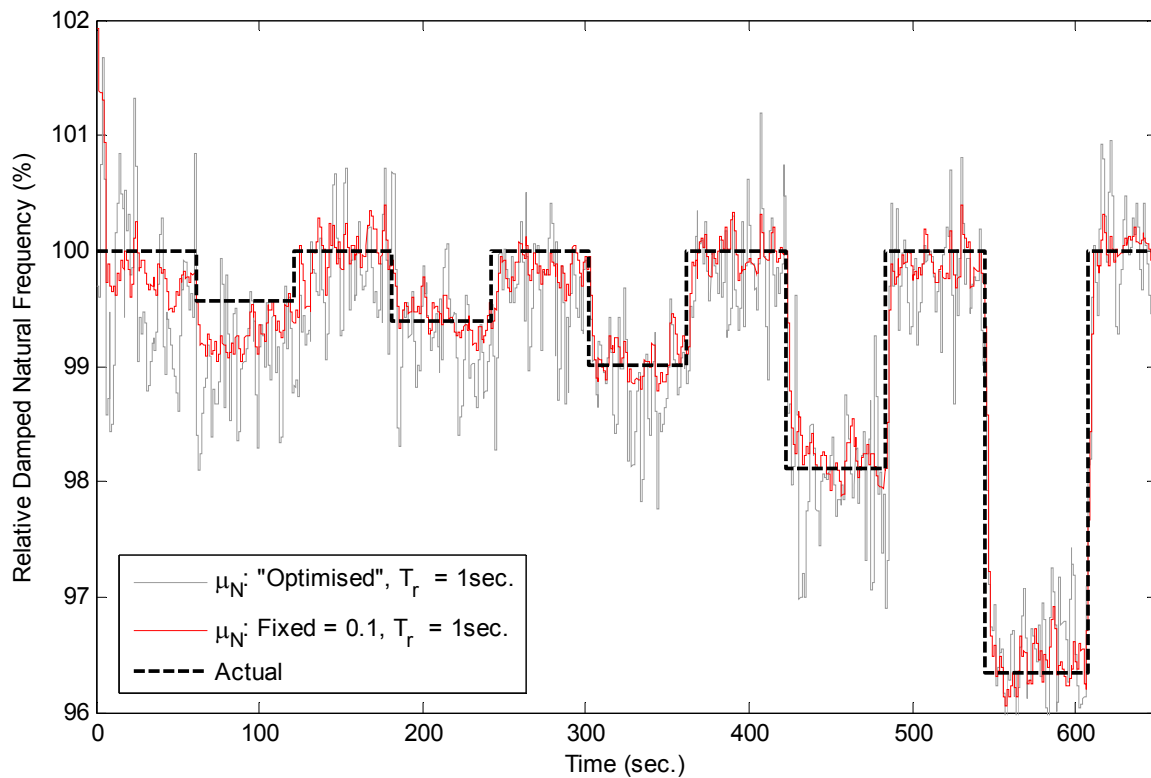


Figure 8-12: Step change results for a physical steel cantilever.

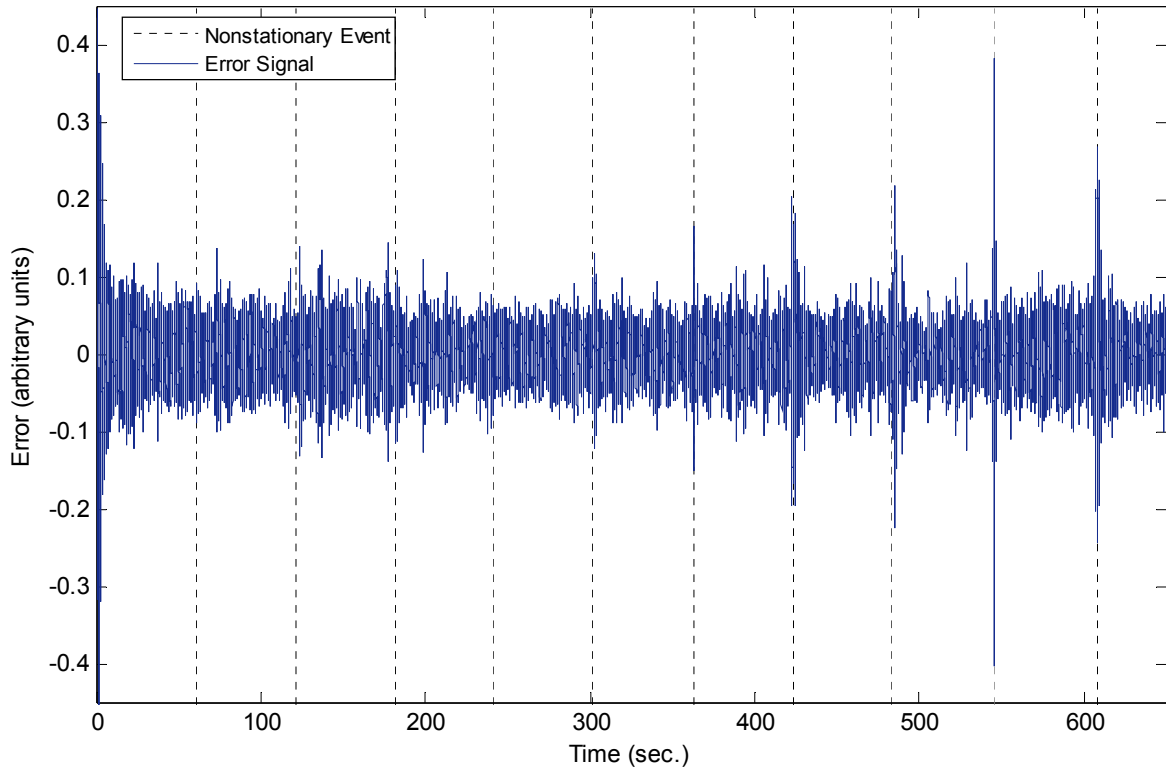


Figure 8-13: Error signal for the fixed step-size the results presented in Figure 8-12.

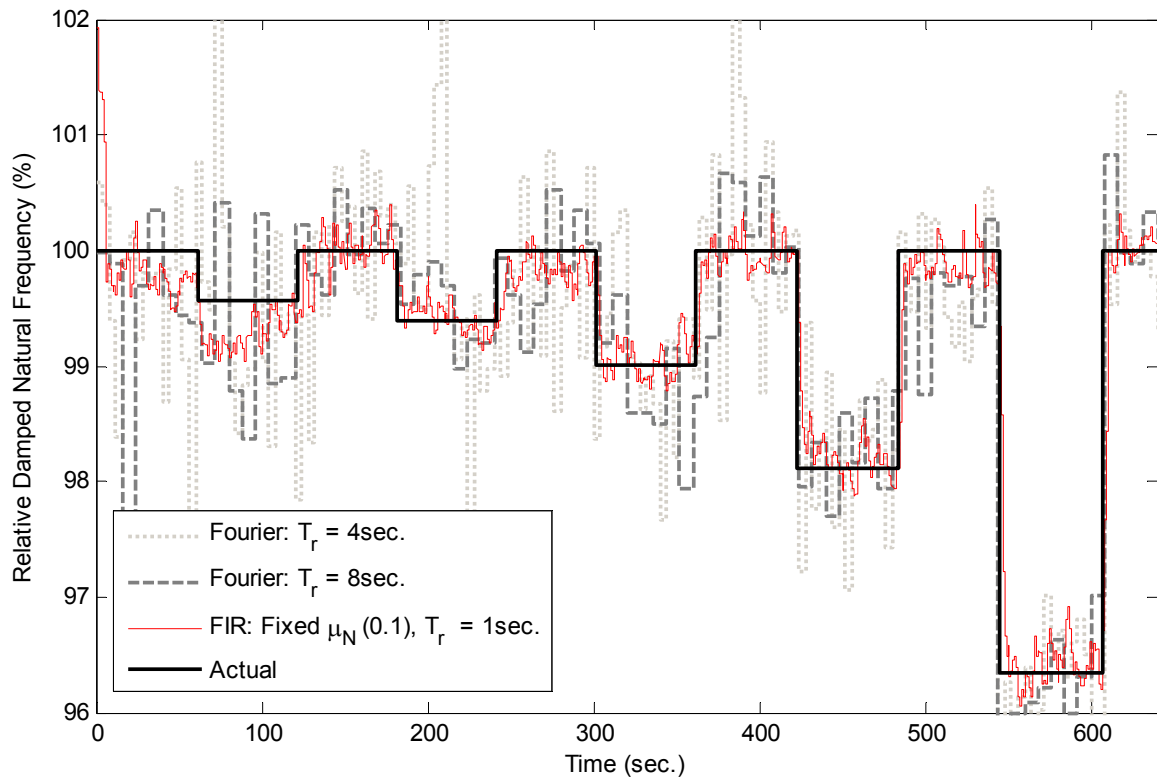


Figure 8-14: Comparison of the adaptive FIR and Fourier based results, steel cantilever.

#### 8.1.4.2. Aluminium cantilever results

The following results were obtained from an aluminium sample configured as a cantilever. The cantilever system had an equivalent viscous damping ratio of approximately 1.25%; the beam had a cross-section of 3X25mm and an initial length of approximately 315mm. The sample was orientated to allow for bending in its weakest axis. A bode plot of the system in its initial state is given in *Figure 8-15*. *Table 8-2* contains the calibration results obtained for the beam at various lengths.

*Table 8-2: Calibration results for aluminium cantilever.*

Increase in Length (mm)	Mean Damped Natural Frequency (Hz)	Coefficient of Variation (%)	Relative Damped Natural Frequency (%)
0±0.01	19.07	0.06	100
0.25±0.01	19.03	0.04	99.83
0.5±0.01	19.00	0.06	99.67
1±0.01	18.95	0.04	99.39
2±0.01	18.84	0.03	98.81
4±0.01	18.65	0.06	97.82

*Figure 8-16* presents the results obtained from the aluminium cantilever using the adaptive FIR response technique with both a fixed step-size of 0.1 and a variable “optimised” step-size which was updated at one second intervals. The results were obtained at a temporal resolution of 0.01 seconds and a moving average filter was applied to achieve a temporal resolution of 1second.

*Figure 8-17* presents the adaptive filter error for the results obtained using a fixed step-size of 0.1.

*Figure 8-18* compares the results obtained using the adaptive FIR technique using a fixed step-size of 0.1 with those obtained using the Fourier based technique at two different temporal resolutions (4 seconds and 8 seconds).

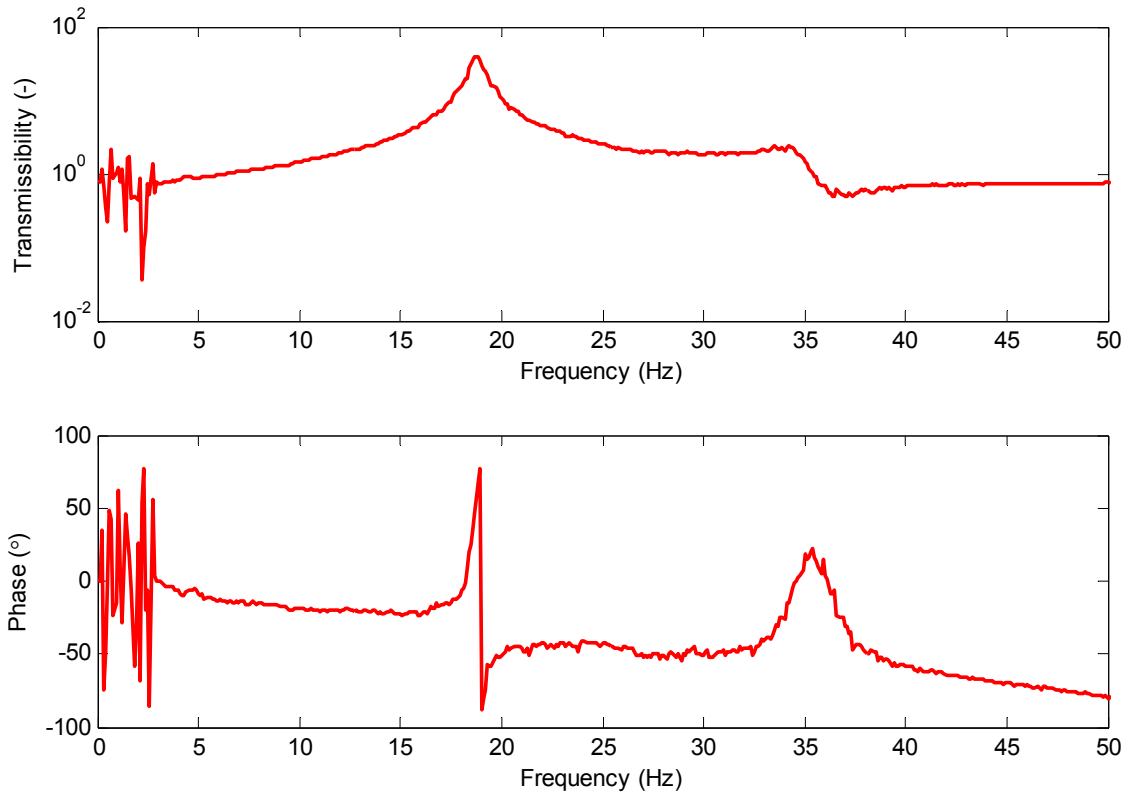


Figure 8-15: Bode plot of physical aluminium cantilever arrangement.

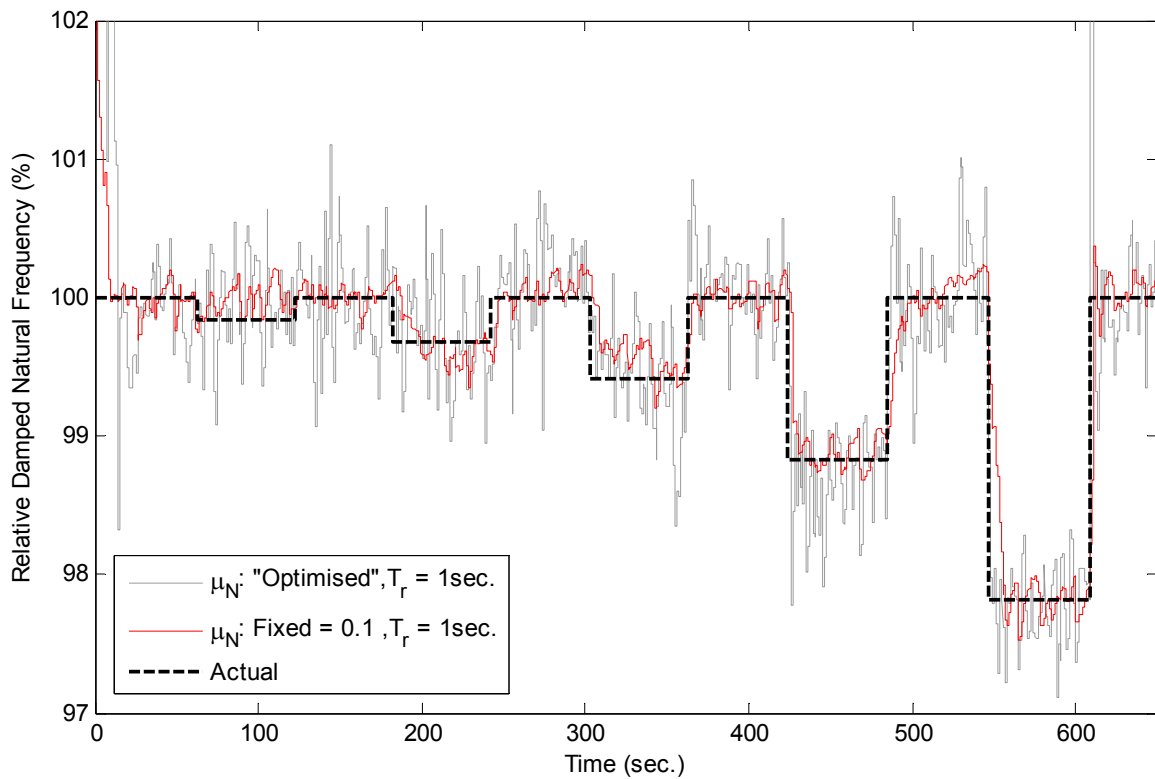


Figure 8-16: Step change results for a physical aluminium cantilever.

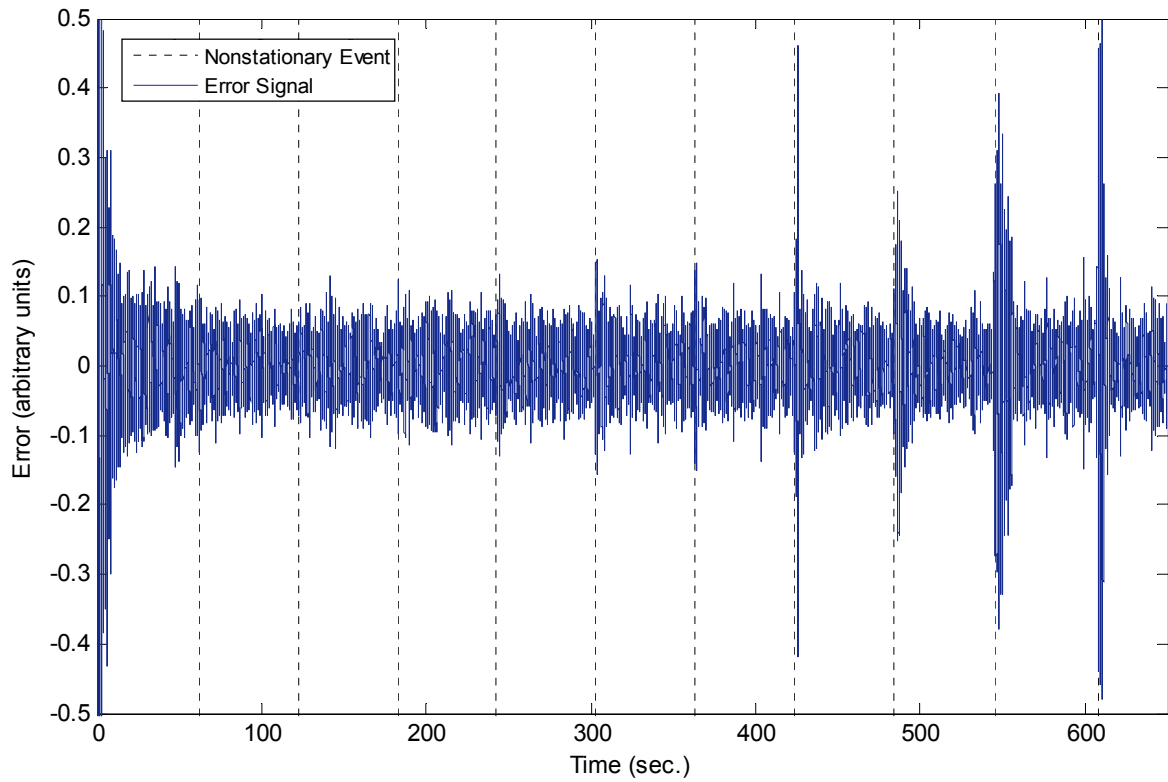


Figure 8-17: Error signal for the fixed step-size the results presented in Figure 8-16.

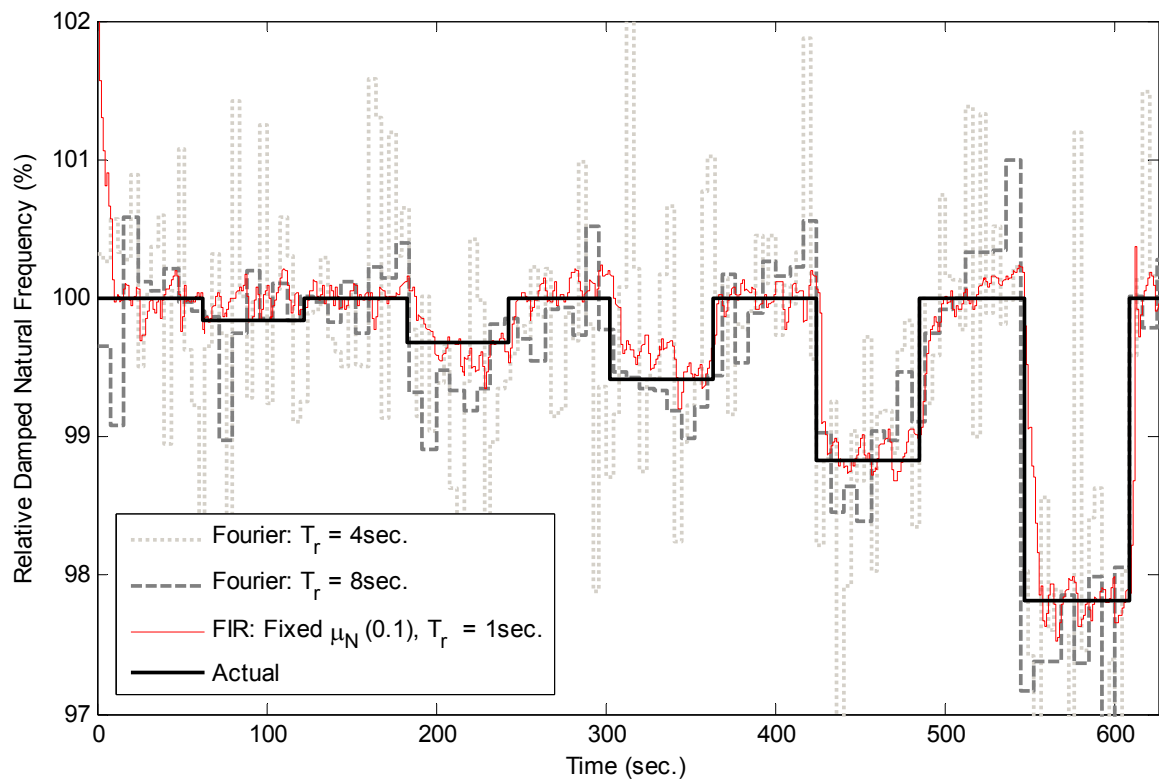


Figure 8-18: Comparison of the adaptive FIR and Fourier based results, aluminium cantilever.

### 8.1.4.3. Acrylic cantilever results

The following results were obtained from an acrylic sample configured as a cantilever. The cantilever system had an equivalent viscous damping ratio of approximately 6.30%; the beam had a cross-section of 4.5X25mm and an initial length of approximately 250mm. The sample was orientated to allow for bending in its weakest axis. A bode plot of the system in its initial state is given in *Figure 8-19*. *Table 8-3* contains the calibration results obtained for the beam at various lengths.

*Table 8-3: Calibration results for acrylic cantilever.*

Increase in Length (mm)	Mean Damped Natural Frequency (Hz)	Coefficient of Variation (%)	Relative Damped Natural Frequency (%)
0±0.01	17.35	0.18	100
0.25±0.01	17.27	0.06	99.56
0.5±0.01	17.24	0.13	99.37
1±0.01	17.21	0.16	99.20
2±0.01	17.01	0.11	98.07
4±0.01	16.77	0.08	96.67

*Figure 8-20* presents the results obtained from the acrylic cantilever using the adaptive FIR response technique with both a fixed step-size of 0.1 and a variable “optimised” step-size which was updated at one second intervals. The results were obtained at a temporal resolution of 0.01 seconds and a moving average filter was applied to achieve a temporal resolution of 1second.

*Figure 8-21* presents the adaptive filter error for the results obtained using a fixed step-size of 0.1.

*Figure 8-22* compares the results obtained using the adaptive FIR technique using a fixed step-size of 0.1 with those obtained using the Fourier based technique at two different temporal resolutions (4 seconds and 8 seconds).

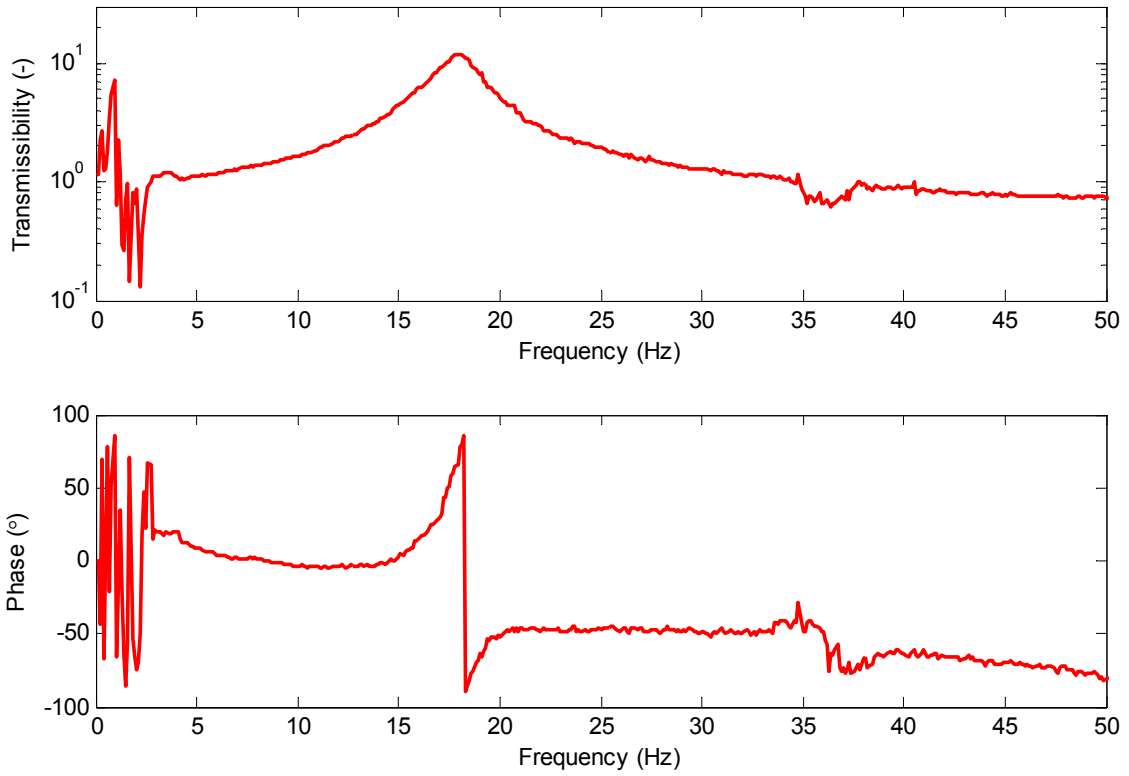


Figure 8-19: Bode plot of physical acrylic cantilever arrangement.

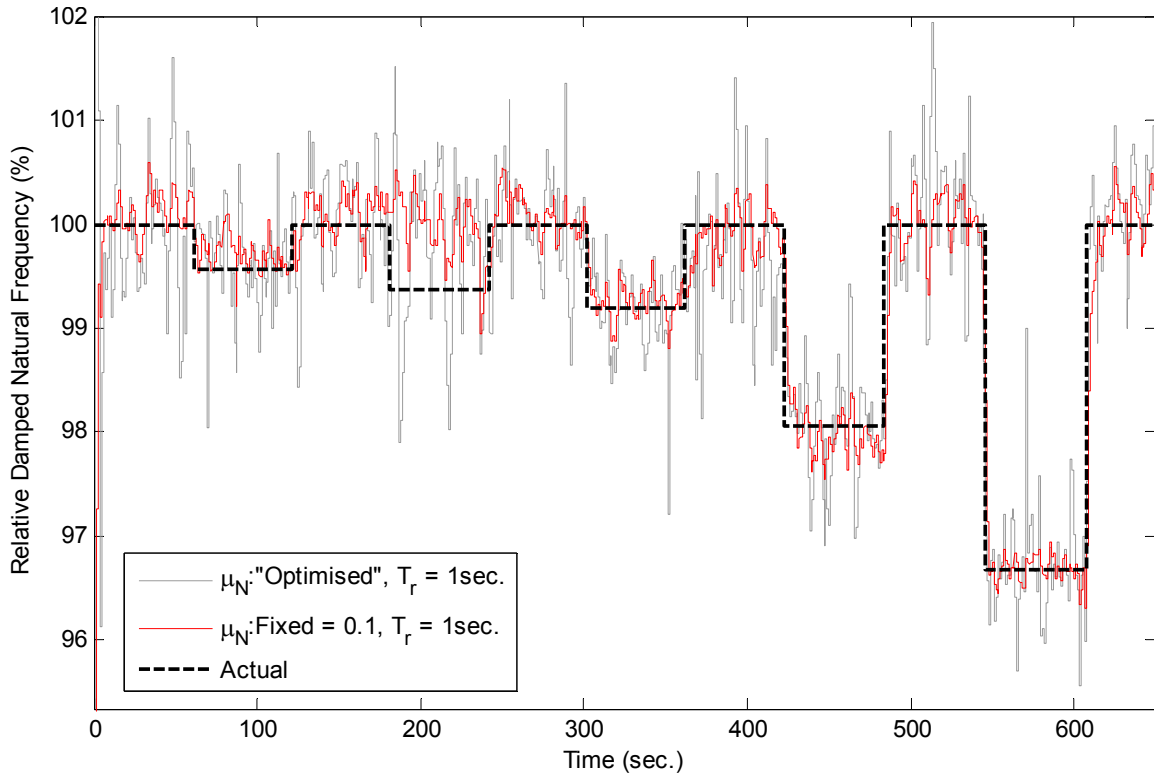


Figure 8-20: Step change results for a physical acrylic cantilever.

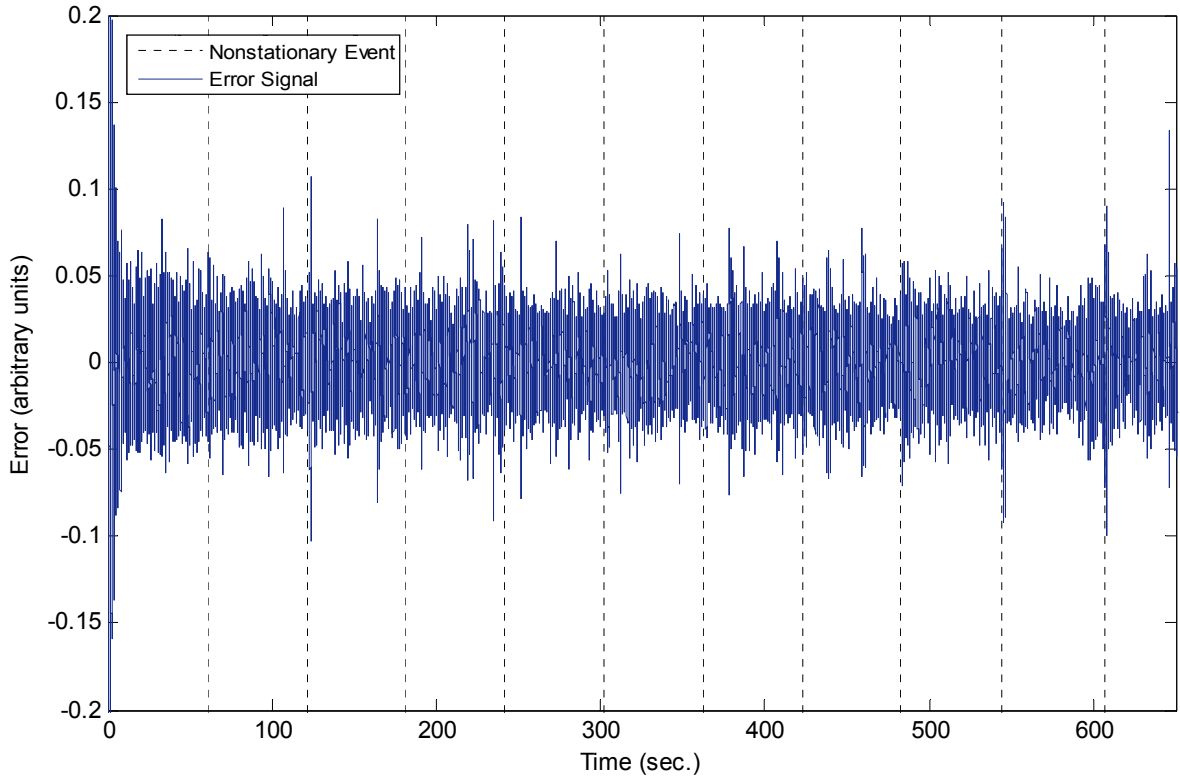


Figure 8-21: Error signal for the fixed step-size results presented in Figure 8-20.

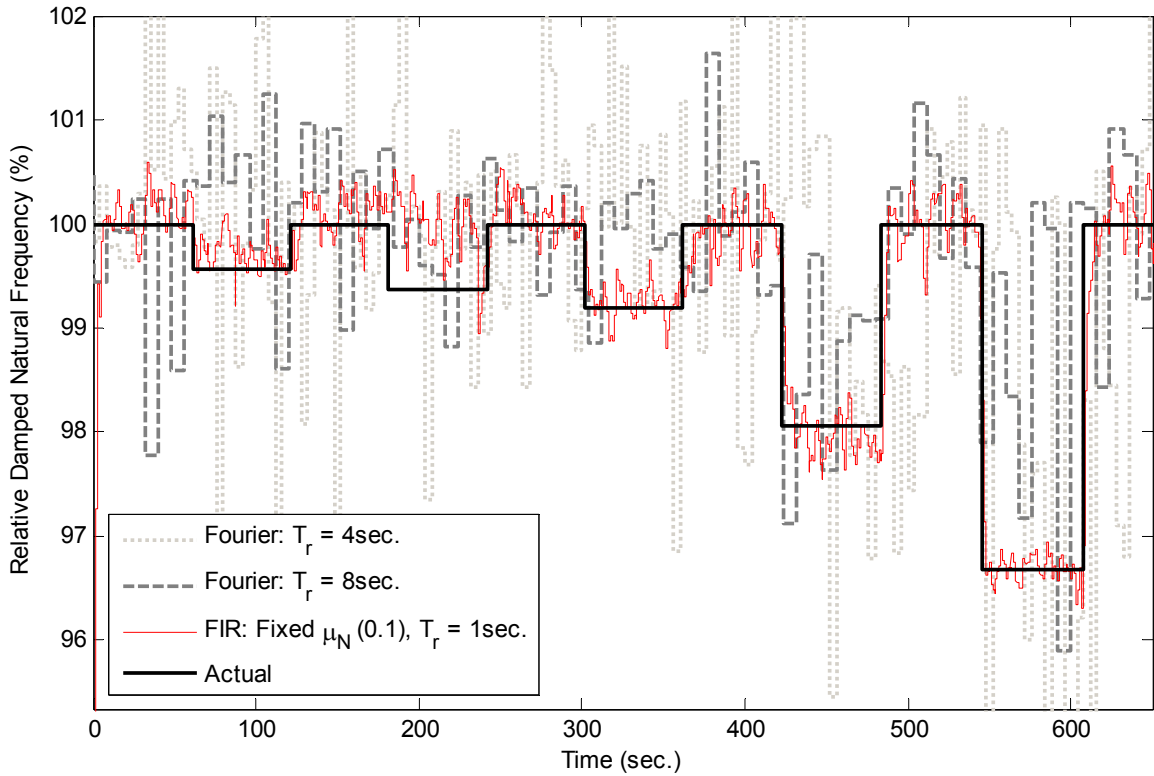


Figure 8-22: Comparison of the adaptive FIR and Fourier based results, acrylic cantilever.

#### 8.1.4.4. Carbon fibre cantilever results

The following results were obtained from a carbon fibre (Carbon Fiber Australia) sample configured as a cantilever. The cantilever system had an equivalent viscous damping ratio of approximately 2.5%; the beam had a cross-section of 3X25mm and an initial length of approximately 325mm. The sample was orientated to allow for bending in its weakest axis. A bode plot of the system in its initial state is given in *Figure 8-23*. *Table 8-4* contains the calibration results obtained for the beam at various lengths.

*Table 8-4: Calibration results for carbon fibre cantilever.*

Increase in Length (mm)	Mean Damped Natural Frequency (Hz)	Coefficient of Variation (%)	Relative Damped Natural Frequency (%)
0±0.01	23.01	0.11	100
0.25±0.01	22.95	0.09	99.74
0.5±0.01	22.84	0.03	99.27
1±0.01	22.78	0.13	98.84
2±0.01	22.61	0.13	98.28
4±0.01	22.22	0.15	96.59

*Figure 8-24* presents the results obtained from the carbon fibre cantilever using the adaptive FIR response technique with both a fixed step-size of 0.1 and a variable “optimised” step-size which was updated at one second intervals. The results were obtained at a temporal resolution of 0.01 seconds and a moving average filter was applied to achieve a temporal resolution of 1second.

*Figure 8-25* presents the adaptive filter error for the results obtained using a fixed step-size of 0.1.

*Figure 8-26* compares the results obtained using the adaptive FIR technique using a fixed step-size of 0.1 with those obtained using the Fourier based technique at two different temporal resolutions (4 seconds and 8 seconds).

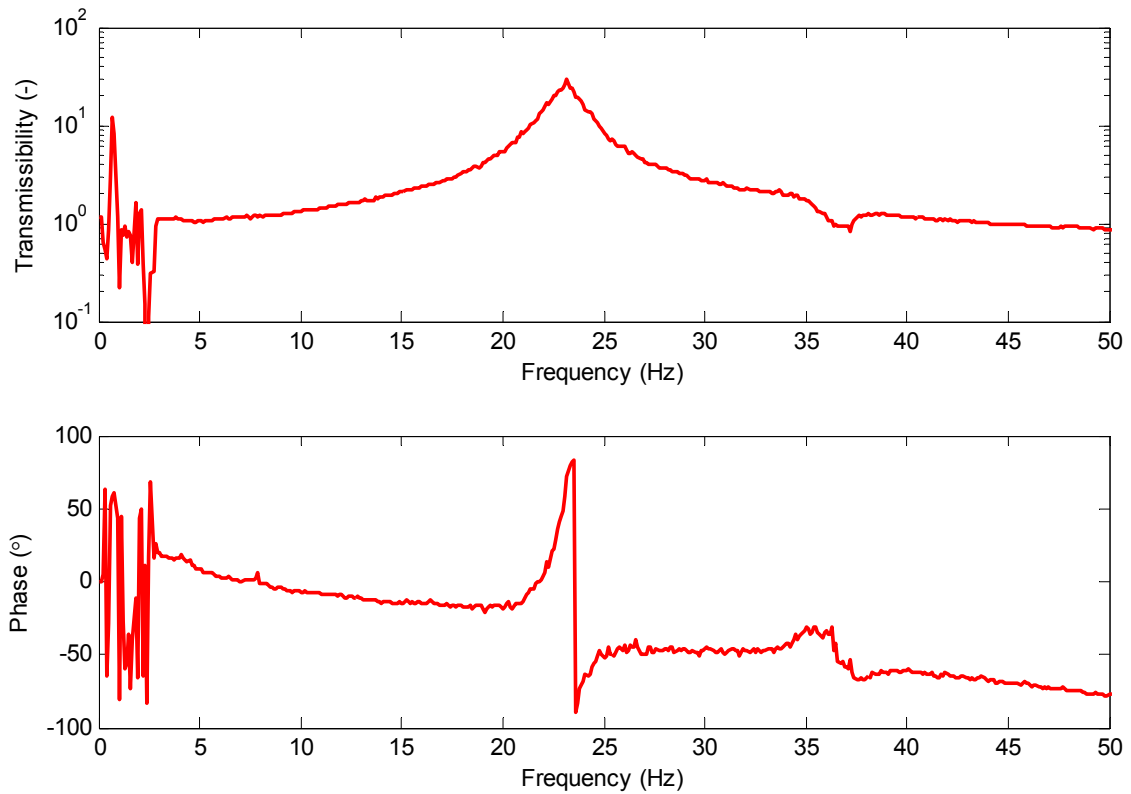


Figure 8-23: Bode plot of physical carbon fibre cantilever arrangement.

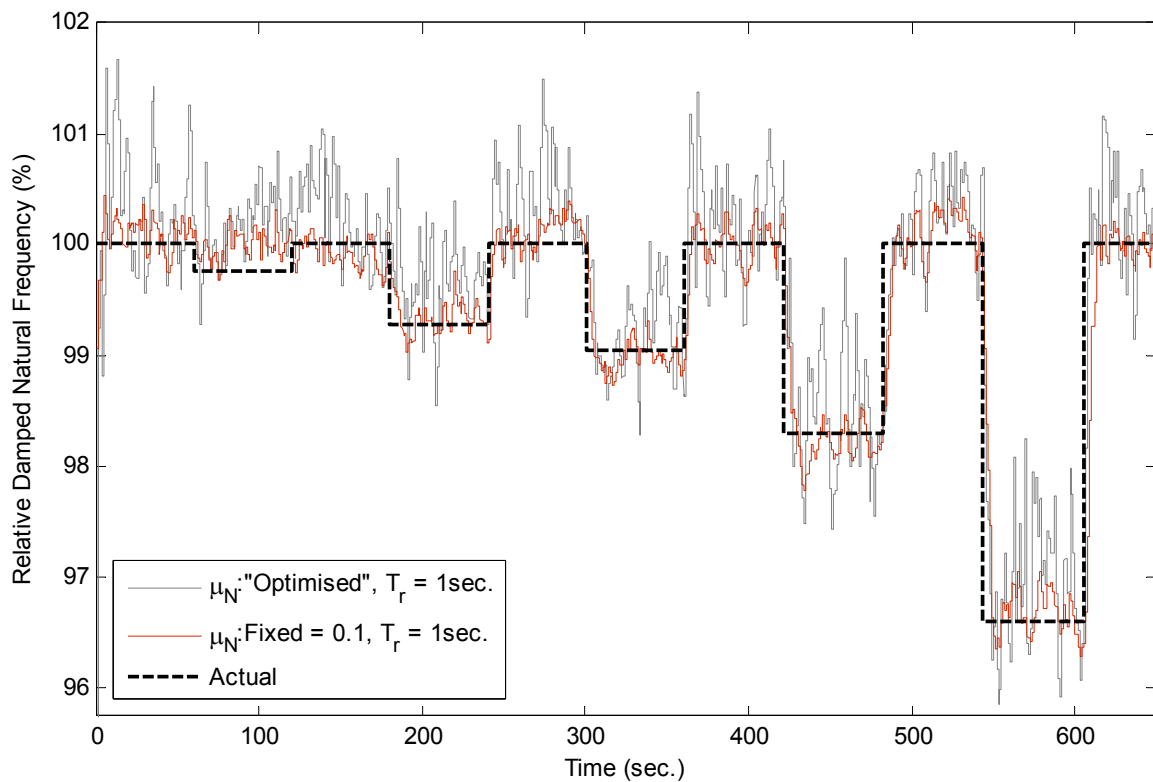


Figure 8-24: Step change results for a physical carbon fibre cantilever.

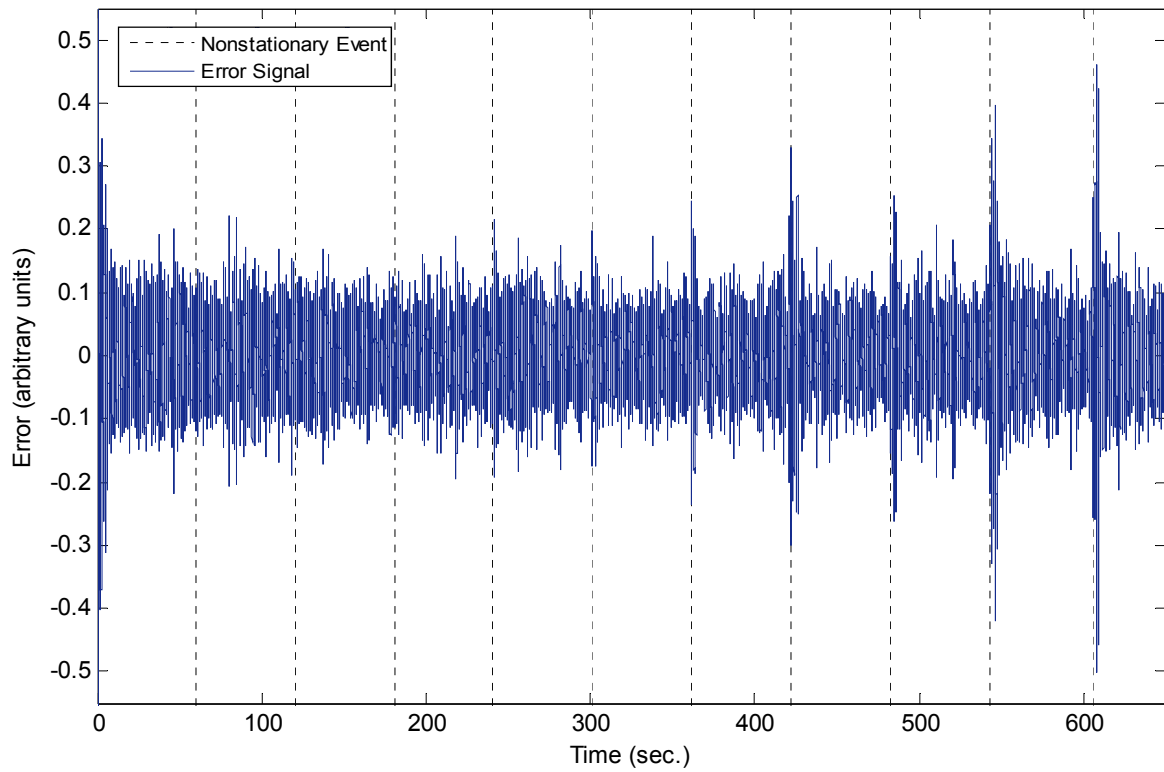


Figure 8-25: Error signal for the fixed step-size results presented in Figure 8-24.

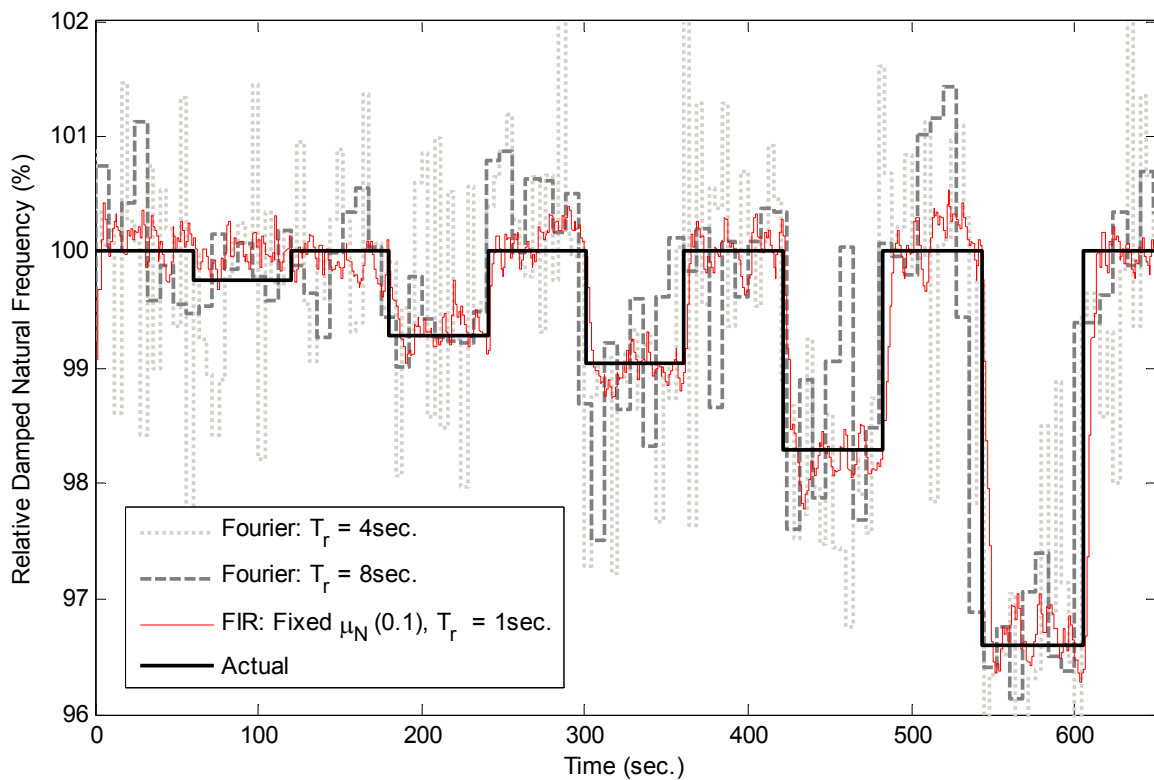


Figure 8-26: Comparison of the adaptive FIR and Fourier based results, carbon fibre cantilever.

### 8.1.5. Discussion of Controlled Experiment Results

The research presented in this section was included to confirm the numerically simulated experiments and to establish the sensitivity of the structural integrity assessment techniques when analysing real materials elements. *Figure 8-3*, *Figure 8-15*, *Figure 8-19* and *Figure 8-23* presented the FRFs (magnitude and phase) obtained from the physical cantilever systems. As can be seen these FRFs deviate, by varying amounts, from those which would be obtained from pure linear SDoF systems, with the FRF presented in *Figure 8-19* (acrylic sample) being the most complex (furthest deviation from a linear SDoF system).

*Figure 8-12*, *Figure 8-16*, *Figure 8-20* and *Figure 8-24* present the results obtained using the adaptive FIR technique to monitor variations in the length of the steel, aluminium, acrylic and carbon fibre samples, respectively. The results presented in these figures re-enforce the results from the preliminary physical experiments, which suggest that, despite the technique's ability to accurately monitor the variations in natural frequency, the optimised step-size technique is unable to yield the step-size which minimises the steady-state error when analysing data from physical experiments. This, as previously discussed, is attributed to the "spikes" in the filter's error signals which are not associated with nonstationary events.

The results presented in *Figure 8-13*, *Figure 8-17*, *Figure 8-21* and *Figure 8-25* suggest that, with suitable signal processing, the filter's error signal alone may provide a means for identifying nonstationary events with increases in error appearing for each adjustment in length (nonstationary event).

*Figure 8-14*, *Figure 8-18*, *Figure 8-22* and *Figure 8-26* compare the performance of the adaptive FIR technique with that of the Fourier based approach. Despite its ability to detect changes in natural frequency, the Fourier based technique is unable to match the performance of the adaptive FIR method, even with a relatively coarse temporal resolution of 8 seconds. Furthermore, as the complexity of the system increased (the acrylic cantilever) the difference in performance between the techniques became greater. This finding was not initially expected, and it is believed that if systems with more complex characteristics are analysed the Fourier based technique may provide better estimates than the adaptive FIR approach.

Overall, results from the controlled physical experiments confirm those obtained from the numerically simulated experiments, which suggest that the adaptive FIR technique is eminently capable of continuously tracking variations in natural frequency. One noticeable difference is a slight increase in uncertainty despite the relatively low noise to signal ratio (when compared to the numerically simulated experiments containing extraneous noise).

This can be attributed to nonlinearities in the physical arrangements as well as the contamination of the first resonant frequency by higher order modes.

## 8.2. ASSESSMENT OF REAL PACKAGING ELEMENTS

Finally, the ability of the integrity assessment techniques to monitor the progression of fatigue within actual protective packaging elements was investigated. This section of the research presents typical results obtained from the analysis of two environmentally acceptable packaging elements:

1. Biodegradable air cushions
2. Empty corrugated paperboard boxes

The compression characteristics of typical Opus<sup>TM</sup> (Green Light Products) air cushions and corrugated paperboard containers are given in *Figure 8-27* and *Figure 8-28*, respectively. As can be seen both elements have highly nonlinear stiffness characteristics. It is also worth mentioning that the corrugated paperboard container compression curves were obtained from three visually identical elements, from the same production batch, yet demonstrate significantly different stiffness, ultimate compressive strength and overall compressive properties. Despite the complex characteristics of the paperboard containers, Garcia-Romeu-Martinez *et al.* (2007) demonstrated that the fit of a linear SDoF model to the FRF (Fourier technique) of such systems is effective in monitoring variations in the stiffness of the system as a result of random compressive loads (provided coarse temporal resolution is sufficient).

During the first series of experiments performed on real protective packaging elements, an Opus biodegradable air cushion was subjected to various preloads (0.3kN-0.7kN) during which the force–deformation characteristics were monitored as shown in *Figure 8-29* (0.3kN compression curve was corrupted before it was able to be plotted). Subsequent to each compressive load being applied, a mass guided by a pneumatic bearing (to minimise friction) was placed atop of the cushion and the system was subjected to random, band-limited (3-50Hz) base excitation (for 100 seconds). The random excitation was set to a low level of 1.0 m/s<sup>2</sup> root-mean-squared (RMS) and the applied load was limited to 2.66kg, in order not to induce further damage to the sample. Both the base table and the guided mass were fitted with accelerometers connected to the previously described data acquisition system. Data was captured using a sampling rate of 1kHz. The captured individual excitation and response records were concatenated (using a Tukey window with the window width parameter  $\alpha$  set to 0.01 to remove the end effects) in order to produce continuous excitation and response

records. These records were analysed using both structural integrity assessment techniques to extract time histories of the variations in the system's damped natural frequency. A photograph of the experimental arrangement is given in *Figure 8-30*.

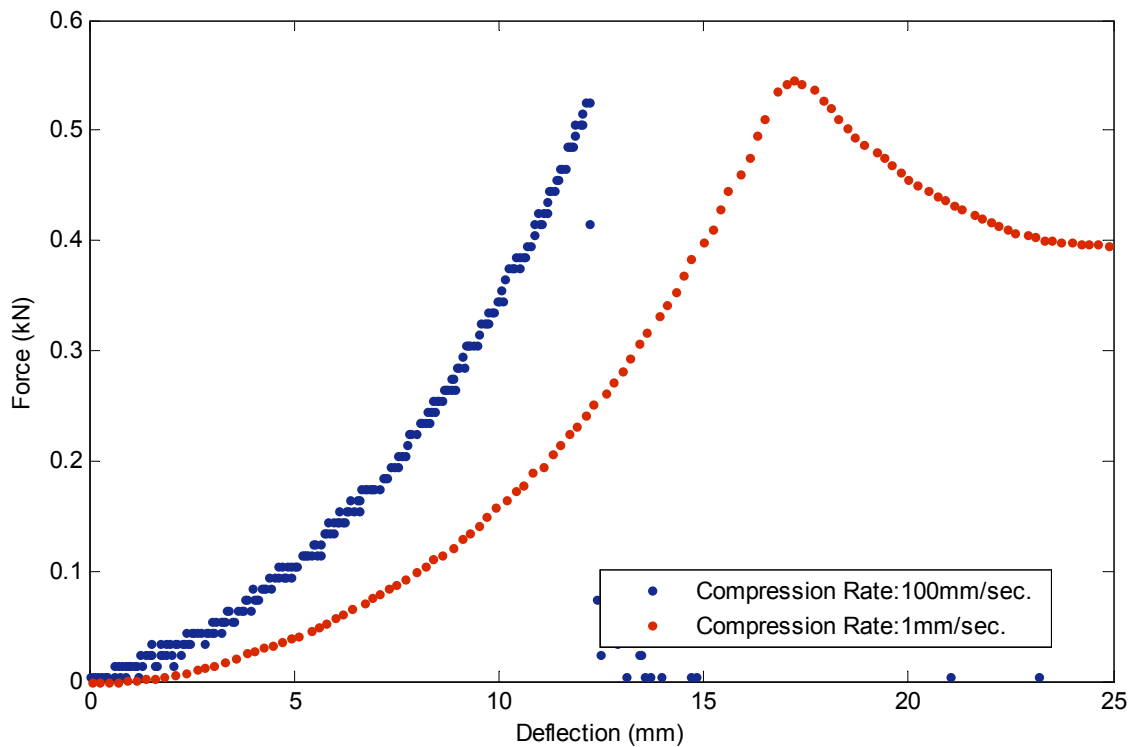


*Figure 8-27: Opus biodegradable air cushion typical compression curves – full compression.*

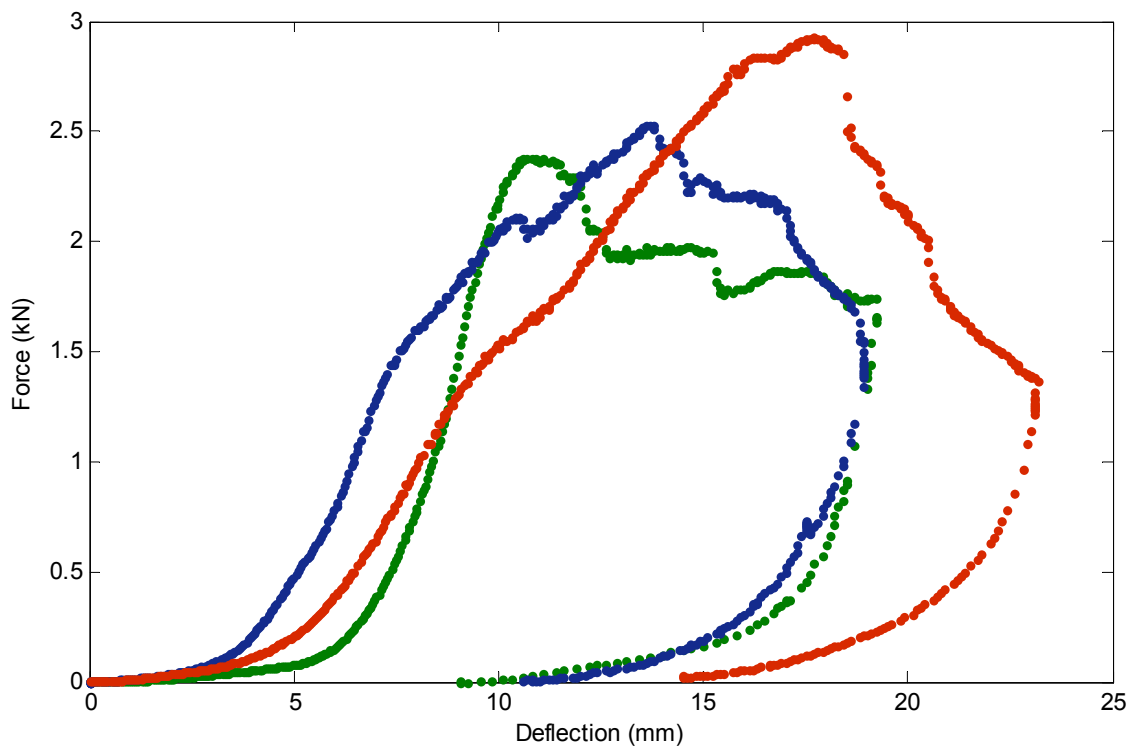


*Figure 8-28: Corrugated paperboard container compression curves – full compression.*

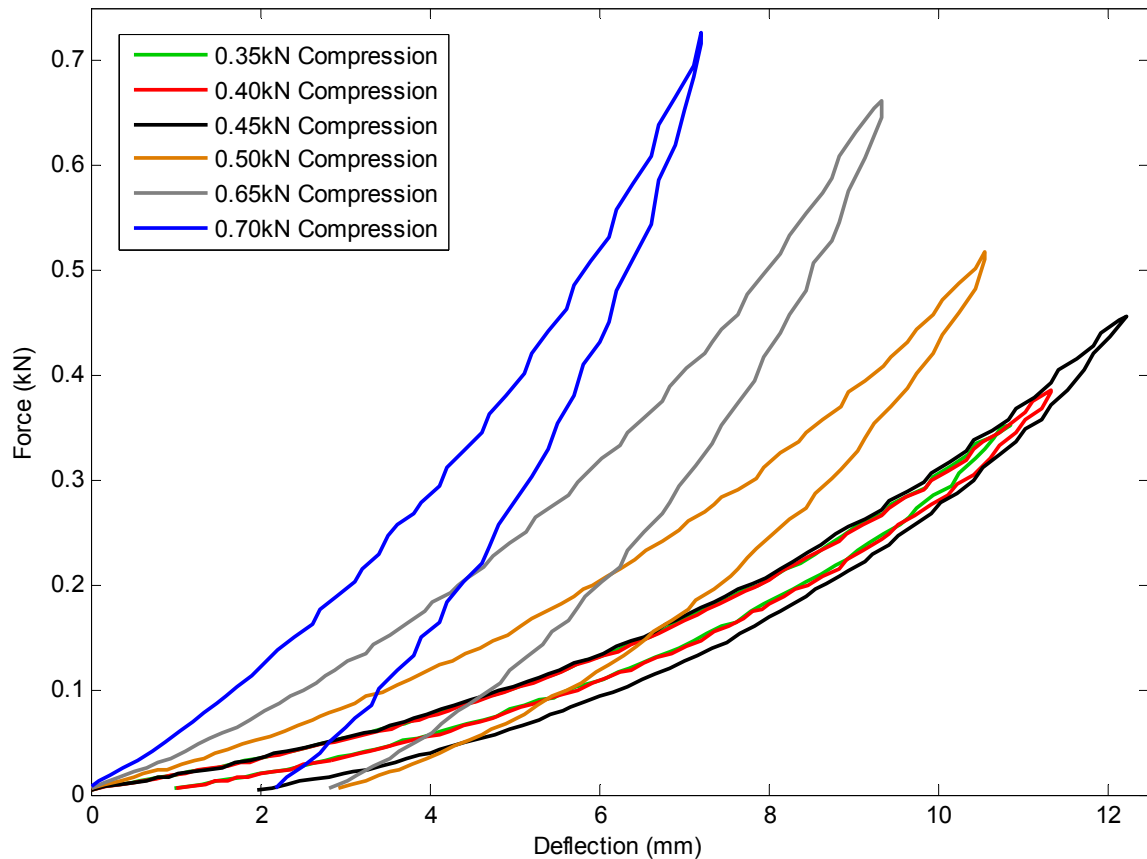
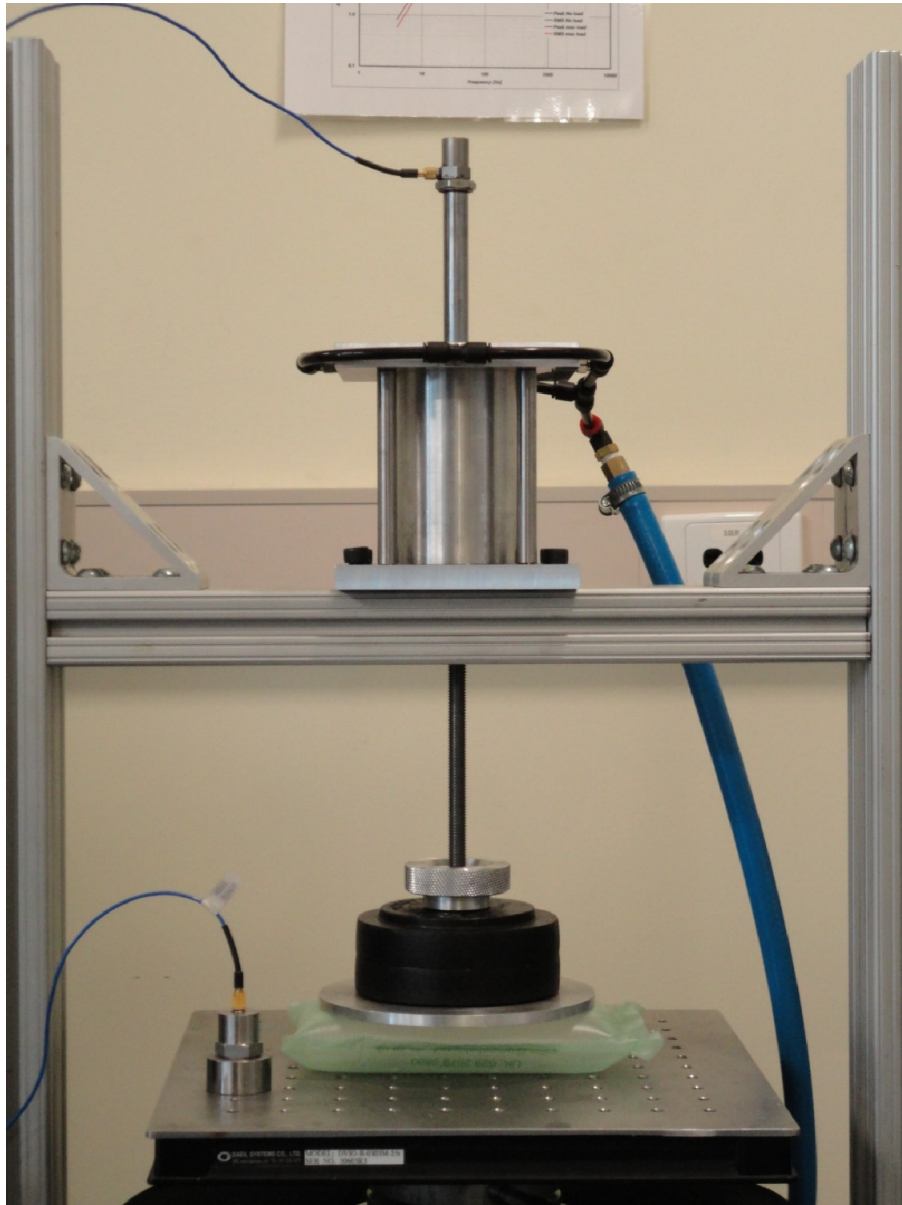


Figure 8-29: *Opus biodegradable air cushion pre-compression characteristics.*

Initially, the force deflection data from each level of pre-compression was to be used to obtain estimates of the system's actual stiffness at each damage level, hence natural frequency. This was to enable a comparison between the estimates extracted using the structural integrity assessment techniques and the actual properties of the system. However, the stiffness results obtained from the force deflection data were insufficiently sensitive.

The results from the analysis of the concatenated acceleration records are given in *Figure 8-31* and *Figure 8-32*. As can be seen, the adaptive FIR technique is more sensitive in detecting small changes in system characteristics. However, as the magnitude of the damage increments increases the performance difference between the two assessment techniques is reduced. This is largely due to the fact that, when using the adaptive FIR technique, the parameters used for analysis (mainly number of filter coefficients and range of data used for curve-fitting) remain constant, irrespective of the changes to the system under analysis. This does not allow for the optimum parameters to be used throughout the analysis period, which presents limitations to the technique when changes in the system's characteristics are large.



*Figure 8-30: Bio-degradable air-cushion experimental arrangement.*

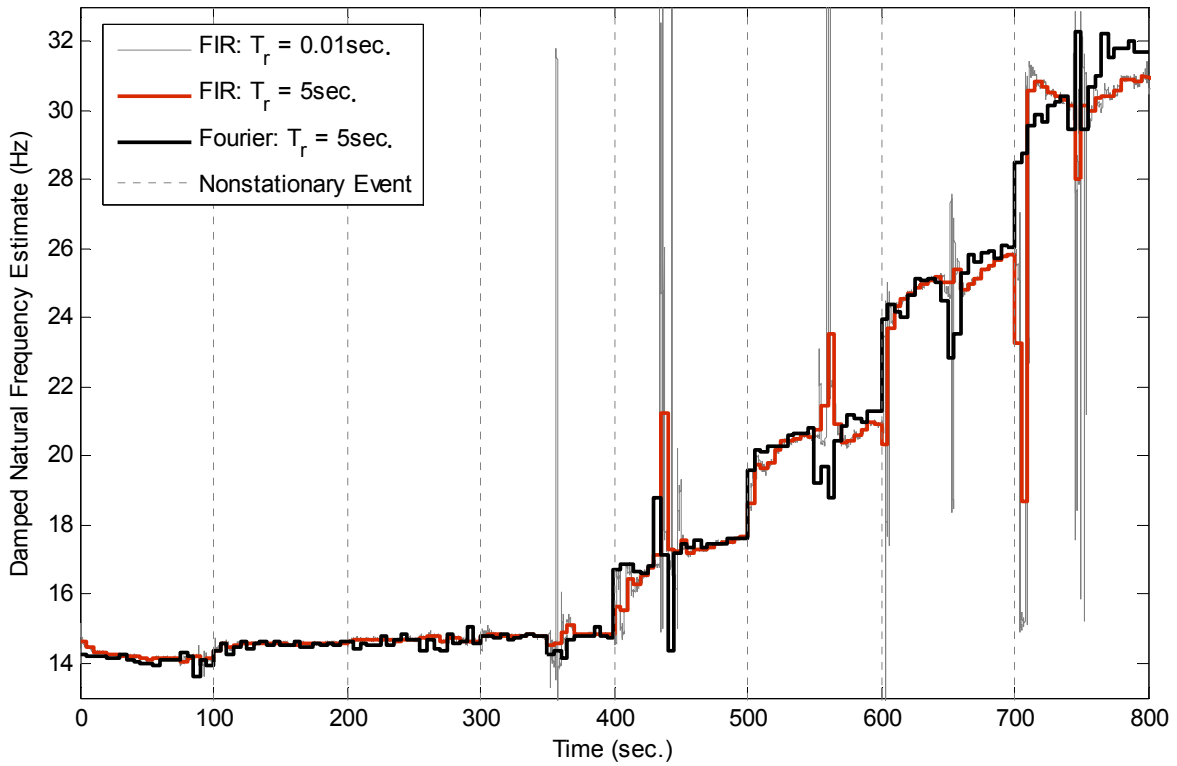


Figure 8-31: Structural integrity assessment results – Opus biodegradable air cushion.

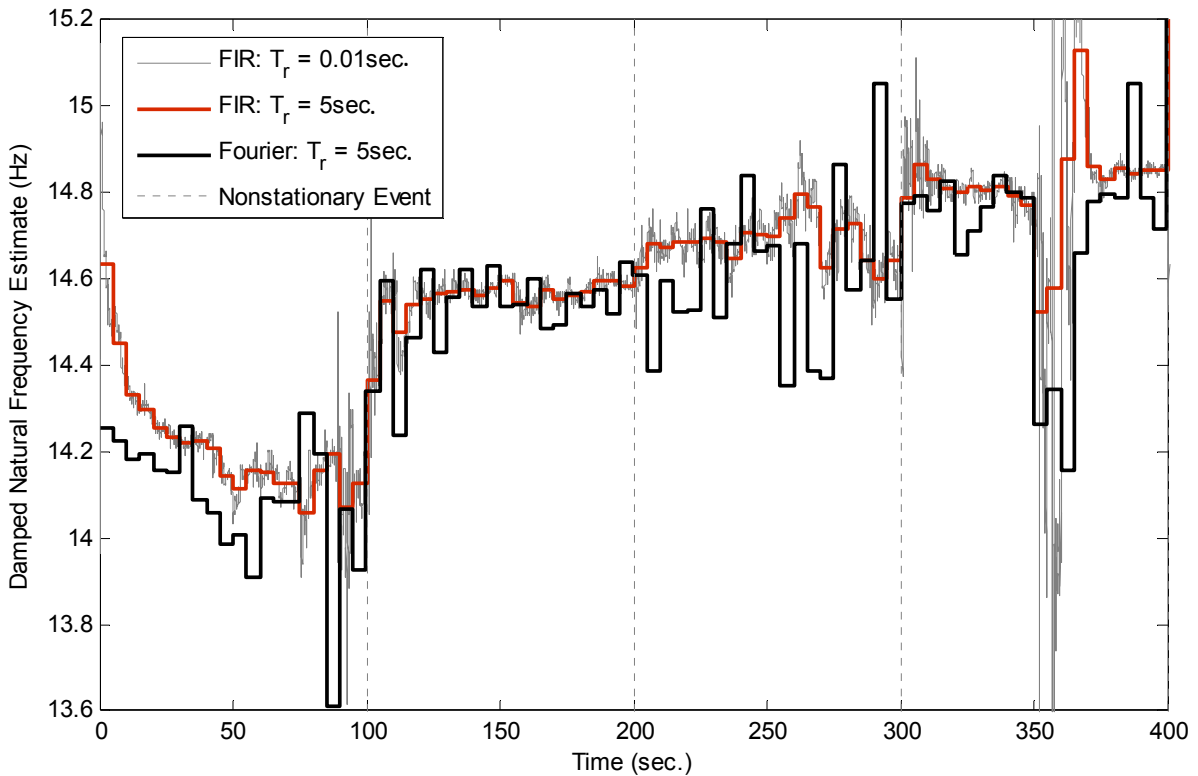


Figure 8-32: Structural integrity assessment results – zoomed section of Figure 8-31.

Figure 8-33 presents the air cushion system's FRF (captured at a temporal resolution of 100 seconds) for each level of pre-compression. As can be seen, the evolution of the FRF clearly follows the trends suggested in Figure 8-31 and Figure 8-32.

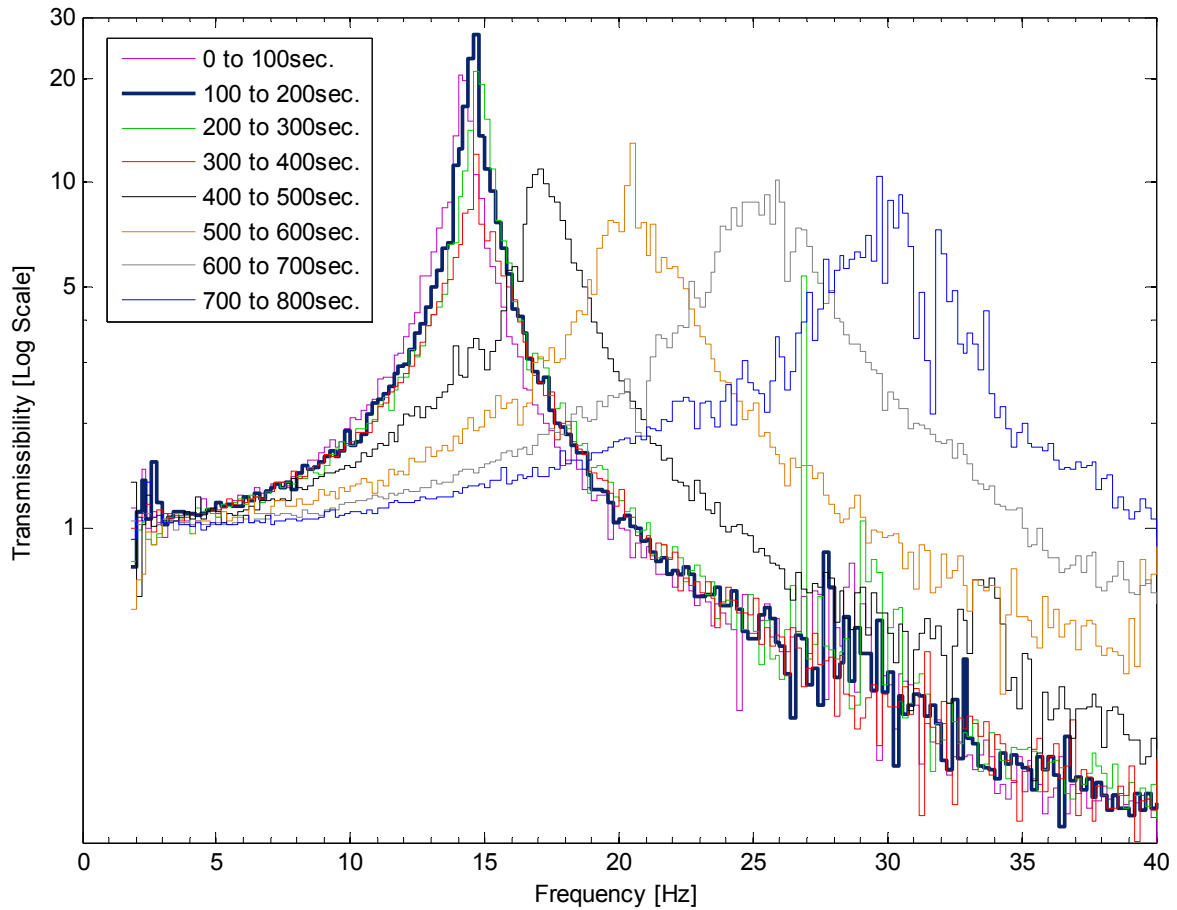


Figure 8-33: Evolution of the air cushion system's FRF with the induction of damage (line colours correspond with those given in Figure 8-29).

The second series of experiments performed on real protective packaging elements were designed to allow for the natural deterioration of the sample under random loading. During this series of experiments a large guided mass (838N) was placed atop of a corrugated paperboard container, while the base of the element was subjected to random excitation (Gaussian white noise, band-limited between 2-100Hz and had an RMS level of  $2.5\text{m/s}^2$ ). An Instron 8501 servo hydraulic testing machine, coupled with the aforementioned random vibration controller, was used to generate the excitation. The level of the excitation was set so as to induce damage to the container sample by virtue of the base while avoiding separation between the package and the guided mass. Data was sampled at a rate of 1kHz. The FRF of the system prior and subsequent (prior to catastrophic failure) to damage is presented in Figure 8-34. The experimental arrangement is pictured in Figure 8-35.

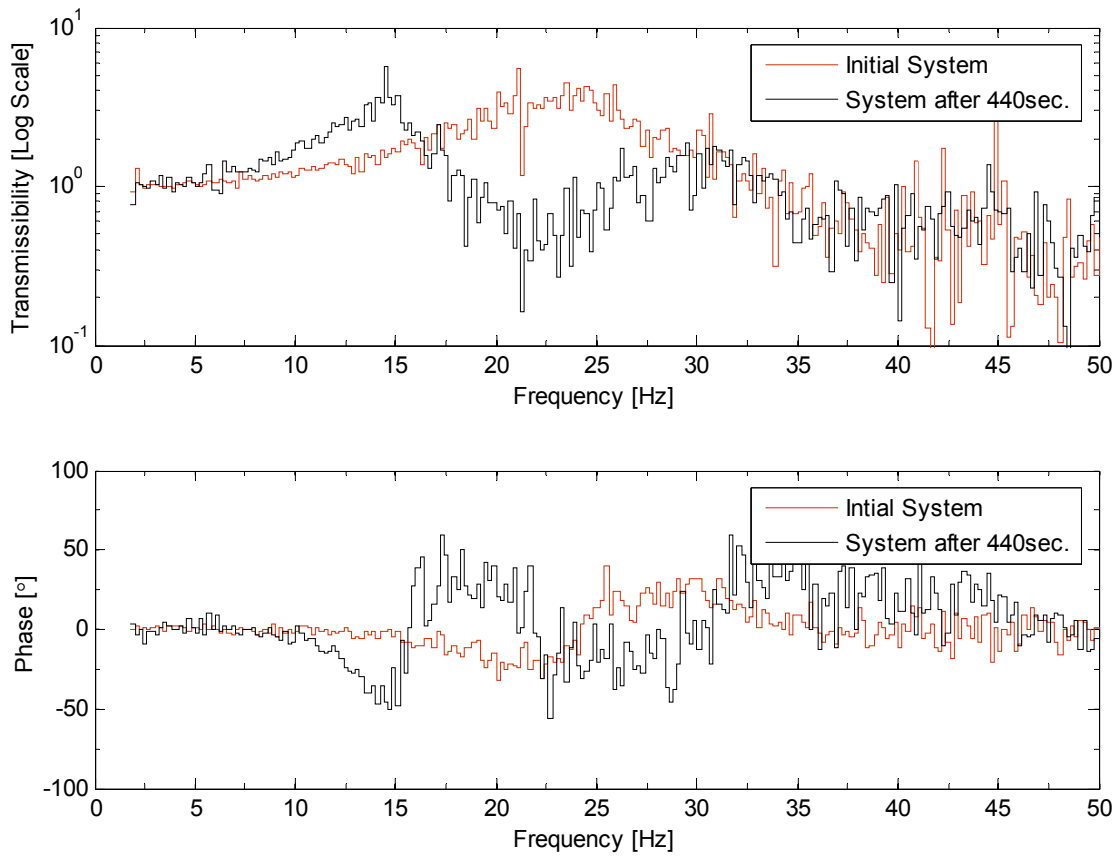


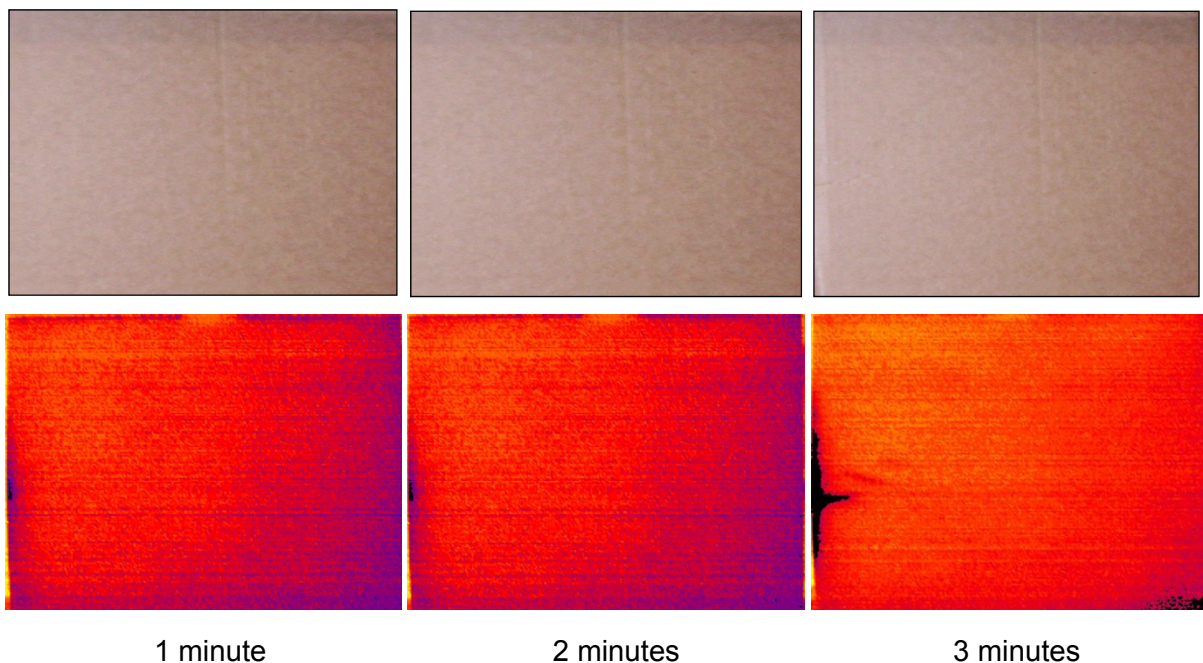
Figure 8-34: Evolution of the paperboard container system's FRF during random fatigue testing.



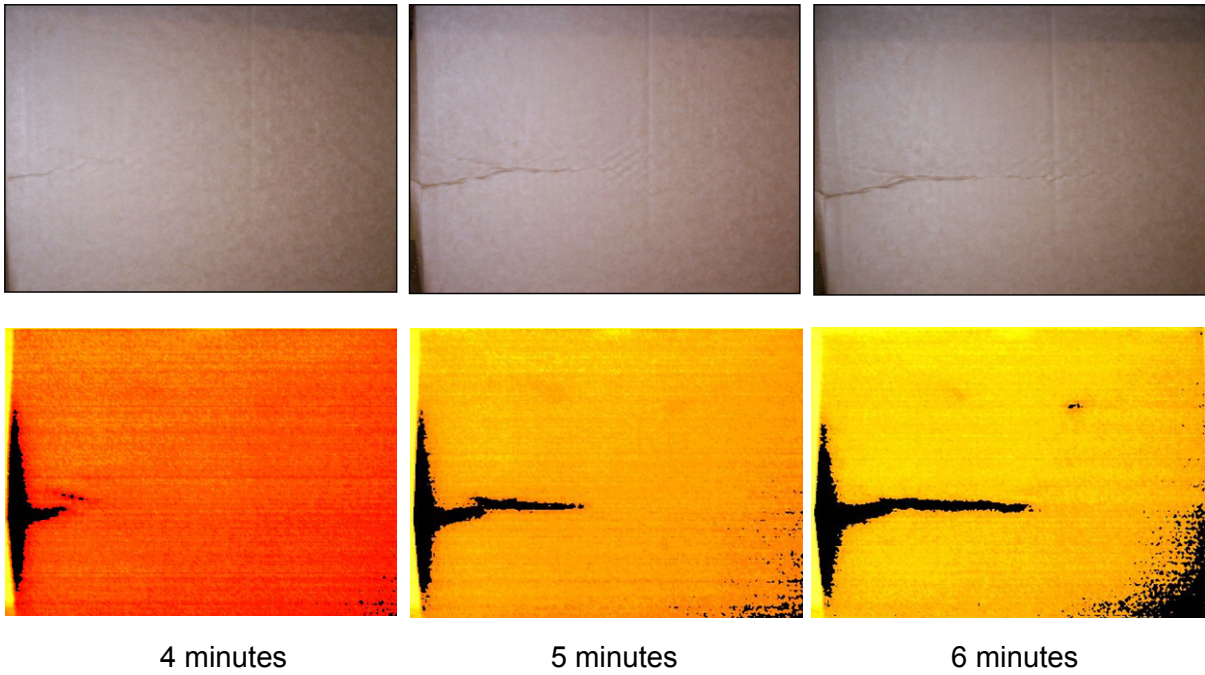
Figure 8-35: Corrugated paperboard experimental arrangement.

As the actual extent of damage to the structure is not known, it is difficult to establish with absolute certainty if the natural frequencies extracted from the two techniques do, in fact, correlate with the evolution of damage within the structure. For this particular experiment, a thermal imaging camera (type Avio 700) was used to identify high temperature regions corresponding to areas of high strain (in turn, corresponding to damage regions in the container wall). A series of thermal images, taken at 1 minute intervals are shown in *Figure 8-36* alongside their visible wavelength equivalents. The final condition of the system, prior to rapid failure (which began between the 7<sup>th</sup> and 8<sup>th</sup> minute of testing), is given in *Figure 8-37*. As can be seen, during the first 7 minutes of testing the structure exhibited consistent crease propagation; this was followed by rapid creasing from the corners of the right hand side of the package, towards the centre crease (some evidence of this creasing is visible in *Figure 8-37*), which in turn resulted in catastrophic failure.

The results obtained from the analysis of the excitation and response records captured during the random fatigue test are presented in *Figure 8-38*. Although not quantifiably accurate, the appearance and evolution of the crease detected by the thermal imaging system does support the results produced by both the Fourier based and the adaptive FIR structural integrity assessment techniques. This is in spite of the significant nonlinearities and complexities present in the system (four walls may result to a behaviour equivalent to four parallel springs of differing properties).



*Figure 8-36: Visual wavelength photograph (top row) and thermal (bottom row) image sequence of sample during random fatigue testing (arbitrary temperature scale).*



4 minutes

5 minutes

6 minutes

*Figure 8-36 Continued: Naked eye (top row) and thermal (bottom row) image sequence of sample during random fatigue testing (arbitrary temperature scale).*

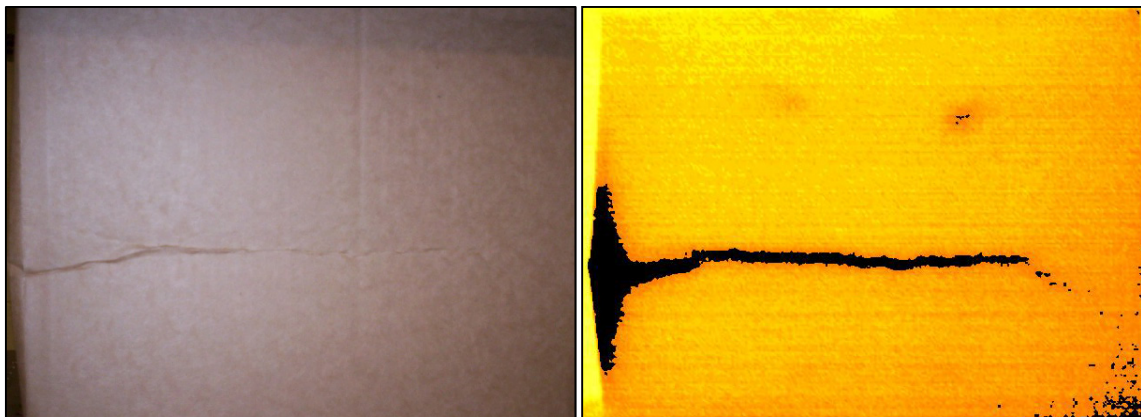


*Figure 8-37: Paperboard container sample at 7<sup>th</sup> minute – Left: Naked eye (top row) Right: Thermal image (arbitrary temperature scale).*

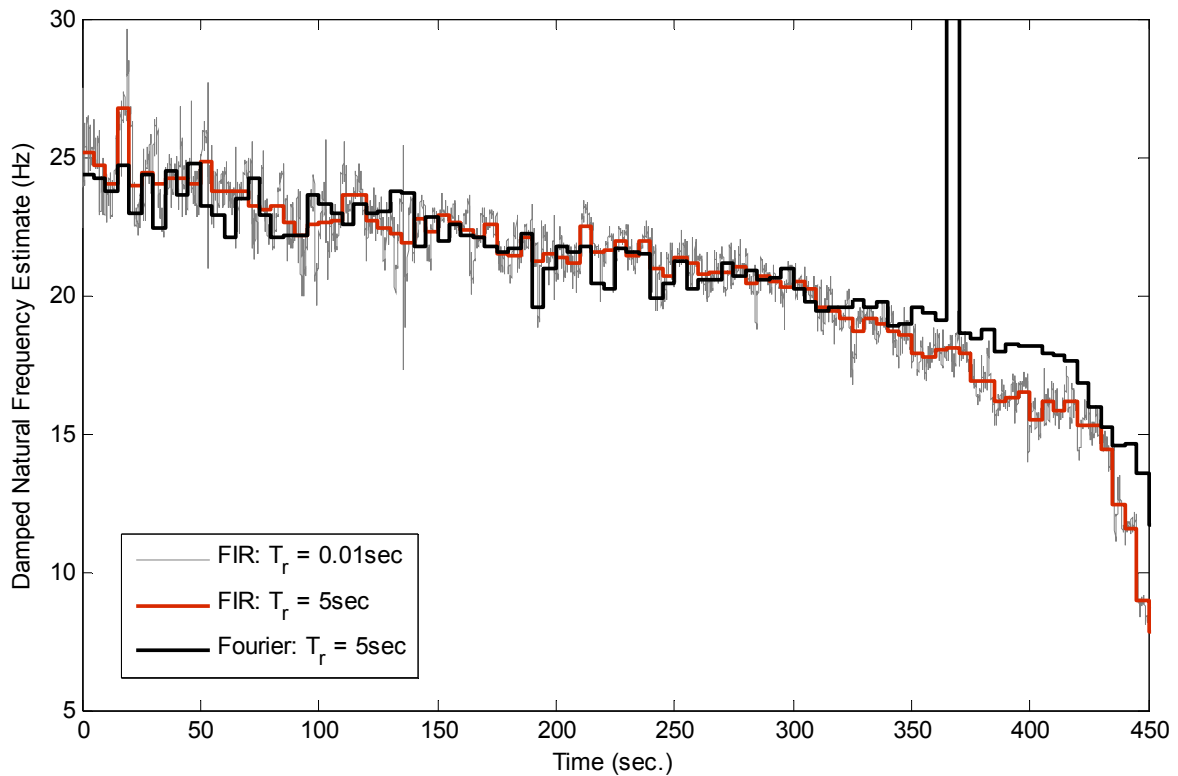


Figure 8-38: Structural integrity assessment results – paperboard container.

### 8.3. CONCLUSION

This chapter presented the results from numerous physical experiments designed to establish the validity and functional limits of the two techniques developed for monitoring structural integrity. Controlled experiments which made use of a variable cantilever arrangement were used to confirm the numerically simulated results. These experiments were performed using samples selected to provide different mechanical properties (specifically damping ratios).

In the main results from the controlled physical experiments confirm those obtained from the numerically simulated experiments. The results showed that both techniques were capable of identifying changes in the natural frequency of the system. However, the adaptive FIR technique provides more accurate estimates (even when the Fourier based approach has a relatively coarse temporal resolution of 8 seconds).

One noticeable difference between the results obtained from the controlled physical and numerically simulated experiments is a slight increase in uncertainty despite the relatively low noise to signal ratio (when compared to the numerically simulated experiments containing extraneous noise). This is attributed to nonlinearities in the physical arrangements as well as the contamination of the first resonant frequency by higher order modes. In addition, the optimised step-size algorithm, which is implemented with the adaptive FIR

technique, was unable to yield the normalised step-size which minimises the steady-state error when analysing data from physical experiments. However, this does not pose a significant limitation to the technique.

Results from the controlled physical experiments were also able to suggest that the error signals obtained using adaptive digital filters (of various types) may provide an alternative approach to monitoring the evolution of damage in structures subjected to random loading.

Finally, the ability of the integrity assessment techniques to monitor changes in the condition of real protective packaging elements was evaluated. Experiments were performed during which the condition of protective packaging elements was continuously monitored while damage to the system was allowed take place naturally (uncontrolled) under the influence of vibrations and an applied load (guided mass). Results from these experiments showed that the natural frequency estimates obtained using both techniques generally agreed and matched visual observations made during the experiments.

Results from the analysis of acceleration records obtained from systems subsequent to various levels of pre-compression also demonstrated that both techniques are capable of detecting sudden changes in the characteristics of real packaging elements; however, the adaptive FIR technique was more sensitive in detecting small changes.

## **REFERENCES**

Garcia-Romeu-Martinez, M.A, Rouillard, V, Sek, M & Cloquell-Ballester, V.A. 2007, 'Monitoring the evolution of fatigue in corrugated paperboard under random loads', *Proceedings of the 5<sup>th</sup> BSSM international conference on advances in experimental mechanics*

Rao, S 2005, *Mechanical Vibrations*, SI Edition, Prentice Hall

## Chapter 9 CONCLUSION

Protective packaging has a significant influence on modern society, particularly at an environmental and economical level. This study discussed the increasing impact of packaging on the environment and the pressures placed on the packaging industry to reduce the level of packaging waste. It was shown that there is a strong case for continued research aimed at developing techniques which can be used to aid the optimisation of engineered protective packaging, thereby reducing packaging waste.

In order to achieve a beneficial level of packaging optimisation, a thorough understanding of the continuous progression of damage, as a result of environmental distribution loads, within the packages is required. A common approach used to evaluate damage within a system is to measure changes in its modal parameters, mainly its stiffness. However, most published modal parameter extraction techniques do not allow for the continuous progression of damage within the system to be established.

This study tested the hypothesis that established constant parameter modal estimation techniques, combined with suitable signal processing approaches, can be used to continually monitor changes in the structural integrity of protective packaging materials.

Two techniques for monitoring structural integrity were considered. The first technique used a modified version of the short-time Fourier transform (STFT) to obtain a series of “instantaneous”, or short-time, frequency response functions (FRF), from which estimates of natural frequency were made. This includes the evaluation of various spectral enhancement techniques, such as zero-padding and data overlapping, used to limit the compromise between the spectral and temporal sensitivities.

The second approach used an adaptive digital finite-impulse-response (FIR) filter to continually extract estimates of the system’s instantaneous FIR function, from which estimates of the system’s instantaneous damped natural frequency were made.

An initial series of numerically simulated experiments were performed to aid the development of both techniques. These experiments were able to clearly demonstrate that the selection of the analysis parameters used when implementing the Fourier based approach has a significant influence on the resulting natural frequency estimates. It was found that, for records containing up to 10% noise, sub-record length (equivalently spectral resolution) has a

more pronounced influence on the accuracy of short-time modal parameter extraction than the level of spectral averaging (equivalently spectral uncertainty). It was also found that while zero-padding may not increase true spectral resolution, it does allow for improved natural frequency estimates with the introduction of interpolated estimates at the non-described frequencies. Finally, it was demonstrated that for short-time modal parameter extraction purposes (in this case natural frequency), increased amounts of overlapped averaging can significantly reduce the variance of the estimates obtained. This is particularly useful as it allows for increased spectral accuracy without compromising temporal resolution. These findings were also confirmed using the results from controlled physical experiments.

The preliminary numerically simulated experiments also aided the development of the adaptive FIR technique. The technique, in its final form, used a normalised least-mean-square (NLMS) adaptive FIR filter to convert random, forced excitation and response data into a series of instantaneous free-response signals. A Hilbert transform based approach was applied to the resulting signals in order to extract estimates of the system's instantaneous damped natural frequency.

The numerically simulated experiments were particularly useful when establishing procedures for selecting the appropriate analysis parameters for the adaptive FIR approach. One important parameter is the normalised step-size. With the aid of results obtained from the numerical simulations a procedure which optimises the adaptation step-size of the NLMS algorithm using the RMS of the adaptive filter's error signal was introduced. It was shown that, for linear SDoF systems with varying amounts of extraneous noise, this procedure can significantly improve the tracking ability of the adaptive FIR technique, particularly when the step-size is re-optimized at regular intervals. The results from further numerical simulations were also able to demonstrate that significant improvements, in terms of both the spectral sensitivity and the rate of initial convergence, can be achieved by iteratively adjusting the filter tap coefficient vector's length and initial filter tap coefficients.

A comparative study directly compared the results obtained from a series of numerically simulated experiments using both integrity assessment techniques for a variety of conditions. The results demonstrated that the adaptive FIR technique was more sensitive to extraneous noise and the damping ratio of the system under analysis. Nevertheless, provided that the damping ratio was not significantly greater than 16% (less than 32%), results extracted with fine temporal resolution had considerably less variation when using the adaptive FIR technique. However, it was also shown that in instances where damage is sudden, and the

system's damping ratio is low ( $\leq 1\%$ ), implementing the Fourier based technique with a coarse temporal resolution can yield estimates with accuracy similar to those obtained using the adaptive FIR technique.

Following the comparative study based on numerically simulated experiments, a number of controlled physical experiments were performed. In the main, results from these experiments confirm those obtained from the numerical simulations. One noticeable difference was a slight increase in the variance of the natural frequency estimates despite a relatively low noise to signal ratio (when compared to the numerically simulated experiments containing extraneous noise). This is attributed to nonlinearities in the physical arrangements and the contamination of the first resonant frequency by higher order modes. In addition, the optimised step-size technique implemented with the adaptive FIR approach was unable to yield the step-size which minimises the steady-state error when analysing data from physical experiments. However, this did not pose a significant limitation to the technique, which again provided more accurate estimates of natural frequency than the Fourier based approach (even when the Fourier based approach used a relatively coarse temporal resolution of 8 seconds).

Finally, the ability of the techniques to monitor changes in the condition of real protective packaging elements was evaluated. The results demonstrated that both techniques were capable of detecting changes in the characteristics of real protective packaging elements. However, the adaptive FIR technique was generally more sensitive in detecting small changes in system properties.

Overall, the results presented in this study demonstrate that vibration endurance tests performed on packaging systems need not be restricted to visual inspection for the identification of damage. It has been shown that constant parameter modal estimation techniques, combined with suitable signal processing approaches, can be used to continually monitor the stiffness of systems (via their natural frequency) during tests. The ability to monitor variations in stiffness allows the rate and manner of structural deterioration to be established. Such an approach will allow packaging engineers to quantitatively compare the performance of various materials and structures with respect to their ability to withstand sustained random loading.

## 9.1. SUMMARY OF GENERAL TECHNICAL CONTRIBUTIONS

In addition to the overview given above, the research has also provided general technical contributions to modal parameter extraction (not limited to packaging systems) which can be applied when using short-time FRFs (obtained using the Fourier transform) to obtain estimates of short-time natural frequency as follows:

- For records containing up to 10% noise, sub-record length has a more pronounced influence on the accuracy of modal parameter extraction than the level of spectral averaging
- Zero-padding allows for improved short-time natural frequency estimates with the introduction of interpolated estimates at the non-described frequencies
- Overlapped averaging can significantly reduce the variance of extracted short-time natural frequency estimates

Furthermore, it was shown that adaptive digital filters provide an alternative to frequency domain analysis and can be manipulated to provide accurate natural frequency estimates with fine temporal sensitivity. It was shown that when extracting estimates of natural frequency using adaptive LMS FIR filters:

- Iteratively adjusting the filter tap coefficient vector's length and initial filter tap coefficients improves spectral sensitivity and the rate of initial convergence
- Leakage factors are likely to create issues associated with convergence and are not recommended in this application
- The number of coefficients should match (or slightly exceed) the natural duration of the impulse response function
- Damping ratios greater than 16% damping present a limitation to the technique as a result of limited curve-fitting data
- Low damping ratios ( $\leq 1\%$ ) present some difficulties related to a reduced rate of convergence

## 9.2. FUTURE WORK

Because the research presented here is the initial stage of a broader research effort, it was deliberately limited to the study of SDoF systems which were mostly linear. The applicability of the techniques to multiple degree-of-freedom systems is an important endeavour that needs to be addressed by future research. Specifically, the effect of isolating natural modes of vibration on the techniques would be of interest. This is particularly the case for the FIR technique, but is also important for the Fourier transform based approach when the systems have high modal density. The analysis of significantly nonlinear systems, particularly using the FIR based approach, is also warranted.

Another aspect of the research that needs further investigation is the influence of uncorrelated or spurious noise on the excitation and response signals. Some discussions of extraneous noise were included in this study. However, the effect of noise on the accuracy and response of the damage detection techniques needs to be evaluated using thorough and systematic investigations. These investigations should combine the influence of extraneous noise and nonlinear effects to establish the practical limits of the damage detection techniques.